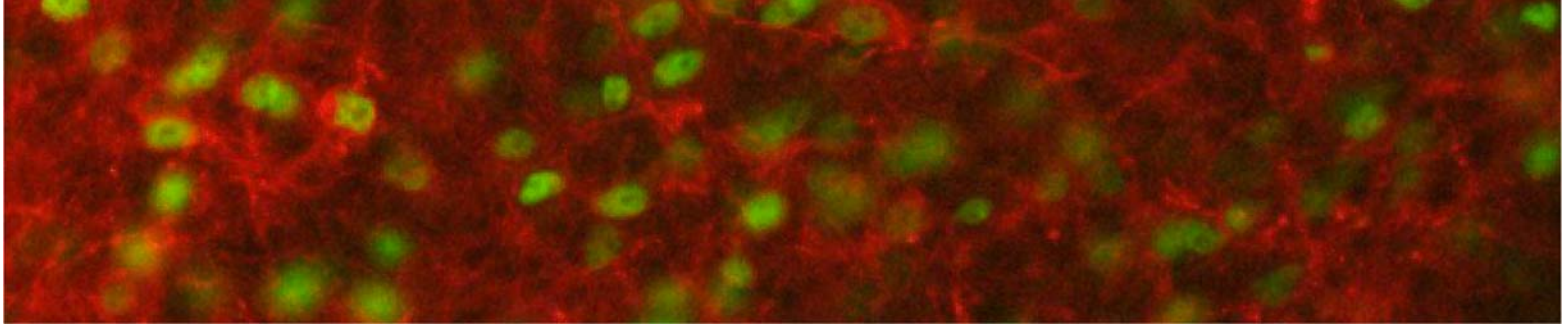

Similitudes y diferencias electrofisiológicas y neurales entre el sueño y la anestesia general.

Tesis de Doctorado en Ciencias Biológicas

Opción Neurociencias

Pedeciba Biología

UdelaR

Alejandra Mondino

2022

Orientador: Giancarlo Vanini (University of Michigan)
Co-Orientador: Pablo Torterolo (Facultad de Medicina, UdelaR)

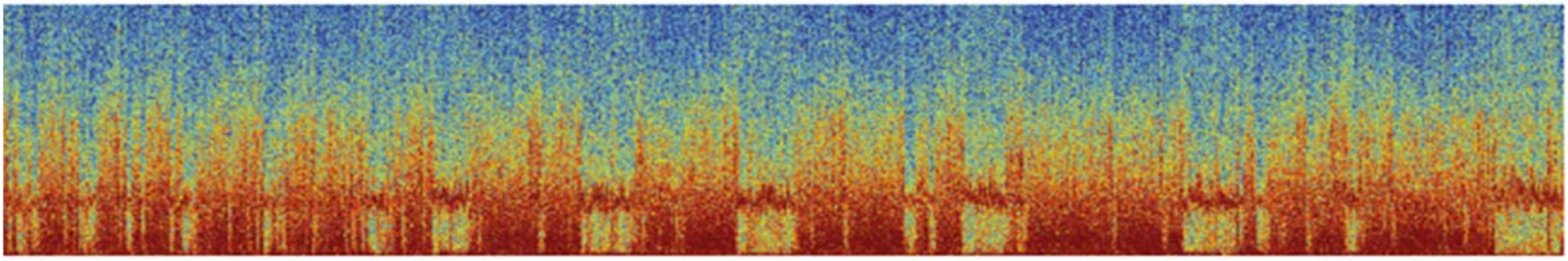

Agradecimientos

En primer lugar, quiero dar mi más sincero agradecimiento a mis tutores, el Dr. Giancarlo Vanini y el Dr. Pablo Torterolo. A Giancarlo por abrirme las puertas de su laboratorio en la Universidad de Michigan, por brindarme toda su ayuda para adaptarme a otro idioma, otra ciudad y otra cultura y hacerme sentir como en casa. Por todo su apoyo, confianza y tiempo en el desarrollo de esta tesis. A Pablo por ser mi gran maestro desde que comencé la maestría, por siempre confiar en mi e impulsarme a llegar a más. Por toda su paciencia y tiempo, por tener siempre las palabras justas, sin importar la distancia. Además de grandes tutores, son dos grandes amigos.

Al Dr. George Mashour, por su gran apoyo y confianza, por estar siempre disponible a pesar de sus ocupaciones y por su gran humildad.

A todos mis compañeros del Vanini Lab en la Universidad de Michigan y del Laboratorio de Neurobiología del Sueño de la Facultad de Medicina, en particular a Joaquín González, por su paciencia para ayudarme con el manejo de la programación y los análisis más complejos.

A la UdelaR, la universidad que me formó y de la que nunca quisiera desvincularme. Gracias por todas las oportunidades brindadas.

A mis padres, quienes me enseñaron el amor por la investigación y la docencia desde que era una niña, gracias por apoyarme siempre, en todas mis decisiones. Gracias a ellos y a mi hermano por ser mi gran soporte y por estar conmigo pese a la distancia física. No sería quien soy sin ellos.

A Gastón, por viajar 9000 km para acompañarme en el desarrollo de mi carrera, por ser mi mayor sostén y compañero de aventuras. Nada habría sido posible sin él.

En especial, a Dulcinea, por sus 15 años de amor incondicional

Índice

Resumen

La anestesia general comparte importantes características con el sueño, siendo la más evidente, la perdida de consciencia reversible. Tal es así, que suele utilizarse la expresión de que un paciente "está dormido" para referirse a que alcanzó un plano anestésico. Estos estados comparten similitudes electrofisiológicas y se ha propuesto que son inducidos por los mismos circuitos neurales. Sin embargo, aún existen muchas interrogantes al respecto. El objetivo principal de esta tesis fue el de determinar las similitudes y diferencias electrofisiológicas y neurales entre el sueño y la anestesia general. Para ello, en el capítulo 1 realizamos una detallada caracterización electroencefalográfica del sueño y la vigilia para contar con una base para comparar con la anestesia general. En el capítulo 2, estudiamos las peculiaridades del electroencefalograma bajo uretano, un anestésico que ha sido propuesto como un modelo farmacológico de sueño dado que es capaz de oscilar entre dos estados, uno similar al sueño No-REM y uno similar al sueño REM. En el capítulo 3, evaluamos el rol de neuronas glutamatérgicas y GABAérgicas de unas de las principales áreas somnogénicas, el área ventrolateral (VLPO) y el núcleo mediano (MnPO) del área preóptica sobre la anestesia general con isoflurano. Por último, el capítulo 4 surgió a raíz de un hallazgo inesperado encontrado en el capítulo 3, que las neuronas glutamatérgicas del VLPO y regiones adyacentes generan vigilia, fragmentan el sueño No-REM y suprimen el sueño REM, desafiando la teoría de que las neuronas del área preóptica que regulan el ciclo sueño-vigilia son exclusivamente somnogénicas. En este capítulo, estudiamos en detalle el rol de estas neuronas en el ciclo sueño-vigilia y la actividad eléctrica cortical. Con esta tesis hemos podido demostrar que la potencia y coherencia del EEG durante el sueño varía de acuerdo al ciclo luz-oscuridad y que es distinta en distintas áreas corticales e incluso entre ambos hemisferios. Por lo tanto, al comparar

la actividad eléctrica cortical del ciclo sueño-vigilia con otro estado, es de gran importancia utilizar la misma disposición de electrodos y realizar los registros en la misma etapa del día. Adicionalmente, si bien durante muchos años se ha sostenido que la anestesia general comparte grandes similitudes con el sueño y que actúa mediante los mismos circuitos neurales, en este trabajo hemos colectado evidencia que contradice estas teorías. Por un lado, existen claras diferencias electroencefalográficas entre la anestesia con uretano (considerada un modelo farmacológico de sueño) y el sueño (tanto No-REM como REM). Por otro lado, la activación del área preóptica del hipotálamo, un área esencial en la generación de sueño no modifica la sensibilidad al isoflurano (un anestésico general ampliamente utilizado). Por último, el estudio del área preóptica en el sueño y la anestesia general nos permitió desafiar el concepto de que las neuronas involucradas en el ciclo sueño-vigilia del área preóptica del hipotálamo son exclusivamente somnogénicas al comprobar que las neuronas glutamatérgicas del área medial y ventrolateral de la región preóptica generan vigilia, fragmentan el sueño No-REM e inhiben el sueño REM.

Introducción

Desde los inicios del siglo XX la ciencia ha tratado de comprender la naturaleza y las bases neurales de la consciencia. Para ello, muchos estudios han evaluado las diferencias entre el estado normal de vigilia consciente y estados en los que ocurre perdida de consciencia, como por ejemplo el sueño o la anestesia general (Mashour, 2011). Desde la primera demostración de la anestesia en 1846 se han utilizado un gran número de diversos agentes anestésicos y se han estudiado sus mecanismos de acción. En los inicios, a partir de la "hipótesis unitaria" formulada por Claude Bernard, se consideraba que todos los anestésicos tenían un mecanismo de acción común ya que todos ellos provocaban perdida de consciencia (Bernard, 1875). En la actualidad, esa hipótesis está obsoleta ya que se conoce que existen diversos grupos de anestésicos con distintos mecanismos de acción. En particular, los anestésicos pueden ser divididos en dos clases principales de acuerdo con su vía de administración; anestésicos intravenosos (usualmente utilizados para la inducción anestésica) y anestésicos inhalatorios (utilizados principalmente para el mantenimiento anestésico). Estos, a su vez pueden clasificarse de acuerdo con su mecanismo de acción. Los anestésicos actúan interactuando con diversos receptores que regulan la transmisión sináptica y distintos receptores presentan distinta sensibilidad a los anestésicos (Franks, 2008). Muchos de los agentes anestésicos, como por ejemplo el propofol, el isoflurano y sevoflurano, actúan sobre los receptores GABA, potenciando las corrientes de cloro. Otros, como la ketamina, un anestésico disociativo, ejercen su acción mediante la inhibición de receptores NMDA (Alkire *et al.*, 2008). Sin embargo, más allá de las diferencias entre los mecanismos de acción, en los últimos años se la neurociencia ha intentado dilucidar los correlatos de inconsciencia comunes de todos ellos, y de otros estados de pérdida de consciencia reversible, como el sueño (Mashour, 2006).

La anestesia general y el sueño comparten importantes características, siendo la principal, la perdida de consciencia reversible y la baja respuesta a estímulos (Mashour & Pal, 2012). Tal es así, que muchas veces es utilizada la expresión de que un paciente "está dormido" para referirse a que alcanzó un plano anestésico (Mashour, 2011; Vacas *et al.*, 2013). En 1994 Lydic y Biebuyck propusieron la hipótesis de circuitos compartidos (*shared circuit hypothesis*) entre el sueño y la anestesia general (Lydic & Biebuyck, 1994). Esta hipótesis propone que ambos estados comparten mecanismos neurales y un amplio número de investigaciones han sido realizadas con el fin de corroborala. Por ejemplo, se ha demostrado que la privación de sueño en la rata disminuye el tiempo necesario para la inducción anestésica, así como también, incrementa el tiempo de recuperación de la misma (Tung *et al.*, 2002). Esto demuestra que un aumento en la presión al sueño incrementa la sensibilidad a los anestésicos. Además, se ha visto que, en animales privados de sueño, la anestesia general tiene un efecto restaurador de sueño, disminuyendo el rebote de sueño post-privación lo que hace pensar que la anestesia general satisface, de manera dependiente de la droga anestésica, la necesidad homeostática de sueño (Tung *et al.*, 2004; Mashour *et al.*, 2010; Pal *et al.*, 2011; Pick *et al.*, 2011). Adicionalmente, mediante tomografía de emisión de positrones, se ha observado que tanto el sueño como la anestesia general generan desactivación del tálamo, giro cingulado y precúneo (Maquet, 2000; Kaisti *et al.*, 2002).

Similitudes electroencefalográficas

En cuanto a la actividad eléctrica cortical, es posible observar grandes similitudes entre la anestesia general y el sueño, específicamente en la fase de sueño de ondas lentas o sueño No-REM. La mayoría de los anestésicos generales generan ondas lentas en la frecuencia delta (1-4 Hz) y husos de sueño (eventos de 0.4 a 2 segundos de duración, caracterizados por una frecuencia de 7-14 Hz)(Keifer *et al.*, 1996; Gugino *et al.*, 2001; Sleigh *et al.*, 2011), al igual que el sueño No-REM

(Uchida *et al.*, 1994). Es interesante destacar que la administración de anestésicos GABAérgicos en la región pontina induce un electroencefalograma que alterna entre un estado caracterizado por ondas lentas (similar a No-REM) y un estado similar al sueño REM, con un incremento de la frecuencia theta (4-8 Hz) (Avigdor *et al.*, 2021). Sin embargo, otros estudios han demostrado diferencias electroencefalográficas entre el sueño y la anestesia general (Murphy *et al.*, 2011; Akeju & Brown, 2017). Por ejemplo, los husos de sueño durante el sueño No-REM aumentan durante la fase positiva de las ondas lentas, mientras que existe muy poca correlación entre las ondas lentas y la actividad de husos en la anestesia general (Murphy *et al.*, 2011). Por otra parte, la anestesia con uretano, ampliamente utilizada en experimentación animal, es considerada un modelo farmacológico de sueño (Horner & Kubin, 1999; Clement *et al.*, 2008). Esta, se caracteriza por dos estados electroencefalográficos que se alternan entre sí, un estado de ondas lentas que recuerda al sueño No-REM, y un estado activado con características similares al sueño REM pero también a la vigilia (Pagliardini *et al.*, 2013; Yagishita *et al.*, 2020). Hasta el momento, las diferencias y similitudes entre el uretano y el sueño fisiológico siguen siendo no del todo comprendidas. Incluso, la similitud del estado activado con la vigilia, han llevado a cuestionar si realmente el uretano provoca perdida de consciencia (Pagliardini *et al.*, 2013; Neves *et al.*, 2018).

Bases neurales

Durante mucho tiempo se consideró que el sueño era un proceso pasivo que no estaba generado por circuitos neurales específicos si no por una disminución generalizada de la actividad cerebral (Reitz & Kelz, 2021). Sin embargo, casi 100 años atrás, durante la epidemia de encefalitis letárgica von Economo propuso la existencia de un centro generador de sueño (el hipotálamo anterior) y uno de vigilia (en el hipotálamo posterior). Esta conclusión fue basada en la correlación entre los signos clínicos de los pacientes (insomnio o sueño excesivo) y las lesiones anatomopatológicas

(von Economo, 1930). Estudios posteriores demostraron un rol esencial de la región preóptica del hipotálamo (POA) en la generación de sueño, principalmente sueño No-REM (Suntsova *et al.*, 2007; Szymusiak *et al.*, 2007; Benedetto *et al.*, 2012). Se ha comprobado que existen grupos de neuronas que se activan durante el sueño en varias subregiones de la POA con una densidad particularmente alta en la región ventrolateral (VLPO) y el núcleo mediano (MnPO) (Suntsova *et al.*, 2002; Szymusiak & McGinty, 2008; Torterolo *et al.*, 2009; Gvilia *et al.*, 2011). Las neuronas GABAérgicas del VLPO y MnPO, en particular generan sueño mediante la inhibición de centros activadores (Vanini *et al.*, 2011). De forma análoga, se ha demostrado que anestésicos generales tanto de administración intravenosa (propofol y barbitúricos), como volátiles (isoflurano), activan neuronas GABAergicas de la POA promotoras de sueño No-REM, principalmente del VLPO (Tung *et al.*, 2001; Nelson *et al.*, 2003; Moore *et al.*, 2012; Han *et al.*, 2014). Sin embargo, si bien estos estudios demuestran una correlación entre la anestesia general y la activación de la POA, no han sido capaces de demostrar causalidad. Además, si bien el MnPO es esencial para la generación y regulación homeostática de sueño, su rol en la anestesia general ha sido poco explorado.

Objetivos y estructura de la Tesis

Debido a que aún existen muchas interrogantes en la relación entre el sueño y la anestesia general, el objetivo principal de esta tesis fue determinar las similitudes tanto a nivel del EEG, como en la actividad neuronal de la POA entre estos estados. Para ello he divido la tesis en 4 capítulos.

El **Capítulo 1** consiste en la caracterización electroencefalográfica del sueño y la vigilia, con el fin de contar con una base detallada para que luego pueda ser comparada con el EEG durante la anestesia general. Si bien, existen diversos trabajos que han analizado el EEG durante sueño y

vigilia, la mayoría de ellos no han estudiado el espectro completo de frecuencias, ni han evaluado diferencias en las diferentes áreas corticales y hemisferios, así como la influencia del ciclo circadiano.

En el **Capítulo 2**, estudiamos las características electroencefalográficas del uretano, el anestésico general que ha sido propuesto como un modelo farmacológico de sueño. En este trabajo comparamos el sueño fisiológico y la vigilia con los dos estados característicos de este tipo de anestesia haciendo especial énfasis en los correlatos electroencefalográficos de perdida de consciencia.

En el **Capítulo 3**, nos enfocamos principalmente en la teoría de los circuitos neurales compartidos entre el sueño y la anestesia, y evaluamos el rol de las neuronas GABAérgicas y glutamatérgicas en el VLPO y el MnPO en el sueño y la inducción y recuperación anestésica.

Por último, el **Capítulo 4** surge como una extensión de un hallazgo inesperado encontrado en el capítulo 3. En este trabajo pudimos demostrar que las neuronas glutamatérgicas del VLPO y regiones adyacentes generan vigilia, fragmentan el sueño No-REM y suprimen el sueño REM, desafiando la teoría establecida durante muchos años de las neuronas de la POA que regulan el ciclo sueño-vigilia son exclusivamente somnogénicas. En este capítulo, estudiamos en detalle el rol de estas neuronas en el ciclo sueño-vigilia y la actividad eléctrica cortical.

Capítulo 1. Caracterización electroencefalográfica del sueño y la vigilia.

El sueño puede ser definido como estado de perdida de consciencia reversible, una disminuida respuesta a estímulos y una reducción del tono y actividad muscular. Además, a nivel comportamental, se caracteriza por inmovilidad y la adopción de una postura típica que permita descansar adecuadamente y conservar el calor corporal (Siegel, 2005; Carskadon & Dement, 2011). El ciclo sueño-vigilia en los mamíferos se organiza en 3 estados principales, la vigilia y dos estados de sueño; el sueño de ondas lentas o sueño No-REM, y el sueño paradójico o sueño REM (de sus siglas en inglés, Rapid Eye Movements) (Saper *et al.*, 2010). Cada uno de estos estados tiene particulares características comportamentales, autonómicas y electroencefalográficas (Torterolo *et al.*, 2019).

El sueño puede ser distinguido de la vigilia por las características de la actividad eléctrica cerebral y muscular mediante el uso de la polisomnografía (Torterolo *et al.*, 2022). En rata y ratón, (modelos animales de esta tesis), la vigilia se caracteriza por un EEG de bajo voltaje y de alta frecuencia asociado a un tono muscular elevado y movimientos musculares visualizados en la actividad registrada por el EMG. Al estudiar el espectro de potencias de la vigilia, existe un pico de potencia de las oscilaciones en la banda de frecuencia theta (4 - 9 Hz) y gamma (> 30 Hz). Las oscilaciones theta son más prominentes en las cortezas occipitales. De la vigilia ocurre la transición al sueño No-REM y las oscilaciones neurales se van enlenteciendo mientras que su amplitud se incrementa debido a una alta sincronización local de la actividad neuronal. Las oscilaciones más prominentes se encuentran en la banda de frecuencia delta (1 – 4 Hz) y se observan husos de sueño (oscilaciones con una frecuencia de 10 – 15 Hz, una duración de al menos 0.4 segundos y una morfología de rampa de ascenso y descenso) Además, durante esta etapa del sueño la actividad muscular

disminuye con respecto a la vigilia (Pace-Schott & Hobson, 2002; Carskadon & Dement, 2011; Torterolo *et al.*, 2019). Por último, del sueño No-REM se ingresa al sueño REM. La actividad del EEG durante esta etapa es muy similar a la vigilia, con oscilaciones de baja amplitud y alta frecuencia y un pico de la actividad theta, por lo cual se lo conoce también con el nombre de sueño paradójico. El REM se diferencia de la vigilia por la presencia de atonía muscular (Carskadon & Dement, 2011).

Además de las diferencias visuales del electroencefalograma de los estados de sueño y vigilia, es posible diferenciar estos estados mediante un análisis cuantitativo del EEG. En este sentido, uno de los análisis más comúnmente realizados es el de la potencia espectral el cual se basa en la determinación del peso de cada uno de los componentes de frecuencias en la señal del EEG. Para calcularla se utiliza la transformada rápida de Fourier que consiste matemáticamente en lo siguiente:

$$Px\ (f) = [x(f)]^2$$

$$\text{Siendo } x(f)\ = \int_{-\infty}^{+\infty} x(t)e^{2\pi ift}dt$$

La potencia de determinada banda de frecuencia refleja el grado de sincronización local de diferentes neuronas a esa frecuencia (Torterolo *et al.*, 2022).

Además de la sincronización local, es posible estimar la sincronización entre diferentes áreas de la corteza cerebral mediante el uso de la coherencia espectral. Este análisis se basa en el cálculo de la correlación de distintas bandas de frecuencia en dos regiones distintas. Para que dos oscilaciones neurales de distintas regiones del cerebro a una frecuencia determinada sean completamente coherentes necesitan tener una fase y relación de amplitud constantes a esa frecuencia. La formula para el cálculo de la coherencia espectral es la siguiente:

$$COH_{xy}(f) = \frac{\left|CSD_{xy}\ (f)\right|^2}{P_x(f)P_y(f)}$$

Siendo CSD: *Cross spectral density* también conocido como análisis de Fourier de la covarianza cruzada. El rango de valores de coherencia va de 0 a 1, siendo 0 totalmente incoherente y 1 totalmente coherente (Bullock & McClune, 1989; Torterolo *et al.*, 2022).

Determinadas características de la potencia y coherencia espectral del EEG son considerados correlatos de consciencia. Por ejemplo, la potencia de las oscilaciones de alta frecuencia como gamma (30-100 Hz) y las llamadas HFO (de sus siglas en inglés *high frequency oscillations* (de 100 a 200 Hz) son características de estados en los que ocurre actividad cognitiva, como la vigilia, pero también como el sueño REM (donde ocurre la mayor cantidad de ensoñaciones) (Cavelli *et al.*, 2015; Cavelli *et al.*, 2018). Por el contrario, durante el sueño No-REM en el cual prácticamente no hay actividad onírica, la potencia de estas frecuencias es baja (Cavelli *et al.*, 2015). Sin embargo, para que ocurra un estado de consciencia alerta (como durante la vigilia) es necesaria una integración de los eventos neurales que ocurren en diversas áreas de la corteza cerebral (Singer, 2006). Es por esto que durante la vigilia la coherencia de las oscilaciones rápidas (gamma y HFO) es alta, mientras que disminuye considerablemente durante el sueño REM (Melloni *et al.*, 2007; Cavelli *et al.*, 2017; Castro-Zaballa *et al.*, 2018; Cavelli *et al.*, 2018). Si bien varios estudios han analizado la potencia y coherencia del EEG durante el sueño y la vigilia, la mayoría se ha centrado en el análisis de algunas bandas de frecuencia determinadas sin evaluar el espectro completo (desde delta a HFO), sin determinar si existen diferencias entre distintas áreas cerebrales, o entre ambos hemisferios, así como tampoco la influencia del ciclo circadiano en las mismas. O a aquellos trabajos que sí lo han hecho, se han basado en una única de estas variables. (Vyazovskiy & Tobler, 2008; Cavelli *et al.*, 2015; Jing *et al.*, 2016; Cavelli *et al.*, 2017; Castro-Zaballa *et al.*, 2018; Cavelli

et al., 2018). La hipótesis de este trabajo fue que la potencia y coherencia del EEG para distintas bandas de frecuencia varía de acuerdo al estado comportamental, las áreas corticales y hemisferios y la fase de luz y oscuridad. Por lo tanto, el objetivo fue realizar un análisis sistemático y detallado del efecto del estado comportamental (vigilia, sueño No-REM y sueño REM), las áreas corticales (evaluando también la presencia de lateralización), y las fases de luz y oscuridad en la potencia y coherencia de las distintas bandas de frecuencia del EEG en la rata.

clocks & sleep

MDPI

Article

Power and Coherence in the EEG of the Rat: Impact of Behavioral States, Cortical Area, Lateralization and Light/Dark Phases

Alejandra Mondino [1,2], Matías Cavelli [1,3], Joaquín González [1], Lucía Osorio [1], Santiago Castro-Zaballa [1], Alicia Costa [1], Giancarlo Vanini [2] and Pablo Torterolo [1,*]

1 Laboratorio de Neurobiología del Sueño, Departamento de Fisiología, Facultad de Medicina, Universidad de la República, Av. Gral. Flores 2125, Montevideo 11800, Uruguay; a.monvero@gmail.com (A.M.); mat.cavelli@gmail.com (M.C.); joaqgonzar@gmail.com (J.G.); luos.mail@gmail.com (L.O.); sancaszab@gmail.com (S.C.-Z.); acosta@fmed.edu.uy (A.C.)
2 Department of Anesthesiology, University of Michigan, 7433 Medical Science Building 1, 1150 West Medical Center Drive, Ann Arbor, MI 48109-5615, USA; gvanini@umich.edu
3 Department of Psychiatry, University of Wisconsin, 6001 Research Park Blvd, Madison, WI 53719, USA
* Correspondence: ptortero@fmed.edu.uy

Received: 22 September 2020; Accepted: 3 December 2020; Published: 9 December 2020

Abstract: The sleep-wake cycle is constituted by three behavioral states: wakefulness (W), non-REM (NREM) and REM sleep. These states are associated with drastic changes in cognitive capacities, mostly determined by the function of the thalamo-cortical system, whose activity can be examined by means of intra-cranial electroencephalogram (iEEG). With the purpose to study in depth the basal activity of the iEEG in adult rats, we analyzed the spectral power and coherence of the iEEG during W and sleep in the paleocortex (olfactory bulb), and in neocortical areas. We also analyzed the laterality of the signals, as well as the influence of the light and dark phases. We found that the iEEG power and coherence of the whole spectrum were largely affected by behavioral states and highly dependent on the cortical areas recorded. We also determined that there are night/day differences in power and coherence during sleep, but not in W. Finally, we observed that, during REM sleep, intra-hemispheric coherence differs between right and left hemispheres. We conclude that the iEEG dynamics are highly dependent on the cortical area and behavioral states. Moreover, there are light/dark phases disparities in the iEEG during sleep, and intra-hemispheric connectivity differs between both hemispheres during REM sleep.

Keywords: sleep; REM; slow waves; oscillations; gamma; spindles

1. Introduction

The brain is a complex system, in which parallel processing coexists with serial operations within highly interconnected networks, but without a single coordinating center. This organ integrates neural events that occur at different times and locations into a unified perceptual experience [1,2]. Cognitive states are mostly determined by the function of the thalamo-cortical system [3]. Part of this neuronal processing can be accurately measured by intra-cranial electroencephalogram (iEEG) or electro-corticogram, which reduces artifacts from non-brain electrical activity, such as eye movement and muscle or electrode noise, and increases the quality of high frequency oscillations in comparison to standard surface electroencephalographic recordings (EEG) [4,5].

The sleep–wake cycle is a critical physiological process and one of the most preserved biological rhythms through evolution [6]. This cycle is composed of wakefulness (W), non-rapid eye movement (NREM) and rapid eye movement (REM) sleep states, that are distinguished by their behavior and

electrophysiological signatures, which can be captured by iEEG signals [3,7]. Accompanying these electro-cortical differences among states, the cognitive capacities drastically change during the cycle. Fundamentally, consciousness is lost during deep NREM sleep, and emerges in an altered fashion during REM sleep, when most vivid dreams occur [3,8].

One of the most-studied neural correlates of consciousness are the cortical EEG oscillations [9], which contain broad and complex frequency spectra that can be examined by means of the fast Fourier transform. The power of the different frequencies of these signals reflect the local degree of synchronization of the extracellular potential, which are deeply modified on passing from W to sleep [10,11]. The power of the frequency components of the iEEG is deeply modified on passing from W to sleep. While W and REM sleep contain high frequency activity together with theta waves (5–9 Hz) in the iEEG, during NREM sleep oscillations with slower frequencies (delta band, 0.5 to 4 Hz) and spindles (sigma band, 11 to 15 Hz) predominate [3,12–14].

Synchronization between oscillations from different areas represent another neural correlate of consciousness [15]. In this regard, the degree of iEEG coherence between two cortical regions reflects the strength of the functional interconnections (re-entries) that occur between them [16]. In other words, the spectral coherence analysis of the iEEG is a valid approach to infer cortical connectivity and communication between distant brain areas [17]. Siegel et al. (2012) proposed that frequency-specific correlated oscillations in distributed cortical networks provide indices or "fingerprints", of the network interactions that underlie cognitive processes [18]. During W, there is a larger coherence in gamma (35–100 Hz) and high frequency oscillations (HFO, up to 200 Hz) than during sleep [11,19–21]. A high degree of delta and sigma synchronization occurs during NREM sleep [22], while theta coherence is large during REM sleep in the rodent iEEG [21].

Although there are several studies that have analyzed the iEEG during W and sleep, most of them have not evaluated the whole spectrum of frequencies (from delta to HFO), the differences between brain areas, lateralization and the phases of the circadian cycle. Additionally, the ones that did, have focused in just one of these parameters without evaluating the effect of all of them [20,21,23–25]. Therefore, a detailed and systematic evaluation, that evaluates the impact of behavioral states, cortical area, lateralization and light/dark phases of power and coherence during behavioral states is still pending. Hence, the purpose of this study was to provide an examination of power and coherence of the basal iEEG activity of the adult rat during W and sleep. To this end, we studied the influence of the cortical site, employing electrodes located on the olfactory bulb (OB), frontal (primary motor or M1), parietal (primary somatosensory, S1) and occipital (secondary visual, V2) cortex, as well as the impact of laterality (differences in signals recorded in the right and left hemispheres) and the influence of dark and light phases. Upon considering this set of factors, we found important patterns of activity characterizing each sleep state along with state independent modulations of iEEG activity.

2. Results

Polysomnographic recordings, hypnogram and spectrogram (power spectrum as a function of time) during the light phase of a representative rat are displayed in Figure 1C,D. As it is exhibited in this figure, the quality of the recordings allowed for an optimal classification of W and sleep epochs.

2.1. Power Spectrum: Effect of Behavioral States and Recording Site

Figure 2 shows the absolute power spectra analysis of the iEEG during W and sleep for the OB and neocortical areas during the light (resting) phase for the right hemisphere. In order to improve the visualization of the power differences among states, in the figure we multiplied the power at each frequency by the frequency itself. It is readily observed that the spectrum is highly variable in function of behavioral states and electrode sites.

A

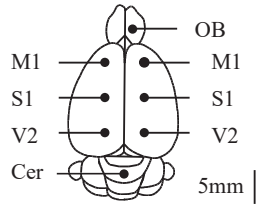

B

Electrode	Medio-lateral	Antero-posterior
rOB	+1.25 mm	+7.5 mm
rM1	+2.5 mm	+2.5 mm
lM1	-2.5 mm	+2.5 mm
rS1	+2.5 mm	-2.5 mm
lS1	-2.5 mm	-2.5 mm
rV2	+2.5 mm	-7.5 mm
lV2	-2.5 mm	-7.5 mm

C

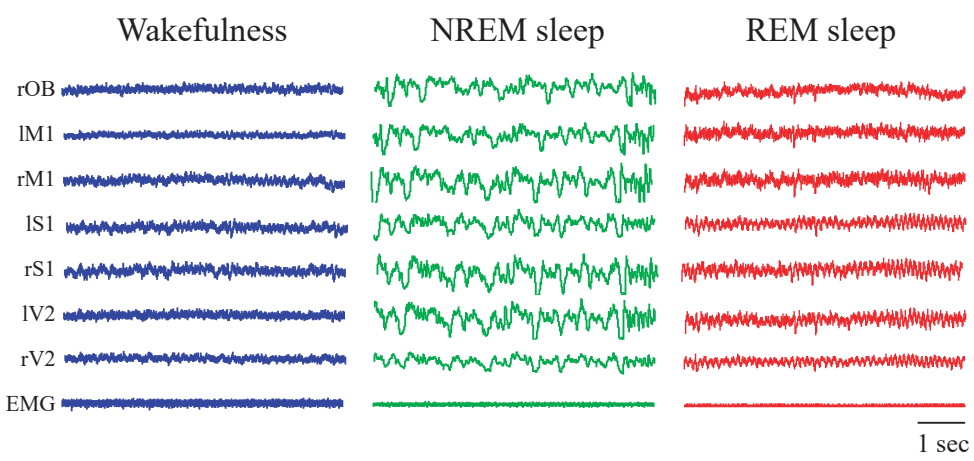

D

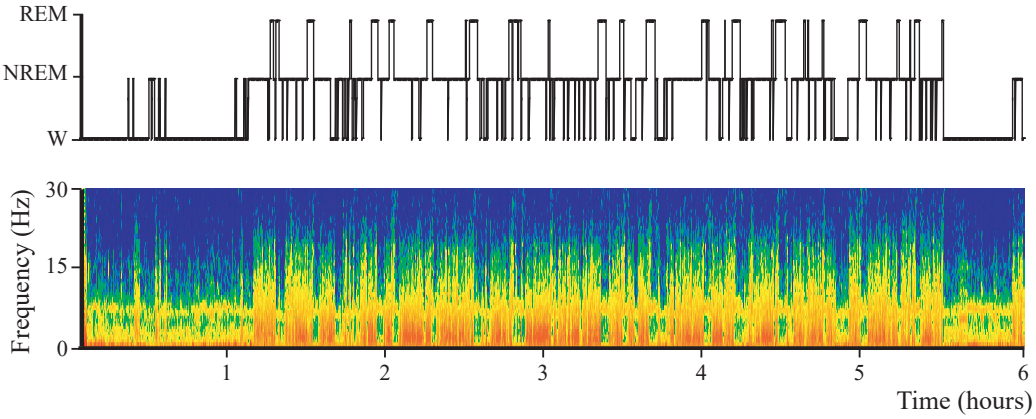

Figure 1. Sleep–wake states in the rat. (**A**) Schematic representation of the electrode position in the brain of the rat. (**B**) Electrodes' positions in reference to *Bregma* [26]. OB, olfactory bulb; M1, primary motor cortex; S1, primary somato-sensory cortex; V2, secondary visual cortex; r, right; l, left. (**C**) Representative iEEG and the neck electromyogram (EMG) recordings during wakefulness (W, blue), NREM (green), and REM sleep (red). From top to bottom, olfactory bulb (OBr), right and left primary motor (M1r/M1l), primary somatosensory (S1r/S1l), and secondary visual (V2r/V2l) cortices. (**D**) Hypnogram (top) according to visually scored behavioral states and spectrogram (0.1 to 30 Hz). During W and REM sleep, theta activity (5–9 Hz) in the spectrogram can be readily observed. During NREM sleep, delta activity (0.5 to 4 Hz) is more prominent and there are intermittent episodes of sigma activity (10–15 Hz) which corresponds to the presence of sleep spindles.

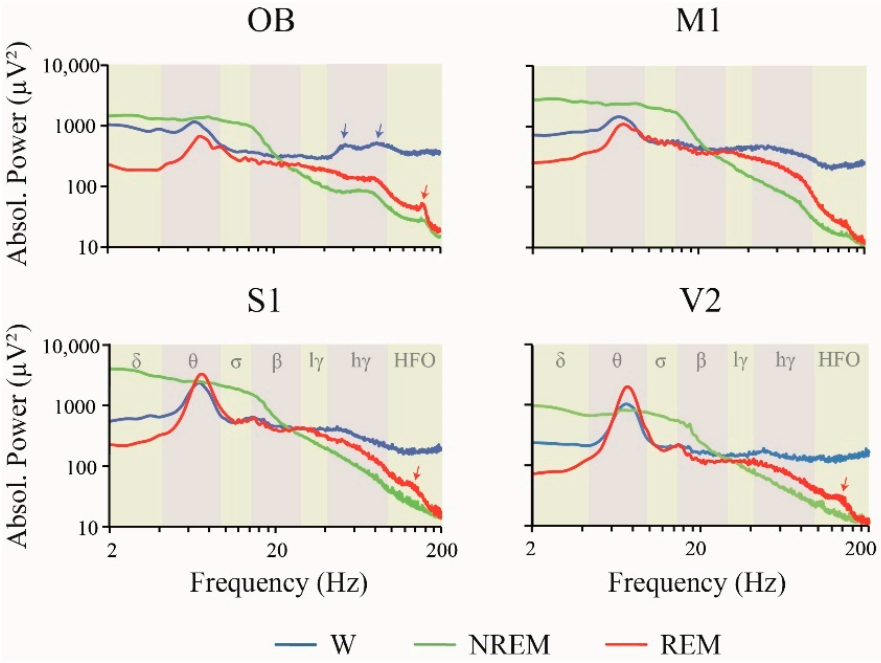

Figure 2. Power spectral profiles. Mean absolute power spectral profiles of the right hemisphere in wakefulness (W), NREM and REM sleep during the light period (n = 11). The frequency bands used for the statistical analysis are indicated by different colors in the background of the graphics. Blue arrows show two small deflections in the HG band during W and red arrows demonstrate a narrow peak in HFO at ≈130 Hz that can be appreciated during REM sleep in OB and somatosensory cortices. OB, olfactory bulb; M1, primary motor cortex; S1, primary somato-sensory cortex; V2, secondary visual cortex; W, wakefulness; r, right; l, left; lγ, low gamma or LG; hγ, high gamma or HG; HFO, high frequency oscillations.

The absolute power of all the frequency bands of the iEEG was affected by behavioral states, localization of electrodes and the interaction of both factors (Table 1). The exceptions were sigma, beta and low gamma (LG) that were not significantly affected by the interactions between behavioral states and electrode locations.

Table 1. Absolute power.

Frequency	Cortex				Behavioral State				Cortex × State			
	df	***p***	**F**	η_p^2	**df**	***p***	**F**	η_p^2	**df**	***p***	**F**	η_p^2
Delta	3, 30	0.0010	7.1	0.415	2, 20	<0.0001	25.0	0.714	6, 57	<0.0001	6.9	0.421
Theta	3, 30	0.0003	8.5	0.459	2, 20	0.0047	7.1	0.415	6, 57	0.0010	4.4	0.316
Sigma	3, 30	0.0003	8.5	0.459	2, 20	<0.0001	24.6	0.711	6, 57	0.0608	2.2	0.188
Beta	3, 30	<0.0001	12.6	0.557	2, 20	0.0488	3.5	0.259	6, 57	0.4312	1.0	0.095
LG	3, 30	0.0066	4.9	0.328	2, 20	0.0017	8.9	0.471	6, 57	0.5688	0.8	0.077
HG	3, 30	0.0001	9.8	0.495	2, 20	<0.0001	59.2	0.855	6, 57	<0.0001	15.5	0.620
HFO	3, 30	0.0002	9.0	0.474	2, 20	<0.0001	57.9	0.852	6, 57	0.0007	4.6	0.326

Statistical evaluation of the absolute spectral power in function of cortical regions, behavioral state, and interaction between both factors. Repeated mixed-effects model. df, degrees of freedom; η_p^2 partial eta squared; LG, low gamma; HG, high gamma; HFO, high frequency oscillations.

A summary of the power spectrum differences between W, NREM and REM sleep is shown in Figure 3 (statistics are shown in Supplementary Figure S1A). The most remarkable results are the following. Delta, theta and sigma power during NREM sleep were significantly higher than during W and REM sleep in M1 and S1. In the OB, delta was larger during NREM compared to REM sleep, while sigma was larger during NREM compared to the other states. LG, HG and HFO powers were higher during W than during NREM in all the cortical areas. Additionally, HG and HFO, during W,

was higher in comparison to REM sleep in most cortical areas. Finally, HG and LG power was also larger in REM sleep than in NREM sleep in M1, while in S1 this fact was observed only for LG.

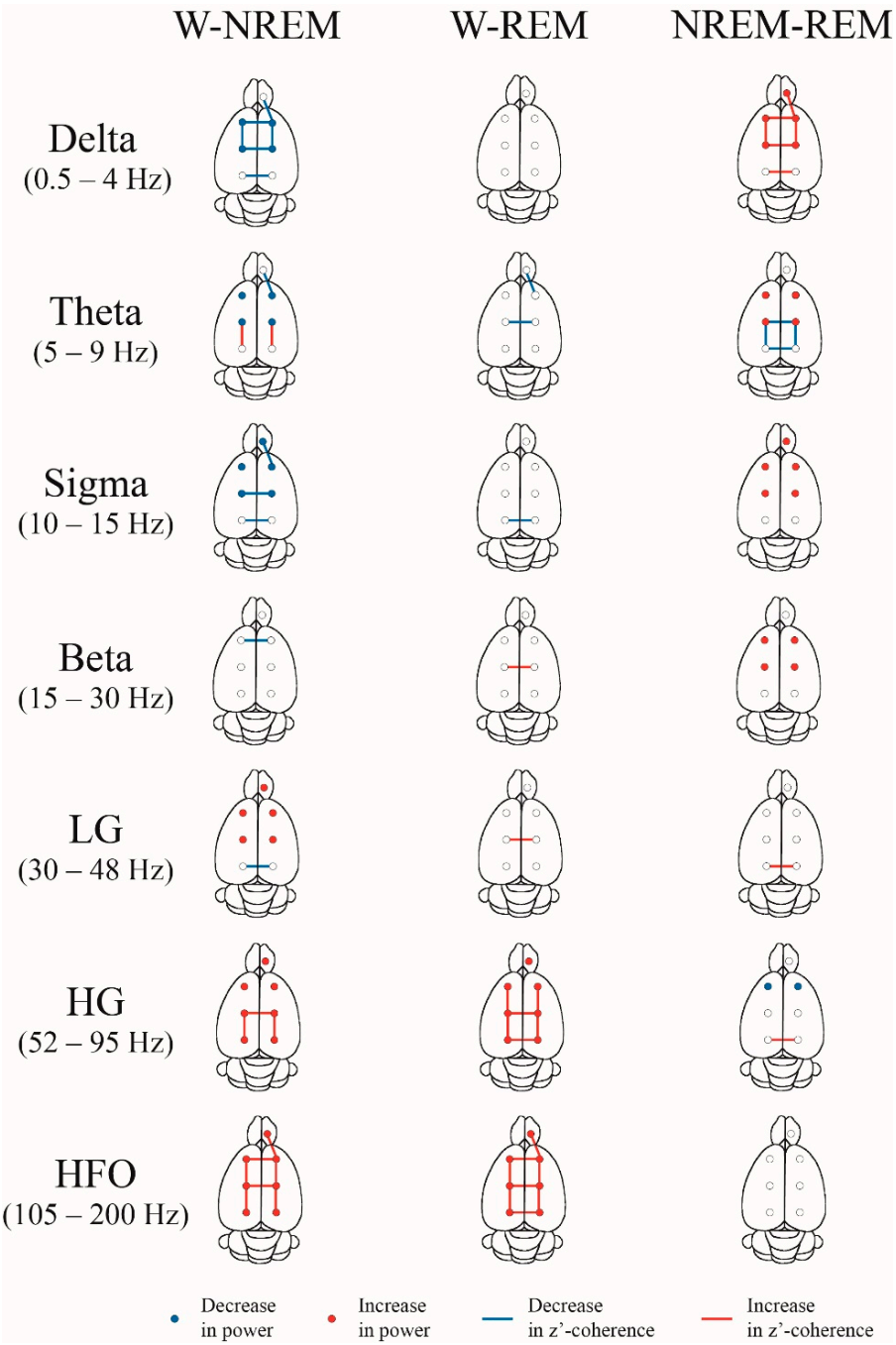

Figure 3. Summary of the power and z'-coherence. Statistically significant differences in absolute power and z'-coherence during wakefulness (W), NREM and REM sleep during the light phase. The circles represent the power for the different electrodes' positions, while the lines represent the coherence for the different derivations. The results were evaluated by means of repeated measures mixed-effects model and Sidak test for multiple comparisons (n = 11). Blue represents a significantly ($p < 0.05$) lower difference between two behavioral states, and red a significantly higher difference. Power data are from the right hemisphere but are represented as bilateral. The complete statistics of these data are shown in Supplementary Figures S1 and S8.

In Supplementary Figure S2, the same tracings of Figure 2 were re-plotted for a more precise comparison as a function of the electrode location; the statistics of these data are shown in Supplementary Figure S1B. However, it is important to consider that the variation in the absolute power in the function of the electrode site is dependent of the distance between the active and the referential electrode (cerebellum). In this regard, as shown in Supplementary Figure S3, the total power was highly modified as a function of the electrode site (total power was also affected by behavioral states and the interaction with electrode localization). Indeed, total power was the lowest in V2 (closer to the reference electrode) reaching significance during W and NREM sleep. Then, we judged it to be more adequate to explore the relative instead of the absolute power in the function of the electrode site (nevertheless, complete statistics of the absolute power in the function of the electrode site are also provided in Supplementary Figure S1B). The analysis of the relative power in the function of the electrode site is exhibited in Figure 4 and Tables 2 and 3 (the analysis of the relative power in the function of behavioral states is shown in Supplementary Figure S4).

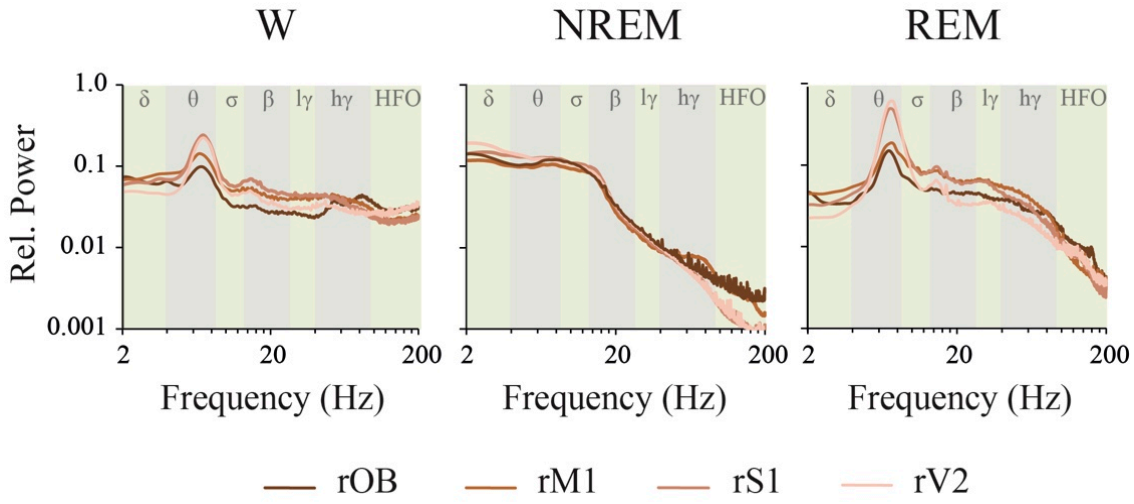

Figure 4. Relative power. Mean relative power profile of each behavioral state of the right hemisphere during the light period (n = 11). This approach removes the effect of the distance between the active and the referential electrode. The analyzed frequency bands are indicated by different colors in the background of the graphics. OB, olfactory bulb; M1, primary motor cortex; S1, primary somato-sensory cortex; V2, secondary visual cortex; W, wakefulness; r, right; l, left; lγ, low gamma or LG; hγ, high gamma or HG; HFO, high frequency oscillations.

Table 2. Relative power. Repeated measures mixed models

Frequency	Cortex				Behavioral State				Cortex × State			
	df	p	F	η_p^2	df	p	F	η_p^2	df	p	F	η_p^2
Delta	3, 30	0.5710	0.7	0.065	2, 20	<0.0001	41.4	0.805	6, 57	<0.0001	14.9	0.611
Theta	3, 30	<0.0001	35.7	0.781	2, 20	0.0009	10.2	0.504	6, 57	<0.0001	61.2	0.866
Sigma	3, 30	0.0005	8.0	0.444	2, 20	<0.0001	15.9	0.613	6, 57	0.2353	1.4	0.128
Beta	3, 30	0.0389	3.2	0.242	2, 20	0.0084	6.1	0.379	6, 57	0.0166	2.9	0.233
LG	3, 30	0.0544	2.8	0.219	2, 20	<0.0001	26.8	0.728	6, 57	<0.0001	4.4	0.316
HG	3, 30	0.0162	4.0	0.286	2, 20	<0.0001	22.5	0.692	6, 57	0.0213	2.7	0.221
HFO	3, 30	0.0052	5.2	0.342	2, 20	<0.0001	33.6	0.770	6, 57	0.1817	1.5	0.136

Statistical evaluation of the relative spectral power in function of the cortical region, behavioral state, and interaction between both factors. Repeated mixed-effects model.

Table 3. Relative power. Sidak multiple comparison test.

State	Comparison	Delta	Theta	Sigma	Beta	LG	HG	HFO
W	OB vs. M1	0.9621	0.8365	0.2279	0.7908	0.0485	0.9294	0.0334
	OB vs. S1	0.6436	0.0452	0.0613	0.0274	0.0494	0.0366	0.0014
	OB vs. V2	0.2194	0.1459	0.6616	0.7521	0.7853	0.0173	0.9786
	M1 vs. S1	0.9897	0.4926	0.9954	0.4594	>0.9999	0.3488	0.9120
	M1 vs. V2	0.7637	0.8360	0.9809	>0.9999	0.5783	0.2254	0.1934
	S1 vs. V2	0.9919	0.9958	0.7595	0.4585	0.5776	>0.9999	0.0137
NREM	OB vs. M1	0.6010	0.9957	0.2926	0.1330	>0.9999	0.9631	0.9925
	OB vs. S1	0.0054	<0.0001	>0.9999	0.9986	>0.9999	0.9711	0.9987
	OB vs. V2	0.8876	0.09998	0.9974	>0.9999	0.9998	0.9986	>0.9999
	M1 vs. S1	0.2591	<0.0001	0.4462	0.3735	>0.9999	>0.9999	>0.9999
	M1 vs. V2	0.9983	0.9957	0.6233	0.0928	0.9998	0.9994	0.9944
	S1 vs. V2	0.0970	<0.0001	0.9999	0.9931	>0.9999	0.9996	0.9991
REM	OB vs. M1	0.9979	0.7428	0.0018	0.0698	0.0872	>0.9999	0.2567
	OB vs. S1	0.5279	<0.0001	0.0318	0.0130	>0.9999	0.1355	0.4773
	OB vs. V2	0.2539	<0.0001	0.9989	0.6463	0.0977	0.0106	0.4965
	M1 vs. S1	0.8384	0.0001	0.9651	0.9854	0.1181	0.0787	0.9999
	M1 vs. V2	0.5548	<0.0001	0.0072	0.8287	<0.0001	0.0051	0.9993
	S1 vs. V2	0.9994	0.3830	0.0930	0.3875	0.1020	0.9561	>0.9999

p-values of the Sidak multiple comparisons test, comparing the differences in the relative power between the different cortical region of the right hemisphere. OB, olfactory bulb; M1, primary motor cortex; S1, primary somato-sensory cortex; V2, secondary visual cortex; df, degrees of freedom; η_p^2 partial eta squared, W, wakefulness; LG, low gamma; HG, high gamma; HFO, high frequency oscillations.

The most remarkable differences in the relative power between the brain regions were noticed during REM sleep, where V2 and S1 theta power was greater than in OB and M1. Another interesting finding was that LG and HG in M1 were higher than in V2. During NREM sleep, S1 power was higher than OB for the delta frequency band, and larger than OB and M1 for the theta band. On the other hand, the power in the OB was lower than M1 and S1 for LG, but became higher for HG and HFO during W.

2.2. Power Spectrum: Light vs. Dark Phases

Next, we examined the effects of the light/dark phases on the iEEG oscillatory activity for the right hemisphere. To simplify, we only show the significant results, while the non-significant effects are shown in the Supplementary Material. Figure 5 shows the light/dark predominance (see the procedure in the figure legend; the same approach was used to show the data in the following figures). We can readily observe that the classic frequency bands show significant differences only during NREM sleep; beta and LG power were larger during the dark than during the light phase in M1. Employing a more precise evaluation using the empirical cluster analysis, we determined that during NREM sleep in M1 clusters of frequencies that include sigma, beta, LG, HG and HFO bands were larger in the dark phase. A cluster of frequencies within the HFO band also increased during the dark phase in the OB during this behavioral state. Regarding REM sleep, although no changes were found in the classical frequency bands, we found a specific cluster within theta frequency band which was higher during the day than during the night in V2.

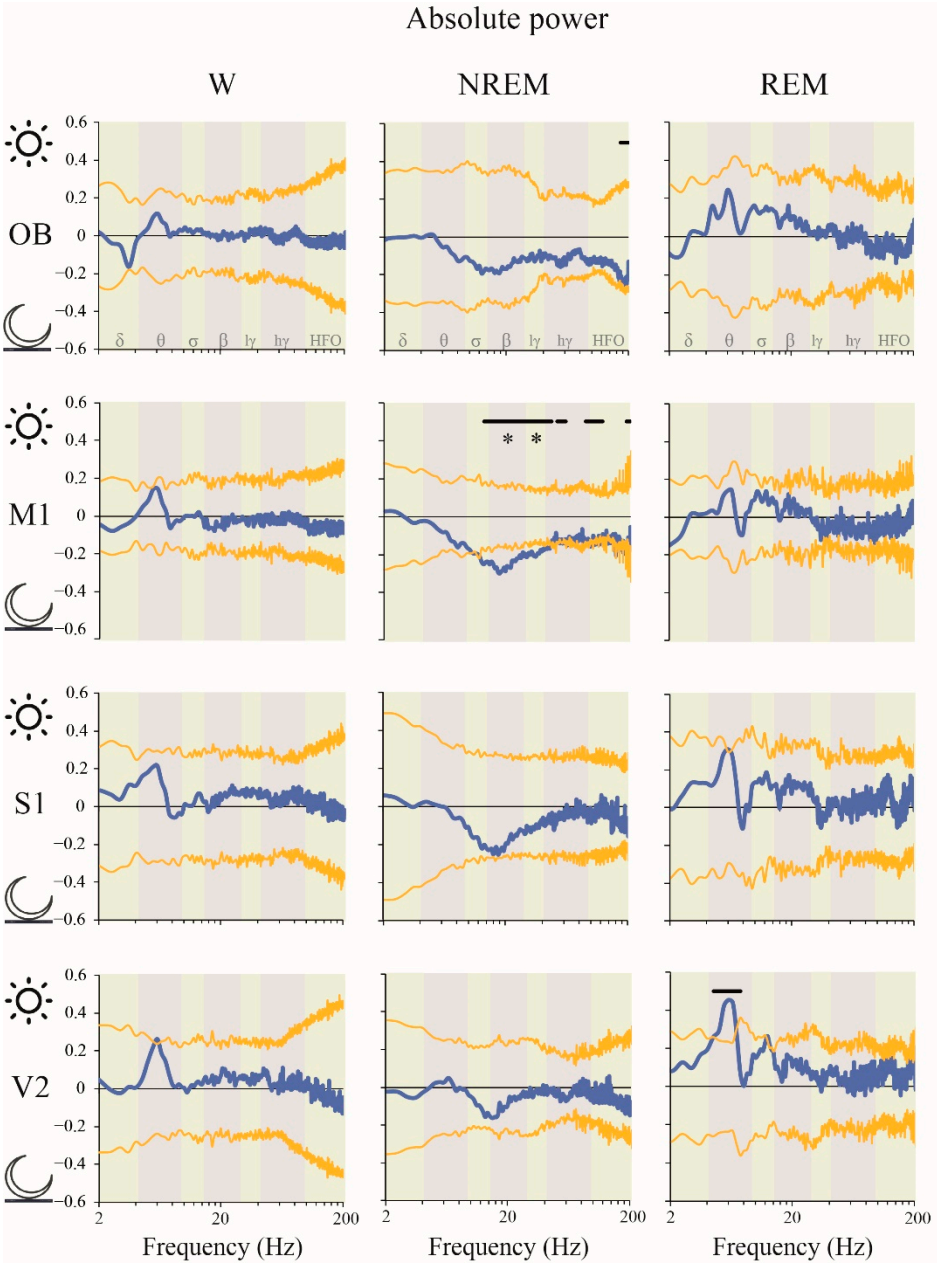

Figure 5. Absolute power: light vs. dark phase differences. The blue traces indicate the mean power difference between light and dark phases. The yellow lines represent the standard deviation of the mean with respect to zero. The statistical evaluation was performed by the two-tailed paired *t*-test with Bonferroni correction for multiple comparisons; * indicates significant differences, $p < 0.0071$ ($n = 11$). We also performed a data-driven approach comparing empirical clusters of frequencies; black lines represent statistical differences in cluster of frequencies, $p < 0.05$. In M1 the following frequency clusters were significantly larger during NREM sleep in the dark phase: 13 to 46 Hz ($p = 0.001$), 51 to 60.5 Hz ($p = 0.016$), 87 to 92 Hz ($p = 0.038$), 93.5 to 100 Hz ($p = 0.025$), 101 to 111 Hz ($p = 0.012$), 112.5 to 119.5 Hz ($p = 0.024$), 124 to 125.5 Hz ($p = 0.047$), 186.5 to 192 Hz ($p = 0.036$) and 193 to 200 Hz ($p = 0.029$). In the OB during NREM sleep, the power of the frequencies 171.5 to 187.5 and 188.5 to 199.5 Hz were larger during the night ($p = 0.018$ and $p = 0.047$, respectively). During REM sleep, the cluster 4.5 to 7.5 Hz was higher during the day than during the night in V2 ($p = 0.038$). The analysis was performed for the right hemisphere. OB, olfactory bulb; M1, primary motor cortex; S1, primary somato-sensory cortex; V2, secondary visual cortex; lγ, low gamma or LG; hγ, high gamma or HG; HFO, high frequency oscillations.

2.3. Power Spectrum: Right vs. Left Hemispheres

iEEG absolute power laterality was analyzed for both the light (Supplementary Figure S5) and dark (Supplementary Figure S6) phases. Neither *t*-test evaluation of classical frequency bands nor cluster analysis showed statistical differences between right and left hemispheres, either during W or sleep.

2.4. Coherence: Effects of Behavioral States and Derivations

The z'-coherence during W, NREM and REM sleep for the right intra-hemispheric and the inter-hemispheric combination of adjacent electrodes during the light period is shown in Figure 6. In Supplementary Figure S7, the data were re-plotted in order to appreciate the differences in function of the derivations. The statistical results of the repeated measures mixed-effects model are shown in Table 4. Interestingly, no significant differences in z'-coherence were observed in the function of the derivation, except for delta and theta bands. However, behavioral states and the interaction between localization and behavioral states modified z'-coherence in all the frequency bands (Table 4).

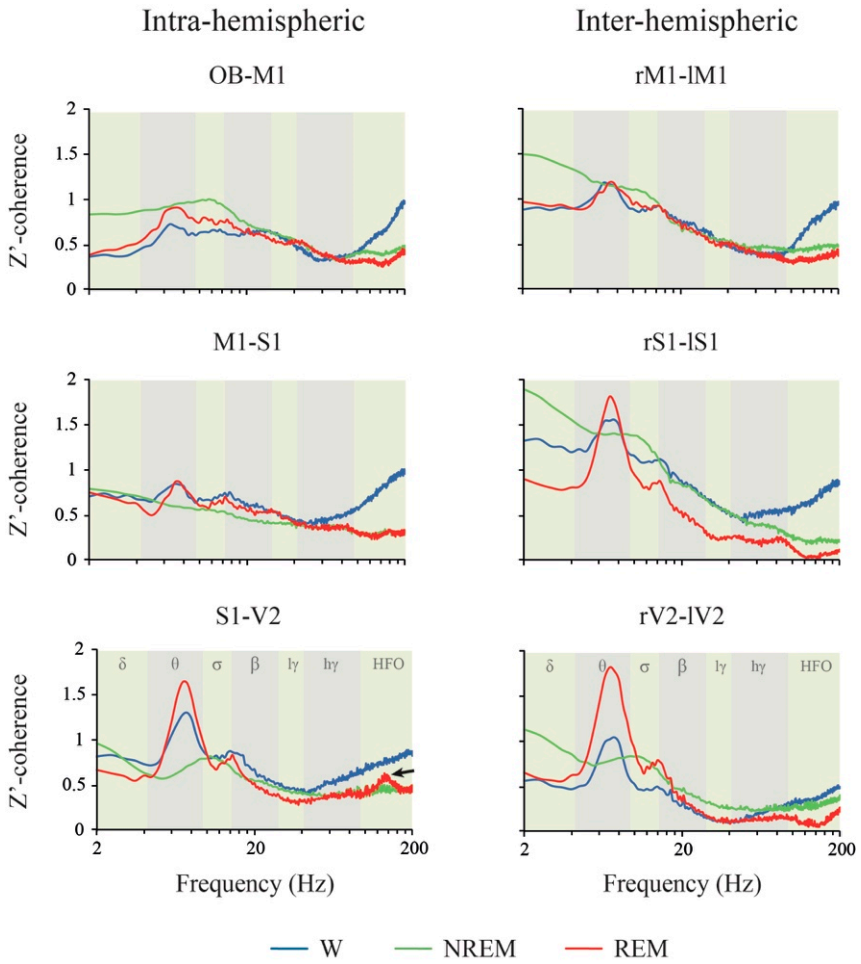

Figure 6. Z'-coherence. Mean z'-coherence profile of the inter-hemispheric and intra-hemispheric derivations (between adjacent areas) during wakefulness (W), NREM and REM sleep in the light phase (n = 11). The analyzed frequency bands are indicated by different colors in the background of the graphics. OB, olfactory bulb; M1, primary motor cortex; S1, primary somato-sensory cortex; V2, secondary visual cortex; r, right; l, left; lγ, low gamma or LG; hγ, high gamma or HG; HFO, high frequency oscillations.

Table 4. Z′-coherence.

Frequency	Derivation				Behavioral State				Derivation × State			
	df	*p*	F	η_p^2	df	*p*	F	η_p^2	df	*p*	F	η_p^2
Delta	5, 50	0.0411	2.5	0.200	2, 20	<0.0001	23.1	0.698	10, 82	0.0121	2.5	0.233
Theta	5, 50	0.0423	2.5	0.200	2, 20	0.0015	9.2	0.479	10, 82	<0.0001	10.7	0.566
Sigma	5, 50	0.1992	1.5	0.130	2, 20	0.0221	4.6	0.315	10, 82	0.0018	3.2	0.280
Beta	5, 50	0.3609	1.86	0.157	2, 20	0.0356	3.9	0.280	10, 82	0.0129	2.4	0.226
LG	5, 50	0.3687	1.1	0.099	2, 20	0.0058	6.7	0.401	10, 82	0.0094	2.6	0.240
HG	5, 50	0.2258	1.4	0.123	2, 20	0.0004	11.7	0.539	10, 82	<0.0001	4.3	0.344
HFO	5, 50	0.0600	2.3	0.187	2, 20	<0.0001	32.1	0.762	10, 82	<0.0001	5.5	0.401

Statistical evaluation of the z′-coherence in function of the derivation, behavioral state, and interaction between both factors. Repeated measures mixed-effects model. df, degrees of freedom; η_p^2 partial eta squared; LG, low gamma; HG, high gamma; HFO, high frequency oscillations.

The spectral z′-coherence of each of the frequency band differences between W, NREM and REM sleep for each electrode combination is also shown in Figure 3; the p values for each comparison are shown in Supplementary Figure S8. The most important results are the following. Delta z′-coherence during NREM sleep was larger than during the other behavioral states in most derivations. Moreover, sigma z′-coherence had higher values during NREM than W in the intra-hemispheric combination OB-M1 and the inter-hemispheric motor and somatosensory cortices. Theta z′-coherence increases during REM sleep in comparison to NREM sleep in the posterior intra and inter-hemispheric combination of electrodes. HG and HFO intra and inter-hemispheric z′-coherence was larger during W compared to REM and NREM sleep in most derivations. Additionally, visual inter-hemispheric LG and HG z′-coherence were lower during REM sleep compared to NREM sleep.

When comparing z′-coherence in the function of the derivation, we could detect very few differences during W and sleep, and in most of the cases, this included differences between intra and inter-hemispheric derivations (Supplementary Figure S9). Therefore, we analyzed the differences between the average inter-hemispheric (right and left M1, S1 and V2 derivations) and intra-hemispheric z′-coherences (OB-M1, M1-S1 and S1-V2 derivations) during W and sleep (Figure 7). We found a significant effect of the interaction between the behavioral state and the derivation type for delta ($F_{(2,14)} = 4.7$, $p = 0.028$, $\eta_p^2 = 0.402$) and HFO bands ($F_{(2,14)} = 3.8$, $p = 0.048$, $\eta_p^2 = 0.351$). During NREM sleep, delta inter-hemispheric was higher than the intra-hemispheric z′-coherence ($p = 0.046$). In contrast, during REM sleep, HFO intra-hemispheric was larger than the inter-hemispheric z′-coherence ($p = 0.038$).

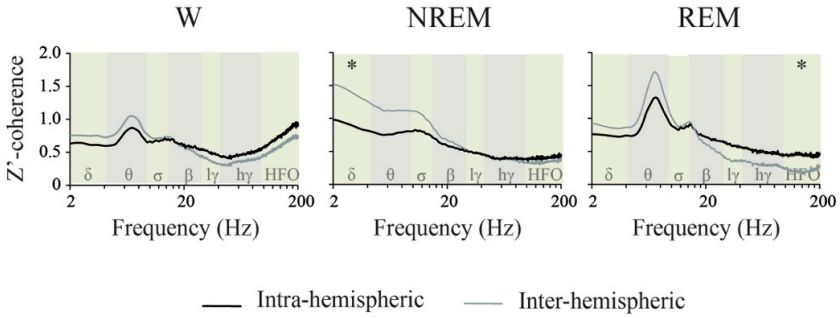

Figure 7. Z′-coherence differences between intra- and inter-hemispheric derivations. z′-coherence profile of the mean intra-hemispheric (OB-M1, M1-S1 and S1-V2) and inter-hemispheric (right–left M1, S1, V2) derivations during wakefulness (W), NREM and REM sleep in the light phase ($n = 11$). The analyzed frequency bands are indicated by different colors in the background of the graphics. OB, olfactory bulb; M1, primary motor cortex; S1, primary somato-sensory cortex; V2, secondary visual cortex; r, right; l, left; lγ, low gamma or LG; hγ, high gamma or HG; HFO, high frequency oscillations. Asterisks indicate significant differences, $p < 0.05$. M1, primary motor cortex; S1, primary somato-sensory cortex; V2, secondary visual cortex; lγ, low gamma or LG; hγ, high gamma or HG; HFO, high frequency oscillations.

2.5. Coherence: Light vs. Dark Phases

The influence of light/dark phases on z'-coherence was also analyzed. There were no significant differences for the classical frequency bands either for inter (Figure 8) or intra-hemispheric (Figure 9) z'-coherence between the dark and light phases during either W or NREM sleep. However, during REM sleep, inter-hemispheric S1 z'-coherence was higher in the dark phase for two clusters of frequencies: 8.5 to 10.5 Hz and 14 to 18.5 Hz (Figure 8). Moreover, REM sleep intra-hemispheric S1-V2 z'-coherence was higher during the light phase for the cluster 173–200 Hz (Figure 9).

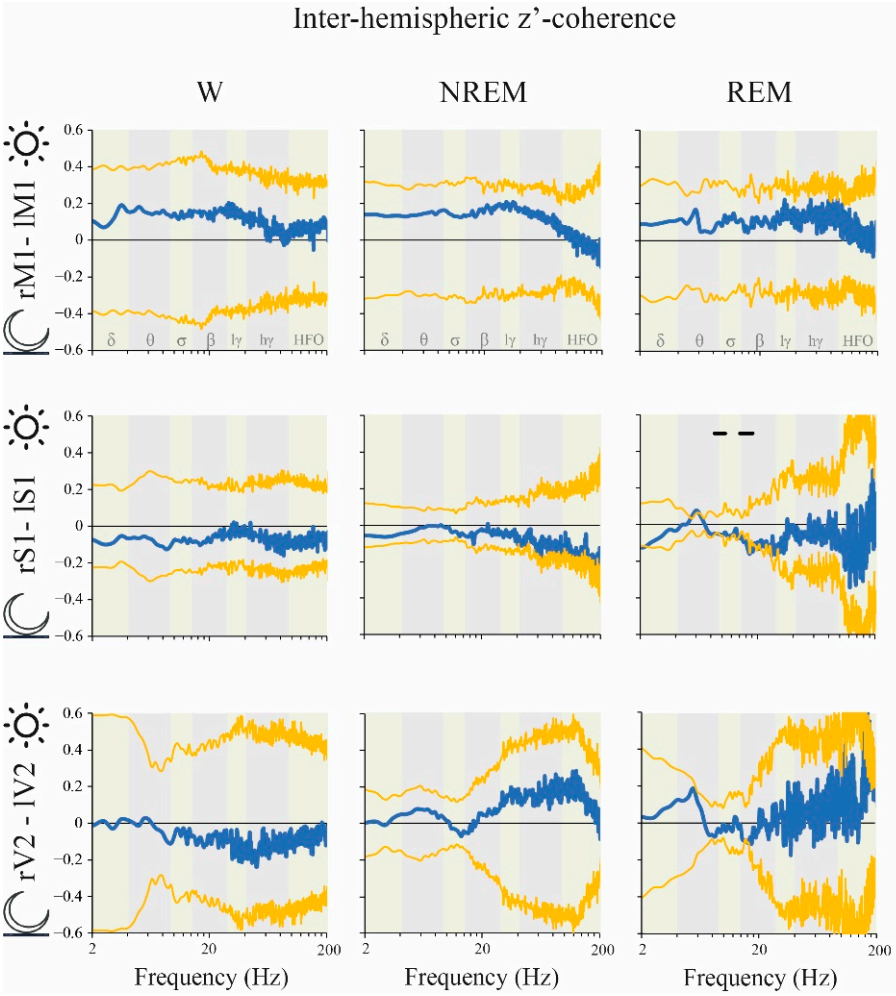

Figure 8. Inter-hemispheric z'-coherence: light vs. dark phases differences. (n = 11). The blue traces indicate the mean coherence difference between light and dark phases. The yellow lines represent the standard deviation of the mean with respect to zero. The statistical evaluation was performed by the two-tailed paired t-test with Bonferroni correction for multiple comparisons; no significant differences were observed. We also performed a data-driven approach comparing empirical clusters of frequencies; black lines represent statistical differences in cluster of frequencies, $p < 0.05$. During REM sleep, inter-hemispheric S1 z'-coherence was higher during the dark phase for the clusters 8.5 to 10.5 Hz (p = 0.008) and 14 to 18.5 Hz (p = 0.005). M1, primary motor cortex; S1, primary somato-sensory cortex; V2, secondary visual cortex; r, right; l, left; lγ, low gamma or LG; hγ, high gamma or HG; HFO, high frequency oscillations.

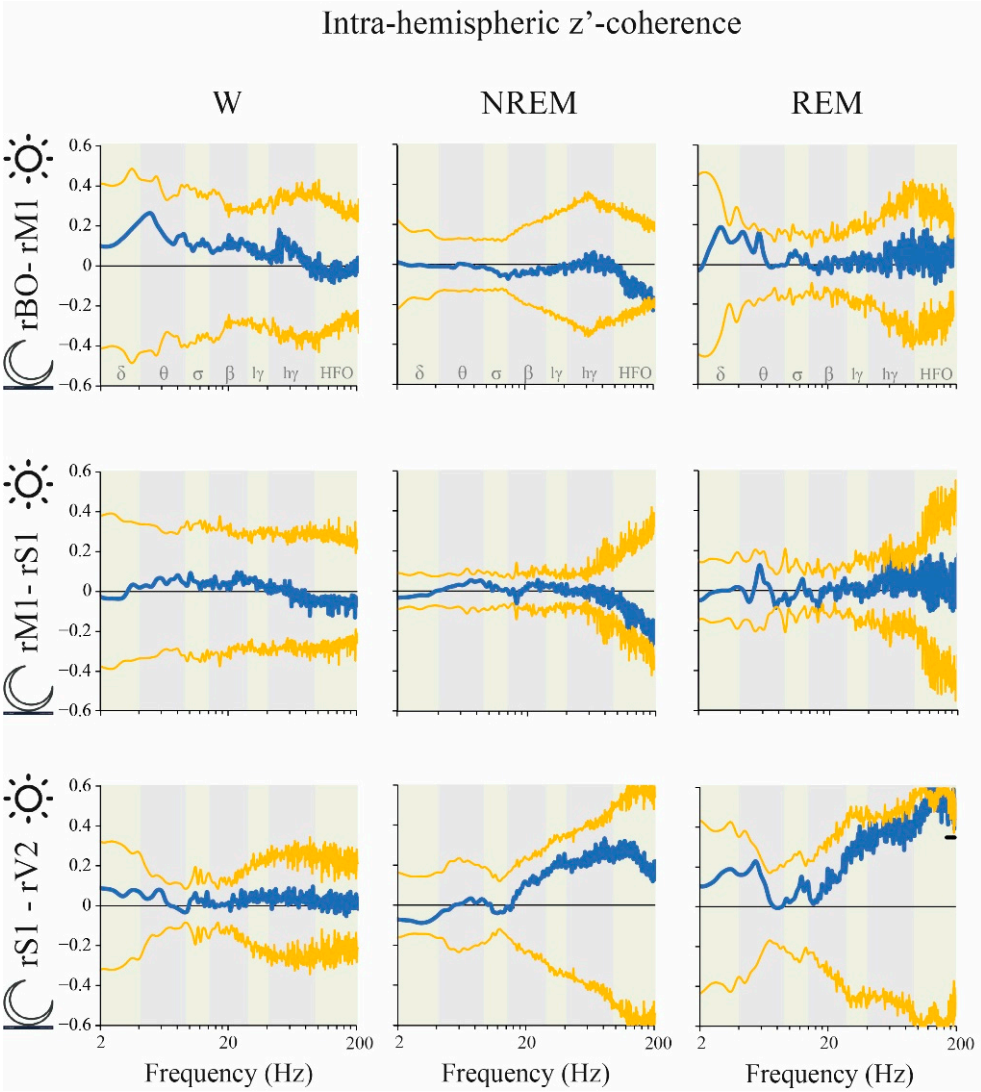

Figure 9. Intra-hemispheric z'-coherence: light vs. dark phases differences. The blue traces indicate the mean z'-coherence difference between light and dark phases. The yellow lines represent the standard deviation of the mean with respect to zero. The statistical evaluation was performed by the two-tailed paired *t*-test with Bonferroni correction for multiple comparisons; no significant differences were observed ($n = 11$). We also performed a data-driven approach comparing empirical clusters of frequencies; black lines represent statistical differences in cluster of frequencies, $p < 0.05$. During REM sleep, intra-hemispheric S1-V2 z'-coherence was higher during the light phase for the cluster 173–200 Hz ($p = 0.005$). OB, olfactory bulb; M1, primary motor cortex; S1, primary somato-sensory cortex; V2, secondary visual cortex; r, right; lγ, low gamma or LG; hγ, high gamma or HG; HFO, high frequency oscillations.

2.6. Coherence: Right vs. Left Hemispheres

Neither *t*-test analysis of classical bands nor cluster analysis showed intra-hemispheric z'-coherence differences between right and left hemispheres during the light phase (Supplementary Figure S11).

During the dark phase, a cluster circumscribed mainly within the theta band in S1-V2 derivation was higher in the right hemisphere during REM sleep. In contrast, clusters of frequencies within LG, HG and HFO were higher in the left hemisphere (Figure 10).

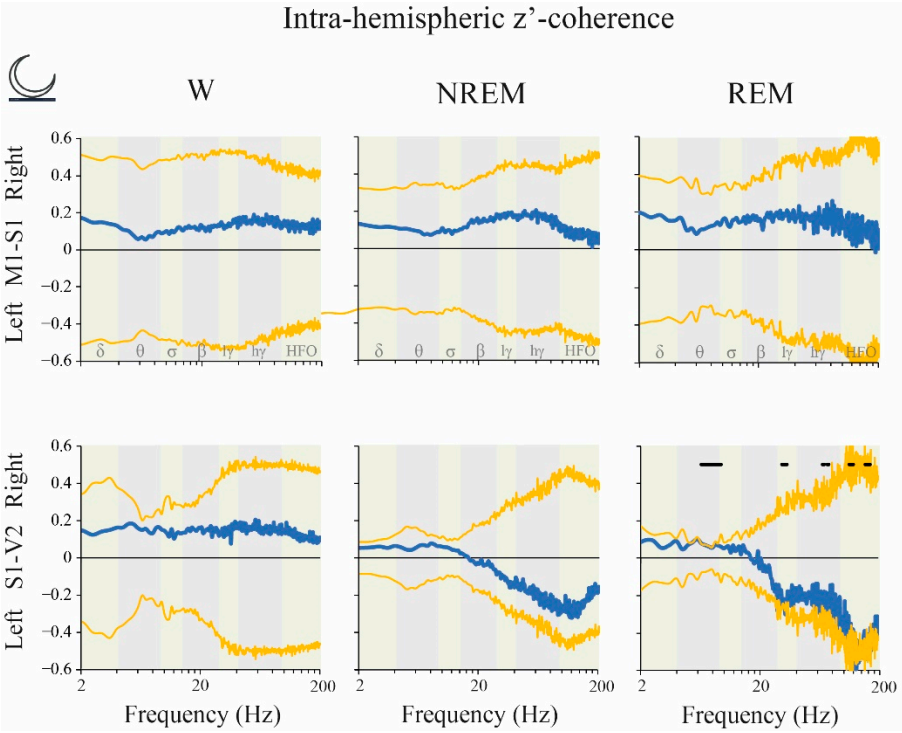

Figure 10. Intra-hemispheric z'-coherence: right vs. left hemispheric difference during the dark phase. The blue traces indicate the mean z'-coherence difference between light and dark phases. The yellow lines represent the standard deviation of the mean with respect to zero. The statistical evaluation was performed by the two-tailed paired *t*-test with Bonferroni correction for multiple comparisons; no significant differences were observed ($n = 11$). We also performed a data-driven approach comparing empirical clusters of frequencies; black lines represent statistical differences in cluster of frequencies, $p < 0.05$. Coherence was higher in the right hemisphere for the cluster between 6.5 to 9.5 Hz ($p = 0.0009$) during REM sleep. In contrast, the clusters between 31 to 34 Hz ($p = 0.022$), 68 to 70 ($p = 0.042$), 74.5 to 76.5 ($p = 0.048$), 114 to 117 ($p = 0.027$), 118 to 123 Hz ($p = 0.015$), 124 to 151.5 ($p = 0.001$), 155.5 to 164 ($p = 0.008$) and 165 to 170 Hz ($p = 0.017$) were higher in the left hemisphere for the same behavioral state. M1, primary motor cortex; S1, primary somato-sensory cortex; V2, secondary visual cortex; lγ, low gamma or LG; hγ, high gamma or HG; HFO, high frequency oscillations.

3. Discussion

In the present study, we performed a comprehensive analysis of the power and coherence of the iEEG signal of the rat, as well as the impact of behavioral states, cortical areas, laterality (differences between hemispheres) and light/dark phases. iEEG power and coherence were largely affected by behavioral states and recording sites. On the contrary, the influence of the light/dark phases was detected only during sleep. Finally, while we did not find right/left differences in power either in W or sleep, we observed that intra and inter-hemispheric coherence differs between both hemispheres during REM sleep.

3.1. Technical Considerations

We performed monopolar recordings (referenced to the cerebellum) utilizing screws (1 mm diameter) in contact with the dura mater as recording electrodes. With this recording design, we observed an important impact of the cortical site. However, as mentioned in the Results Section, the absolute power is highly dependent on the distance between the recording and reference electrodes. In order to discern the relative weight of the power of specific frequency bands in each channel, we also computed the relative power (absolute individual frequencies power normalized by total power). Hence, although complete analyses are provided in the Supplementary Data, in the description of the

result, we did not focus on the absolute power as a function of the cortical area or in the total power. In other words, we emphasized the absolute power in the function of behavioral states, and the relative power in the function of the electrode site.

However, it is important to note that total power in OB is lower than in M1 and S1 during NREM sleep (Supplementary Figure S3); this result is not an artifact of the electrode separation (that is the longest in this case), suggesting that the amplitude of the slow waves during NREM sleep in the paleocortex is lower than in the neocortex.

The present as well as most of the studies that analyzed the iEEG spectrum focus on "classical" or "standard" frequency bands, that are associated with behavioral states and cognitive functions [11,19,21,27–29]. Nevertheless, the effect of different variables such as moment of the day and laterality on power and coherence could be circumscribed to only a subset of frequencies within a "classical" band or could include changes that extend over these band limits. In these cases, smaller changes could remain undetected when analyzing a whole "classical" frequency band [30]. Because of this, for day/night and laterality analyses, we also performed the result-driven analysis of clusters of frequencies. This methodology allowed us to unveil changes in the iEEG power that not coincide exactly with "standard" or "classical" frequency bands.

3.2. iEEG Power

During W, gamma and HFO power reached the maximal level [20,21]; however, although in our analysis we eliminated the epochs with movements artifacts, we cannot rule out the possibility that part of the signal corresponds to muscle activity contamination that reaches cortical electrodes through volume conduction. Interestingly, in the OB, two small deflections in the HG band during W (signaled by blue arrows in Figure 2) are readily observed. Gamma oscillations in the OB have been known since the pioneering study of Adrian (1942) [31]; these oscillations are in phase with the respiratory potentials and significantly increase during active exploration [32,33]. In accordance with this, we found that HG power was higher in the OB during W than during sleep.

NREM sleep was characterized by a higher power spectrum profile, associated with large absolute and relative power values in slow frequency bands (delta, theta and sigma), that can be observed throughout the cortex (Figure 2 and Tables 2 and 3). A remarkable change in the slope is readily observed at lower frequency bins of the beta band; from this point, there is a marked and constant decrease in power as a function of the frequency. As mentioned in the Introduction, delta (and low theta) is related to the cortical and thalamic slow oscillations, while sigma power is related to sleep spindles; both electrographic features that characterize NREM sleep. As expected, delta and sigma band power during NREM were larger than during W and REM sleep in most of the cortical areas. Furthermore, we found that absolute theta power was higher in NREM than in W and REM sleep in the motor and somatosensory cortices. Hence, even if W and REM sleep exhibit a clear peak at ≈7 Hz in posterior areas, and the relative theta rhythm predominates over other frequency bands, the absolute theta power (considering the whole band) is not as high as in NREM sleep.

During REM sleep, the relative weight of the theta band is highlighted with the analysis of the relative power (Tables 2 and 3). The main origin of theta rhythm is in the hippocampus; this hippocampal theta rhythm modulates cortical neuronal activity [14,21,34,35]. A prominent peak in theta and relatively large power in gamma and HFO (larger than during NREM sleep) characterize REM sleep [21]. In fact, in the present study, we found that HG power was higher during REM than during NREM sleep in the motor cortex. Additionally, as described before [21], a narrow peak in HFO at ≈130 Hz can be appreciated during REM sleep in the OB and sensory cortices (signaled with red arrows in Figure 2). HFO is implicated in sensory processing [36], and a recent study suggests that the OB is a source of HFO [37]. However, HFO power was not significantly different between NREM and REM sleep, probably because the set of frequencies involved in the peak is much narrower than the whole HFO band.

3.3. iEEG Coherence

The spectral coherence is a tool to examine the functional interactions between different cortices as a function of the frequency [19,38]. In accordance with previous studies [19–21], during W, large values of intra and inter-hemispheric coherence were observed for high frequencies (HG and HFO) in almost all the derivations. Hence, during W, both gamma and HFO power (that reflects local synchronization) and coherence (that suggest synchronization between areas) are high.

During NREM sleep, delta coherence was higher than during W and REM sleep; thus, large delta power and coherence characterize NREM sleep. However, Pal et al. (2016) [39] found that, during NREM, there was a reduction in the cortico-cortical delta coherence in comparison to W. Of note is that these authors used the mean global coherence (an average of the coherence for the individual channel pairs), and they only evaluated the inter-hemispheric combination of electrodes. It was interesting that delta coherence was larger in homologous inter-hemispheric than in intra-hemispheric derivations (Figure 7); this fact was also demonstrated in humans [22].

Similar to our previous report [21], we found that REM sleep is characterized by large theta coherence, especially between visual and/or somatosensory electrodes. Another valuable issue is that HG and HFO coherence during REM sleep is lower than in W. Similar results have been described in rats [20,39]. Additionally in cats, there are very low gamma coherence values (both LG and HG) during REM sleep [19,27]. In accordance with Cavelli et al. (2018) [21], HFO coherence for intra-hemispheric posterior (S1-V2, sensory) derivations has a clear "peak" during REM sleep (indicated by a black arrow in Figure 6); this peak did not reach statistical significance in comparison to NREM sleep when we analyzed the whole HFO band. In spite of this, it is important to note that HFO intra-hemispheric z'-coherence was significantly higher than inter-hemispheric coherence during REM sleep (Figure 7).

3.4. Impact of the Light/Dark Phases

In the present report, we analyzed the iEEG during the subjective day (9 a.m. to 3 p.m.) and compared it with the subjective night (9 p.m. to 3 a.m.); the lights were on from 6 a.m. to 6 p.m. Hence, we evaluated the average of 6 h periods of the light/dark phases in the middle of these phases. In other words, the 3 h at the beginning and at the end of the phases, that should be more unsteady, were not analyzed. This is important to take it into account because previous studies showed an important modification in the hour-to-hour iEEG oscillations [40,41].

Albino rats have short sleep cycles (on average ≈11 min) and are more active during the dark phase; i.e., light phase is their main resting period [42–44]. Interestingly, during REM sleep, there was a clear predominance of theta power (≈5–7 Hz) in the light phase (Figure 5); this effect reached the maximum in V2, and it was statistically significant between 4.5 to 7.5 Hz. This predominance during the light phase could be explained by more consolidated REM sleep in the resting phase. In contrast, during NREM sleep, high frequency powers of the iEEG were skewed toward the dark phase (Figure 5). These phenomena could be related to a shallow NREM sleep during the active phase.

To the best of our knowledge, the light/dark phases differences in the iEEG spectral coherence were not studied before. Cluster analysis revealed that there were light/dark phase differences, but only during REM sleep. We found a dark phase predominance within theta, sigma and beta bands in S1 inter-hemispheric derivation (Figure 7). In contrast, there was a light phase predominance for frequencies higher than 173 Hz in S1-V2 intra-hemispheric derivation during this behavioral state (Figure 8). The functional meaning of these day/night differences in electro-cortical coherence confined just to REM sleep is unknown, but may be related to the circadian strength of the cognitive function executed during this behavioral state, such as memory processing [45,46].

3.5. Right/Left Hemispheric Differences in Electro-Cortical Activity

There were no differences between the right/left hemispheres' iEEG power either during light or dark phases during W. Vyazovskiy and Tobler (2008) [24] described iEEG laterality at 4.5–6.0 Hz during a hand preference task; however, as in our results, the authors did not find differences in naïve animals.

During NREM sleep, Vyazovskiy et al. (2002) [41] showed a left-hemispheric predominance of low-frequency power in the parietal cortex at the beginning of the light period, when sleep pressure is high. The left-hemispheric dominance changed to a right-hemispheric dominance in the course of the resting phase when sleep pressure dissipated. Additionally, during recovery from sleep deprivation, parietal left-hemispheric predominance was enhanced. We did not see hemispheric laterality in any frequency band, probably because we did not record the first 3 h of the light phase, which seems to be the time where laterality is mostly developed.

During REM sleep, right-hemispheric predominance in the theta band power was elucidated [41]. Although, no significant differences were observed, in accordance with these authors, there was a clear tendency for right predominance in the theta band power in M1 and S1 during REM sleep, both during light and dark phases (Supplementary Figures S5 and S6).

We did not find previous reports that compared the effect of laterality in the iEEG coherence in rodents; however, changes in iEEG coherence during W have been shown in humans in relation to their skilled hand [47]. In the present report, right/left significant differences in coherence were found only during REM sleep in the dark phase (Figure 10). We found a right predominance of frequencies within the theta range in S1-V2 derivation, and a left predominance for clusters within the gamma and HFO bands. New experimental approaches are needed to explain these differences between both hemispheres.

4. Materials and Methods

4.1. Experimental Animals

Eleven Wistar male adult rats (270–300 g) were used for this study. The number of animals was selected based on previous studies [21,39,48,49]. The rats were determined to be in good health by veterinarians of the institution. All experimental procedures were conducted in agreement with the National Animal Care Law (#18611) and with the "Guide to the care and use of laboratory animals" (8th edition, National Academy Press, Washington, DC, USA, 2010). Furthermore, the Institutional Animal Care Committee approved the experimental procedures (No 070153-000332-16). Adequate measures were taken to minimize the pain, discomfort or stress of the animals, and all efforts were made to use the minimal number of animals necessary to obtain reliable scientific data. Animals were maintained on a 12-h light/dark cycle (lights on at 6.00 a.m.) and housed five to six per cage before the experimental procedures. Food and water were freely available. Rats were habituated to be cabled to the rotating connector in the sleep chamber for four days before the experiments.

4.2. Surgical Procedures

We employed surgical procedures similar to those used in our previous studies [21,50,51]. The animals were chronically implanted with intracranial electrodes. Anesthesia was induced with a mixture of ketamine-xylazine (90 mg/kg; 5 mg/kg i.p., respectively). Rats were positioned in a stereotaxic frame and the skull was exposed. In order to record the iEEG, stainless steel screw electrodes were placed on the skull above the right and left M1, S1 and V2, as well as on the right OB and cerebellum (reference electrode). A representation of the electrode positions and their coordinates, according to [26], are shown in Figure 1A,B. In order to record the electromyogram (EMG), a bipolar electrode was inserted into the neck muscle. The electrodes were soldered into a 12-pin socket and fixed to the skull with acrylic cement. At the end of the surgical procedures, an analgesic (Ketoprofen, 1 mg/kg subcutaneous) was administered. Incision margins were kept clean and a topical antibiotic

was applied on a daily basis. After the animals recovered from the preceding surgical procedures, they were adapted to the recording chamber for one week.

4.3. Sleep Recordings

Animals were housed individually in transparent cages (40 × 30 × 20 cm) containing wood shaving material in a temperature-controlled (21–24 °C) room, with water and food ad libitum, under a 12:12 h light/dark cycle (lights on at 6 a.m.). Experimental sessions were conducted during the light (9 a.m. to 3 p.m.) and dark periods (9 p.m. to 3 a.m.) in a sound-attenuated chamber that also acts as a Faraday box. The recordings were performed through a rotating connector, to allow the rats to move freely within the recording box. Bioelectric signals were amplified (×1000), filtered (0.1–500 Hz), sampled (1024 Hz, 16 bits) and stored in a PC using Spike 2 software version 9.04 (Cambridge Electronic Design, Cambridge, UK).

4.4. Data Analysis

The states of sleep and W were determined in 10 s epochs. W was defined as low voltage fast waves in frontal cortex, a mixed theta rhythm in occipital cortex and relatively high EMG activity. Light sleep (LS) was determined as high voltage slow cortical waves interrupted by low voltage fast iEEG activity. Slow wave sleep (SWS) was defined as continuous high amplitude slow (1–4 Hz) neocortical waves and sleep spindles combined with a reduced EMG activity. LS and SWS were grouped as NREM sleep. REM sleep was defined as low voltage fast frontal waves, a regular theta rhythm in parietal and occipital cortices, and a silent EMG except for occasional twitching. In order to analyze power spectrum (in each channel) and coherence (between pairs of iEEG channels or derivations) we used procedures similar to those done in our previous studies [20,21,50]. The maximum number of non-transitional and artifact-free periods of 30 s was selected during each behavioral state to determine the mean power and coherence for each rat. Power spectrum was estimated by means of the *pwelch* built-in function in MATLAB version R2020a (The MathWorks Inc, Natick, MA, USA) using the following parameters: window = 30 s, noverlap = [], nfft = 2048, fs = 1024, which correspond to employing 30 s sliding windows with half window overlap with a 0.5 Hz resolution. Right M1 was excluded in one rat due to the presence of artifacts.

The coherence between selected pairs of iEEG channels was analyzed in 30 s epochs. We chose for the analysis all the intra-hemispheric and inter-hemispheric pairwise combination of adjacent cortices (the distance between adjacent neocortical electrodes was 5 mm; Figure 1B). For each period, the Magnitude Squared Coherence for each channel (for details about coherence definition see [19,38], was calculated with the *mscohere* built-in MATLAB (parameters: window = 30 s, noverlap, nfft = 2048, fs = 1024). In order to normalize the data and conduct parametric statistical tests, we applied the Fisher z' transform to the coherence values [19]. The analysis of the data was performed for the classically defined frequency band in rodents: delta, 1–4 Hz; theta, 5–9 Hz; sigma, 10–15 Hz; beta, 16–30 Hz; low gamma (LG), 31–48 Hz; high gamma (HG) 52–95 Hz; high frequency oscillations (HFO), 105–200 Hz [21,50]. Frequencies around 50 and 100 Hz were not analyzed to avoid alternating current artifacts. For the coherence analysis, NREM data were excluded in two rats, and REM data were excluded in one rat, due to artifacts that made processing unfeasible.

Differences in mean power and coherence among states (W, NREM and REM sleep) and electrode position or derivation, were evaluated by means of a two-ways repeated measures mixed-effects model, and Sidak as a correction for multiple comparisons test. We employed a mixed-effects model because we had to remove the information of noisy iEEG channels in 3 rats. We also computed the relative power as the absolute power of a specific frequency band/the sum of the power from 0.5 to 200 Hz. This analysis was performed independently for each state. Statistical significance was set at $p < 0.05$. Partial eta squared (η_p^2) was used to evaluate the effect size [52].

In order to determine if power and coherence were different between the time of the day (light vs. dark phases) or between hemispheres (right vs. left), a paired two-tailed Student test was performed

for each of the abovementioned bands. As we analyzed seven frequency bands, a Bonferroni correction for multiple comparisons was applied. With this correction $p < 0.0071$ was considered statistically significant. The predominance was calculated by means of the formula: (a − b)/(a + b). "a" represents the mean power for each frequency in the light phase or in the right side, and "b" the mean power in the dark period or in the left side. A positive value means that power during the light period (or right side) was higher than during dark period (or left side) and vice versa.

We are aware that the specific start- and end-points of each frequency band is arbitrary, and vary between subjects [30,53]. Because of this, for the day/night and laterality analyses we also performed a second evaluation by means of a cluster-based permutation test, consisting of comparing empirical clusters of frequencies against a randomized distribution, thus allowing the frequency bands to be delimited in a statistical approach without the need of a previous convention. This method consisted of comparing individual frequencies (512 frequencies) in each condition by means of paired *t*-tests (alpha = 0.05). Once p values were obtained for each frequency, all consecutive significant frequencies were grouped into empirical clusters (defining a minimum cluster size of 4 frequency points), and a new statistic was formed by summing the t-statistic of each frequency inside the cluster. To determine if a given cluster was significant, a null hypothesis distribution of cluster statistics was constructed by randomizing labels (day/night or left/right) and repeating the cluster construction method for a total of 10,000 randomizations. The p values of the empirical clusters were obtained by comparing each cluster statistic to the randomized cluster statistic distribution (X). A one-tailed comparison was employed, where the *p* value was calculated as *p* value = P (X < Xobs) [54].

In summary, as recommended by Simmons et al. (2012), we have reported how we defined our sample size, all data exclusions, all manipulations, and all measures [55].

5. Conclusions

In the present study, we carried out a thorough analysis of the spectral power and coherence of the rat iEEG. We found major effects on these parameters in the function of both behavioral states and cortical areas. We also revealed that there are night/day differences in power and coherence during sleep, but not during W. Additionally, while we did not find right/left differences in power either in W or sleep, we observed that, during REM sleep, intra-hemispheric coherence differs between both hemispheres. We consider that this systematic analysis of the iEEG dynamics during physiological W and sleep provides a template or reference for comparison with pharmacological, toxicological or pathological challenges.

Supplementary Materials: The following are available online at http://www.mdpi.com/2624-5175/2/4/39/s1, Figure S1: Absolute power in function of behavioral states and cortical regions, Figure S2: Mean absolute power in function of cortical regions, Figure S3: Total power, Figure S4: Differences in relative power in function of behavioral states, Figure S5: Absolute power: right vs. left hemispheric difference during the light phase, Figure S6: Absolute power: right vs. left hemispheric difference during the dark phase, Figure S7: Z'-coherence in function of the derivations, Figure S8: Differences in z'-coherence in function of behavioral states, Figure S9: Z'-coherence in function of the derivation, Figure S10: Intra-hemispheric z'-coherence: right vs. left hemispheric difference during the light phase.

Author Contributions: Conceptualization, A.M., M.C., J.G., L.O., S.C.-Z., A.C. and P.T.; methodology, A.M., M.C., J.G. and S.C.-Z.; software, M.C. and J.G.; validation, A.M., M.C., J.G., L.O. and S.C.-Z.; formal analysis, A.M.; investigation, A.M.; resources, P.T.; data curation, J.G.; writing—original draft preparation, A.M. and P.T.; writing—review and editing, M.C., J.G., A.C., G.V. and P.T.; visualization, A.M.; supervision, A.C., G.V. and P.T.; project administration, P.T.; funding acquisition, P.T. All authors have read and agreed to the published version of the manuscript.

Funding: This research was funded by grants from the Agencia Nacional de Investigación e Innovación (ANII) FCE-1-2011-1-5997, Comisión Sectorial de Investigación Científica (CSIC) I+D-2016-589, and Programa de Desarrollo de Ciencias Básicas (PEDECIBA), Uruguay.

Conflicts of Interest: The authors declare no conflict of interest.

Abbreviations

EEG	Electroencephalogram
iEEG	Intra-cranial electroencephalogram
HFO	High frequency oscillations
HG	High gamma
LG	Low gamma
M1	Primary motor cortex
NREM	Non-REM
OB	Olfactory bulb
REM	Rapid eye movement
S1	Primary somatosensory cortex
V2	Secondary visual cortex
W	Wakefulness

References

1. Singer, W. Complexity as Substrate for Neuronal Computations. In *Complexity and Analogy in Science*; Libreria Editrice Vaticana: Vatican City, 2015; pp. 1–10.
2. Singer, W. Binding by synchrony. *Scholarpedia* **2007**, *2*, 1657. [CrossRef]
3. Torterolo, P.; Castro-Zaballa, S.; Cavelli, M.; Gonzalez, J. Arousal and normal conscious cognition. In *Arousal in Neurological and Psychiatric Diseases*; Garcia-Rill, E., Ed.; Academic Press: Cambridge, MA, USA, 2019; pp. 1–24.
4. Andrade-Valenca, L.; Dubeau, F.; Mari, F.; Zelmann, R.; Gotman, J. High-Frequency Oscillations Recorded on Scalp EEG. *Neurology* **2011**, *77*, 524–531. [CrossRef] [PubMed]
5. Besio, W.G.; Martinez-Juarez, I.E.; Makeyev, O.; Gaitanis, J.N.; Blum, A.S.; Fisher, R.S.; Medvedev, A.V. High-Frequency Oscillations Recorded on the Scalp of Patients With Epilepsy Using Tripolar Concentric Ring Electrodes. *IEEE J. Transl. Eng. Health Med.* **2014**, *2*, 2000111. [CrossRef] [PubMed]
6. Torterolo, P.; Monti, J.; Vanini, G. Neurochemistry and Pharmacology of Sleep. In *The Behavioral, Molecular, Pharmacological, and Clinical Basis of the Sleep-Wake Cycle*; Murillo, E., Ed.; Elsevier Inc.: Amsterdam, The Netherlands, 2019; pp. 45–83.
7. Steriade, M.; McCormick, D.A.; Sejnowski, T.J. Thalamocortical oscillations in the sleeping and aroused brain. *Science* **1993**, *262*, 679–685. [CrossRef] [PubMed]
8. Tononi, G.; Laureys, S. (Eds.) The neurology of consciousness: An overview. In *The Neurology of Consciousness: Cognitive Neuroscience and Neuropathology*; Elsevier: San Diego, CA, USA, 2009; pp. 375–412.
9. Crick, F.; Koch, C. Some reflections on visual awareness. In *Cold Spring Harbor Symposia on Quantitative Biology*; Cold Spring Harbor Laboratory Press: Cold Spring Harbor, NY, USA, 1990; Volume 55, pp. 953–962.
10. Buzsaki, G.; Anastassiou, C.A.; Koch, C. The origin of extracellular fields and currents-EEG, ECoG, LFP and spikes. *Nat. Rev. Neurosci.* **2012**, *13*, 407–420. [CrossRef]
11. Cavelli, M.; Castro-Zaballa, S.; Mondino, A.; Gonzalez, J.; Falconi, A.; Torterolo, P. Absence of EEG gamma coherence in a local activated neocortical state: A conserved trait of REM sleep. *Transl. Brain Rhytm.* **2017**, *2*, 1–13.
12. Achermann, P. EEG Analysis Applied to Sleep. *Epileptologie* **2009**, *26*, 28–33.
13. Vanderwolf, C.H. Hippocampal electrical activity and voluntary movement in the rat. *Electroencephalogr. Clin. Neurophysiol.* **1969**, *26*, 407–418. [CrossRef]
14. Winson, J. Patterns of hippocampal theta rhythm in the freely moving rat. *Electroencephalogr. Clin. Neurophysiol.* **1974**, *36*, 291–301. [CrossRef]
15. John, E.R. The neurophysics of consciousness. *Brain Res. Rev.* **2002**, *39*, 1–28. [CrossRef]
16. Edelman, G.M.; Tononi, G. *A Universe of Consciousness*; Basic Books: New York, NY, USA, 2000.
17. Cantero, J.L.; Atienza, M.; Salas, R.M. Clinical value of EEG coherence as electrophysiological index of cortico-cortical connections during sleep. *Rev. Neurol.* **2000**, *31*, 442–454. [PubMed]
18. Siegel, M.; Donner, T.H.; Engel, A.K. Spectral fingerprints of large-scale neuronal interactions. *Nat. Rev. Neurosci.* **2012**, *13*, 121–134. [CrossRef] [PubMed]

19. Castro, S.; Falconi, A.; Chase, M.H.; Torterolo, P. Coherent neocortical 40-Hz oscillations are not present during REM sleep. *Eur. J. Neurosci.* **2013**, *37*, 1330–1339. [CrossRef] [PubMed]
20. Cavelli, M.; Castro, S.; Schwarzkopf, N.; Chase, M.H.; Falconi, A.; Torterolo, P. Coherent neocortical gamma oscillations decrease during REM sleep in the rat. *Behav. Brain Res.* **2015**, *281*, 318–325. [CrossRef]
21. Cavelli, M.; Rojas-Libano, D.; Schwarzkopf, N.; Castro-Zaballa, S.; Gonzalez, J.; Mondino, A.; Santana, N.; Benedetto, L.; Falconi, A.; Torterolo, P. Power and coherence of cortical high-frequency oscillations during wakefulness and sleep. *Eur. J. Neurosci.* **2018**, *48*, 2728–2737. [CrossRef]
22. Achermann, P.; Borbely, A.A. Coherence analysis of the human sleep electroencephalogram. *Neuroscience* **1998**, *85*, 1195–1208. [CrossRef]
23. Jing, W.; Wang, Y.; Fang, G.; Chen, M.; Xue, M.; Guo, D.; Yao, D.; Xia, Y. EEG Bands of Wakeful Rest, Slow-Wave and Rapid-Eye-Movement Sleep at Different Brain Areas in Rats. *Front. Comput. Neurosci.* **2016**, *10*, 79. [CrossRef]
24. Vyazovskiy, V.V.; Tobler, I. Handedness leads to interhemispheric EEG asymmetry during sleep in the rat. *J. Neurophysiol.* **2008**, *99*, 969–975. [CrossRef]
25. Swift, K.M.; Keus, K.; Echeverria, C.G.; Cabrera, Y.; Jimenez, J.; Holloway, J.; Clawson, B.C.; Poe, G.R. Sex differences within sleep in gonadally intact rats. *Sleep* **2020**, *43*, zsz289. [CrossRef]
26. Paxinos, G.; Watson, C. *The Rat Brain*; Academic Press: New York, NY, USA, 2005.
27. Castro, S.; Cavelli, M.; Vollono, P.; Chase, M.H.; Falconi, A.; Torterolo, P. Inter-hemispheric coherence of neocortical gamma oscillations during sleep and wakefulness. *Neurosci. Lett.* **2014**, *578*, 197–202. [CrossRef]
28. Nyhus, E.; Curran, T. Functional role of gamma and theta oscillations in episodic memory. *Neurosci. Biobehav. Rev.* **2010**, *34*, 1023–1035. [CrossRef] [PubMed]
29. Mahjoory, K.; Cesnaite, E.; Hohlefeld, F.U.; Villringer, A.; Nikulin, V.V. Power and temporal dynamics of alpha oscillations at rest differentiate cognitive performance involving sustained and phasic cognitive control. *Neuroimage* **2019**, *188*, 135–144. [CrossRef]
30. Myrden, A.; Chau, T. Feature clustering for robust frequency-domain classification of EEG activity. *J. Neurosci. Methods* **2016**, *262*, 77–84. [CrossRef] [PubMed]
31. Adrian, E.D. Olfactory reactions in the brain of the hedgehog. *J. Physiol.* **1942**, *100*, 459–473. [CrossRef] [PubMed]
32. Cavelli, M.; Castro-Zaballa, S.; Gonzalez, J.; Rojas-Libano, D.; Rubido, N.; Velasquez, N.; Torterolo, P. Nasal respiration entrains neocortical long-range gamma coherence during wakefulness. *Eur. J. Neurosci.* **2020**, *51*, 1463–1477. [CrossRef] [PubMed]
33. Zhuang, L.; Zhang, B.; Qin, Z.; Wang, P. Nasal Respiration is Necessary for the Generation of gamma Oscillation in the Olfactory Bulb. *Neuroscience* **2019**, *398*, 218–230. [CrossRef] [PubMed]
34. Sirota, A.; Montgomery, S.; Fujisawa, S.; Isomura, Y.; Zugaro, M.; Buzsaki, G. Entrainment of neocortical neurons and gamma oscillations by the hippocampal theta rhythm. *Neuron* **2008**, *60*, 683–697. [CrossRef] [PubMed]
35. Gonzalez, J.; Cavelli, M.; Mondino, A.; Rubido, N.; Tort, A.B.L.; Torterolo, P. Communication through coherence by means of cross-frequency coupling. *Neuroscience* **2020**. [CrossRef] [PubMed]
36. Bauer, M.; Stenner, M.P.; Friston, K.J.; Dolan, R.J. Attentional modulation of alpha/beta and gamma oscillations reflect functionally distinct processes. *J. Neurosci.* **2014**, *34*, 16117–16125. [CrossRef] [PubMed]
37. Hunt, M.J.; Adams, N.E.; Sredniawa, W.; Wojcik, D.K.; Simon, A.; Kasicki, S.; Whittington, M.A. The olfactory bulb is a source of high-frequency oscillations (130–180 Hz) associated with a subanesthetic dose of ketamine in rodents. *Neuropsychopharmacology* **2019**, *44*, 435–442. [CrossRef] [PubMed]
38. Bullock, T.H.; McClune, M.C. Lateral coherence of the electrocorticogram: A new measure of brain synchrony. *Electroencephalogr. Clin. Neurophysiol.* **1989**, *73*, 479–498. [CrossRef]
39. Pal, D.; Silverstein, B.H.; Lee, H.; Mashour, G.A. Neural Correlates of Wakefulness, Sleep, and General Anesthesia: An Experimental Study in Rat. *Anesthesiology* **2016**, *125*, 929–942. [CrossRef] [PubMed]
40. Osorio, L.; Mondino, A.; Cavelli, M.; Gonzalez, J.; Torterolo, P.; Costa, A. EEG power spectrum daily variations in sleep and wakefulness. *Sleep Sci.* **2020**. [CrossRef]
41. Vyazovskiy, V.V.; Borbely, A.A.; Tobler, I. Interhemispheric sleep EEG asymmetry in the rat is enhanced by sleep deprivation. *J. Neurophysiol.* **2002**, *88*, 2280–2286. [CrossRef] [PubMed]
42. Trachsel, L.; Tobler, I.; Achermann, P.; Borbely, A.A. Sleep continuity and the REM-nonREM cycle in the rat under baseline conditions and after sleep deprivation. *Physiol. Behav.* **1991**, *49*, 575–580. [CrossRef]

43. Datta, S.; Hobson, J.A. The rat as an experimental model for sleep neurophysiology. *Behav. Neurosci.* **2000**, *114*, 1239–1244. [CrossRef]
44. Stephenson, R.; Lim, J.; Famina, S.; Caron, A.M.; Dowse, H.B. Sleep-wake behavior in the rat: Ultradian rhythms in a light-dark cycle and continuous bright light. *J. Biol. Rhythms* **2012**, *27*, 490–501. [CrossRef]
45. Poe, G.R. Sleep Is for Forgetting. *J. Neurosci.* **2017**, *37*, 464–473. [CrossRef]
46. Sara, S.J. Sleep to Remember. *J. Neurosci.* **2017**, *37*, 457–463. [CrossRef]
47. Boldyreva, G.N.; Zhavoronkova, L.A. Interhemispheric asymmetry of EEG coherence as a reflection of different functional states of the human brain. *Biomed. Sci.* **1991**, *2*, 266–270.
48. Pal, D.; Hambrecht-Wiedbusch, V.S.; Silverstein, B.H.; Mashour, G.A. Electroencephalographic coherence and cortical acetylcholine during ketamine-induced unconsciousness. *Br. J. Anaesth.* **2015**, *114*, 976–989. [CrossRef] [PubMed]
49. Guidera, J.A.; Taylor, N.E.; Lee, J.T.; Vlasov, K.Y.; Pei, J.; Stephen, E.P.; Mayo, J.P.; Brown, E.N.; Solt, K. Sevoflurane Induces Coherent Slow-Delta Oscillations in Rats. *Front. Neural Circuits* **2017**, *11*, 36. [CrossRef] [PubMed]
50. Mondino, A.; Cavelli, M.; Gonzalez, J.; Santana, N.; Castro-Zaballa, S.; Mechoso, B.; Bracesco, N.; Fernandez, S.; Garcia-Carnelli, C.; Castro, M.J.; et al. Acute effect of vaporized Cannabis on sleep and electrocortical activity. *Pharmacol. Biochem. Behav.* **2019**, *179*, 113–123. [CrossRef] [PubMed]
51. Gonzalez, J.; Cavelli, M.; Mondino, A.; Pascovich, C.; Castro-Zaballa, S.; Torterolo, P.; Rubido, N. Decreased electrocortical temporal complexity distinguishes sleep from wakefulness. *Sci. Rep.* **2019**, *9*, 18457. [CrossRef]
52. Lakens, D. Calculating and reporting effect sizes to facilitate cumulative science: A practical primer for *t*-tests and ANOVAs. *Front. Psychol.* **2013**, *4*, 863. [CrossRef]
53. Haegens, S.; Cousijn, H.; Wallis, G.; Harrison, P.J.; Nobre, A.C. Inter- and intra-individual variability in alpha peak frequency. *Neuroimage* **2014**, *92*, 46–55. [CrossRef]
54. Gonzalez, J.; Cavelli, M.; Castro-Zaballa, S.; Mondino, A.; Tort, A.B.L.; Rubido, N.; Carrera, I.; Torterolo, P. Gamma band alterations and REM-like traits underpin the acute effect of the atypical psychedelic ibogaine. *bioRxiv* **2020**. [CrossRef]
55. Simmons, J.; Nelson, L.; Simonsohn, U. A 21 word solution. *Dialogue* **2012**, *26*, 4–7. [CrossRef]

A

Cortex	Comparison	Delta	Theta	Sigma	Beta	LG	HG	HFO
OB	W vs NREM	0.6445	0.4622	0.0123	0.9732	0.0199	<0.0001	<0.0001
	W vs REM	0.1889	0.7319	0.9566	0.4866	0.0957	<0.0001	<0.0001
	NREM vs REM	0.0138	0.0774	0.0031	0.2634	0.9026	0.8339	0.9684
M1	W vs NREM	<0.0001	0.0004	<0.0001	0.2875	0.0006	<0.0001	<0.0001
	W vs REM	0.6163	0.6545	>0.9999	0.7885	0.1984	<0.0001	<0.0001
	NREM vs REM	<0.0001	<0.0001	<0.0001	0.0464	0.1231	0.0133	0.3058
S1	W vs NREM	<0.0001	0.0064	<0.0001	0.1379	0.0321	<0.0001	<0.0001
	W vs REM	0.8051	0.8555	0.9998	0.9115	0.6745	0.0020	<0.0001
	NREM vs REM	<0.0001	0.0474	<0.0001	0.0331	0.3065	0.0716	0.9649
V2	W vs NREM	0.1540	0.8113	0.1495	0.9978	0.1898	0.0023	0.0002
	W vs REM	0.9614	0.7019	0.9994	0.8749	0.1905	0.0451	0.0004
	NREM vs REM	0.0562	0.9973	0.1182	0.9398	>0.9999	0.6695	0.9937

B

States	Comparison	Delta	Theta	Sigma	Beta	LG	HG	HFO
W	OB vs M1	0.9741	0.9921	0.9767	0.5754	0.2381	0.0723	0.0001
	OB vs S1	0.8577	0.2735	0.9494	0.2945	0.5623	<0.0001	<0.0001
	OB vs V2	0.2606	0.9897	0.9889	0.7840	>0.9999	<0.0001	<0.0001
	M1 vs S1	0.9995	0.6663	0.9999	0.9981	0.9983	0.0375	0.9171
	M1 vs V2	0.7673	0.7844	0.6850	0.0442	0.1482	<0.0001	0.1486
	S1 vs V2	0.9533	0.0676	0.6048	0.0146	0.4103	0.0016	0.7756
NREM	OB vs M1	0.0090	0.0062	0.0124	0.0389	0.9557	0.9998	0.8640
	OB vs S1	<0.0001	0.0010	0.0095	0.0030	0.5119	>0.9999	0.9923
	OB vs V2	0.9203	0.8132	0.4517	0.3883	0.9637	0.8570	0.9568
	M1 vs S1	0.0468	0.9888	>0.9999	0.9344	0.9664	0.9954	0.9981
	M1 vs V2	0.0003	<0.0001	<0.0001	<0.0001	>0.9999	0.9667	>0.9999
	S1 vs V2	<0.0001	<0.0001	<0.0001	<0.0001	0.9591	0.7301	>0.9999
REM	OB vs M1	>0.9999	0.9977	0.7833	0.2688	0.1028	0.3289	>0.9999
	OB vs S1	>0.9999	0.0027	0.6559	0.0636	0.0472	0.3550	0.9946
	OB vs V2	0.9997	0.7065	>0.9999	0.9922	>0.9999	0.9576	0.8884
	M1 vs S1	>0.9999	0.0120	>0.9999	0.9844	0.9994	>0.9999	0.9626
	M1 vs V2	0.9978	0.9490	0.5988	0.0685	0.1408	0.0486	0.7387
	S1 vs V2	0.9993	0.1208	0.4684	0.0122	0.0664	0.0581	0.9984

Supplementary Figure 1. Absolute power in function of behavioral states and cortical regions. p values of the Sidak multiple comparisons test, comparing the differences in the absolute power between behavioral states (A) and cortical regions (B). Data show in A are summarized in Figure 3. The data are from the right hemisphere during the light phase. OB, olfactory bulb; M1, primary motor cortex; S1, primary somato-sensory cortex; V2, secondary visual cortex; W, wakefulness; LG, low gamma; HG, high gamma; HFO, high frequency oscillations.

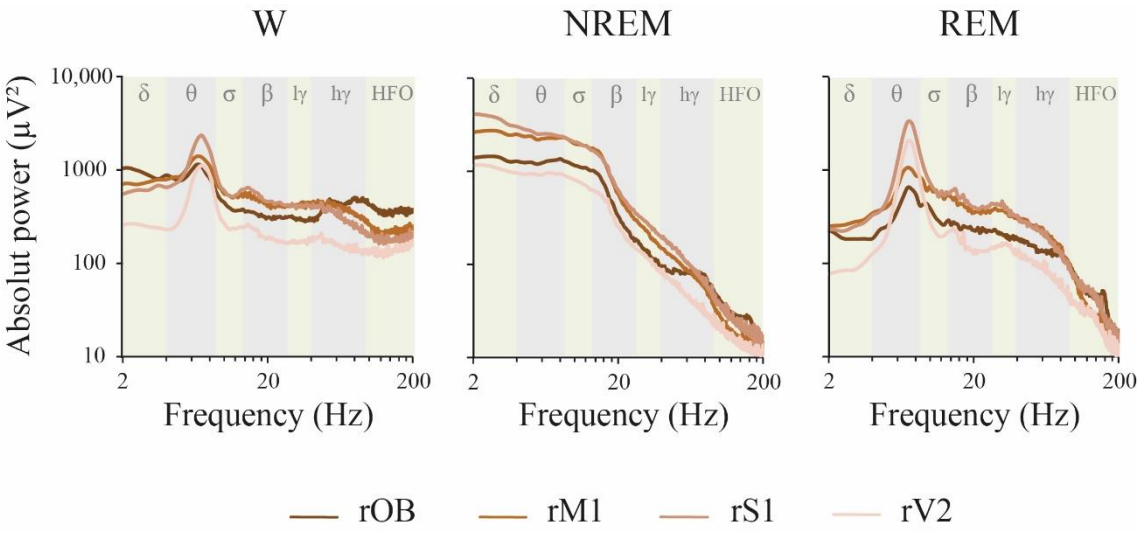

Supplementary Figure 2. Mean absolute power in function of cortical regions. Mean absolute power spectral profile of each behavioral state during the light period for all the electrodes of the right hemisphere. The analyzed frequency bands are indicated by different colors in the background of the graphics. OB, olfactory bulb; M1, primary motor cortex; S1, primary somato-sensory cortex; V2, secondary visual cortex; W, wakefulness; lγ, low gamma or LG; hγ, high gamma or HG; HFO, high frequency oscillations.

Total Power

A

	Localization			Behavioral State			Localization x State		
	Df	p	F	df	p	F	df	P	F
Total power	3,30	0.0001	9.6	2, 20	<0.0001	20.0	6, 57	0.0003	5.2

B

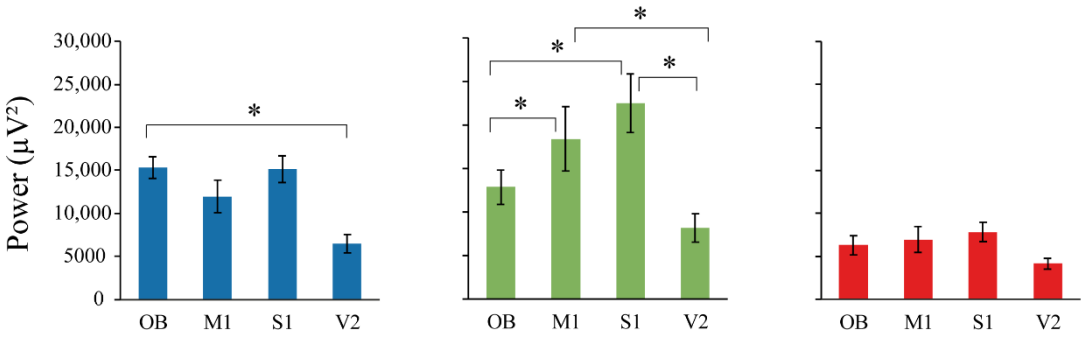

C

State	Comparison	p value
W	OB vs M1	0.4853
	OB vs S1	0.2315
	OB vs V2	0.0005
	M1 vs S1	0.9991
	M1 vs V2	0.1122
	S1 vs V2	0.2784
NREM	OB vs M1	0.0163
	OB vs S1	0.0004
	OB vs V2	0.5393
	M1 vs S1	0.8690
	M1 vs V2	<0.0001
	S1 vs V2	<0.0001
REM	OB vs M1	0.8917
	OB vs S1	0.9284
	OB vs V2	0.9800
	M1 vs S1	>0.9999
	M1 vs V2	0.4337
	S1 vs V2	0.5000

D

Cortex	Comparison	p value
OB	W vs NREM	0.1968
	W vs REM	<0.0001
	NREM vs REM	0.0312
M1	W vs NREM	0.0144
	W vs REM	0.2855
	NREM vs REM	<0.0001
S1	W vs NREM	0.0001
	W vs REM	0.4712
	NREM vs REM	<0.0001
V2	W vs NREM	0.8431
	W vs REM	0.6690
	NREM vs REM	0.2245

Supplementary Figure 3. Total power. A. Statistical evaluation of the total power in function of cortical regions, behavioral state, and interaction between both factors. Repeated mixed-effects model. B. Mean total power in function of cortical regions. Total power is lower in the V2 probably because it is closer to the reference electrode located in the cerebellum. The error bars show the standard error of the mean. Asterisks indicate significant differences, $p < 0.05$. C. p values of the Sidak multiple comparisons test, comparing the differences in the total power between the different cortical localizations of the right hemisphere for each behavioral state. D. p values of the Sidak multiple comparisons test, comparing the differences in the total power between the different behavioral states in each right cortex. OB, olfactory bulb; M1,

primary motor cortex; S1, primary somato-sensory cortex; V2, secondary visual cortex; W, wakefulness.

Cortex	Comparison	Delta	Theta	Sigma	Beta	LG	HG	HFO
OB	W vs NREM	0.0032	0.6824	<0.0001	0.0015	0.0314	<0.0001	<0.0001
	W vs REM	0.0926	0.9053	0.1590	0.8238	0.0068	0.1815	<0.0001
	NREM vs REM	<0.0001	0.9710	0.0134	0.0165	<0.0001	<0.0001	0.0964
M1	W vs NREM	<0.0001	0.8538	<0.0001	0.0001	<0.0001	<0.0001	<0.0001
	W vs REM	0.2034	0.8360	0.0066	0.2606	0.0172	0.7641	0.0002
	NREM vs REM	<0.0001	>0.9999	0.3633	0.0272	<0.0001	<0.0001	0.6090
S1	W vs NREM	<0.0001	<0.0001	0.0195	0.1988	<0.0001	<0.0001	<0.0001
	W vs REM	0.0677	0.0022	0.1235	0.7243	0.8881	0.4177	0.0049
	NREM vs REM	<0.0001	<0.0001	0.8450	0.7589	<0.0001	0.0071	0.5565
V2	W vs NREM	<0.0001	0.7643	0.0003	0.0294	0.0028	0.0002	<0.0001
	W vs REM	0.1089	<0.0001	0.5729	0.7624	0.9970	0.1371	<0.0001
	NREM vs REM	<0.0001	<0.0001	0.0115	0.2260	0.0049	0.0861	0.6982

Supplementary Figure 4. Differences in relative power in function of behavioral states. p values of the Sidak multiple comparisons test, comparing the differences in the absolute power in function of behavioral states for each cortical region (of the right hemisphere). OB, olfactory bulb; M1, primary motor cortex; S1, primary somato-sensory cortex; V2, secondary visual cortex; df, degrees of freedom; W, wakefulness; LG, low gamma; HG, high gamma; HFO, high frequency oscillations.

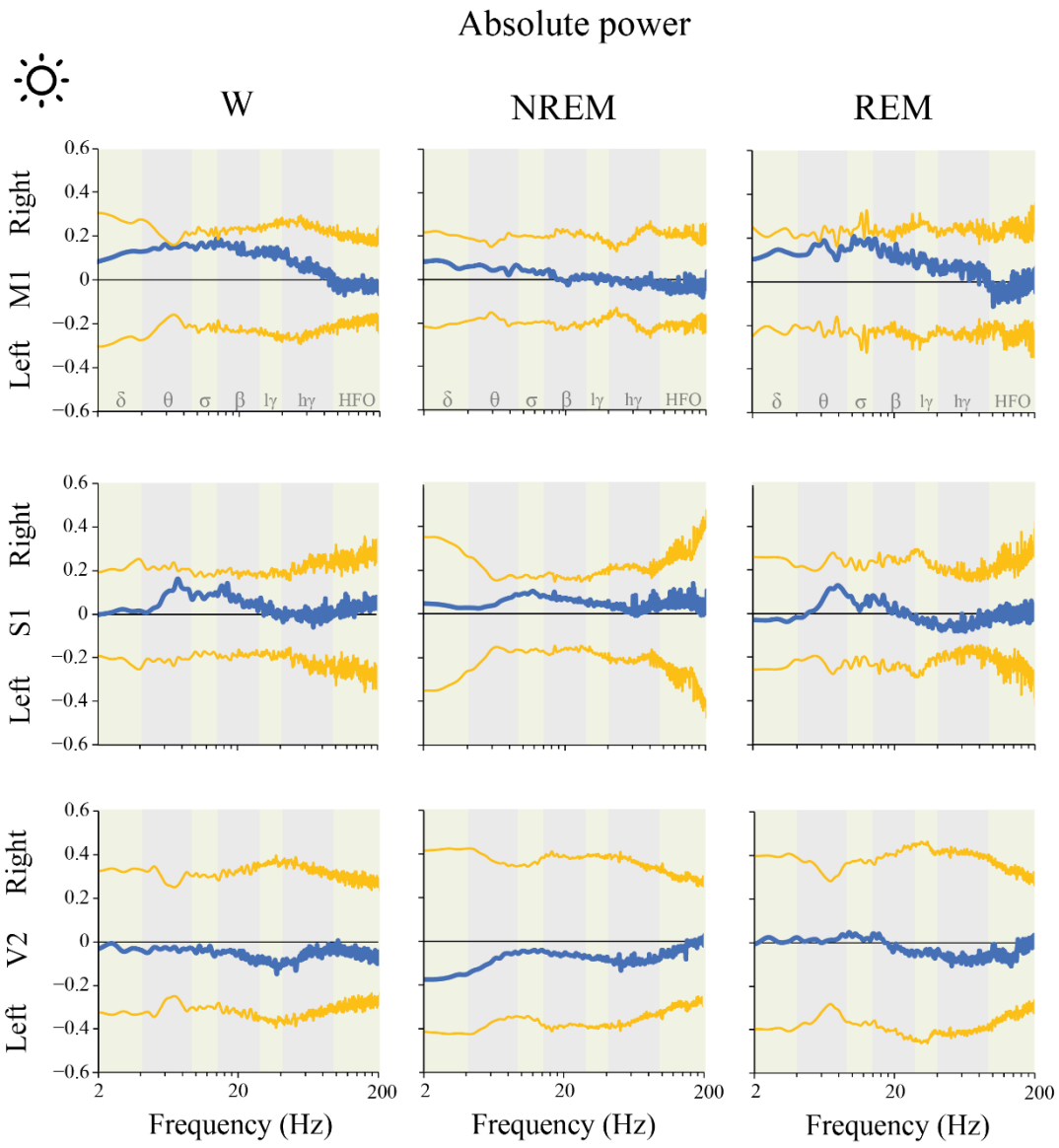

Supplementary Figure 5. Absolute power: right Vs. left hemispheric difference during the light phase. The predominance was calculated by means of the formula: (a-b)/(a+b). "a" represents the mean power for each frequency in the right hemisphere, and "b" the mean power in the left hemisphere. A positive value means that power in the right was higher than in the left hemisphere and *vice versa*. The blue traces indicate the mean power difference between right and dark hemispheres. The yellow lines represent the standard deviation of the mean with respect to zero. The statistical evaluation was performed by the two-tailed paired t-test with Bonferroni correction for multiple comparisons; no significant differences were observed. M1, primary motor cortex; S1, primary somato-sensory cortex; V2, secondary visual cortex; lγ, low gamma or LG; hγ, high gamma or HG; HFO, high frequency oscillations.

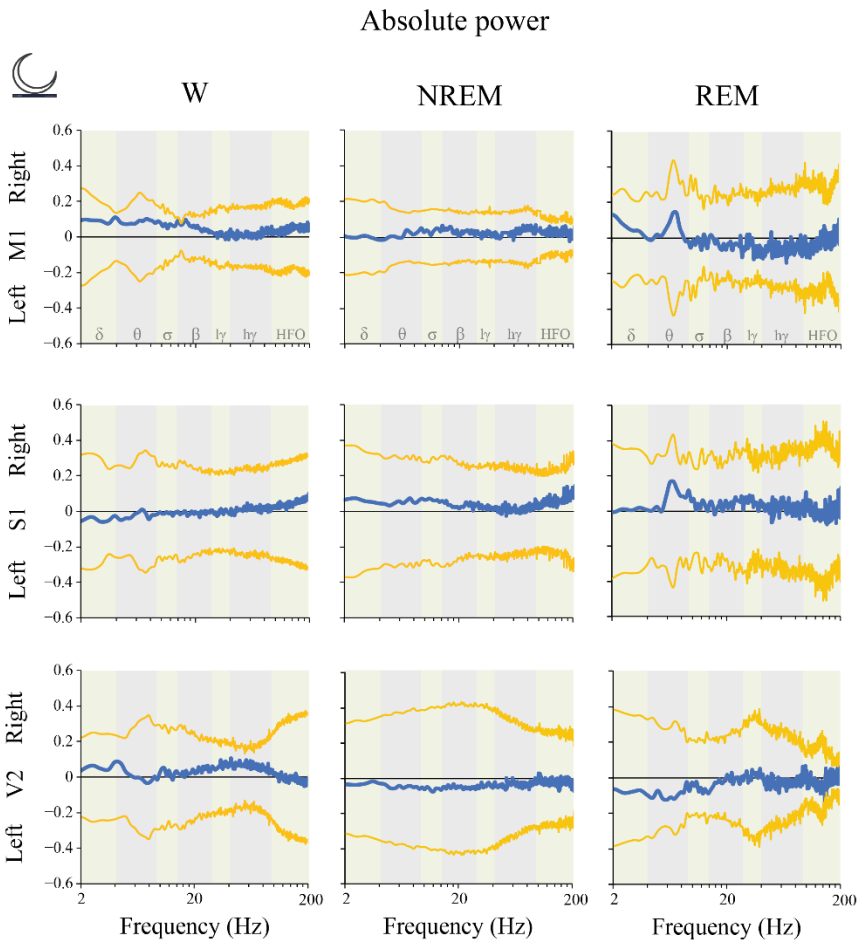

Supplementary Figure 6. Absolute power: right Vs. left hemispheric difference during the dark phase. The predominance was calculated by means of the formula: (a-b)/(a+b). "a" represents the mean power for each frequency in the right hemisphere, and "b" the mean power in the left hemisphere. A positive value means that power in the right was higher than in the left hemisphere and *vice versa*. The blue traces indicate the mean power difference between right and dark hemispheres. The yellow lines represent the standard deviation of the mean with respect to zero. The statistical evaluation was performed by the two-tailed paired t-test with Bonferroni correction for multiple comparisons; no significant differences were observed. M1, primary motor cortex; S1, primary somato-sensory cortex; V2, secondary visual cortex; lγ, low gamma or LG; hγ, high gamma or HG; HFO, high frequency oscillations.

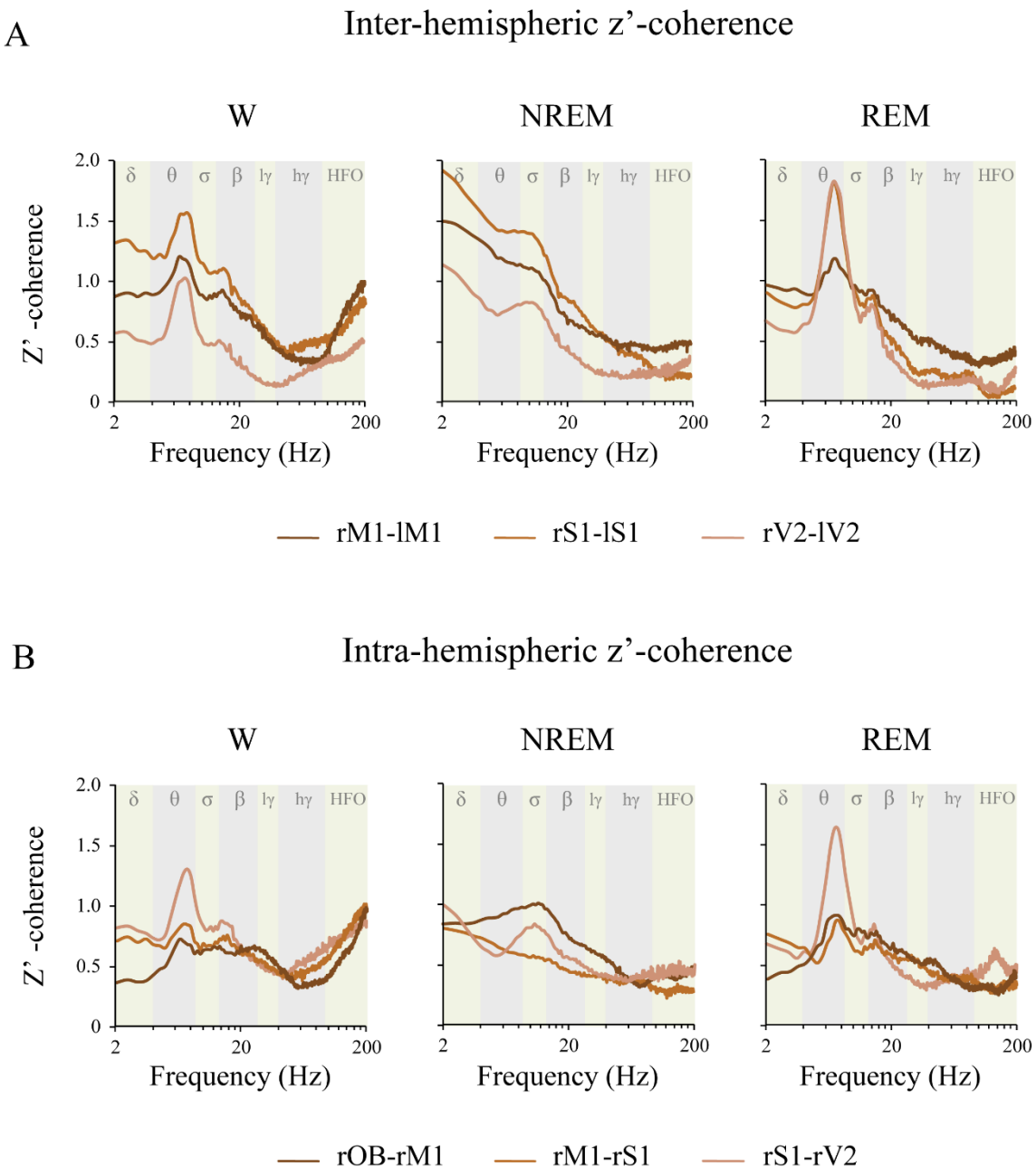

Supplementary Figure 7. Z'-coherence in function of the derivations. Mean z'-coherence profile of the intra-hemispheric (A, for the right hemisphere) and inter-hemispheric (B) derivations during wakefulness (W), NREM and REM sleep in the light phase. The analyzed frequency bands are indicated by different colors in the background of the graphics. OB, olfactory bulb; M1, primary motor cortex; S1, primary somato-sensory cortex; V2, secondary visual cortex; r, right; l, left; lγ, low gamma or LG; hγ, high gamma or HG; HFO, high frequency oscillations.

Derivation		Delta	Theta	Sigma	Beta	LG	HG	HFO
	Intra-hemispheric z'coherence							
rOB – rM1	W vs NREM	0.0014	0.0287	0.0004	0.6053	0.8309	0.9930	0.0007
	W vs REM	0.8569	0.0778	0.1541	0.9999	0.8453	>0.9999	<0.0001
	NREM vs REM	0.0129	0.9520	0.1089	0.6477	>0.9999	0.9935	0.7875
rM1 – rS1	W vs NREM	0.0030	0.9974	0.9635	0.0966	0.8563	0.0898	<0.0001
	W vs REM	>0.9999	0.9664	0.7950	0.6974	0.9471	0.0103	<0.0001
	NREM vs REM	0.0030	0.9192	0.9772	0.9410	0.9929	0.8696	0.9122
rS1 – rV2	W vs NREM	0.9485	<0.0001	0.7063	0.4468	0.9998	0.0021	<0.0001
	W vs REM	0.4460	0.0731	0.9510	0.1566	0.1528	0.0004	<0.0001
	NREM vs REM	0.2151	<0.0001	0.9416	0.9410	0.2083	0.9872	0.9676
	Inter-hemispheric z'coherence							
rM1 – lM1	W vs NREM	<0.0001	0.4673	0.0438	0.9834	0.3244	0.3029	0.0002
	W vs REM	0.9196	0.9992	0.9847	0.6268	0.9990	0.8330	<0.0001
	NREM vs REM	<0.0001	0.3982	0.0937	0.8552	0.2631	0.0648	0.3631
rS1 – lS1	W vs NREM	0.0004	0.6795	0.8996	0.0922	0.4033	<0.0001	<0.0001
	W vs REM	0.5178	0.0446	0.7298	0.0011	0.0034	<0.0001	<0.0001
	NREM vs REM	<0.0001	0.0031	0.3474	0.4359	0.2082	>0.9999	0.6549
rV2 – lV2	W vs NREM	0.0002	0.6415	0.0062	0.0283	0.0011	>0.9999	0.4611
	W vs REM	0.9918	<0.0001	0.0019	0.7857	0.9989	0.0322	0.0006
	NREM vs REM	0.0005	<0.0001	0.9944	0.1954	0.0007	0.0479	0.0567

Supplementary Figure 8. Differences in z'-coherence in function of behavioral states. p values of the Sidak multiple comparisons test, comparing the differences in the z'-coherence in function of behavioral states for each frequency band. OB, olfactory bulb; M1, primary motor cortex; S1, primary somato-sensory cortex; V2, secondary visual cortex; r, right; l, left; W, wakefulness; LG, low gamma; HG, high gamma; HFO, high frequency oscillations.

A

Comparison	Delta	Theta	Sigma	Beta	LG	HG	HFO
rOB-rM1 vs rM1-rS1	0.9955	>0.9999	>0.9999	>0.9999	>0.9999	>0.9999	0.9988
rOB-rM1 vs rM1-rV2	0.1567	0.0751	0.5571	0.9847	0.9947	0.2005	0.4356
rOB-rM1 vs rM1-lM1	0.8031	0.8266	0.9969	>0.9999	>0.9999	>0.9999	>0.9999
rOB-rM1 vs rS1-lS1	0.0235	0.0461	0.3920	0.9867	>0.9999	0.9520	0.9995
rOB-rM1 vs rV2-lV2	>0.9999	0.9985	>0.9999	0.9967	0.8911	>0.9999	0.7529
rM1-rS1 vs rS1-rV2	0.8703	0.2318	0,7258	0.9695	0.9755	0.6631	0.9533
rM1-rS1 vs rM1-lM1	>0.9999	0.9846	0.9998	>0.9999	>0.9999	>0.9999	>0.9999
rM1-rS1 vs rS1-lS1	0.3692	0.1547	0.5566	0.9730	>0.9999	>0.9999	>0.9999
rM1-rS1 vs rV2-lV2	>0.9999	>0.9999	>0.9999	0.9830	0.9592	0.9946	0.1782
rS1-rV2 vs rM1-lM1	0.9986	0.9755	0.9981	0.9999	0.9926	0.2924	0.7587
rS1-rV2 vs rS1-lS1	>0.9999	>0.9999	>0.9999	>0.9999	>0.9999	0.9890	0.9727
rS1-rV2 vs rV2-lV2	0.5609	0.5958	0.2650	0.2091	0.1661	0.0673	0.0027
rM1-lM1 vs rS1-lS1	0.8428	0.9313	0.9860	0.9999	>0.9999	0.9847	>0.9999
rM1-lM1 vs rV2-lV2	0.9960	>0.9999	0.9340	0.7698	0.9079	>0.9999	0.4025
rS1-lS1 vs rV2-lV2	0.1430	0.4580	0.9963	0.2179	0.5124	0.7255	0.1447

B

Comparison	Delta	Theta	Sigma	Beta	LG	HG	HFO
rOB-rM1 vs rM1-rS1	0.9998	>0.9999	>0.9999	>0.9999	>0.9999	>0.9999	>0.9999
rOB-rM1 vs rM1-rV2	0.6713	0.0777	0.9631	0.9998	>0.9999	0.8373	0.3460
rOB-rM1 vs rM1-lM1	0.8441	0.9997	>0.9999	>0.9999	>0.9999	>0.9999	>0.9999
rOB-rM1 vs rS1-lS1	0.1835	0.0395	0.9393	>0.9999	>0.9999	>0.9999	0.9976
rOB-rM1 vs rV2-lV2	>0.9999	0.4186	>0.9999	0.9891	0.8162	0.9974	0.9729
rM1-rS1 vs rS1-rV2	0.9951	0.0203	0.6591	0.9928	0.9966	0.8247	0.1439
rM1-rS1 vs rM1-lM1	0.9997	0.9701	0.9921	>0.9999	>0.9999	>0.9999	>0.9999
rM1-rS1 vs rS1-lS1	0.7377	0.0094	0.5897	>0.9999	>0.9999	>0.9999	>0.9999
rM1-rS1 vs rV2-lV2	>0.9999	0.1581	>0.9999	0.9995	0.9721	0.9979	0.9993
rS1-rV2 vs rM1-lM1	>0.9999	0.5115	>0.9999	>0.9999	0.9997	0.8352	0.2841
rS1-rV2 vs rS1-lS1	>0.9999	>0.9999	>0.9999	>0.9999	0.9999	0.9349	0.0257
rS1-rV2 vs rV2-lV2	0.9442	>0.9999	0.9692	0.5786	0.3192	0.1553	0.0104
rM1-lM1 vs rS1-lS1	0.9986	0.3355	0.9997	>0.9999	>0.9999	>0.9999	0.9992
rM1-lM1 vs rV2-lV2	0.9895	0.9614	>0.9999	0.9549	0.9088	0.9975	0.9867
rS1-lS1 vs rV2-lV2	0.4753	0.9985	0.9481	0.8407	0.8832	0.9835	>0.9999

C

Comparison	Delta	Theta	Sigma	Beta	LG	HG	HFO
rOB-rM1 vs rM1-rS1	0.9985	>0.9999	0.9963	>0.9999	>0.9999	>0.9999	>0.9999
rOB-rM1 vs rM1-rV2	0.9362	>0.9999	>0.9999	>0.9999	0.9988	0.8319	0.8575
rOB-rM1 vs rM1-lM1	0.2233	0.9882	>0.9999	>0.9999	>0.9999	>0.9999	>0.9999
rOB-rM1 vs rS1-lS1	0.0182	0.7371	0.9798	>0.9999	>0.9999	>0.9999	0.9994
rOB-rM1 vs rV2-lV2	0.9997	>0.9999	>0.9999	0.9975	0.9960	>0.9999	>0.9999
rM1-rS1 vs rS1-rV2	>0.9999	0.9996	0.8436	0.9275	0.9538	0.8801	0.4688
rM1-rS1 vs rM1-lM1	0.8948	0.8642	0.8392	0.9995	>0.9999	>0.9999	0.9999
rM1-rS1 vs rS1-lS1	0.2544	0.4073	0.3459	0.9755	>0.9999	>0.9999	>0.9999
rM1-rS1 vs rV2-lV2	>0.9999	>0.9999	>0.9999	>0.9999	>0.9999	>0.9999	>0.9999
rS1-rV2 vs rM1-lM1	0.9954	>0.9999	>0.9999	>0.9999	0.9996	0.9895	0.9579
rS1-rV2 vs rS1-lS1	0.5884	0.9619	>0.9999	>0.9999	0.9999	0.9125	0.2274
rS1-rV2 vs rV2-lV2	>0.9999	0.9999	0.9834	0.7859	0.5706	0.4580	0.5166
rM1-lM1 vs rS1-lS1	0.9992	>0.9999	>0.9999	>0.999	>0.9999	>0.9999	0.9917
rM1-lM1 vs rV2-lV2	0.8305	0.9025	0.9824	0.9910	0.9906	0.9982	>0.9999
rS1-lS1 vs rV2-lV2	0.1946	0.4658	0.6645	0.8924	0.9828	>0.9999	>0.9999

Supplementary Figure 9. Z'-coherence in function of the derivation. p values of the Sidak multiple comparisons test, comparing the differences in the z'-coherence according to the derivation, during wakefulness (A), NREM (B) and REM sleep (C). OB, olfactory bulb; M1, primary motor cortex; S1, primary somato-sensory cortex; V2, secondary visual cortex; LG, low gamma; HG, high gamma; HFO, high frequency oscillations.

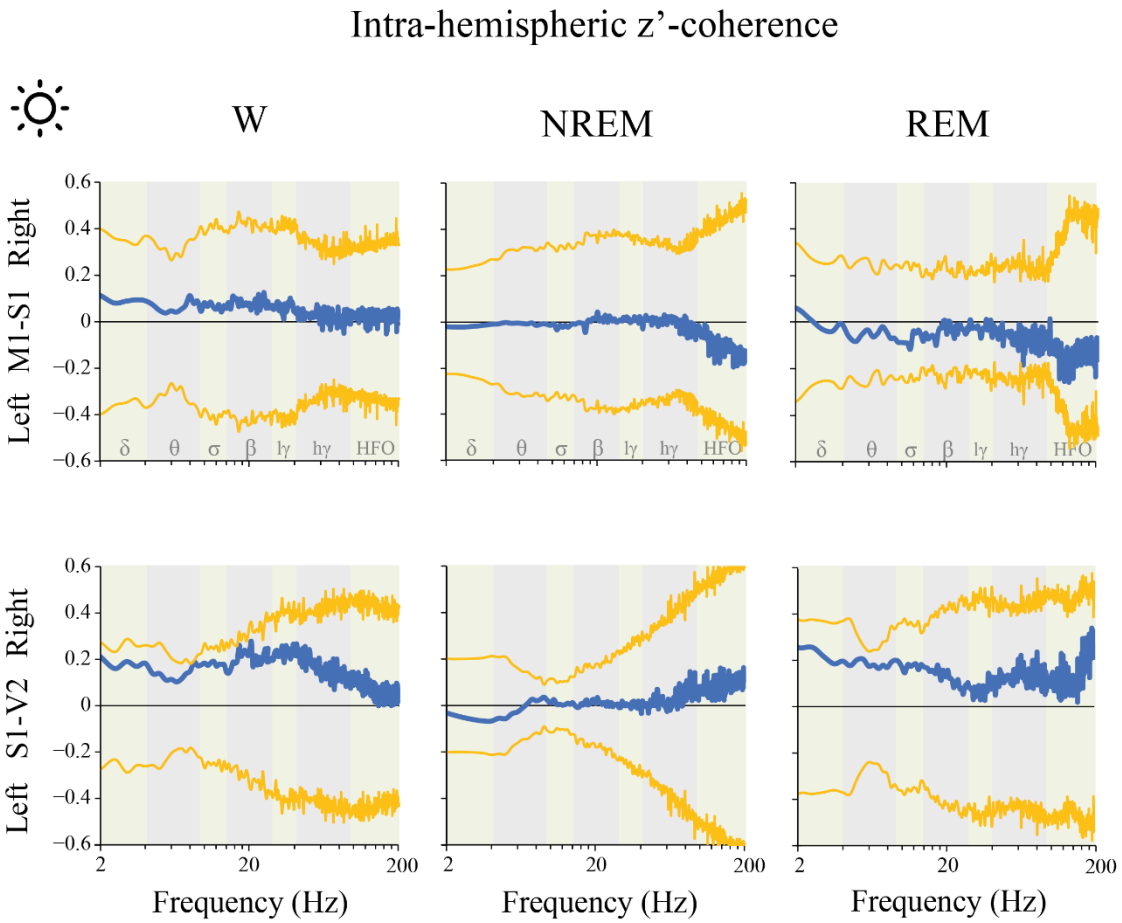

Supplementary Figure 10. Intra-hemispheric z'-coherence: right Vs. left hemispheric difference during the light phase. The predominance was calculated by means of the formula: (a-b)/(a+b). "a" represents the mean z'-coherence for each frequency in the light phase, and "b" the mean coherence during the dark period. A positive value means that z'-coherence in the light period was higher than during dark period and *vice versa*. The blue traces indicate the mean z'-coherence difference between light and dark phases. The yellow lines represent the standard deviation of the mean with respect to zero. The statistical evaluation was performed by the two-tailed paired t-test with Bonferroni correction for multiple comparisons; no significant differences were observed. M1, primary motor cortex; S1, primary somato-sensory cortex; V2, secondary visual cortex; lγ, low gamma or LG; hγ, high gamma or HG; HFO, high frequency oscillations.

Comentarios adicionales a la discusión del artículo

Respecto a las diferencias encontradas entre el día y la noche, pudimos observar cambios en el sueño tanto No-REM como REM. Sin embargo, no fueron evidenciadas diferencias en la vigilia. Posteriormente, nuestro equipo de trabajo realizó otro estudio más detallado, evaluando los cambios de potencia y coherencia hora por hora en registros de 24 horas (Osorio *et al.*, 2020). En este trabajo, encontramos cambios en la frecuencia de theta en sueño REM entre el día y la noche, siendo el theta más lento durante el día. Esto podría explicar el aumento de theta encontrado en el Artículo 1 en las frecuencias de 4.5 a 7.5 Hz durante el día. El artículo de Osorio et al. (2020) ha sido incluido en la tesis como **Anexo 1**.

Capítulo 2. Semejanzas electroencefalográficas entre el sueño y la anestesia general, ¿es realmente el Uretano un modelo farmacológico de sueño?

Como fue discutido anteriormente, existen grandes similitudes en la actividad eléctrica cerebral durante la anestesia general y el sueño. Pero esta similitud se da principalmente entre algunos anestésicos generales (principalmente anestésicos inhalatorios y aquellos anestésicos fijos que actúan sobre receptores GABA como el Propofol y barbitúricos) y el sueño No-REM (Murphy *et al.*, 2011; Vanini *et al.*, 2011; Vacas *et al.*, 2013; Pal *et al.*, 2016). Otros anestésicos como la ketamina, un inhibidor de los receptores NMDA provocan características electroencefalográficas distintas del sueño No-REM y que se asemejan más al sueño REM (Akeju *et al.*, 2016; Castro-Zaballa *et al.*, 2018). De hecho, se ha demostrado que la administración intercalada de Propofol y ketamina imita las dinámicas del sueño fisiológico con características de sueño No-REM y REM respectivamente (Guang *et al.*, 2021). Sin embargo, el único anestésico que es capaz de generar una actividad electroencefalográfica cíclica, entre episodios similares a sueño No-REM y episodios similares a sueño REM es el uretano (etil carbamato) (Clement *et al.*, 2008). Sin embargo, algunos autores proponen que el estado similar al sueño REM, es, en realidad, un estado semejante a la vigilia (Pagliardini *et al.*, 2013; Neves *et al.*, 2018). La hipótesis de este trabajo fue que la anestesia con uretano tanto en su estado de ondas lentas como su estado activado presenta correlatos electrofisiológicos de inconsciencia y que es similar al sueño natural. En el artículo evaluamos en detalle diferentes características electroencefalográficas presentes durante la anestesia con uretano y los comparamos con los estados de sueño natural. Además, hicimos especial foco en los correlatos neurales de pérdida de consciencia para determinar si durante el estado similar al REM o activado bajo anestesia con uretano, existe realmente pérdida de consciencia. Como mencionamos, a pesar de que diversos anestésicos pueden generar un patrón

electroencefalográfico distinto (como por ejemplo el propofol y la ketamina), todos comparten con el sueño determinados correlatos de pérdida de consciencia (Pal *et al.*, 2016) por ejemplo, la caída de coherencia y conectividad fronto-parietal de la banda de frecuencia gamma así como la disminución de la complejidad del EEG (Hudetz *et al.*, 2016; Wang *et al.*, 2017; Mashour & Hudetz, 2018).

Urethane Anesthesia Exhibits Neurophysiological Correlates of Unconsciousness and is Distinct from Sleep

Alejandra Mondino[1], Joaquín González[1], Duan Li[2,3,4], Diego Mateos[5,6], Lucía Osorio[1], Matías Cavelli[1,7], Alicia Costa[1], Giancarlo Vanini[2,3,4], George Mashour[2,3,4], Pablo Torterolo[1]*

1. Departamento de Fisiología, Facultad de Medicina, Universidad de la República, 11800, Montevideo, Uruguay

2. Department of Anesthesiology, University of Michigan, Ann Arbor, Michigan 48109-5615.

3. Center for Consciousness Science, University of Michigan, Ann Arbor, Michigan 48109.

4. Neuroscience Graduate Program, University of Michigan, Ann Arbor, Michigan 48109-2215.

5. Instituto de Matemática Aplicada del Litoral–CONICET–UNL, CCT CONICET, Santa Fe, Argentina.

6. Facultad de Ciencia y Tecnología, Universidad Autónoma de Entre Ríos, Entre Ríos, Argentina.

7. Department of Psychiatry, University of Wisconsin, 6001 Research Park Blvd, Madison, WI 53719, USA

* Correspondence: Dr. Pablo Torterolo

Email: ptortero@fmed.edu.uy

Abstract

Urethane is a general anesthetic widely used in animal research. It is unique among anesthetics because urethane anesthesia alternates between macroscopically distinct electrographic states: a slow-wave state that resembles NREM sleep (NREMure), and an activated state with features of both REM sleep and wakefulness (REMure). However, the relationship between urethane anesthesia and physiological sleep is still unclear. In this study, electroencephalography (EEG) and electromyography were recorded in chronically prepared rats during natural sleep-wake states and during urethane anesthesia. We subsequently analyzed the EEG signatures associated with the loss of consciousness and found that, in comparison to natural sleep-wake states, the power, coherence, directed connectivity and complexity of brain oscillations are distinct during urethane. We also demonstrate that both urethane states have clear EEG signatures of general anesthesia. Thus, despite superficial similarities that have led others to conclude that urethane is a model of sleep, the electrocortical traits of depressed and activated states during urethane anesthesia differ from physiological sleep states.

Keywords: sleep, NREM, REM, paradoxical sleep, anesthesia, consciousness, awareness

Introduction

Urethane is an anesthetic that is widely used in animal research because of its unique characteristics. It induces long-term narcosis and immobilization with minimal effect on physiological variables (Maggi & Meli, 1986). Furthermore, it produces a spontaneous cycle between two different states: one characterized by slow wave oscillations in the electroencephalogram (EEG), similar to natural non-rapid eye movements (NREM) sleep, and an activated state with rhythmic activity in the slow theta range that qualitatively resembles the EEG pattern either of wakefulness (W) or REM sleep (Détári & Vanderwolf, 1987; Murakami *et al.*, 2005; Pagliardini *et al.*, 2013; Yagishita *et al.*, 2020). Because of the resemblance to a sleep cycle, urethane anesthesia has been proposed as a pharmacological model to study sleep (Horner & Kubin, 1999; Clement *et al.*, 2008; Pagliardini *et al.*, 2013).

Whether the activated state of urethane anesthesia reflects a wake-like or a REM sleep-like state remains an open question. On the one hand, some authors have proposed that this state corresponds to a reduced level of anesthesia (or a W-like state) because nociceptive stimuli evoke a shift from the NREM-like state to the activated state (Pagliardini *et al.*, 2013; Neves *et al.*, 2018). Other findings supporting this hypothesis are that rapid eye movements do not occur during the activated state and increasing doses of urethane decrease the relative amount of time spent in that state well as that (Clement *et al.*, 2008). In addition, while midline thalamic neuronal firing increases during REM sleep (up to five times higher in comparison to NREM sleep), this increase was less pronounced during the activated urethane state compared to the NREM-like state (Hay, 2021). On the other hand, there is evidence that this activated state resembles REM sleep, including: 1) there are no differences between both urethane states in a withdrawal response to a noxious stimulus (Clement *et al.*, 2008); 2) the

alternation between the activated and NREM-like state under urethane anesthesia resembles the natural NREM and REM sleep cycle (Clement *et al.*, 2008; Pagliardini *et al.*, 2013); 3) muscle tone is reduced during the activated state in comparison to the NREM-like state (Clement *et al.*, 2008); and 4) there is a similar modulation of breathing between the REM-like state and REM sleep (Pagliardini *et al.*, 2012).

In the past years, behavior-independent measures of consciousness and unconsciousness have been developed (Mashour & Hudetz, 2018), providing a novel opportunity to study urethane states. For instance, neural oscillations differ between conscious and unconscious states. Specifically, gamma oscillations (30-150 Hz), hypothesized to relate to cognitive processes, appear during W and REM and are reduced during NREM or anesthesia (Hudetz *et al.*, 2011; Cavelli *et al.*, 2015; Mondino *et al.*, 2020). Conversely, delta oscillations (0.1-4 Hz) occur both during NREM and anesthesia, possibly disrupting the neural interactions supporting consciousness (Steriade *et al.*, 1993; Pigorini *et al.*, 2015; Tononi *et al.*, 2016; Arena *et al.*, 2021). In addition, synchronization between high frequency neural oscillations at different brain areas is another major correlate of consciousness (Varela *et al.*, 2001; Melloni *et al.*, 2007). Gamma oscillations are synchronous during alert and awake states, but they decouple during NREM, anesthesia and even REM sleep (Lee *et al.*, 2013; Cavelli *et al.*, 2015; Pal *et al.*, 2016; Castro-Zaballa *et al.*, 2018; Mondino *et al.*, 2020). The directionality of the connectivity is another important feature to consider, as feedforward and feedback interactions between anterior and posterior cortices decrease during sleep and different anesthetics (Pal *et al.*, 2016). Finally, the complexity of brain oscillations changes between conscious and unconscious states, suggesting that complex neuronal interactions are necessary for awareness (Schartner *et al.*, 2015; Mateos *et al.*,

2017; Schartner *et al.*, 2017; Demertzi *et al.*, 2019; Gonzalez *et al.*, 2019; Gonzalez *et al.*, 2020; Sarasso *et al.*, 2021).

In the present report, we characterize the EEG correlates of urethane anesthesia. Specifically, we compared electrocortical activity (power, coherence, directionality and complexity) between physiologic sleep-wake states and NREM-like urethane (NREMure) and REM-like urethane (REMure) states of anesthesia. We found that the urethane states show a consistent decline in the EEG correlates of consciousness, suggesting that—despite the cyclic alternation between EEG profiles—urethane induces sustained unconsciousness. In addition, we demonstrate well-defined EEG differences between NREMure and REMure and their correspondent sleep state. Based on these differences we conclude that, despite superficial similarities, urethane anesthesia is not an accurate model of sleep.

Materials and Methods

Experimental animals

Nine Wistar male adult rats (270–300 g) were studied. Veterinarians of the institution certified that the rats were in good health at the time of the study. All experimental procedures were conducted in agreement with the National Animal Care Law (#18611) and with the "Guide for the care and use of laboratory animals" (8th edition, National Academy Press, Washington, DC, USA, 2010). Furthermore, the Institutional Animal Care Committee approved the experimental procedures (No 070153-000332-16). Adequate procedures were taken to minimize animals' pain, discomfort, and stress.

We utilized the minimum number of animals necessary to acquire reliable scientific information. The rats were housed in groups of four to five per cage prior to

the experiments. Before and during the experiments they were kept in a temperature-controlled (21–24 ◦C) room, on a 12:12 h light/dark cycle (lights on at 6.00 a.m.) with food and water available *ad libitum*.

Surgical Procedures

We employed the same surgical procedure that we used in our previous studies (Gonzalez *et al.*, 2018; Mondino *et al.*, 2019; Mondino *et al.*, 2020). Anesthesia was induced with a combination of ketamine and xylazine (90 mg/kg; 5 mg/kg, i.p., respectively). Ketoprofen, 1 mg/kg subcutaneous was administered to provide analgesia. Rats were positioned in a stereotaxic frame; the skull was exposed, and seven stainless-steel screw electrodes were implanted in the skull in order to record the intracranial EEG or electrocorticogram. The electrodes were localized above the right and left primary motor cortex (M1), primary somatosensory cortex (S1) and secondary visual cortex (V2). Another electrode was placed in the right olfactory bulb (OB). Finally, a reference electrode was implanted in the cerebellum. The electromyogram (EMG) was recorded by means of a bipolar electrode inserted into the neck muscles. A representation of the electrode positions is shown in Figure 1A. The electrodes were soldered to a socket and fixed to the skull with dental cement. A topical antibiotic was applied to the margins of the incision. Animals were allowed to recover from the surgical procedure for seven days. Thereafter, they were housed independently in transparent cages (40 × 30 × 20 cm) and habituated for five days to the recording condition in a sound-attenuated chamber.

Sleep Recordings

Experimental sessions were performed between 9:00 AM and 1:00 PM. The recordings were carried out using a rotating connector that allows the rats to freely move within the recording chamber. Bioelectric signals were amplified (×1000), band-pass filtered (0.1–500 Hz), sampled (1024 Hz, 16 bits) and acquired using using DASYlab, (National Instruments, Austin, TX, US).

Baseline polysomnographic recordings were performed for two hours. Thereafter, the rats were anesthetized with urethane (1.2 to 1.5 g/kg, i.p.), and recorded for another two hours. During anesthesia, animals were warmed with a heating pad at 37ºC. Video recordings were also performed during the recording sessions.

States of W, NREM and REM sleep were manually scored using Spike 2 software version 9.04 (Cambridge Electronic Design, Cambridge, UK) in 5s epochs. W was defined by low-amplitude, high-frequency EEG activity accompanied by high EMG activity. NREM sleep was defined by high-amplitude slow waves as well as sleep spindles associated with a reduced muscular tone, while REM sleep was identified by low-amplitude, fast waves with a regular theta rhythm, particularly in the posterior cortex, and by an EMG atonia except for occasional twitches. During urethane anesthesia two states were defined according to the EEG profile. NREMure displayed high-amplitude low-frequency EEG similar to NREM sleep, whereas REMure was characterized by low-amplitude and high-frequency EEG associated with regular theta rhythm. These states were also scored in 5s epochs. We determined the total time spent in each state as well as the number and duration of epochs.

EEG signal analysis

We analyzed all EEG epochs without artifacts or state transitions. The frequency bands were defined as delta (1-4 Hz), theta (4-10 Hz), sigma (10-15 Hz), Beta (15-30

Hz), low gamma (LG, 30-45 Hz), high gamma (HG, 55-95 Hz) and high frequency oscillations (HFO, 105-145, and 155-195 Hz). Frequencies around the alternating current (50 Hz in Uruguay) and harmonics were excluded from the analysis.

The power spectrum was calculated by means of the *pwelch* built-in function on Matlab (version 2020a; MathWorks, Inc., Natick, MA) with a 5s window size, half-window overlap, frequency sample of 1024 Hz and a resolution of 0.5 Hz. Absolute power values were normalized for each animal as the mean power of each frequency band divided by the total power (i.e., sum of the power of each frequency band) (Mondino *et al.*, 2020; González *et al.*, 2021). Spectral coherence was determined as a measure of undirected functional connectivity between EEG electrodes (Bullock & McClune, 1989), using the same procedure as Mondino et al. (2020). We determined the coherence between interhemispheric and intrahemispheric adjacent electrodes (the distance between neocortical contiguous electrodes was 5 mm). The *mscohere* built-in Matlab function was employed for this analysis with a 5s window size, half-window overlap, frequency sample of 1024 Hz and a resolution of 0.5 Hz. Coherence values were normalized by the Fisher's z-transform to get the z'coherence. For the power and coherence analysis, the rOB, rV2, lM1 and lS1 had to be excluded in one rat during the baseline recordings, and rV2 and lM1 during anesthetized recordings due to artifacts that made processing unfeasible. Additionally, rS1-rV2 z'coherence of another rat was excluded from the analysis because it was a clear outlier with extremely high values for all the frequency bands.

Normalized symbolic transfer entropy (NSTE) was used to determine directed connectivity between the rM1 (anterior) and rV2 (posterior) cortices (Borjigin *et al.*, 2013; Lee *et al.*, 2013; Pal *et al.*, 2016). rM1 and rV2 EEG signals were filtered into the frequency bands described above and segmented into non-overlapped 5s windows. We

used the same strategy for parameter selection as in our previous studies (Li *et al.*, 2017; Mondino *et al.*, 2021). The embedding dimension was fixed at dE = 3 and we used the time delay (τ) = 128, 51, 34, 17, 11, 5, 3 corresponding respectively to delta, theta, sigma, beta, LG, HG and HFO. In every window, we examined the transfer time (δ) = 1-100 (corresponding to 1-100 ms approximately) and chose the one that generated the maximum feedback (anterior to posterior) and feedforward (posterior to anterior) NSTE, respectively.

Finally, we evaluated the complexity of the EEG signal by means of Lempel-Ziv Complexity (LZC) (Lempel & Ziv, 1976). This is an information theoretic measure based on Kolmogorov complexity, that calculates the minimal "information" contained in the sequence (Cover & Thomas, 2006). LZC has been shown to be an important tool to explore the temporal complexity of brain activity (Schartner *et al.*, 2015; Hudetz *et al.*, 2016). To estimate the complexity of a time series $\mathcal{X}(t) \equiv \{x_t; t = 1, \cdots, T\}$, a sequence $X(t)$ is parsed into a number of words W by considering any subsequent series that has not yet been encountered as a new word. The LZC c_{LZ} is the minimum number of W required to reconstruct the information contained in the original time series. Continuous sequences such as an EEG signal, need to be discretized to analyze LZC. Different methods can be employed for this purpose and could lead to slightly differing results. In this work, we employed the binarization by mean-value (referred to as bin LZC) to calculate the complexity of each EEG channel. Although Lempel and Ziv originally developed the method for binary sequences, this approach can be easily generalized to multivariate discrete processes by extending the alphabet size (Zozor *et al.*, 2005). Consider an m-dimensional stationary process $X(m)$, that generates the sequences $x_{t,i} = x_{1,i}, \ldots, x_{T,i}$ with $i = 1, \ldots, m$ each one of them from an alphabet of α

symbols. Let $z_t = z_1, \ldots, z_T$ to be a new sequence defined over an extended alphabet of size α_m

$$z_t = \sum_{i=1}^{m} \alpha^{i-1} x_{t,i}$$

Using this approach, we also calculated the global complexity of neurophysiologic activity, referred as joint Lempel–Ziv complexity (JLZC) of the x_i-sequence as the complexity of the new sequences z_t $C_{LZ}(x_{t,i}) = C_{LZ}(z_t)$. In this case, $x_{i,t}$ is the EEG signal per channel and z_t is a new sequence that represents the information from all channels. The JLZC was binarized ($\alpha = 2$) using the mean value (Zozor *et al.*, 2005).

Statistical analyses

Statistical analyses were done with PRISM v9.0 (GraphPad Software Inc., La Jolla, CA). All data were presented as mean ± standard error of the mean (SEM). Comparisons between W, NREMure and REMure were performed by means of a repeated measures one-way ANOVA and Holm-Sidak as a *post hoc* test; adjusted p value < 0.05 was considered significant. Two-tailed paired Student t tests were used to determine differences between NREM and NREMure as well as REM and REMure. p values were also corrected for multiple comparisons using Holm-Sidak test.

Results

Rats under urethane anesthesia cycle between two different states

A representative hypnogram, spectrogram (power spectrum as a function of time), as well as the EEG recordings of baseline and following urethane anesthesia during two hours of recordings are shown in Figure 1B. During baseline, rats exhibit the

states of W, NREM and REM sleep, while under urethane anesthesia they cycled between two different states, a slow wave activity state (NREMure), and an activated state (REMure). In Figure 1C, the distinctive characteristics of the EEG and EMG of each state can be observed. Although muscle activity in most of the rats was higher in REMure than during NREMure, no difference in the EMG power was observed when the whole population was analyzed (Figure 1D). As can be appreciated in Figure 1E-G during the baseline recordings rats spent 2702 ± 422.6 s (37.52% of the total time) in W, 3977 ± 367.8 s (55.23%) in NREM sleep and 522 ± 76.52 s (7.25%) in REM sleep. If we consider the total amount of sleep, NREM sleep represented 88.4% while REM sleep represented 11.6%. In average, the number of bouts of W was 32.78 ± 3.79 with a mean duration of 21.45 ± 7.08 s, the number of NREM bouts was 33.78 ± 4.15 with a duration of 24.65 ± 1.82 s, and the number of REM bouts was 6.44 ± 1.23 and lasted 17.58 ± 2.36 s. After urethane injection, rats spent a similar amount of time in NREMure and REMure; 3292 ± 434.15 s (45.73% of total time) and 3908 ± 434.15 s (54.27%), respectively [$t(8) = 0.708$; $p = 0.4985$]. The number of bouts of NREMure was 33.78 ± 7.63, and of REMure 33.67 ± 7.59 [$t(8) = 0.00$; $p > 0.9999$]. There was no difference in bout duration between the two states (35.54 ± 37.32 s for NREMure and 42.60 ± 14.36 for REMure [$t(8) = 1.067$; $p = 0.3172$]).

Urethane increases low and decreases high frequency bands of the EEG

To study brain oscillations, we analyzed the EEG power spectrum from OB, M1, S1 and V2. We compared both urethane states to the physiological W to identify EEG features of unconsciousness during urethane (Figure 2A). Detailed statistics are shown in Supplementary Table 1. We found that delta oscillations increased in all cortical locations during NREMure compared to either REMure or W. In addition, W had more

power in the rest of the bands compared to NREMure. This can be fully appreciated looking at low-gamma, high-gamma and HFO bands, which decrease in all cortical locations during NREMure. In contrast, the distinction between W and REMure was less marked, and was evidenced by a power decrease in the frequencies above low-gamma. In particular, HFOs decreased during REMure in all cortical locations (significant in OB, M1 and S1), while low and high gamma also significantly decreased in M1 and S1. We also observed a noticeable decrease in the theta peak frequency during REMure compared to W and REM [Mean ± SEM, 4.75 ± 0.16 for REMure, 6.87 ± 0.12 for REM sleep, and 6.94 ± 0.15 for W; [$F(2,7) = 79.40$, $p < 0.0001$]. For this analysis, we calculated the differences between the maximum value in each state in V2, where theta oscillations are fully expressed.

Next, we compared both urethane states to study how the various brain oscillations differ between them; statistics are shown in Supplementary Tables 1 and 2. Importantly, we found that delta power was higher during NREMure in all locations. Similar to W, REMure showed higher power in all frequency bands above delta, which was significant for theta in OB, M1, S1; for sigma in S1; and for Beta, LG, HG and HFO in all locations except for HFO in the visual cortex.

To complete the characterization of brain oscillations under urethane anesthesia, we compared each urethane state to its physiological analog; i.e, NREMure vs NREM, and REMure vs REM. Statistics are shown in Supplementary Table 3. Comparing each pair, we found that delta oscillations are larger under both urethane states compared to their physiological counterparts in all cortical sites. The rest of the frequency bands showed a tendency to decrease under urethane. For instance, all bands (>delta) were reduced in NREMure compared to NREM (except for HG and HFO in V2), the same

occurred comparing REMure to REM; the exception was HFO in the neocortex as well as beta and gamma bands in V2.

In summary, urethane promotes slow delta oscillations, while reducing higher frequency bands, especially gamma and HFOs.

Urethane alters corticocortical synchronization

For a more complete characterization of urethane's neurophysiological correlates, we analyzed the spatial synchronization between neural oscillations. We first analyzed the interhemispheric z'coherence comparing between W and the urethane states (Figure 3A). The complete statistical analysis is shown in Supplementary Table 4A and 5. We found that during NREMure, the inter-hemispheric delta coherence increased with respect to the other states, which was significant in rM1-lM1 comparing NREMure to REMure or W, and rS1-lS1 comparing NREMure to W. Moreover, higher frequency bands were more coherent during W than during both urethane states. For instance, rS1-lS1 theta and sigma coherences decreased during REMure compared to W, while rS1-lS1 HG and HFO decreased for both urethane states compared to W.

Comparing each urethane state to its natural analog, we found differences suggesting that inter-hemispheric synchronization is compromised compared to physiological sleep states. Details of these statistics are shown in Supplementary Table 7. Comparing NREMure to NREM, we found that theta, sigma and beta coherences decreased in both rS1-lS1 and rV2-lV2, and that LG and HG coherences decreased in rS1-lS1 (Figure 3B). The REMure vs REM comparison showed that theta and sigma oscillations are also less coherent during REMure in rS1-lS1 and rV2-lV2 (Figure 3C).

To more fully characterize how urethane alters cortical synchronization, we also studied the intra-hemispheric z'coherence between adjacent electrodes on the right

hemisphere. We found that delta coherence increased for both urethane states in OB-M1 compared to W. Moreover, HG coherence between M1-S1 and S1-V2 decreased during NREMure compared to W, while HFO S1-V2 coherence also decreased during both urethane states compared to W (Figure 4A). When we compared each urethane state to its analog, we found no significant differences (Figure 4B and C).

Thus, these results show that urethane promotes synchronized delta waves between areas, while higher frequency synchronization, such as gamma, decreases during both urethane states.

Urethane compromises feedback connectivity

To evaluate the directed connectivity between the rM1 (anterior) and rV2 (posterior) cortices, we calculated feedback and feedforward NSTE for each frequency band. As is illustrated in Figure 5, when comparing W to the anesthetized states, both feedback and feedforward NSTE were affected by behavioral states in the theta frequency band [$F(2,8) = 9.523$, $p = 0.0081$ and $F(2,8) = 7.433$, $p = 0.017$ respectively]. NREMure had a lower connectivity than W and REMure in both feedback ($p = 0.049$ and 0.026, respectively) and feedforward directions ($p = 0.029$ and 0.002, respectively). No differences were found between W and REMure for feedback or feedforward connectivity ($p = 0.140$ and 0.499 respectively). Additionally, feedback but not feedforward connectivity was affected by the states in HG frequency band [$F(2,8) = 6.620$, $p = 0.0136$ and $F(2,8) = 0.783$, $p = 0.425$, respectively]. W feedback NSTE was higher than REMure ($p = 0.049$) but not than NREMure ($p = 0.140$). Lastly, both anesthetized states did not differ in HG feedback NSTE ($p = 0.361$). Delta, sigma, beta, LG and HFO frequency bands did not show differences between W and the anesthetized states neither for the feedback NSTE [$F(2,8) = 4.536$, $p = 0.055$, $F(2,8) = 2.436$, $p =$

0.150, F(2,8) = 1.056, p = 0.348, F(2,8) = 0.344, p = 0.621 and F(2,8) = 3.522, p = 0.078 respectively] nor for the feedforward NSTE [F(2,8) = 0.077, p = 0.827, F(2,8) = 4.479, p = 0.063, F(2,8) = 0.601, p = 0.487, F(2,8) = 0.739, p = 0.459 and F(2,8) = 3.509, p = 0.077 respectively].

When comparing the anesthetized states with its analogous state during sleep, we did not see any differences in feedback or feedforward connectivity. The statistics are shown in Supplementary Table 9.

Urethane decreases EEG complexity

We studied the complexity of the EEG signal during each state by means of the binarized Lempel Ziv Complexity (LZC). First, we analyzed the complexity of the whole signal (1-195 Hz). In all the electrode locations the ANOVA showed significant differences between W and urethane states [rOB. F (2,7) = 25.48 p = 0.0002], [rM1 F (2,8) = 46.53 p <0.0001], [rS1 F (2,8) = 69.89 p <0.0001] and [rV2 F (2,8) = 64.02 p = <0.0001]. As can be observed in Figure 6A, in rOB, rM1, rS1 and rV2 the complexity of the EEG signal during NREMure was lower than during W (p = 0.0022, <0.0001 and <0.0001, respectively) and REMure (p = 0.0036, 0.0004, <0.0001 and <0.0001, respectively). Additionally, W had a higher complexity than REMure in rOB, rM1 and rS1 (p = 0.0064, 0.0139 and 0.0042, respectively) but not in rV2 (p = 0.0849). When comparing the NREMure with NREM sleep, no differences in complexity were found in any of the electrode locations (rOB p = 0.1038, rM1 p = 0.0691, rS1 p = 0.6627, rV2 p = 0.0835). The same occurred between REMure and REM sleep (rOB p = 0.4280, rM1 p = 0.5359, rS1 p =0.2824, rV2 p = 0.3638). Because sleep is characterized by slow oscillations, we measured the LZC for the signal between 1 to 15 Hz. Like the whole signal analysis, the ANOVA showed significant differences between W and the

anesthetized states [rOB F (2,7) = 13.75 p = 0.0007], [rM1 F (2,8) = 43.30 p = <0.0001], [rS1 F (2,8) = 94.97, p <0.0001] and [rV2 F (2,8) = 71.90, p <0.0001]. In all cortical areas NREMure had a lower complexity than W (rOB p = 0.0027, rM1 p <0.0001, rS1 p <0.0001, rV2 p <0.0001) and REMure (rOB p = 0.0144, rM1 p = 0.0036, rS1 p = 0.0005 and rV2 p = 0.0007). In addition, W had a higher complexity than REMure in rM1 (p = 0.0004), rS1 (p <0.0001) and rV2 (p = 0.0001) but not in rOB (p = 0.5278). Additionally, we compared the complexity during the anesthetized states and in analogous states during sleep, observing clear differences between them. For instance, NREMure had lower complexity in the low frequency oscillations than NREM sleep in all electrode locations (rOB p = 0.0007, rM1 p <0.0001, rS1 p <0.0001 and rV2 p <0.0001). Similarly, REMure had lower complexity than REM sleep (rOB p = 0.0008, rM1 p <0.0001, rS1 p <0.0001 and rV2 p <0.0001).

Thus, unlike directed connectivity measures, complexity analysis distinguished between physiological sleep and urethane-induced states.

Urethane disrupts whole-brain complexity

Finally, to understand how the complexity of the EEG signal within the whole brain varies between states, we computed a joint Lempel Ziv for 1–195 Hz and for 1 – 15 Hz. The results are displayed in Figure 7. ANOVA demonstrated a clear difference between the complexity during W and the anesthetized states for 1 – 195 Hz F(2,8) = 82.63 p < 0.0001. W had a higher complexity than NREMure p < 0.0001and REMure p = 0.0099. Also, REMure had a higher complexity than NREMure (p = < 0.0001). Similar results were found for the 1 – 15 Hz oscillations F(2,8) = 55.27 p < 0.0001. W had a higher complexity than NREMure p < 0.0001 and REMure p = 0.0099. Furthermore, REMure had a higher complexity than NREMure (p < 0.0009).

Differences between sleep states and anesthetized states were seen for the 1 - 15 Hz analysis NREM sleep had higher complexity than NREMure ($p = 0.0002$), and REM sleep had higher complexity than REMure ($p < 0.0001$). For the 1 – 195 Hz analysis these differences were lost (NREM sleep vs NREMure $p = 0.2125$, and REM sleep vs REMure $p = 0.1693$).

Discussion

We performed an extensive analysis of the EEG signal during urethane anesthesia. We demonstrated that, in comparison to W, the EEG signal quantified by different metrics is significantly modified during both urethane-induced states, i.e., NREMure and REMure. In addition, while urethane anesthesia resembles natural sleep, the EEG profiles under urethane anesthesia and sleep are not the same. This brings into question whether urethane can serve as a pharmacological model for sleep.

General features of urethane-induced states

Urethane evokes a cycle between two states that resemble natural sleep states. However, despite the shared phenotype, our EEG analysis suggests that the underlying oscillations and neurobiology of sleep and urethane anesthesia are different. REMure did not show the characteristic muscle atonia that occurs in REM sleep. In fact, no differences were observed between the two anesthetized states in the total power of the EMG (Figure 1D). This finding is in disagreement with the finding of Clement *et al.* (2008), that observed a decreased EMG signal during REMure in comparison with NREMure (Clement *et al.*, 2008). Horner and Kubin (1999) demonstrated that the microinjection of carbachol into the pontine reticular formation potentiates the REM-like state in rats anesthetized with urethane, evoking clear muscle atonia (Horner &

Kubin, 1999); however, when those rats were sensory stimulated (pinch in the hindlimb) they showed an EEG with theta oscillations similar to REM sleep but with an increase in muscle tone.

We have demonstrated that urethane anesthesia and physiological sleep differ in the duration of the alternating cycles (Figure 1 E, F and G). In the natural sleep cycle, REM sleep represented 11.6% of the total time, while NREM represented 88.4%. During the anesthetized states, the time spent in NREMure and REMure was almost evenly divided at 45.73% Vs. 54.27%, respectively. This was due to equivalent number and duration of bouts in each state. This is in accordance with other studies that found similar amounts of REMure and NREMure during urethane anesthesia (Pagliardini *et al.*, 2012). Interestingly, Clement et al. (2008) found that an increase in the depth of anesthesia reduces the time spent in REMure while the cyclicity is maintained (Clement *et al.*, 2008).

EEG during urethane anesthesia

We determined that urethane anesthesia affects the spectral power of the EEG in different frequency bands. Clear differences were found between W and the anesthetized states. Compared to the waking state, NREMure had a large increase in delta power as well as a reduction in power across all other frequency bands (theta, sigma, beta, LG, HG and HFO). Additionally, W was characterized by a higher power than REMure, especially in the higher frequency bands (HFO in rOB, rM1, rS1; HG and LG in rM1 and rS1 and beta in rS1). This is particularly interesting because higher frequency bands have been associated with consciousness and cognitive processing (Kucewicz *et al.*, 2014; Pal *et al.*, 2016; Castro-Zaballa *et al.*, 2018).

The spectral power during NREMure also differs from physiological NREM sleep. Lower delta was higher in NREMure, while at approximately 3 Hz, NREM sleep had similar or even higher power than NREMure. Since EEG oscillations follow a power-law scaling, by which slower oscillations have higher power values (Miller *et al.*, 2009), it is possible that during NREMure there was a shift in the peak frequency of the delta oscillations, with slower delta waves during the anesthetized states in comparison with natural NREM sleep. Interestingly, while delta oscillations during anesthesia with propofol or isoflurane have been shown to have a similar amplitude than NREM sleep delta oscillations (Murphy *et al.*, 2011; Akeju & Brown, 2017), the frequency of delta oscillations is slower during anesthesia with ketamine and medetomidine (Torao-Angosto *et al.*, 2021).

On the other hand, the power of higher frequency bands was higher in NREM sleep in most cortical locations (see below). Sigma band (10-15 Hz) encompasses the frequency range of sleep spindles, a characteristic electroencephalographic feature of NREM sleep. In fact, NREM sleep is characterized by a higher sigma power than W and REM sleep (Mondino *et al.*, 2020). In this study, NREMure showed lower sigma power values than NREM sleep (Figure 2B) and lower than REMure (Figure 2A). Interestingly, Murphy *et* al. (2011) showed in humans that while NREM sleep and propofol anesthesia EEG characteristics shared several similarities, propofol failed to effectively generate spindles (Murphy *et al.*, 2011). In the present study the number and duration of sleep spindles was not calculated, but Clement et al. (2008) showed that sleep spindles did occur during urethane anesthesia (Clement *et al.*, 2008). However, this study found that spindles occur more frequently during transitions between NREMure and REMure, which is also seen during spontaneous NREM-REM transitions

(Bandarabadi *et al.*, 2020). These transitional epochs were not considered in the present study.

When comparing REMure with REM sleep, we found that delta power was higher during REMure. It is interesting that in both states of urethane, delta power was higher than during their analogous state in the physiological sleep. Of note, an increase in delta oscillations characterizes general anesthesia with GABA agents (Hagihira, 2015; Mondino *et al.*, 2020). On the contrary, the power of most other frequency bands was larger in REM sleep than in REMure, mainly in anterior locations. This could be related to the intense cognitive processing associated with sleep and possibly related to memory consolidation.

We observed a clear decrease of the peak of the theta band frequency under REMure. In fact, Fenik and Kubin (2009) have already described that hippocampal theta-like rhythms had a lower frequency range in rats anesthetized with urethane (3-5 Hz) than in awake rats (6-8 Hz); however, Dringenber and Vanderwolf (1998) and Vertes (1984), suggested that these rhythms are generated by similar neuronal networks and that can be triggered by similar stimuli (Vertes, 1984; Dringenberg & Vanderwolf, 1998; Fenik & Kubin, 2009). Clement et al. (2008) found that the spindles under urethane anesthesia also have a lower frequency (≈8Hz; i.e., in the theta frequency band range) than physiological sleep spindles (Clement *et al.*, 2008). However, the mechanisms of the reduction in the theta or spindles frequency are not understood. Our results are consistent with previous studies identifying a decreased frequency of hippocampal theta during isoflurane anesthesia (Perouansky *et al.*, 2007; Mashour *et al.*, 2010)

Additionally, we observed a decrease in power of the high frequency oscillations in both NREMure and REMure. This finding is typically associated with

NREM sleep and general anesthesia with isoflurane, but not with ketamine (a NMDA receptor antagonist) (Kortelainen *et al.*, 2012; Akeju *et al.*, 2016; Castro-Zaballa *et al.*, 2018; Mondino *et al.*, 2020). Of note, a clear peak in HFO power, suggesting a true HFO oscillation during REM sleep have been described in the OB and posterior cortices (Cavelli *et al.*, 2018; Mondino *et al.*, 2020).

We also analyzed the inter and intra-hemispheric coherence. When comparing W and both anesthetized states, delta z'coherence was larger in NREMure, primarily for interhemispheric derivatives, suggesting the presence of synchronized slow wave activity in both hemispheres. By contrast, high frequency (HG and HFO) z'coherence was larger during W reaching significance for S1 interhemispheric, M1-S1 and S1-V2 (only for gamma) derivatives. Interestingly, high frequency z'coherence is lost during both GABA agents and ketamine general anesthesia (Purdon *et al.*, 2013; Pal *et al.*, 2015), as well as during NREM and REM sleep (Cavelli *et al.*, 2015; Cavelli *et al.*, 2017; Castro-Zaballa *et al.*, 2018).

We also analyzed the anteroposterior (rM1–rV2) directed connectivity by means of NSTE. We demonstrated that under NREMure there was a decrease of theta connectivity both in FF and FB direction. Furthermore, in comparison to W, REMure showed a reduction of HG band connectivity in the FB directionality but not in the FF, which is consistent with the reduction or loss in gamma FB transfer entropy during sleep and anesthesia with different agents (Lee *et al.*, 2013; Pal *et al.*, 2016; Li *et al.*, 2017).

EEG complexity was also analyzed using the Lempel-Ziv algorithm. Compared to W, LZC was reduced in most cortical locations in both anesthetized states; the decrease in complexity was larger during NREMure than REMure, similar to what has been shown to occur with physiological sleep states (Abásolo *et al.*, 2015). In addition,

when only low frequencies (1-15 Hz) were analyzed, NREMure and REMure had reduced complexity in comparison to their analogous natural states. In this regard, Gonzalez et al. (2019) have shown that complexity, assessed by permutation entropy, is higher during W than both sleep states (Gonzalez *et al.*, 2019). Furthermore, EEG complexity decreases under general anesthesia (Zhang *et al.*, 2001; Hudetz *et al.*, 2016). Notably, in comparison to W, we also found a decrease in complexity during NREMure and REMure assessed by permutation entropy (data not shown).

We also introduced the novel analysis of JLZC, which provides a broader view of cortical complexity. For example, homogenous cortical activity results in low JLZC while the opposite occurs when the activity is differentiated across cortical areas. This analysis showed that, in comparison to W, JLZC decreases during both anesthetized states, but the decrease is larger during NREMure (Mateos *et al.*, 2017). Moreover, if we isolated low-frequency activity, JLZC is lower under urethane in comparison to the analogous natural sleep states. Interestingly, Mateos et. al (2017) analyzed standard EEG in humans and found that, at low frequencies (4-12 Hz), JLZC was lower during NREM than during W, but JLZC during REM sleep was similar or even higher than during W. This could be associated with the cognitive processes that takes place during REM sleep (Hobson, 2009). These authors also found that JLZC was exceptionally low during comatose states and epileptic seizures with loss of consciousness, showing that JLZC is an important candidate as a correlate of consciousness. According to these findings, we could assume that the state of consciousness is reduced during urethane anesthesia in comparison with its analog during sleep. To our knowledge, this is the first report of the effect of an anesthetic on JLZC.

EEG correlates of consciousness are lost in urethane anesthesia

The concept of "neural correlates of consciousness" (NCC) represents the minimal set of neural events and structures sufficient to generate any kind of experience (Koch *et al.*, 2016; Mashour & Hudetz, 2018; Torterolo *et al.*, 2019; Sarasso *et al.*, 2021). In a very schematic way, the main EEG correlates of W consciousness, and the modifications under NREMure and REMure are listed in Table 1. W presents a relative low delta, as well as high gamma and HFO power and coherence in the EEG. While all these signatures are altered by NREMure, under REMure high frequency oscillations power and coherence are lost in most cortical locations and derivates. During REMure there was a decrease in the HG FB directionality of the signal, a feature that has been established as a correlate of loss of consciousness (Pal *et al.*, 2016). Interestingly, while the values during NREMure were lower than during W, significance was not achieved. Finally, high EEG complexity also characterizes normal W and is decreased during both NREMure and REMure; high complexity is also considered a marker of consciousness (Abásolo *et al.*, 2015; Mateos *et al.*, 2017). Hence, EEG features strongly suggest that urethane produces unconsciousness not only under NREMure, that have similarities with the EEG effect of GABA anesthetic agents and deep NREM sleep, but also under the activated state of REMure.

Urethane anesthesia is not a faithful model of sleep

Despite the superficial similarity of the EEG between NREMure and natural NREM sleep, as well as between REMure and REM sleep, a deeper analysis shows strong differences between physiological and pharmacological states.

NREM sleep, especially during deep NREM sleep or N3 where EEG slow waves are fully developed, is considered a state where oneiric behavior is scarce (Siclari *et al.*, 2017). However, NREM sleep has a critical function in cognitive functions such as memory consolidation (Stickgold, 2005; Berner *et al.*, 2006; Wei *et al.*, 2018). The

EEG profile of NREMure strongly differs from natural NREM sleep. Compared to NREM sleep, NREMure exhibits a potentiation of delta waves power associated with a decrease in higher frequency power. In addition, NREMure shows a decrease in theta to gamma inter-hemispheric coherence in V2 and/or S1 derivates. Finally, considering only the lower (< 15 Hz) frequency oscillations, we also found that NREMure has lower LZC and JLZC.

REM sleep is an activated state where the neural activity and neurochemical milieu create conditions for the emergence of phenomenal experience in the form of dreams (Hobson, 2009; Siclari *et al.*, 2017). The EEG profile under REMure also differs from the natural counterpart. Compared to REM sleep, REMure showed a clear decrease in theta oscillation frequency more consistent with an anesthetized state. Moreover, while delta power was higher in REMure, the power of higher frequencies decreased in this anesthetized state, mainly in anterior cortices. Decreases in interhemispheric coherence in theta and sigma band during REMure were also detected in posterior cortices, while an increase in HFO in S1 interhemispheric coherence was also observed. As in NREMure, a decrease in complexity (both LZC and JLZC) was also detected.

To summarize, these analyses demonstrate that, despite their similarities, the EEG in urethane-anaesthetized states differs from sleep. Hence it is possible that cognitive functions that are known to be carried on during sleep, such as memory consolidation (Stickgold, 2005; Hobson, 2009), are not taking place under urethane anesthesia. Of note, intense research has been carried out trying to uncover the precise mechanisms by which anesthetics induce unconsciousness. In the past two decades there has been a focus on the shared mechanisms between anesthesia and sleep with a body of correlative suggesting that anesthetics and sleep share the same neural circuits.

However, in a recent study, we have demonstrated that the activation of GABAergic or glutamatergic neurons in the preoptic area of the hypothalamus, a key area for sleep generation, alters sleep-wake architecture but does not modulate the anesthetized state (Vanini *et al.*, 2020). The results from this paper can be considered as additional evidence against a strong mechanistic overlap between sleep and anesthesia. This is especially compelling because urethane was considered to be the only general anesthetic that could mimic the full spectrum of natural sleep. However, despite the similarities between urethane anesthesia and sleep, this detailed analysis revealed key differences.

Limitations

Our study has several limitations, first, we have not evaluated different doses of urethane anesthesia; therefore, lighter or deeper planes of anesthesia could show different results. Additionally, anesthesia was achieved by a single intraperitoneal injection of urethane and no supplementary injections were given, therefore, the anesthetic effects could have been attenuated over time. However, other authors evaluated the effect of additional injections over time and showed that urethane cyclicity is not affected by the absolute concentration of urethane in blood(Clement *et al.*, 2008). Finally, this study was performed with male rats, and therefore we could be losing some sex-differences of urethane anesthesia.

Conclusions

Urethane produces two different alternating electrographic states: a NREM sleep -like state and an activated state that has features of either REM sleep or waking. Our study revealed EEG signatures of unconsciousness in both urethane-induced states. In addition, NREM-like and REM-like states during urethane anesthesia differ from natural sleep states.

References

Abásolo, D., Simons, S., Morgado da Silva, R., Tononi, G. & Vyazovskiy, V.V. (2015) Lempel-Ziv complexity of cortical activity during sleep and waking in rats. *Journal of neurophysiology*, **113**, 2742-2752.

Akeju, O. & Brown, E.N. (2017) Neural oscillations demonstrate that general anesthesia and sedative states are neurophysiologically distinct from sleep. *Curr Opin Neurobiol*, **44**, 178-185.

Akeju, O., Song, A.H., Hamilos, A.E., Pavone, K.J., Flores, F.J., Brown, E.N. & Purdon, P.L. (2016) Electroencephalogram signatures of ketamine anesthesia-induced unconsciousness. *Clin Neurophysiol*, **127**, 2414-2422.

Arena, A., Comolatti, R., Thon, S., Casali, A.G. & Storm, J.F. (2021) General Anesthesia Disrupts Complex Cortical Dynamics in Response to Intracranial Electrical Stimulation in Rats. *eNeuro*, **8**.

Bandarabadi, M., Herrera, C.G., Gent, T.C., Bassetti, C., Schindler, K. & Adamantidis, A.R. (2020) A role for spindles in the onset of rapid eye movement sleep. *Nat Commun*, **11**, 5247.

Berner, I., Schabus, M., Wienerroither, T. & Klimesch, W. (2006) The significance of sigma neurofeedback training on sleep spindles and aspects of declarative memory. *Appl Psychophysiol Biofeedback*, **31**, 97-114.

Borjigin, J., Lee, U., Liu, T., Pal, D., Huff, S., Klarr, D., Sloboda, J., Hernandez, J., Wang, M.M. & Mashour, G.A. (2013) Surge of neurophysiological coherence and connectivity in the dying brain. *Proc Natl Acad Sci U S A*, **110**, 14432-14437.

Bullock, T. & McClune, M. (1989) Lateral coherence of the electrocorticogram: a new measure of brain synchrony. *Electroencephalography and clinical Neurophysiology*, **73**, 479-498.

Castro-Zaballa, S., Cavelli, M.L., Gonzalez, J., Nardi, A.E., Machado, S., Scorza, C. & Torterolo, P. (2018) EEG 40 Hz Coherence Decreases in REM Sleep and Ketamine Model of Psychosis. *Front Psychiatry*, **9**, 766.

Cavelli, M., Castro-Zaballa, S., Mondino, A., Gonzalez, J., Falconi, A. & Torterolo, P. (2017) Absence of EEG gamma coherence in a local activated cortical state: a conserved trait of REM sleep. *Translational Brain Rhythmicity*, **2**.

Cavelli, M., Castro, S., Schwarzkopf, N., Chase, M.H., Falconi, A. & Torterolo, P. (2015) Coherent neocortical gamma oscillations decrease during REM sleep in the rat. *Behav Brain Res*, **281**, 318-325.

Cavelli, M., Rojas-Libano, D., Schwarzkopf, N., Castro-Zaballa, S., Gonzalez, J., Mondino, A., Santana, N., Benedetto, L., Falconi, A. & Torterolo, P. (2018) Power and coherence of cortical high-frequency oscillations during wakefulness and sleep. *Eur J Neurosci*, **48**, 2728-2737.

Clement, E.A., Richard, A., Thwaites, M., Ailon, J., Peters, S. & Dickson, C.T. (2008) Cyclic and sleep-like spontaneous alternations of brain state under urethane anaesthesia. *PLoS One*, **3**, e2004.

Demertzi, A., Tagliazucchi, E., Dehaene, S., Deco, G., Barttfeld, P., Raimondo, F., Martial, C., Fernández-Espejo, D., Rohaut, B., Voss, H.U., Schiff, N.D., Owen, A.M., Laureys, S., Naccache, L. & Sitt, J.D. (2019) Human consciousness is supported by dynamic complex patterns of brain signal coordination. **5**, eaat7603.

Détári, L. & Vanderwolf, C.H. (1987) Activity of identified cortically projecting and other basal forebrain neurones during large slow waves and cortical activation in anaesthetized rats. *Brain Research*, **437**, 1-8.

Dringenberg, H.C. & Vanderwolf, C.H. (1998) Involvement of Direct and Indirect Pathways in Electrocorticographic Activation. *Neuroscience & Biobehavioral Reviews*, **22**, 243-257.

Fenik, V.B. & Kubin, L. (2009) Differential localization of carbachol- and bicuculline-sensitive pontine sites for eliciting REM sleep-like effects in anesthetized rats. *J Sleep Res*, **18**, 99-112.

González, J., Cavelli, M., Castro-Zaballa, S., Mondino, A., Tort, A.B.L., Rubido, N., Carrera, I. & Torterolo, P. (2021) EEG Gamma Band Alterations and REM-like Traits Underpin the Acute Effect of the Atypical Psychedelic Ibogaine in the Rat. *ACS Pharmacology & Translational Science*.

Gonzalez, J., Cavelli, M., Mondino, A., Pascovich, C., Castro-Zaballa, S., Rubido, N. & Torterolo, P. (2020) Electrocortical temporal complexity during wakefulness and sleep: an updated account. *Sleep Science*, 47-50.

Gonzalez, J., Cavelli, M., Mondino, A., Pascovich, C., Castro-Zaballa, S., Torterolo, P. & Rubido, N. (2019) Decreased electrocortical temporal complexity distinguishes sleep from wakefulness. *Sci Rep*, **9**, 18457.

Gonzalez, J., Prieto, J.P., Rodriguez, P., Cavelli, M., Benedetto, L., Mondino, A., Pazos, M., Seoane, G., Carrera, I., Scorza, C. & Torterolo, P. (2018) Ibogaine Acute Administration in Rats Promotes Wakefulness, Long-Lasting REM Sleep Suppression, and a Distinctive Motor Profile. *Front Pharmacol*, **9**, 374.

Hagihira, S. (2015) Changes in the electroencephalogram during anaesthesia and their physiological basis. *Br J Anaesth*, **115 Suppl 1**, i27-i31.

Hay, Y.A. (2021) Brainstem cholinergic modulation of the thalamocortical activity in urethane anesthetized mice. *Preprint bioRxiv*.

Hobson, J.A. (2009) REM sleep and dreaming: towards a theory of protoconsciousness. *Nat Rev Neurosci*, **10**, 803-813.

Horner, R.L. & Kubin, L. (1999) Pontine Carbachol Elicits Multiple Rapid Eye Movement Sleep-Like Neural Events in Urethane-Anesthetized Rats. *Neuroscience*, **93**, 215-226.

Hudetz, A.G., Liu, X., Pillay, S., Boly, M. & Tononi, G. (2016) Propofol anesthesia reduces Lempel-Ziv complexity of spontaneous brain activity in rats. *Neurosci Lett*, **628**, 132-135.

Hudetz, A.G., Vizuete, J.A. & Pillay, S. (2011) Differential effects of isoflurane on high-frequency and low-frequency gamma oscillations in the cerebral cortex and hippocampus in freely moving rats. *Anesthesiology*, **114**, 588-595.

Koch, C., Massimini, M., Boly, M. & Tononi, G. (2016) Neural correlates of consciousness: progress and problems. *Nature Reviews Neuroscience*, **17**, 307-321.

Kortelainen, J., Jia, X., Seppanen, T. & Thakor, N. (2012) Increased electroencephalographic gamma activity reveals awakening from isoflurane anaesthesia in rats. *Br J Anaesth*, **109**, 782-789.

Kucewicz, M.T., Cimbalnik, J., Matsumoto, J.Y., Brinkmann, B.H., Bower, M.R., Vasoli, V., Sulc, V., Meyer, F., Marsh, W.R., Stead, S.M. & Worrell, G.A. (2014) High frequency oscillations are associated with cognitive processing in human recognition memory. *Brain*, **137**, 2231-2244.

Lee, U., Ku, S., Noh, G., Baek, S., Choi, B. & Mashour, G.A. (2013) Disruption of frontal-parietal communication by ketamine, propofol, and sevoflurane. *Anesthesiology*, **118**, 1264-1275.

Lempel, A. & Ziv, J. (1976) On the Complexity of Finite Sequences. *IEEE Transactions on Information Theory*, **22**, 75-81.

Li, D., Hambrecht-Wiedbusch, V.S. & Mashour, G.A. (2017) Accelerated Recovery of Consciousness after General Anesthesia Is Associated with Increased Functional Brain Connectivity in the High-Gamma Bandwidth. *Front Syst Neurosci*, **11**, 16.

Maggi, C. & Meli, A. (1986) Suitability of urethane anesthesia for physiopharmacological investigations in various systems. Part 1: General considerations. *Experientia*, **42**, 109-210.

Mashour, G.A. & Hudetz, A.G. (2018) Neural Correlates of Unconsciousness in Large-Scale Brain Networks. *Trends Neurosci*, **41**, 150-160.

Mashour, G.A., Lipinski, W.J., Matlen, L.B., Walker, A.J., Turner, A.M., Schoen, W., Lee, U. & Poe, G.R. (2010) Isoflurane anesthesia does not satisfy the homeostatic need for rapid eye movement sleep. *Anesth Analg*, **110**, 1283-1289.

Mateos, D.M., Wennberg, R., Guevara, R. & Perez Velazquez, J.L. (2017) Consciousness as a global property of brain dynamic activity. *Physical Review E*, **96**, 062410.

Melloni, L., Molina, C., Pena, M., Torres, D., Singer, W. & Rodriguez, E. (2007) Synchronization of neural activity across cortical areas correlates with conscious perception. *J Neurosci*, **27**, 2858-2865.

Miller, K.J., Sorensen, L.B., Ojemann, J.G. & den Nijs, M. (2009) Power-law scaling in the brain surface electric potential. *PLoS Comput Biol*, **5**, e1000609.

Mondino, A., Cavelli, M., Gonzalez, J., Osorio, L., Castro-Zaballa, S., Costa, A., Vanini, G. & Torterolo, P. (2020) Power and Coherence in the EEG of the Rat: Impact of Behavioral States, Cortical Area, Lateralization and Light/Dark Phases. *Clocks Sleep*, **2**, 536-556.

Mondino, A., Cavelli, M., Gonzalez, J., Santana, N., Castro-Zaballa, S., Mechoso, B., Bracesco, N., Fernandez, S., Garcia-Carnelli, C., Castro, M.J., Umpierrez, E., Murillo-Rodriguez, E., Torterolo, P. & Falconi, A. (2019) Acute effect of vaporized Cannabis on sleep and electrocortical activity. *Pharmacol Biochem Behav*, **179**, 113-123.

Mondino, A., Hambrecht-Wiedbusch, V., Li, D., York, A.K., Pal, D., Gonzalez, J., Torterolo, P., Mashour, G.A. & Vanini, G. (2021) Glutamatergic neurons in the preoptic hypothalamus promote wakefulness, destabilize NREM sleep, suppress REM sleep, and regulate cortical dynamics. *J Neurosci*.

Murakami, M., Kashiwadani, H., Kirino, Y. & Mori, K. (2005) State-dependent sensory gating in olfactory cortex. *Neuron*, **46**, 285-296.

Murphy, M., Bruno, M.A., Riedner, B., Boveroux, P., Noirhomme, Q., Landsness, E., Brichant, J., Phillips, C., Massimini, M., Laureys, S., Tononi, G. & Melanie, B. (2011) Propofol anesthesia and sleep: a high-density EEG study. *Sleep*, **34**, 283-291.

Neves, R.M., van Keulen, S., Yang, M., Logothetis, N.K. & Eschenko, O. (2018) Locus coeruleus phasic discharge is essential for stimulus-induced gamma oscillations in the prefrontal cortex. *J Neurophysiol*, **119**, 904-920.

Pagliardini, S., Gosgnach, S. & Dickson, C.T. (2013) Spontaneous sleep-like brain state alternations and breathing characteristics in urethane anesthetized mice. *PLoS One*, **8**, e70411.

Pagliardini, S., Greer, J.J., Funk, G.D. & Dickson, C.T. (2012) State-dependent modulation of breathing in urethane-anesthetized rats. *J Neurosci*, **32**, 11259-11270.

Pal, D., Hambrecht-Wiedbusch, V.S., Silverstein, B.H. & Mashour, G.A. (2015) Electroencephalographic coherence and cortical acetylcholine during ketamine-induced unconsciousness. *Br J Anaesth*, **114**, 979-989.

Pal, D., Silverstein, B.H., Lee, H. & Mashour, G.A. (2016) Neural Correlates of Wakefulness, Sleep, and General Anesthesia: An Experimental Study in Rat. *Anesthesiology*, **125**, 929-942.

Perouansky, M., H., H., Perkins, M. & Pearce, R.A. (2007) Amnesic concentrations of the nonimmobilizer 1,2-dichlorohexafluorocyclobutane (F6, 2N) and isoflurane alter hippocampal theta oscillations in vivo. *Anesthesiology*, **106**, 1168-1176.

Pigorini, A., Sarasso, S., Proserpio, P., Szymanski, C., Arnulfo, G., Casarotto, S., Fecchio, M., Rosanova, M., Mariotti, M., Lo Russo, G., Palva, J.M., Nobili, L. & Massimini, M. (2015) Bistability breaks-off deterministic responses to intracortical stimulation during non-REM sleep. *Neuroimage*, **15**, 105-113.

Purdon, P.L., Pierce, E.T., Mukamel, E.A., Prerau, M.J., Walsh, J.L., Wong, K.F., Salazar-Gomez, A.F., Harrell, P.G., Sampson, A.L., Cimenser, A., Ching, S., Kopell, N.J., Tavares-Stoeckel, C., Habeeb, K., Merhar, R. & Brown, E.N. (2013) Electroencephalogram signatures of loss and recovery of consciousness from propofol. *Proc Natl Acad Sci U S A*, **110**, E1142-1151.

Sarasso, S., Casali, A.G., Casarotto, S., Rosanova, M., Sinigaglia, C. & M., M. (2021) Consciousness and complexity: a consilience of evidence. *Neuroscience of Consciousness*, **7**, 1-24.

Schartner, M., Seth, A., Noirhomme, Q., Boly, M., Bruno, M.A., Laureys, S. & Barrett, A. (2015) Complexity of Multi-Dimensional Spontaneous EEG Decreases during Propofol Induced General Anaesthesia. *PLoS One*, **10**, e0133532.

Schartner, M.M., Pigorini, A., Gibbs, S.A., Arnulfo, G., Sarasso, S., Barnett, L., Nobili, L., Massimini, M., Seth, A.K. & Barrett, A.B. (2017) Global and local complexity of intracranial EEG decreases during NREM sleep. *Neurosci Conscious*, **2017**, niw022.

Siclari, F., Baird, B., Perogamvros, L., Bernardi, G., LaRocque, J.J., Riedner, B., Boly, M., Postle, B.R. & Tononi, G. (2017) The neural correlates of dreaming. *Nat Neurosci*, **20**, 872-878.

Steriade, M., Nunez, A. & Amzica, F. (1993) A novel slow (< 1 Hz) oscillation of neocortical neurons in vivo: depolarizing and hyperpolarizing components. *J Neurosci*, **13**, 3252-3265.

Stickgold, R. (2005) Sleep-dependent memory consolidation. *Nature*, **437**, 1272-1278.

Tononi, G., Boly, M., Massimini, M. & Koch, C. (2016) Integrated information theory: from consciousness to its physical substrate. *Nat Rev Neurosci*, **17**, 450-461.

Torao-Angosto, M., Manasanch, A., Mattia, M. & Sanchez-Vives, M.V. (2021) Up and Down States During Slow Oscillations in Slow-Wave Sleep and Different Levels of Anesthesia. *Front Syst Neurosci*, **15**, 609645.

Torterolo, P., Castro-Zaballa, S., Cavelli, M. & Gonzalez, J. (2019) Arousal and normal conscious cognition *Arousal in Neurological and Psychiatric Diseases*, pp. 1-24.

Vanini, G., Bassana, M., Mast, M., Mondino, A., Cerda, I., Phyle, M., Chen, V., Colmenero, A.V., Hambrecht-Wiedbusch, V.S. & Mashour, G.A. (2020) Activation of Preoptic GABAergic or Glutamatergic Neurons Modulates Sleep-Wake Architecture, but Not Anesthetic State Transitions. *Curr Biol*, **30**, 779-787 e774.

Varela, F., Lachaux, J., Rodriguez, E. & Martinerie, J. (2001) The BrainWeb: Phase Sinchronization and Large-Scale Integration. *Nature Reviews Neurosciences*, **2**, 229-239.

Vertes, R. (1984) Brainstem Control of The Events of REM Sleep. *Progress in Neurobiology*, **22**, 241 - 288.

Wei, Y., Krishnan, G.P., Komarov, M. & Bazhenov, M. (2018) Differential roles of sleep spindles and sleep slow oscillations in memory consolidation. *PLoS Comput Biol*, **14**, e1006322.

Yagishita, H., Nishimura, Y., Noguchi, A., Shikano, Y., Ikegaya, Y. & Sasaki, T. (2020) Urethane anesthesia suppresses hippocampal subthreshold activity and neuronal synchronization. *Brain Res*, **1749**, 147137.

Zhang, X., Roy, R. & Jensen, E. (2001) EEG Complexity as a Measure of Depth of Anesthesia for Patients. *IEEE TRANSACTIONS ON BIOMEDICAL ENGINEERING*, **48**, 1424-1433.

Zozor, S., Ravier, P. & Buttelli, O. (2005) On Lempel–Ziv complexity for multidimensional data analysis. *Physica A: Statistical Mechanics and its Applications*, **345**, 285-302.

Figure legends.

Figure 1. Sleep–wake and urethane states in the rat. (**A**) Schematic representation of the electrode position in the brain of the rat. OB, olfactory bulb; M1, primary motor cortex; S1, primary somato-sensory cortex; V2, secondary visual cortex; r, right; l, left. (**B**) Hypnogram (top) according to visually scored behavioral states and spectrogram (0.1 to 30 Hz) of one representative animal. Left panel shows baseline recordings and right panel shows recordings under urethane anesthesia. During W, REM sleep and REMure theta activity (4–10 Hz) in the spectrogram can be readily observed. **(C)** Representative electroencephalogram (EEG) of the somatosensory cortex (S1Cx) and neck electromyogram (EMG) recordings during W, NREM sleep, REM sleep, NREMure and REMure. Similarities between the sleep and anesthetized states can be observed with delta (0.5 – 4 Hz) oscillations characterizing NREM sleep and NREMure and theta (4-10 Hz) and high frequency oscillations characterizing W, REM sleep and REMure. Notice that REMure doesn't show the REM sleep characteristic atonia. **(D)** Electromyography power during NREMure and REMure, both states showed no significant (ns) differences. **(E)** Mean and SEM of the total time spent in each behavioral state during baseline recordings (left) and urethane anesthesia (right). **(F)** Mean and SEM of the number of bouts of each behavioral state during baseline recordings (left) and urethane anesthesia (right). **(G)** Mean and SEM of the duration of bouts of each behavioral state during baseline (left) and urethane anesthesia (right).

Figure 2. Power spectral profiles. **(A)** Mean and SEM (shadow) normalized power spectral profiles of the right hemisphere during wakefulness (W) and the anesthetized states (NREMure and REMure). Significant diffrerences are indicated by symbols: ✱, W Vs. NREMure; ✝, W Vs. REMure; ✱, NREMure Vs. REMure; *, differences among all conditions. **(B)** Mean and SEM (shadow) of normalized power spectral profiles of the right hemisphere during NREM sleep and NREMure. *, indicates significant differences. **(C)** Mean and SEM (shadow) normalized power spectral profiles of the right hemisphere during REM sleep and REMure. *, indicates significant differences. The frequency bands used for the statistical analysis are indicated by colors in the background of the chart. OB, olfactory bulb; M1, primary motor cortex; S1, primary somato-sensory cortex; V2, secondary visual cortex; W, wakefulness; r, right; l, left; l; δ, delta; θ, theta; σ, sigma; β, beta; lγ, low gamma or LG; hγ, high gamma or HG; HFO, high frequency oscillations.

Figure 3. Interhemispheric z'coherence. **(A)** Mean and SEM (shadow) interhemispheric z'coherence during wakefulness (W) and the anesthetized states (NREMure and REMure). Significant diffrerences are indicated by symbols: ✱, W Vs. NREMure; ✝, W Vs. REMure; ✱, NREMure Vs. REMure; *, differences among all conditions. **(B)** Mean and SEM (shadow) interhemispheric z'coherence during NREM sleep and NREMure. *, indicates significant differences. **(C)** Mean and SEM (shadow) interhemispheric z'coherence during REM sleep and REMure. *, indicates significant differences. M1, primary motor cortex; S1, primary somato-sensory cortex; V2, secondary visual cortex; W, wakefulness; r, right; l, left; l, δ, delta; θ, theta; σ, sigma; β, beta; lγ, low gamma or LG; hγ, high gamma or HG; HFO, high frequency oscillations

Figure 4. Right Intrahemispheric z'coherence. **(A)** Mean and SEM (shadow) right intrahemispheric z'coherence during wakefulness (W) and the anesthetized states (NREMure and REMure). Significant diffrerences are indicated by symbols: ✱, W Vs. NREMure; ✝, W Vs. REMure; ✱, NREMure Vs. REMure; *, differences among all conditions. **(B)** Mean and SEM (shadow) right intrahemispheric Z'coherence during NREM sleep and NREMure. *,

indicates significant differences. **(C)** Mean and SEM (shadow) right intrahemispheric Z'coherence during REM sleep and REMure. OB, olfactory bulb; M1, primary motor cortex; S1, primary somato-sensory cortex; V2, secondary visual cortex; W, wakefulness; r, right; l, left; l, δ, delta; θ, theta; σ, sigma; β, beta; lγ, low gamma or LG; hγ, high gamma or HG; HFO, high frequency oscillations

Figure 5. Normalized Transfer Entropy. Feedback (FB) and Feedforward (FF) Normalized transfer entropy (NSTE) for Theta and HG frequency bands during W and the anesthetized states. Frequency bands with no significant differences between states are not shown. *, indicates significant differences. Comparisons of NSTE between sleep states and its analogous during anesthesia can be find in Supplementary Table 9.

Figure 6. Lempel Ziv Complexity (LZC). (A) Lempel Ziv Complexity for frequencies between 1-195 Hz during W and the anesthetized states (Left), NREM sleep and NREMure (middle) and REM sleep and REMure (right) for each electrode localization in the right hemisphere. *, indicates significant differences. **(B)** Lempel Ziv Complexity for frequencies between 1 -15 Hz (low frequencies, LF) during W and the anesthetized states (Left), NREM sleep and NREMure (middle) and REM sleep and REMure (right) for each electrode localization in the right hemisphere. *, indicates significant differences. OB, olfactory bulb; M1, primary motor cortex; S1, primary somato-sensory cortex; V2, secondary visual cortex; W, wakefulness; r, right; l, left.

Figure 7. Joint Lempel Ziv Complexity (JLZC). (A) Comparison of Lempel Ziv Complexity for frequencies between 1-195 Hz (top) and 1-15 Hz (bottom) for W and the anesthetized states (Left), NREM sleep and NREMure (middle) and REM sleep and REMure (right). *indicates significant differences. OB, olfactory bulb; M1, primary motor cortex; S1, primary somato-sensory cortex; V2, secondary visual cortex; W, wakefulness; r, right; l, left.

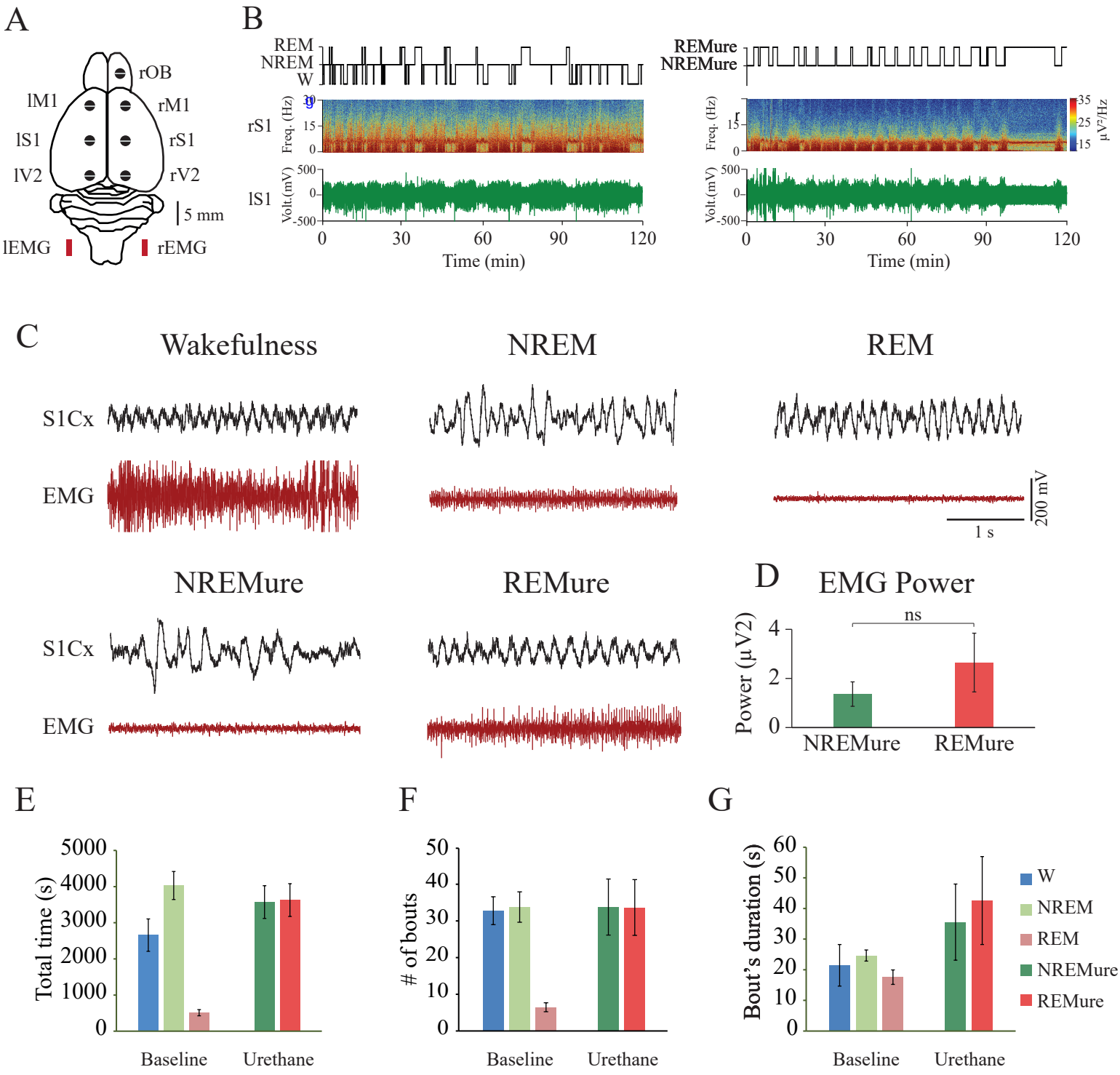
A
rOB
lM1
rM1
lS1
rS1
lV2
rV2
5 mm
lEMG
rEMG
B
REM
NREM
W
REMure
NREMure
rS1
lS1
Freq. (Hz)
Volt.(mV)
Time (min)
C
Wakefulness
NREM
REM
S1Cx
EMG
200 mV
1 s
NREMure
REMure
D
EMG Power
ns
Power (μV2)
E
Total time (s)
Baseline
Urethane
F
# of bouts
G
Bout's duration (s)
W
NREM
REM
NREMure
REMure

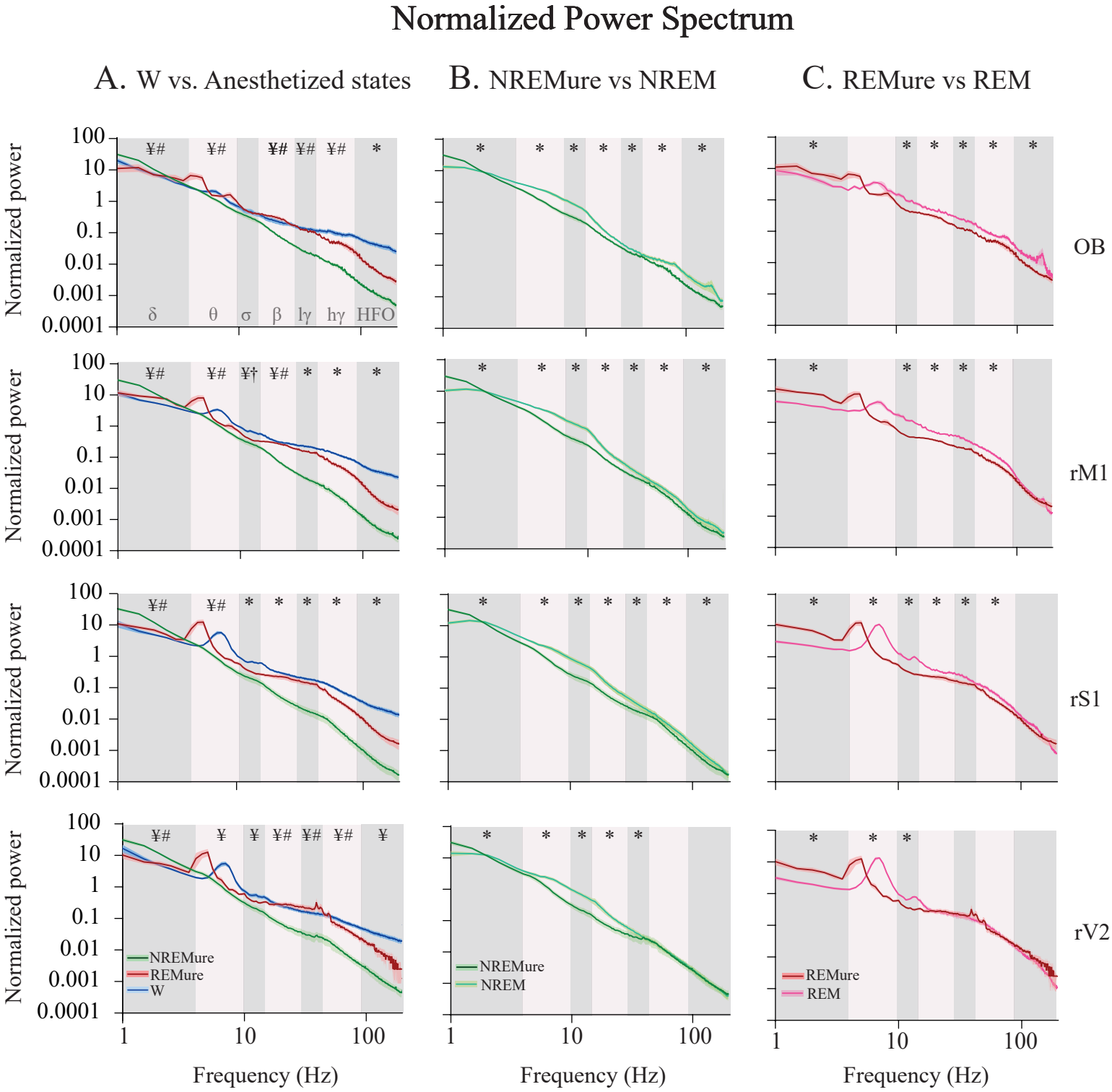
Normalized Power Spectrum
A. W vs. Anesthetized states
B. NREMure vs NREM
C. REMure vs REM
Normalized power
100
10
1
0.1
0.01
0.001
0.0001
δ
θ
σ
β
lγ
hγ
HFO
OB
rM1
rS1
rV2
NREMure
REMure
W
NREM
REM
1
10
100
Frequency (Hz)

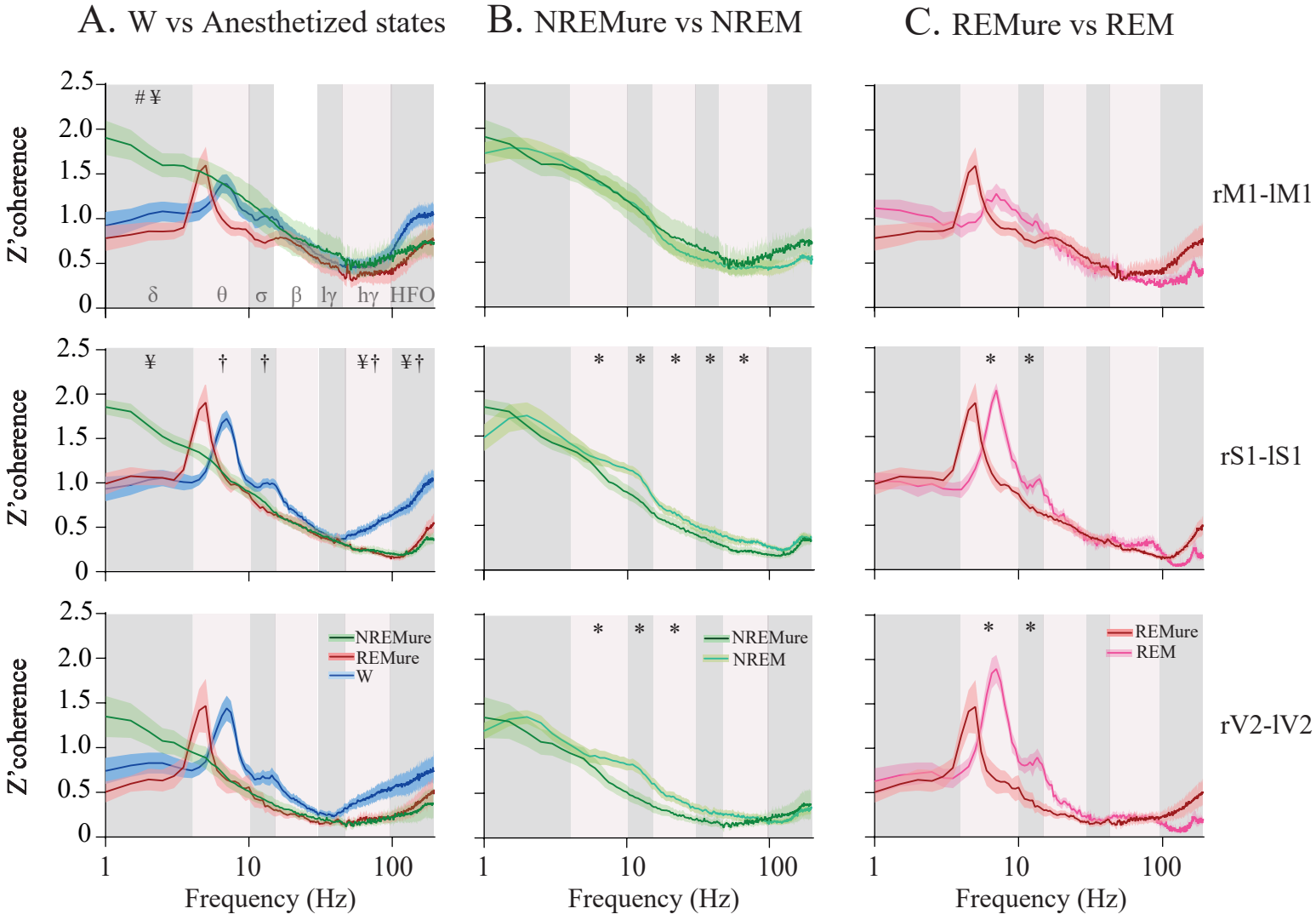
Interhemispheric z'coherence
A. W vs Anesthetized states
B. NREMure vs NREM
C. REMure vs REM
Z'coherence
rM1-lM1
rS1-lS1
rV2-lV2
¥
δ θ σ β lγ hγ HFO
¥ † † ¥† ¥†
* * * * *
NREMure
REMure
W
NREM
REM
2.5
2.0
1.5
1.0
0.5
0
1
10
100
Frequency (Hz)

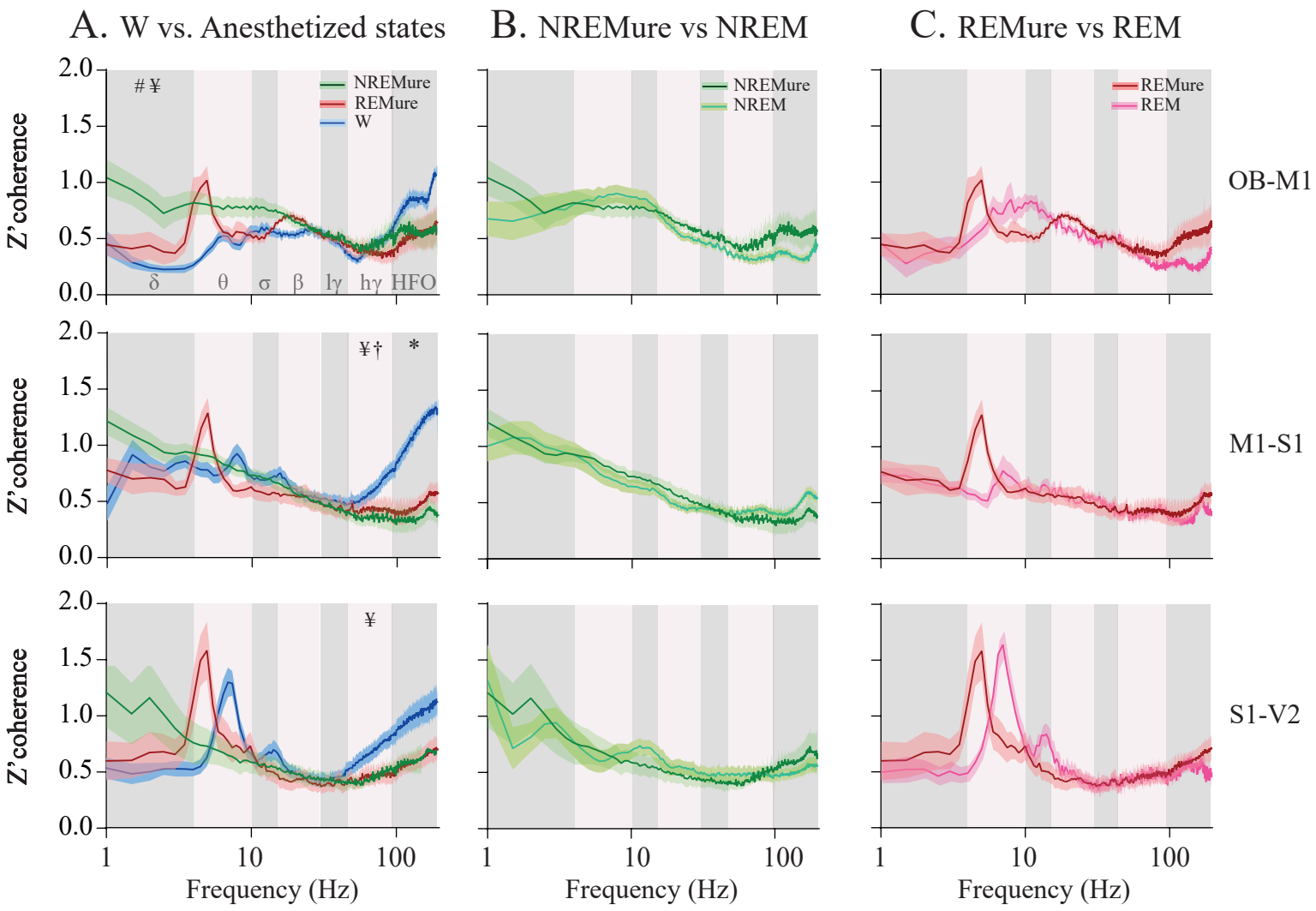
Intrahemispheric z'coherence
A. W vs. Anesthetized states
B. NREMure vs NREM
C. REMure vs REM
NREMure
REMure
W
NREM
REM
OB-M1
M1-S1
S1-V2
Z'coherence
Frequency (Hz)
δ θ σ β lγ hγ HFO

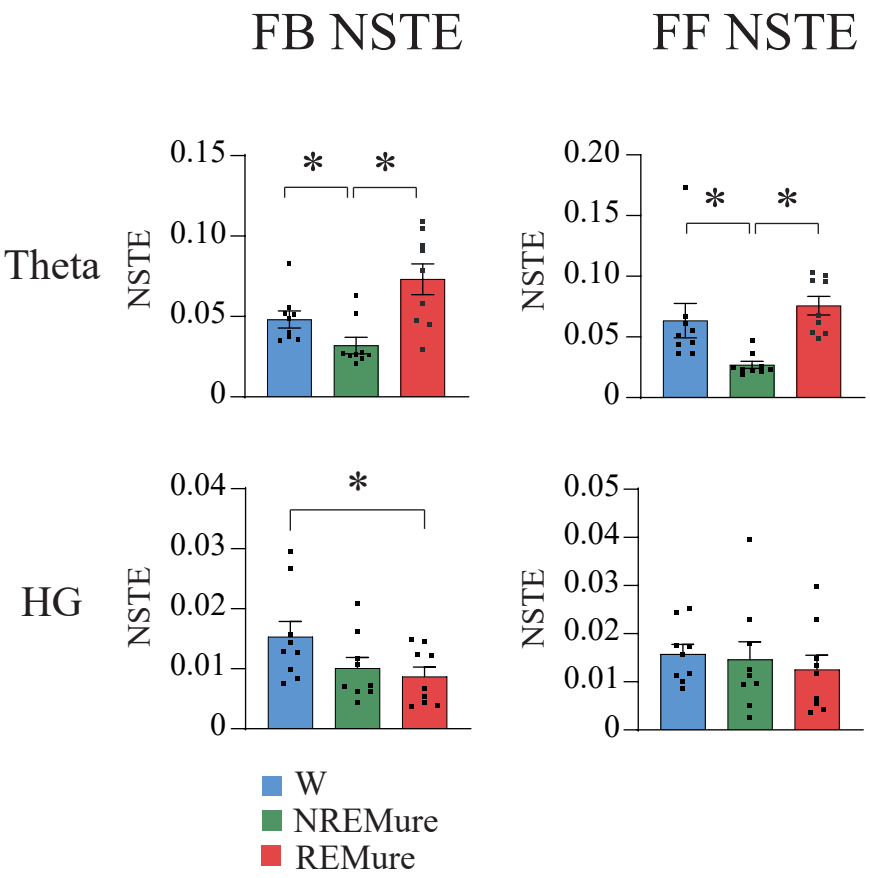
FB NSTE
FF NSTE
Theta
HG
NSTE
0.15
0.10
0.05
0
0.20
0.04
0.03
0.02
0.01
*
W
NREMure
REMure

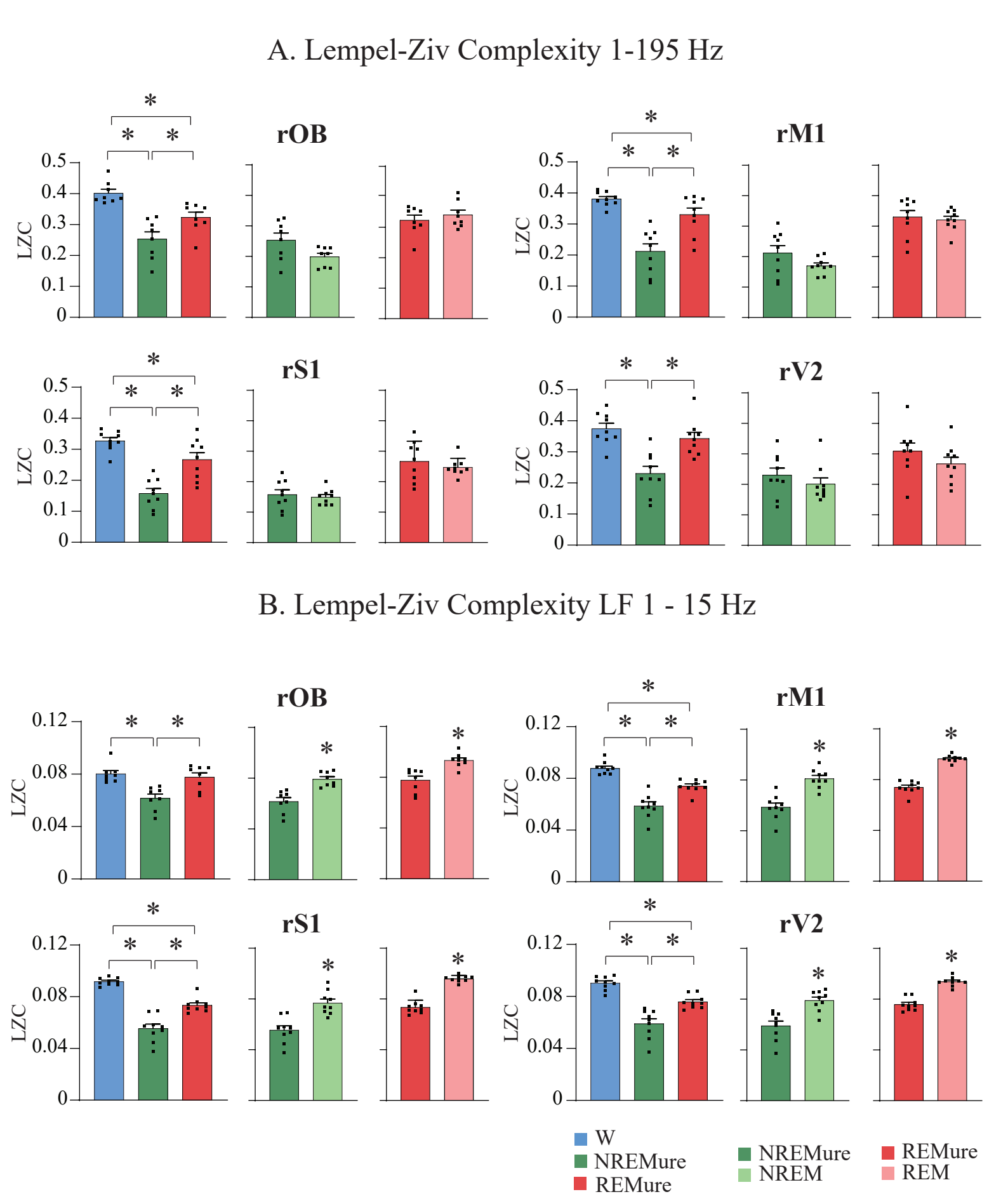
A. Lempel-Ziv Complexity 1-195 Hz
rOB
rM1
rS1
rV2
LZC
0.5
0.4
0.3
0.2
0.1
0
B. Lempel-Ziv Complexity LF 1 - 15 Hz
0.12
0.08
0.04
W
NREMure
REMure
NREMure
NREM
REMure
REM

Joint Lempel-Ziv Complexity

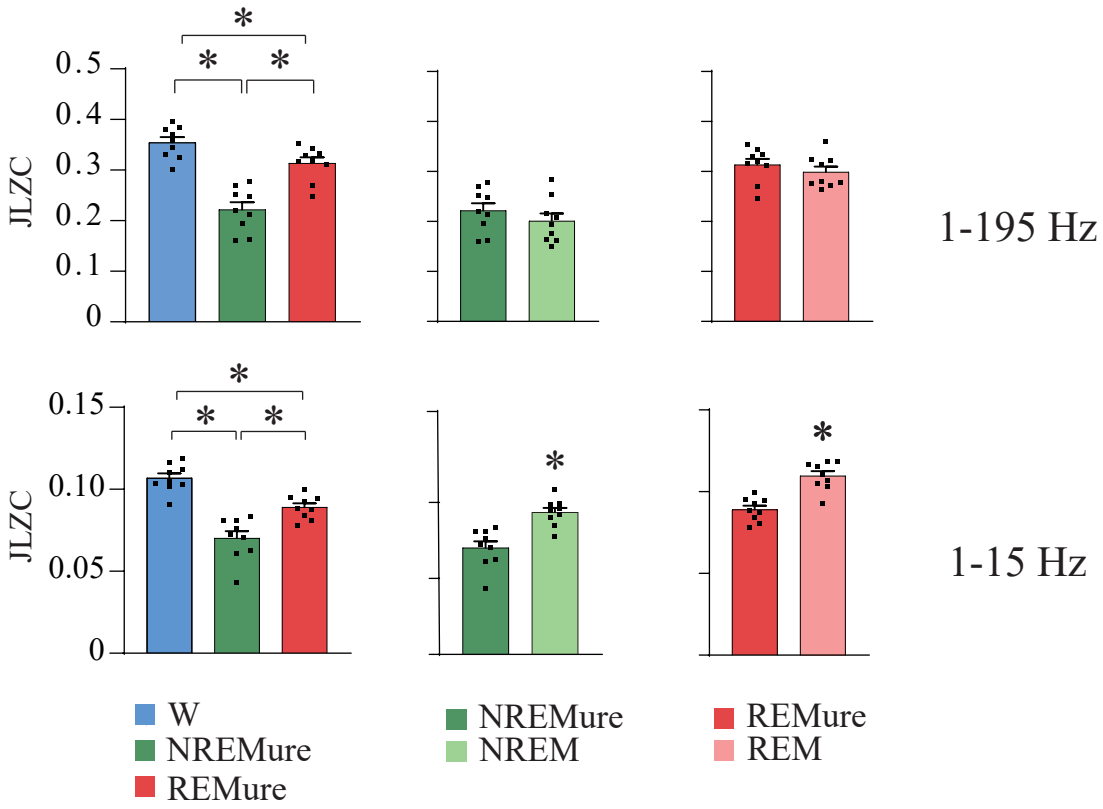

Table 1. Parameters associated with consciousness/unconsciousness during anesthetized states and physiological sleep, in comparison to wakefulness.

	NREMure	NREM sleep	REMure	REM sleep
Delta power	↑ ↑	↑[a]	↑	n/c [a]
Gamma and HFO power	↓ ↓	↓[a]	↓	n/c [a]
Gamma and HFO coherence	↓	↓[a]	↓	↓[a]
HG FB Gamma NSTE	n/c	↓[b]	↓	↓[b]
LZC	↓	↓[c]	↓	n/c[c]
JLZC	↓	↓[d]	↓	n/c[d]

EEG features suggest that urethane produces unconsciousness during both NREMure and REMure. Increase (+) or decrease (-) in comparison to wakefulness. n/c, no changes. [a]Mondino et. al (2020), [b]Pal et. al (2016), [c]Abásolo et. al (2015), [d]Mateos et al. 2017

Table 1. Normalized Power. Repeated measures one-way ANOVA.

	OB			M1			S1			V2		
Frequency	**df**	**F**	**p**	**df**	**F**	**p**	**df**	**F**	**p**	**df**	**F**	**p**
Delta	2,7	19.24	0.001*	2,8	45.87	<0.001*	2,8	54.90	<0.001*	2,7	23.04	0.001*
Theta	2,7	13.77	0.005*	2,8	12.26	0.004*	2,8	18.19	0.002*	2,7	9.28	0.009*
Sigma	2,7	3.717	0.053	2,8	21.00	<0.001*	2,8	56.86	<0.001*	2,7	19.10	0.001*
Beta	2,7	19.12	0.001*	2,8	45.45	<0.001*	2,8	57.61	<0.001*	2,7	19.64	0.001*
LG	2,7	31.49	0.001*	2,8	90.21	<0.001*	2,8	66.21	<0.001*	2,7	12.25	0.008*
HG	2,7	24.63	0.001*	2,8	115.2	<0.001*	2,8	74.13	<0.001*	2,7	26.20	0.001*
HFO	2,7	29.84	0.001*	2,8	45.34	<0.001*	2,8	30.43	0.001*	2,7	20.43	0.002*

Results of the Repeated measures one-way ANOVA comparing W with the anesthetized states (NREMure and REMure). Data are plotted in Figure 2.

Table 2. Normalized Power. Holm-Šídák *post-hoc* test.

	OB			M1			S1			V2		
Frequency	**W vs. NREMure**	**W vs. REMure**	**NREMure vs. REMure**	**W vs. NREMure**	**W vs. REMure**	**NREMure vs. REMure**	**W vs. NREMure**	**W vs. REMure**	**NREMure vs. REMure**	**W vs. NREMure**	**W vs. REMure**	**NREMure vs. REMure**
Delta	0.0070*	0.9570	0.0084*	0.0021*	0.0791	0.0048*	0.0021*	0.0905	0.0021*	0.0021*	0.9288	0.0048*
Theta	0.0198*	0.1191	0.0198*	0.0021*	0.4682	0.0228*	0.0021*	0.0905	0.0088*	0.0107*	0.9288	0.0706
Sigma	N/A	N/A	N/A	0.0027*	0.0220*	0.1244	0.0021*	0.0030*	0.0287*	0.0040*	0.1934	0.0706
Beta	0.0243*	0.3870	0.0088*	0.0021*	0.1244	0.0021*	0.0021*	0.0448*	0.0024*	0.0040*	0.9288	0.0060*
LG	0.0064*	0.5882	0.0018*	0.0021*	0.0098*	0.0021*	0.0021*	0.0287*	0.0024*	0.0040*	0.6448	0.0229*
HG	0.0064*	0.0548	0.0109*	0.0021*	0.0021*	0.0022*	0.0021*	0.0021*	0.0021*	0.0040*	0.1494	0.0104*
HFO	0.0078*	0.0143*	0.0034*	0.0021*	0.0022*	0.0021*	0.0030*	0.0088*	0.0088*	0.0098*	0.0706	0.0706

Adjusted p values from Holm-Šídák multiple comparison test. We analyzed only frequency bands for which ANOVA was significant. The ones not analyzed are represented by "N/A". Data are plotted in Figure 2A.

Table 3. Normalized Power. Comparison between anesthetized states and NREM and REM sleep

A. Normalized power adjusted p values NREMure Vs. NREM												
	rOB			**rM1**			**rS1**			**rV2**		
Frequency	**df**	**t**	**p**	**df**	**t**	**p**	**df**	**t**	**p**	**df**	**t**	**p**
Delta	8	8.566	<0.001*	8	7.273	<0.001*	8	6.491	0.001*	7	6.341	0.002*
Theta	8	7.602	<0.001*	8	9.500	<0.001*	8	6.983	0.001*	7	4.789	0.007*
Sigma	8	8.737	<0.001*	8	5.669	0.002*	8	5.895	0.002*	7	7.230	0.001*
Beta	8	4.604	0.010*	8	4.281	0.011*	8	4.686	0.006*	7	5.430	0.005*
LG	8	2.980	0.041*	8	3.287	0.033*	8	4.574	0.006*	7	1.503	0.007*
HG	8	3.622	0.025*	8	3.197	0.033*	8	3.806	0.010*	7	0.403	0.8977
HFO	8	2.909	0.041*	8	3.169	0.033*	8	3.340	0.010*	7	0.138	0.8977
B. Normalized power adjusted p values REMure Vs. REM												
	rOB			**rM1**			**rS1**			**rV2**		
Frequency	**df**	**t**	**p**	**df**	**t**	**P**	**df**	**t**	**p**	**df**	**t**	**p**
Delta	8	3.722	0.029*	8	6.110	0.001*	8	5.581	0.002*	7	4.621	0.014*
Theta	8	0.688	0.513	8	1.171	0.475	8	3.404	0.018*	7	4.349	0.017*
Sigma	8	4.333	0.017*	8	7.396	0.001*	8	8.399	0.001*	7	10.12	0.001*
Beta	8	5.900	0.004*	8	13.63	0.001*	8	5.038	0.005*	7	0.235	0.958
LG	8	6.415	0.003*	8	6.380	0.001*	8	4.255	0.008*	7	0.440	0.824
HG	8	2.808	0.077	8	5.528	0.002*	8	4.831	0.005*	7	0.794	0.958
HFO	8	2.681	0.077	8	0.923	0.475	8	1.361	0.210*	7	0.307	0.770

Statistical results from two-tailed paired Student t tests comparing NREMure with NREM sleep (A) and REMure with REM sleep (B). p values were adjusted by Holm-Šídák multiple comparison test. Data are plotted in Figure 2B and 2C respectively.

Table 4. Inter-hemispheric and Intra-hemispheric z'coherence.

A. Inter-hemispheric z'coherence									
	rM1-lM1			**rS1-lS1**			**rV2-lV2**		
Frequency	**df**	**F**	**p**	**df**	**F**	**P**	**df**	**F**	**p**
Delta	2,7	14.66	0.001*	2,7	15.80	0.001*	2,7	2.876	0.113
Theta	2,7	2.711	0.131	2,7	9.36	0.007*	2,7	6.458	0.027*
Sigma	2,7	2.515	0.152	2,7	26.16	0.001*	2,7	5.624	0.042*
Beta	2,7	0.353	0.588	2,7	8.086	0.005*	2,7	6.524	0.023*
LG	2,7	1.436	0.270	2,7	1.179	0.333	2,7	4.058	0.048*
HG	2,7	2.635	0.141	2,7	37.30	<0.001*	2,7	10.24	0.012*
HFO	2,7	0.311	0.672	2,7	32.77	<0.001*	2,7	3.789	0.088
B. Intra-hemispheric z'coherence									
	rOB-rM1			**rM1-rS1**			**rS1-rV2**		
Frequency	**df**	**F**	**p**	**df**	**F**	**P**	**df**	**F**	**P**
Delta	2,7	11.77	0.007*	2,8	3.758	0.067	2,6	3.040	0.123
Theta	2,7	7.756	0.007*	2,8	0.434	0.564	2,6	4.956	0.046*
Sigma	2,7	7.300	0.007*	2,8	1.206	0.308	2,6	0.813	0.407
Beta	2,7	3.841	0.071	2,8	0.085	0.794	2,6	0.295	0.639
LG	2,7	1.201	0.326	2,8	1.034	0.345	2,6	0.286	0.684
HG	2,7	1.158	0.325	2,8	23.04	<0.001*	2,6	12.29	0.004*
HFO	2,7	3.217	0.094	2,8	85.11	<0.001*	2,6	7.393	0.012*

Inter-hemispheric and Intra-hemispheric z'coherence. Comparison between wakefulness and anesthetized states. Repeated measures one-way ANOVA. Data are plotted in Figure 3 and 4.

Table 5. Inter-hemispheric z'coherence between wakefulness and anesthetized states. Holm-Šídák *post-hoc*.

	rM1-lM1			rS1-lS1			rV2-lV2		
Frequency	**W vs. NREMure**	**W vs. REMure**	**NREMure vs. REMure**	**W vs. NREMure**	**W vs. REMure**	**NREMure vs. REMure**	**W vs. NREMure**	**W vs. REMure**	**NREMure vs. REMure**
Delta	0.018*	0.732	0.050*	0.002*	0.258	0.205	N/A	N/A	N/A
Theta	N/A	N/A	N/A	0.087	0.026*	0.772	0.151	0.399	0.814
Sigma	N/A	N/A	N/A	0.064	0.002*	0.288	0.290	0.400	0.814
Beta	N/A	N/A	N/A	0.104	0.104	0.928	0.399	0.241	0.725
LG	N/A	N/A	N/A	N/A	N/A	N/A	0.399	0.399	0.814
HG	N/A	N/A	N/A	0.002*	0.007*	0.894	0.131	0.233	0.814
HFO	N/A	N/A	N/A	0.003*	0.007*	0.737	N/A	N/A	N/A

Adjusted p values from Holm-Šídák multiple comparison test. We analyzed only frequency bands for which ANOVA was significant. The ones not analyzed are represented by "N/A". Data are plotted in Figure 3.

Table 6. Intra-hemispheric z'coherence. between wakefulness and anesthetized states. Holm-Šídák post-hoc.

	rOB-rM1			rM1-rS1			rS1-rV2		
Frequency	**W vs. NREMure**	**W vs. REMure**	**NREMure vs. REMure**	**W vs. NREMure**	**W vs. REMure**	**NREMure vs. REMure**	**W vs. NREMure**	**W vs. REMure**	**NREMure vs. REMure**
Delta	0.045*	0.223	0.008*	N/A	N/A	0.205	N/A	N/A	N/A
Theta	0.065	0.223	0.223	N/A	N/A	0.772	0.154	0.845	0.077
Sigma	0.106	0.785	0.065	N/A	N/A	0.288	N/A	N/A	N/A
Beta	N/A	N/A	N/A	N/A	N/A	0.928	N/A	N/A	N/A
LG	N/A	N/A	N/A	N/A	N/A	N/A	N/A	N/A	N/A
HG	N/A	N/A	N/A	0.001*	0.004*	0.045*	0.077	0.233	0.999
HFO	N/A	N/A	N/A	0.001*	0.004*	0.017*	0.153	0.064	0.996

Adjusted p values from Holm-Šídák multiple comparison test. We analyzed only frequency bands for which ANOVA was significant. The ones not analyzed are represented by "N/A". Data are plotted in Figure 4.

Table 7. Inter-hemispheric z'coherence between NREMure and NREM, and REMure and REM

A. Inter-hemispheric z'coherence p values NREMure Vs. NREM									
	rM1-lM1			**rS1-lS1**			**rV2-lV2**		
Frequency	**df**	**t**	**P**	**df**	**t**	**P**	**df**	**t**	**p**
Delta	7	0.952	0.915	8	0.913	0.406	7	0.521	0.854
Theta	7	0.114	0.991	8	3.795	0.026	7	4.988	0.011
Sigma	7	0.123	0.991	8	7.540	0.001	7	4.675	0.014
Beta	7	1.022	0.916	8	5.417	0.005	7	3.714	0.037
LG	7	0.958	0.916	8	6.142	0.003	7	2.875	0.092
HG	7	1.029	0.916	8	3.806	0.026	7	0.844	0.811
HFO	7	1.461	0.766	8	1.317	0.406	7	0.373	0.854
B. Inter-hemispheric z'coherence p values REMure Vs. REM									
	rM1-lM1			**rS1-lS1**			**rV2-lV2**		
Frequency	**df**	**t**	**p**	**df**	**t**	**P**	**df**	**t**	**p**
Delta	7	0.120	0.907	8	2.435	0.169	7	0.127	0976
Theta	7	0.969	0.597	8	6.023	0.003	7	4.403	0.018
Sigma	7	2.309	0.323	8	7.148	0.001	7	5.203	0.008
Beta	7	0.157	0.534	8	0.990	0.584	7	3.089	0.085
LG	7	0.227	0.538	8	0.060	0.953	7	1.160	0.634
HG	7	0.124	0.534	8	1.430	0.480	7	0.204	0.976
HFO	7	0.119	0.534	8	3.699	0.038	7	2.000	0.301

Statistical results from two-tailed paired Student t tests between NREMure and NREM (A) and REMure and REM(B). Adjusted p values (Holm-Šídák correction for multiple comparisons). Data are plotted in Figure 3.

Table 8. Intra-hemispheric z'coherence between NREMure and NREM, and REMure and REM.

A. Intra-hemispheric z'coherence p values NREMure Vs. NREM									
	rOB-rM1			**rM1-rS1**			**rS1-rV2**		
Frequency	**df**	**T**	**p**	**df**	**T**	**p**	**df**	**T**	**p**
Delta	7	0.876	0.558	8	0.199	0.976	6	0.231	0.985
Theta	7	1.288	0.558	8	1.150	0.820	6	0.326	0.985
Sigma	7	1.053	0.558	8	1.037	0.820	6	1.331	0.842
Beta	7	2.057	0.437	8	1.144	0.820	6	0.726	0.942
LG	7	2.012	0.437	8	0.133	0.976	6	0.836	0.942
HG	7	1.608	0.483	8	1.243	0.820	6	0.297	0.985
HFO	7	1.769	0.473	8	1.557	0.700	6	1.128	0.885
B. Intra-hemispheric z'coherence p values REMure Vs. REM									
	rOB-rM1			**rM1-rS1**			**rS1-rV2**		
Frequency	**df**	**T**	**p**	**df**	**T**	**P**	**df**	T	**p**
Delta	7	2.802	0.149	8	1.072	0.911	6	3.141	0.132
Theta	7	1.475	0.456	8	0.594	0.985	6	2.282	0.321
Sigma	7	3.473	0.071	8	0.402	0.992	6	2.035	0.369
Beta	7	1.986	0.364	8	0.204	0.992	6	0.371	0.979
LG	7	0.255	0.806	8	0.376	0.992	6	0.063	0.998
HG	7	1.124	0.507	8	0.110	0.992	6	0.021	0.998
HFO	7	1.993	0.364	8	1.129	0.911	6	1.394	0.616

Statistical results from two-tailed paired Student t tests between NREMure and NREM (A) and REMure and REM(B). Adjusted p values (Holm-Šídák correction for multiple comparisons). Data are plotted in Figure 4.

Table 9. Normalized transfer entropy between NREMure and NREM, and REMure and REM.

Normalized transfer entropy						
A. NREMure vs NREM						
	FB			**FF**		
Frequency	**df**	**t**	**p**	**df**	**t**	**p**
Delta	8	0.298	0.997	8	0.572	0.970
Theta	8	1.806	0.552	8	1.394	0.739
Sigma	8	0.606	0.984	8	1.200	0.785
Beta	8	0.127	0.997	8	0.471	0.970
LG	8	0.140	0.997	8	0.074	0.970
HG	8	0.205	0.997	8	0.571	0.970
HFO	8	0.994	0.924	8	1.613	0.667
B. REMure vs REM						
	FB			**FF**		
Frequency	**df**	**t**	**p**	**df**	**t**	**p**
Delta	8	0.371	0.971	8	0.406	0.9863
Theta	8	0.923	0.966	8	0.435	0.9863
Sigma	8	0.923	0.966	8	1.884	0.5078
Beta	8	0.962	0.971	8	0.181	0.9863
LG	8	0.815	0.971	8	0.075	0.9863
HG	8	0.526	0.966	8	1.218	0.7748
HFO	8	0.403	0.966	8	1.566	0.6385

Statistical results from two-tailed paired Student t tests between NREMure and NREM (A) and REMure and REM(B). Adjusted p values (Holm-Šídák correction for multiple comparisons).

Comentarios adicionales a la discusión del artículo

En este trabajo demostramos que la anestesia general con uretano se caracteriza por presentar correlatos de pérdida de consciencia, refutando la teoría de que el estado similar a REM o estado activado podría ser un estado similar a la vigilia en el cual el animal podría estar carente de respuesta e inmóvil pero consciente. Adicionalmente, hemos demostrado que, si bien la anestesia bajo uretano recuerda al sueño fisiológico, presenta importantes diferencias con el mismo, hallazgo que se muestra como una evidencia en contra de la teoría de una sobreposición neurofisiológica entre el sueño y la anestesia general. En este sentido, la revisión de Akeju y Brown (2007) recopila diversos hallazgos que demuestran diferencias en las oscilaciones neurales entre el sueño y diversos agentes anestésicos y sedantes (Akeju & Brown, 2017). Por ejemplo, los autores remarcan que mientras las oscilaciones delta durante el sueño No-REM son sincrónicas, mientras que las generadas por propofol son asincrónicas con períodos de inactividad cortical. En cuanto a la similitud entre la anestesia con Ketamina y el sueño REM, el tipo de oscilaciones gamma presentes también son diferentes en estos dos estados ya que durante la anestesia con ketamina existe una alternancia entre oscilaciones gamma y oscilaciones delta (Akeju *et al.*, 2016). En este sentido, resulta interesante mencionar que un artículo publicado recientemente desarrolla el concepto de "anestesia paradojal" refiriéndose con este nombre a un estado similar a REM o vigilia que ocurre cuando agentes GABAérgicos son inyectados en la región tegmental mesopontina. Estos autores demostraron que si bien cuando anestésicos como el pentobarbital son inyectados de forma sistémica, ocurre una actividad electroencefalográfica caracterizada por la presencia de ondas lentas, al inyectarlos directamente en la región tegmental mesopontina ocurre un ciclado entre un estado de ondas lentas (similar al sueño No-REM) y un estado activado, similar al REM (o a la vigilia). Sin embargo, estos autores también encontraron diferencias en las características

electroencefalográficas de la anestesia paradojal y el sueño REM, principalmente una mayor potencia y coherencia delta de la primera con respecto al sueño REM natural, similar a nuestros hallazgos con uretano (Avigdor *et al.*, 2021).

Capítulo 3. Teoría de circuitos compartidos. ¿Qué rol juega el área preóptica del hipotálamo en la anestesia general?

Como fue mencionado anteriormente, Lydic y Biebuyck propusieron, en 1994 la hipótesis de que la anestesia general actúa en los mismos circuitos neurales encargados de la generación de sueño (Lydic & Biebuyck, 1994). Las principales áreas generadoras de sueño No-REM en el encéfalo de mamíferos son el área preóptica del hipotálamo (Saper *et al.*, 2005; Benedetto *et al.*, 2012) y un grupo de neuronas GABAérgicas en el prosencéfalo basal (Lee *et al.*, 2004; Xu *et al.*, 2015).

Por otra parte, la generación de REM está dada principalmente por neuronas ubicadas en el área tegmental laterodorsal, el núcleo tegmental pedunculopontino y el núcleo tegmental sublaterodorsal (Boucetta *et al.*, 2014; Van Dort *et al.*, 2015).

El área preóptica del hipotálamo puede dividirse en 4 áreas anatómicas principales: El núcleo mediano (MnPO), el área medial (MPO), el área lateral (LPO) y el área ventrolateral (VLPO) (Reitz & Kelz, 2021). Dentro de estas áreas, las principales involucradas en la generación del sueño NREM han sido el MnPO y el VLPO (Gvilia et al., 2011; Suntsova et al., 2002; Szymusiak & McGinty, 2008; Torterolo et al., 2009). Las neuronas GABAérgicas y galaninérgicas del VLPO y MnPO generan sueño mediante la inhibición de centros activadores (Vanini et al., 2011). La actividad de estas neuronas es diferente entre ambas regiones. Mediante c-Fos se ha visto que muchas de las neuronas GABAérgicas del MnPO se activan en respuesta a la presión de sueño, mientras que en el VLPO la descarga de las neuronas GABAérgicas incrementa cuando el animal está dormido (Gvilia, 2006). Es por esto que, si bien se ha demostrado que ambas regiones son esenciales en la regulación homeostática del sueño, se han sido sugeridos roles diferenciales de la VLPO y el MnPO (Gvilia et al., 2006). El MnPO sería más importante en promover la transición de la vigilia al sueño, mientras el VLPO contribuiría al mantenimiento del sueño NREM (Gvilia,

2010). Los anestésicos generales tanto de administración intravenosa (propofol y barbitúricos) como volátiles (isoflurano) activan neuronas GABAergicas de la POA que son presumiblemente promotoras de sueño NREM (Moore et al., 2012; Nelson et al., 2003; Tung et al., 2001). Sin embargo, aún quedan elementos por esclarecer. Por un lado, mientras que el rol de las neuronas GABAérgicas o galaninérgicas en el VLPO en el control del sueño y anestesia está bien documentado en la literatura, el rol de otros tipos neuronales, como las neuronas glutamátergicas no ha sido estudiado en detalle (Modirrousta *et al.*, 2004; Kroeger *et al.*, 2018). A su vez, el rol del VLPO en la anestesia ha sido estudiado más ampliamente que el del MnPO (Lu *et al.*, 2008; Moore *et al.*, 2012; Han *et al.*, 2014). Por último, la mayoría de los trabajos se han basado en correlaciones, pero no existían hasta el momento trabajos que hubieran evaluado un rol causal de estas áreas en la anestesia general.

La hipótesis de este capítulo fue que la activación de neuronas glutamatérgicas y/o GABAérgicas del MnPO y VLPO modificarían los tiempos de inducción y recuperación anestésica.

El objetivo fue evaluar el rol de distintos subgrupos neuronales (neuronas glutamatérgicas y GABAérgicas) del VLPO y el MnPO en la inducción y recuperación anestésica.

Estrategia experimental

Para los trabajos contenidos dentro de este capítulo y el siguiente, fue utilizado el ratón como modelo animal. Esto fue necesario ya que para estimular selectivamente determinados grupos neuronales utilizamos quimiogenética, lo que requirió del uso de líneas de animales genéticamente modificados y estas líneas están más desarrolladas en ratones que en ratas.

La quimiogenética es una técnica que permite la modulación selectiva de grupos neuronales específicos. Consiste en la modificación de proteínas (en general receptores neuronales) para que sean capaces de interactuar con ligandos que no eran capaces de reconocer previamente (Roth,

2016). Actualmente, los Receptores de Diseño Exclusivamente Activados por Drogas de Diseño (DREADDs – Designed Repectors Activated Exclusively by Designed Drugs), son las proteínas modificadas más ampliamente utilizadas (Roth, 2016; Smith *et al.*, 2016). Los DREADDs consisten en receptores acoplados a proteína G, como por ejemplo los receptores muscarínicos de acetilcolina, modificados para que pierdan la sensibilidad a su ligando natural y se vuelvan sensibles a una droga inerte. Una de las drogas más utilizadas es el CNO (de sus siglas en inglés, Clozapine-N-oxide). Existen diversas opciones para expresar DREADDs en neuronas, una de las más utilizadas, y la que utilizamos en este trabajo, es el uso de vectores virales como, por ejemplo, virus adeno-asociados (AAV). Estos virus transportan la información genética necesaria para inducir la expresión de los DREADDs en las neuronas que infectan. De esta manera, es posible reducir la expresión de estos receptores al área de inyección del AAV. Sin embargo, para poder seleccionar únicamente determinados grupos neuronales en esas áreas, es necesario utilizar AAV dependientes de Cre-recombinasa (Roth, 2016; Smith *et al.*, 2016; Whissell *et al.*, 2016). La enzima Cre-recombinasa reconoce secuencias direccionales de 34 pares de bases (sitos Lox-P) formados por 2 sitios de reconocimiento de 13 pares de bases separados por una secuencia espaciadora de 8 pares de bases. Al unirse a las secuencias Lox-P la Cre-recombinasa produce una recombinación del material genético. Es posible entonces, lograr que la expresión de DREADDs ocurra solamente en neuronas que expresan Cre-recombinasa, por ejemplo, añadiendo una secuencia de STOP entre sitios Lox-P antes de la que codifica para el DREADD; sólo las neuronas que expresan Cre-recombinasa podrán escindir esa secuencia STOP y el gen de interés podrá expresarse (Taniguchi, 2014; Zhou *et al.*, 2017). Existen líneas de ratones modificados genéticamente que cuentan con expresión de Cre-recombinasa en grupos neuronales específicos.

En nuestro trabajo utilizamos ratones Vglut2-IRES-Cre y Vgat-IRES-Cre que expresan Cre-recombinasa en neuronas glutamatérgicas y GABAérgicas respectivamente.

Current Biology
Article

Activation of Preoptic GABAergic or Glutamatergic Neurons Modulates Sleep-Wake Architecture, but Not Anesthetic State Transitions

Giancarlo Vanini,[1,2,3,4,*] Marina Bassana,[1,2,3] Megumi Mast,[1] Alejandra Mondino,[1] Ivo Cerda,[1] Margaret Phyle,[1] Vivian Chen,[1] Angelo V. Colmenero,[1] Viviane S. Hambrecht-Wiedbusch,[1,2] and George A. Mashour[1,2,3]
[1]Department of Anesthesiology, University of Michigan, 7433 Medical Science Building 1, 1150 West Medical Center Drive, Ann Arbor, MI 48109-5615, USA
[2]Center for Consciousness Science, University of Michigan, Ann Arbor, MI 48109, USA
[3]Neuroscience Graduate Program, University of Michigan, 4137 Undergraduate Science Building, 204 Washtenaw Avenue, Ann Arbor, MI 48109-2215, USA
[4]Lead Contact
*Correspondence: gvanini@umich.edu
https://doi.org/10.1016/j.cub.2019.12.063

SUMMARY

The precise mechanism of general anesthesia remains unclear. In the last two decades, there has been considerable focus on the hypothesis that anesthetics co-opt the neural mechanisms regulating sleep. This hypothesis is supported by ample correlative evidence at the level of sleep-promoting nuclei, but causal investigations of potent inhaled anesthetics have not been conducted. Here, we tested the hypothesis that chemogenetic activation of discrete neuronal subpopulations within the median preoptic nucleus (MnPO) and ventrolateral preoptic nucleus (VLPO) of the hypothalamus would modulate sleep/wake states and alter the time to loss and resumption of consciousness associated with isoflurane, a potent halogenated ether in common clinical use. We show that activating MnPO/VLPO GABAergic or glutamatergic neurons does not alter anesthetic induction or recovery time. However, activation of these neuronal subpopulations did alter sleep-wake architecture. Notably, we report the novel finding that stimulation of VLPO glutamatergic neurons causes a strong increase in wakefulness. We conclude that activation of preoptic GABAergic or glutamatergic neurons that increase sleep or wakefulness does not substantively influence anesthetic state transitions. These data indicate that the correlative evidence for a mechanistic overlap of sleep and anesthesia at the level of an individual nucleus might not necessarily have strong causal significance.

INTRODUCTION

General anesthetics have been in continuous clinical use for more than 170 years, but the precise mechanisms by which these drugs reversibly suppress consciousness remain unknown. Within the past two decades, there has been increased attention on the relationship between sleep and general anesthesia, with ample correlative evidence suggesting that anesthetics act by co-opting subcortical nuclei that generate sleep and wakefulness [1–4]. To date, research on the mechanisms underlying the sleep-anesthesia connection has focused predominantly on the preoptic region of the hypothalamus, particularly the medial preoptic area [5] and ventrolateral preoptic nucleus (VLPO) [2, 4, 6–8]. Consistent with what has been termed the shared circuits hypothesis, putative sleep-promoting GABAergic neurons in the VLPO express cFos during the loss of consciousness induced by isoflurane, which directly activates these neurons [2]. However, despite biological plausibility and compelling correlative data, there have been no causal investigations to date that demonstrate a role for discrete neuronal subpopulations in the preoptic area of the hypothalamus in the mechanism of general anesthesia. Additionally, the median preoptic nucleus (MnPO) of the hypothalamus is critical for both sleep generation and the regulation of sleep homeostasis [9–12], but its influence on the anesthetized state remains virtually unexplored. In this study, we tested the hypothesis that activation of neuronal subpopulations within the preoptic area of the hypothalamus that promote sleep or wakefulness would modulate the entry to or exit from general anesthesia induced by isoflurane, a potent halogenated ether in common clinical use. To test this hypothesis, we used a chemogenetic approach to examine the role of GABAergic and glutamatergic neurons of both the MnPO and VLPO in anesthetic state transitions. We report that, despite altering sleep-wake states, activation of preoptic GABAergic or glutamatergic neurons had no substantive effect on the entry to or emergence from isoflurane anesthesia. These findings prompt a reconsideration of the hypothesis that general anesthesia is produced by activating nuclei in the preoptic hypothalamus known to promote or regulate sleep.

RESULTS

Activation of Neuronal Subpopulations in the Median Preoptic Nucleus Did Not Alter Anesthetic-State Transitions

To determine whether activation of GABAergic or glutamatergic neurons in the MnPO (Figure S4) modulates anesthetic induction and recovery time, mice were exposed to a clinically relevant

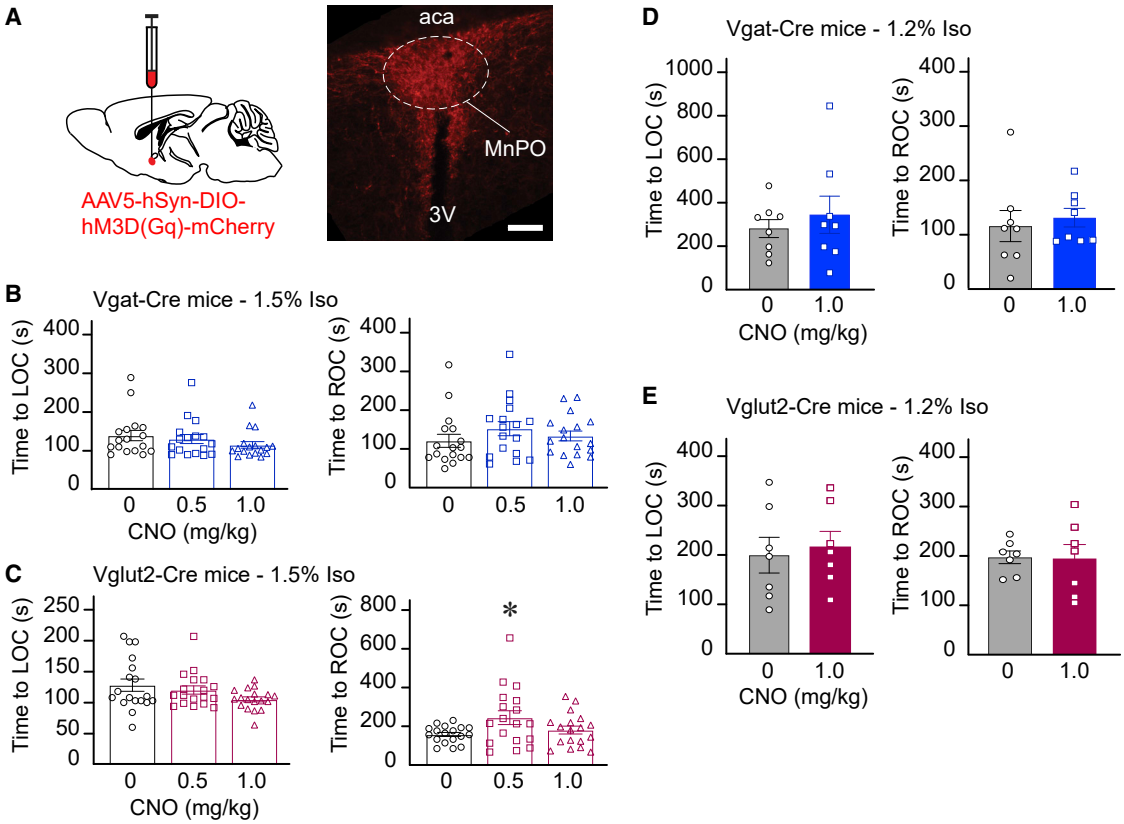

Figure 1. Chemogenetic Stimulation of GABAergic and Glutamatergic Neurons in the MnPO Did Not Alter Anesthetic State Transitions

(A) Schematic representation of adeno-associated virus (AAV) injection into the median preoptic nucleus (MnPO). mCherry (red) indicates the expression of the excitatory designer receptor hM3Dq within the MnPO of a Vglut2-Cre mouse.

(B) Time to loss (left) and resumption of consciousness (right) in Vgat-Cre mice exposed to 1.5% isoflurane.

(C) Time to loss (left) and resumption of consciousness (right) in Vglut2-Cre mice exposed to 1.5% isoflurane.

(D and E) Time to loss and resumption of consciousness (left and right panels, respectively) in Vgat-Cre and Vglut2-Cre mice (D and E, respectively) exposed to 1.2% isoflurane.

The asterisk in (C) indicates a significant difference (*$p < 0.05$) from vehicle control (0 mg/kg CNO). Statistical comparisons were conducted using a Friedman test followed (when applicable) by a post hoc Dunn's (B and C) or a two-tailed Wilcoxon test (D and E). Scale bar in (A), 50 μm. Data in (B)–(E) are shown as mean ± SEM. aca, anterior commissure; CNO, clozapine-N-oxide; LOC, loss of consciousness; ROC, resumption of consciousness; 3V, third ventricle.

See also Figures S1, S2, and S4.

(1.5%) or a sub-anesthetic (1.2%) concentration of isoflurane for 30 min. Relative to vehicle, activation of GABAergic neurons in the MnPO (n = 17 mice) prior to exposure to 1.5% isoflurane did not alter anesthetic induction ($p = 0.1256$) or recovery time ($p = 0.2198$; Figure 1B). Activation of glutamatergic neurons (n = 18 mice) did not change induction time ($p = 0.3577$); recovery time was increased ($p = 0.0071$) after injection of 0.5 mg/kg clozapine-N-oxide (CNO) only (p value for saline versus 1.0 mg/kg CNO > 0.9999; Figure 1C). The statistical significance between 0.5 mg/kg CNO and vehicle was caused by a single outlier (p value without outlier = 0.2919). The estrous cycle stage was identified in all female mice after each anesthesia experiment by histological assessment of vaginal smears. Female mice were used in 78 experiments, 60% of which were conducted during diestrus, 25% during metestrus, and 15% during estrous or proestrus. Changes in the cycle stage between control versus 0.5 mg/kg CNO and control versus 1.0 mg/kg CNO were observed, respectively, in 18% and 19% of the experiments. Relative to control, there were no significant differences in induction and recovery time as a function of sex or estrous cycle stage. Similarly, activation of MnPO GABAergic and glutamatergic neurons prior to exposure to 1.2% isoflurane (a sub-anesthetic concentration) did not change anesthetic induction and recovery time (n = 8 Vgat-Cre mice, $p = 0.5469$ and 0.6406; n = 7 Vglut2-Cre mice, $p = 0.6875$ and 0.7813; Figures 1D and 1E). Consistent with these behavioral findings, there was no difference in breathing rates between treatment conditions ($p > 0.1$) at 1.5% or 1.2% isoflurane. Mice exposed to 1.2% exhibited a few transient wake-like episodes during anesthesia, ranging from limb movements to the resumption of righting. Post hoc analysis revealed no differences in the amount of wake-like episodes between vehicle and CNO ($p > 0.9999$). To rule out any non-specific effect of CNO, an adverse effect from the vector injection (i.e., mechanical and/or inflammatory tissue damage), or Cre-associated toxicity [13] on anesthetic induction/recovery time, we conducted additional anesthesia experiments using the following groups of Vgat-Cre and Vglut2-Cre mice: (1) mice injected with the vector but without

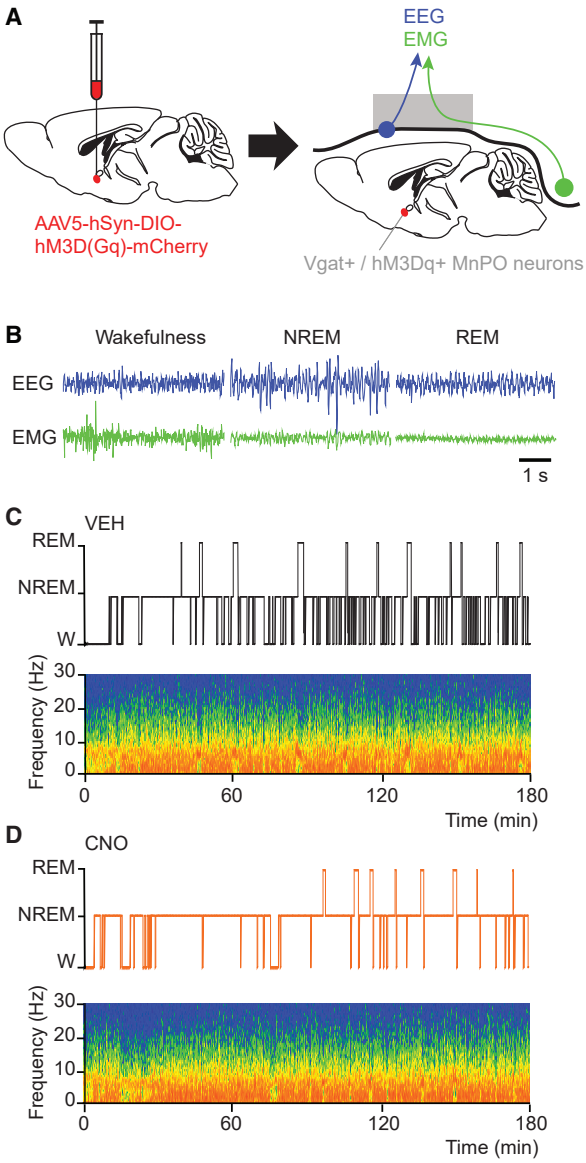

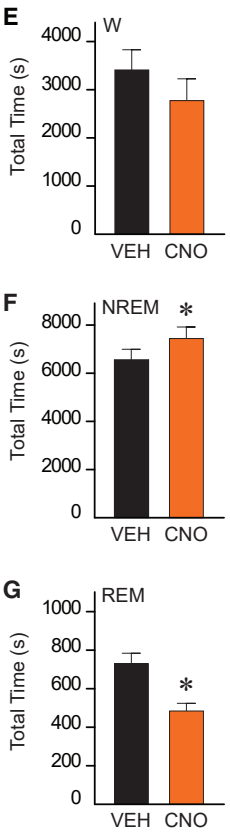

Figure 2. Chemogenetic Stimulation of GABAergic Neurons in the MnPO Increased NREM Sleep and Decreased REM Sleep

(A) Schematic representation of AAV injection into the MnPO for expression of the excitatory designer receptor hM3Dq. Following the expression of hM3Dq receptors in the MnPO, mice were implanted with electrodes for recording the electroencephalogram (EEG) (blue) and electromyogram (EMG) (green).

(B) Representative EEG and EMG traces recorded from the same Vgat-Cre mouse during wakefulness, non-rapid eye movement (NREM) sleep, and rapid eye movement (REM) sleep.

(C and D) Hypnograms displaying the time course of sleep and wakefulness during the 3-h recording period after vehicle (VEH; C) and CNO (D) injection. The spectrograms below each hypnogram show state-specific changes in frontal power density (red, maximum; blue, minimum) across the respective recording session. Time 0 on the abscissa indicates the time at which VEH or CNO (1.0 mg/kg) was injected.

(E–G) Effect of CNO administration on the duration (in s) of wakefulness (W; E), NREM sleep (F), and REM sleep (G) over the 3-h recording period. Asterisk indicates a significant difference (*$p < 0.05$) from vehicle control using a one-tailed Wilcoxon test. Data are shown as mean ± SEM.

See also Figures S3 and S4.

expression of hM3Dq receptors (Figure S1; Vgat-Cre, n = 7 and Vglut2-Cre, n = 6); (2) sham operated Vgat-Cre (n = 6) and Vglut2-Cre (n = 5); and (3) naive mice (n = 5 in each mouse line; the results from both groups are shown in Figure S2). Relative to vehicle, 1.0 mg/kg CNO administration did not alter anesthetic state transitions in any of the three control groups.

Activation of Neuronal Subpopulations in the Median Preoptic Nucleus Altered Sleep-Wake Architecture and Reduced Core Body Temperature

In a second set of experiments, we tested whether selective activation of MnPO GABAergic and glutamatergic neurons (during the same time period during which the anesthesia experiments were conducted) modulates sleep-wake architecture (n = 6 Vgat-Cre and n = 7 Vglut2-Cre mice). Figure 2 shows representative examples of electrophysiological recordings during wakefulness, non-rapid eye movement (NREM) sleep, and rapid eye movement (REM) sleep (Figure 2B) and sleep-wake patterns with their respective spectrograms after injection of vehicle (Figure 2C) or 1.0 mg/kg CNO (Figure 2D) in Vgat-Cre mice. Group data plotted in Figures 2E–2G revealed that activation of GABAergic neurons in the MnPO increased the time spent in NREM sleep ($p = 0.0313$) and decreased REM sleep ($p = 0.0156$); total time in wakefulness was not significantly different ($p = 0.0781$). CNO caused a significant reduction in the number of wakefulness ($p = 0.0156$), NREM sleep ($p = 0.0156$), and REM sleep ($p = 0.0313$) bouts and an increase in NREM bout duration ($p = 0.0156$; e.g., more consolidated sleep). Activation of MnPO glutamatergic neurons decreased REM sleep ($p = 0.0391$) but did not alter wakefulness and NREM sleep ($p = 0.3438$ and 0.5000, respectively). The decrease in REM sleep (695.70 s ± 71.95 versus 382.12 s ± 72.21) is at the expense of non-significant increases in the time spent in wakefulness (3,956 s ± 584.70 versus 4,199 s ± 434; $p = 0.3804$) and NREM sleep (6,148 s ± 534.50 versus 6,219 s ± 423.50; $p = 0.4596$). To control for potential adverse effects of the vector injection and non-specific effects of 1.0 mg/kg CNO on sleep-wake architecture, additional studies were conducted in sham Vgat-Cre (n = 5) and Vglut2-Cre (n = 5) mice. Duration of wakefulness, NREM sleep, and REM sleep were not different in sham versus transfected mice, and CNO administration to sham mice did not alter the duration of sleep and wakefulness states (Figure S3).

Given the recently identified role of MnPO glutamatergic neurons in regulating both temperature and sleep [9, 10], changes in

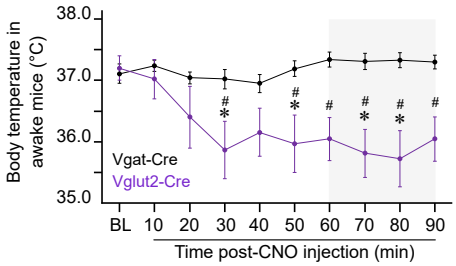

Figure 3. Stimulation of Glutamatergic (but Not GABAergic) Neurons in the MnPO Produced Hypothermia in Awake Mice

The figure plots the change in core body temperature in awake mice before and after an intraperitoneal injection of CNO (1.0 mg/kg). Asterisk indicates significant differences (*$p < 0.05$) from baseline, and hashtag symbols indicate significant differences between mouse lines. Statistical comparisons were conducted using a two-way ANOVA with Bonferroni's correction for multiple comparisons. The gray area indicates the time period (60–90 min) during which the time to loss and resumption of consciousness was assessed in anesthesia experiments. Data are shown as mean ± SEM. See also Figure S4.

body temperature were assessed in a subset of awake mice before and during 90 min after 1.0 mg/kg CNO administration. As expected [10], CNO administration to Vglut2-Cre mice (n = 9) induced a sustained reduction in body temperature (treatment effect; $F(1, 170) = 65.41$; $p < 0.0001$), although there was no temperature change in Vgat-Cre mice (n = 10; Figure 3). There was no significant correlation between the number of mCherry-positive glutamatergic neurons and the magnitude of temperature change. In both mouse lines, CNO administration (1.0 mg/kg) significantly increased cFos expression in MnPO hM3Dq-positive neurons ($p < 0.0001$ in Vgat-Cre and $p = 0.0002$ in Vglut2-Cre mice; Figure 4). Together, these data indicate that activation of MnPO GABAergic and glutamatergic neurons results in the expected changes of promoting sleep and reducing temperature but does not alter anesthetic state transitions.

Activation of Neuronal Subpopulations in the Ventrolateral Preoptic Nucleus Did Not Alter Anesthetic-State Transitions

The expression pattern of hM3Dq designer receptors in this study (Figure S5) is consistent with what has been termed the extended VLPO [14, 15], but we will hereafter refer to it as VLPO. Given the unexpected finding that selective manipulation of two neuronal subpopulations within the MnPO did not modulate the entry to and exit from the anesthetized state, we conducted the same experiments in VLPO, a hypothalamic nucleus that is critical for the generation of NREM sleep, as a control site [15]. Figure 5 shows that activation of GABAergic or glutamatergic neurons in the VLPO, prior to exposure to 1.5% (n = 10 Vgat-Cre and n = 6 Vglut2-Cre mice) or 1.2% (n = 4 Vgat-Cre and n = 4 Vglut2-Cre mice) isoflurane, did not alter anesthetic induction or recovery time.

Activation of Neuronal Subpopulations in the Ventrolateral Preoptic Nucleus Altered Sleep-Wake Architecture

Following anesthesia experiments, we conducted sleep studies to determine whether similar conditions of activated GABAergic and glutamatergic VLPO neurons play a role in sleep-wake control. These sleep studies were conducted during the same time period (i.e., 3 h spanning CNO/vehicle injection to emergence) as the anesthesia experiments. Representative examples of the electrophysiological signatures of wake, NREM sleep, and REM sleep in Vglut2-Cre mice are shown in Figure 6B. The temporal organization of sleep-wake states and changes in power spectral density after vehicle or 1.0 mg/kg CNO administration are depicted in Figures 6C and 6D, respectively. Group data plotted in Figures 6E–6G demonstrate that activation of glutamatergic neurons in the VLPO (n = 4 mice) increases the time in wakefulness ($p = 0.0233$; 79% increase) and reduces NREM sleep ($p = 0.0351$) and REM sleep ($p = 0.0176$). There were no significant changes in the number of bouts or bout duration in any of the three states. Chemogenetic stimulation of GABAergic neurons in the VLPO (n = 4 mice) did not alter sleep-wake architecture ($p > 0.1000$ for wakefulness, NREM, and REM sleep). Collectively, activation of GABAergic or glutamatergic neurons in the VLPO does not alter state transitions induced by isoflurane, despite a robust alteration of sleep-wake architecture induced by activation of glutamatergic subpopulations.

DISCUSSION

These data show that chemogenetic stimulation of GABAergic or glutamatergic neurons in the MnPO and VLPO does not substantially alter state transitions related to isoflurane anesthesia. To our knowledge, this is the first direct assessment of a causal role for two major sleep-promoting nuclei [9, 10, 15], to the resolution of a single-cell subtype, in the mechanisms of inhaled general anesthesia. Our results are highly relevant—and rather unexpected—because a prevailing hypothesis in the field posits that general anesthetics produce the loss of consciousness by co-opting nuclei that regulate sleep-wake states [1, 2, 16]. This hypothesis has been supported by abundant correlative evidence suggesting that the preoptic region of the hypothalamus, particularly the medial preoptic area [5] and VLPO [2, 4, 6–8], plays a key role in the relationship between sleep and anesthesia. Consistent with the shared circuits hypothesis, previous work using cFos-dependent tagging and selective stimulation of previously active (tagged) neurons showed that sedation with dexmedetomidine and NREM sleep are produced, in part, by the same neuronal array within the preoptic area [17]. Preoptic galanin neurons mediate, in part, sleep homeostasis as well as the sedative and hypothermic effect of dexmedetomidine [18]. However, dexmedetomidine is clinically used in humans as a sedative, and its hypnotic, NREM-sleep-like effect is readily reversible upon stimulation, unlike general anesthesia with isoflurane, a halogenated ether used at clinically relevant concentrations in the current study.

Importantly, our study shows that activation of GABAergic and glutamatergic neurons in the MnPO and VLPO altered sleep-wake architecture during a similar time period in which anesthesia experiments were conducted. Consistent with previously published work [9, 10], activation of GABAergic neurons in the MnPO increased the amount of NREM sleep. Another remarkable finding was that activation of glutamatergic neurons in the VLPO caused a strong increase in wakefulness and a reduction in both NREM and REM sleep. These data are novel because no previous studies have examined the role of VLPO

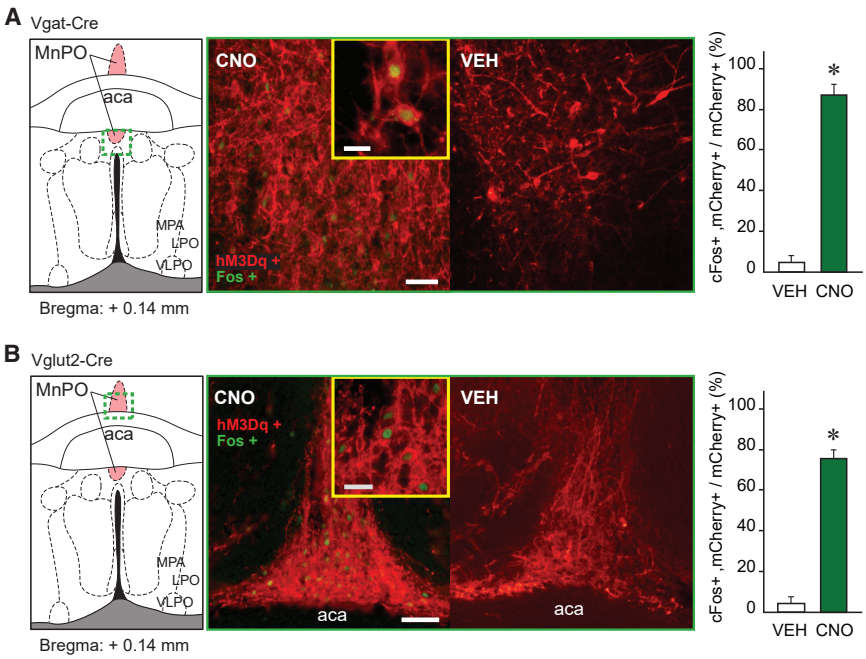

Figure 4. Verification of MnPO Vgat+ and Vglut2+ Cell Activation by CNO

(A and B) cFos expression (green nuclei) in mCherry expressing (red) neurons within the MnPO of Vgat-Cre (A) and Vglut2-Cre (B) mice, 90 min after an intraperitoneal injection of CNO (1.0 mg/kg) or VEH. The bar graphs plot the percentage (mean + SEM) of mCherry-expressing neurons that also express cFos over the total number of mCherry-positive cells after vehicle or CNO administration. Asterisk indicates a significant difference (*$p < 0.05$) from vehicle control using a one-tailed Mann Whitney test. The strong increase in cFos expression in GABAergic (Vgat+) and glutamatergic (Vglut2+) neurons provides further validation of hM3Dq receptors in the MnPO. Scale bars in (A) and (B), 50 μm and 20 μm (inset). LPO, lateral preoptic area; MPA, medial preoptic area; VLPO, ventrolateral preoptic nucleus.

glutamatergic neurons in the regulation of sleep and wakefulness. Neurons in the MnPO and VLPO play a dual role in sleep generation and sleep homeostasis [11, 17, 19]. The modulation of sleep and wakefulness caused by stimulation of preoptic neurons is of relevance to our study because of the well-known relationship between sleep homeostasis and anesthesia. For example, sleep deprivation or sleep loss caused by chronic VLPO lesions potentiates the hypnotic effect of propofol and the inhalational anesthetic sevoflurane [6, 20, 21]. Additionally, general anesthesia has been shown to satisfy the homeostatic sleep drive in a drug-specific manner [21–23]. Thus, the dual role of these preoptic neurons in sleep generation and the regulation of sleep homeostasis strengthened our prediction that stimulation of preoptic sleep- or wake-promoting neurons would alter anesthetic induction and recovery time. Contrary to our prediction, activation of preoptic neurons that increase sleep or wakefulness did not affect anesthetic state transitions. An interesting possibility that remains to be explored is whether increasing the time between CNO injection and behavioral testing, allowing more time for the sleep/wake drive to accrue, or varying the circadian time of the experiment (i.e., early morning versus evening) would yield a different outcome. It is also important to consider other subcortical nodes that are not classically considered critical for sleep regulation but might play a more relevant role in general anesthetic mechanisms. For example, recent and noteworthy studies showed that glutamatergic neurons in the lateral habenula facilitate the hypnotic effect of the intravenous anesthetic propofol [24], and neuroendocrine cells within the supraoptic nucleus promote NREM sleep and facilitate general anesthesia [25]. These studies, in conjunction with our complementary findings, should prompt the field to consider exploring additional brain regions and nuclei beyond those classically known to regulate sleep and wakefulness. Furthermore, it is becoming increasingly evident that widespread neural networks encompassing multiple nuclei within the rostral hypothalamus orchestrate the features of complex behaviors and states, such as sleep, sedation, and anesthesia [10, 11, 17, 18, 26, 27].

An unexpected finding was that activation of glutamatergic neurons in the MnPO reduced REM sleep and did not alter NREM sleep. Harding et al. [10] recently demonstrated that sleep generation and the reduction of body temperature are controlled by the same subset of glutamatergic neurons (Vglut2 and nNOS1) localized within the MnPO and the medial preoptic area. This is important because we show that activation of glutamatergic neurons in the MnPO caused a sustained decrease in body temperature, indicating that we activated at least a proportion of the glutamatergic cells that also promote sleep. Contrasting our results with those obtained in control mice, it seems unlikely that tissue damage caused by the injection procedure or the vector itself [13] selectively lesioned the sleep-promoting cells, sparing a neuronal group that causes hypothermia. The fact that VLPO GABAergic neurons did not increase sleep during the light period is not inconsistent with prior studies. GABAergic neurons in the VLPO that co-express galanin project to (among other major wake-promoting centers) the tuberomammillary nucleus of the hypothalamus [28]. Optogenetic and chemogenetic stimulation of VLPO GABAergic/galaninergic neurons increases NREM sleep, but chemogenetic activation during the light period only produces a modest increase [15]. An evident limitation of our study is that our approach did not allow us to assess different subpopulations of VLPO GABAergic cells by targeting, for example, projection-specific or galanin-positive neurons. However, the discrepancy between our findings and the evidence reviewed above may also be attributable to the vast neurochemical and functional diversity of both GABAergic and glutamatergic neurons in the preoptic area [9, 10, 29]. It is important to note that the reduction of body temperature in Vglut2-Cre mice, as well as the changes in sleep architecture and Fos expression in both Vgat-Cre and Vglut2-Cre mice, provided functional validation of hM3Dq receptors in the MnPO and VLPO.

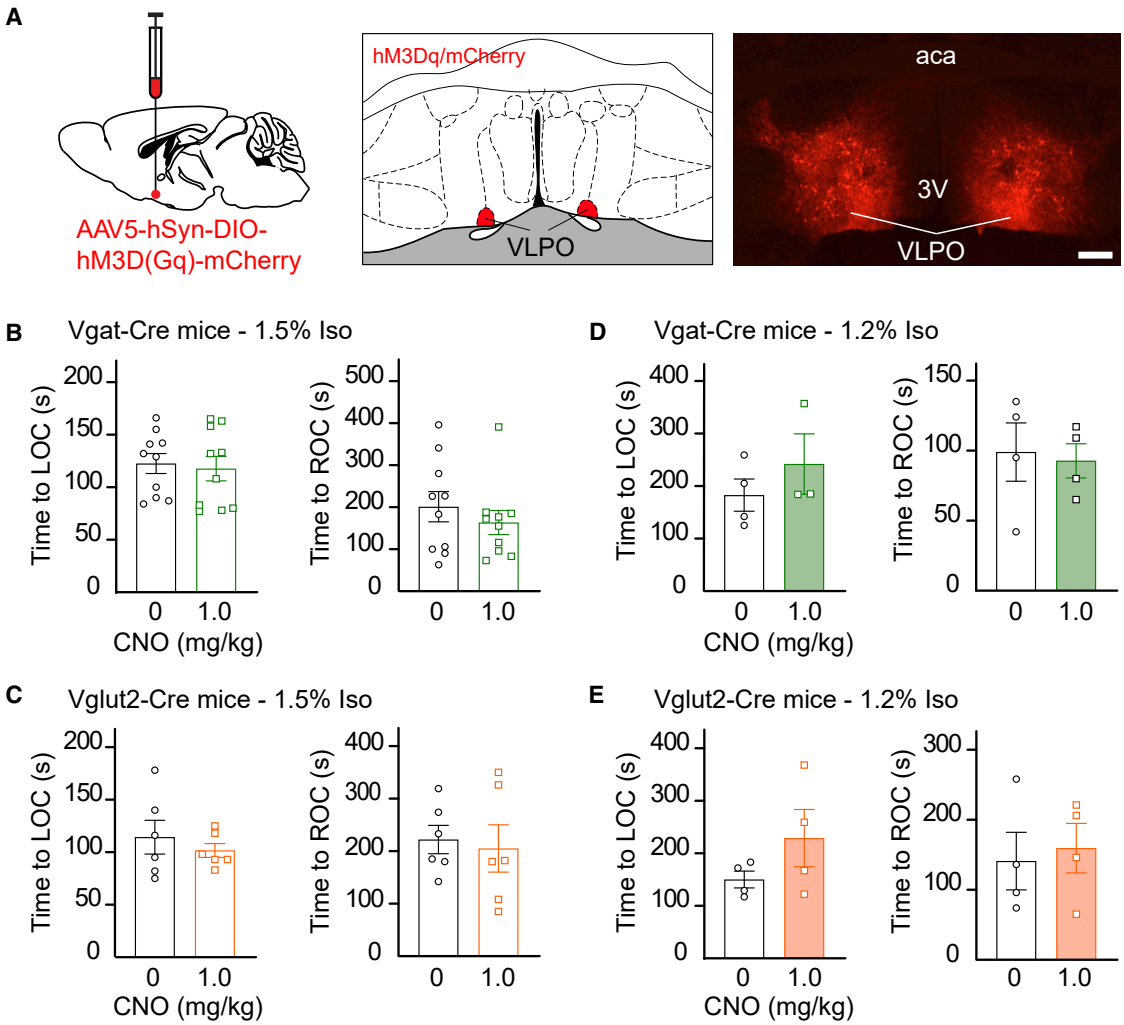

Figure 5. Chemogenetic Stimulation of GABAergic and Glutamatergic Neurons in the VLPO Did Not Alter Anesthetic State Transitions

(A) Schematic representation of bilateral AAV injections into the VLPO. mCherry (red) indicates the expression of the excitatory designer receptor hM3Dq within the VLPO of a Vglut2-Cre mouse.

(B) Time to loss (left) and resumption of consciousness (right) in Vgat-Cre mice exposed to 1.5% isoflurane.

(C) Time to loss (left) and resumption of consciousness (right) in Vglut2-Cre mice exposed to 1.5% isoflurane.

(D and E) Time to loss (left) and resumption of consciousness (right) in Vgat-Cre (D) and Vglut2-Cre (E) mice exposed to 1.2% isoflurane. Statistical comparisons were conducted using two-tailed Wilcoxon test.

Scale bar in (A), 50 μm. Data in (B)–(E) are shown as mean ± SEM.

See also Figures S2 and S5.

Collectively, our data suggest that activation of preoptic GABAergic or glutamatergic neurons that increase sleep or wakefulness does not substantially influence anesthetic state transitions. These data also suggest that the correlative evidence for a mechanistic overlap of sleep and anesthesia at the level of an individual nucleus, or even individual cell subtypes, might not necessarily have strong causal significance. The present study is limited in its restriction to one anesthetic and only used neuronal stimulation techniques, but the findings bring into question the long-standing hypothesis in the field that activation of individual nuclei associated with the promotion of sleep is a major contributor to the mechanism of general anesthesia. Furthermore, given the strong biological plausibility and correlative evidence supporting the shared circuits hypothesis, these data also suggest that the systems neuroscience of general anesthesia requires causal investigations and cannot rely upon *a priori* or theoretical bases regarding the circuits mediating anesthetic-induced unconsciousness.

STAR★METHODS

Detailed methods are provided in the online version of this paper and include the following:

- KEY RESOURCES TABLE
- LEAD CONTACT AND MATERIALS AVAILABILITY
- EXPERIMENTAL MODEL AND SUBJECT DETAILS
  - Mice

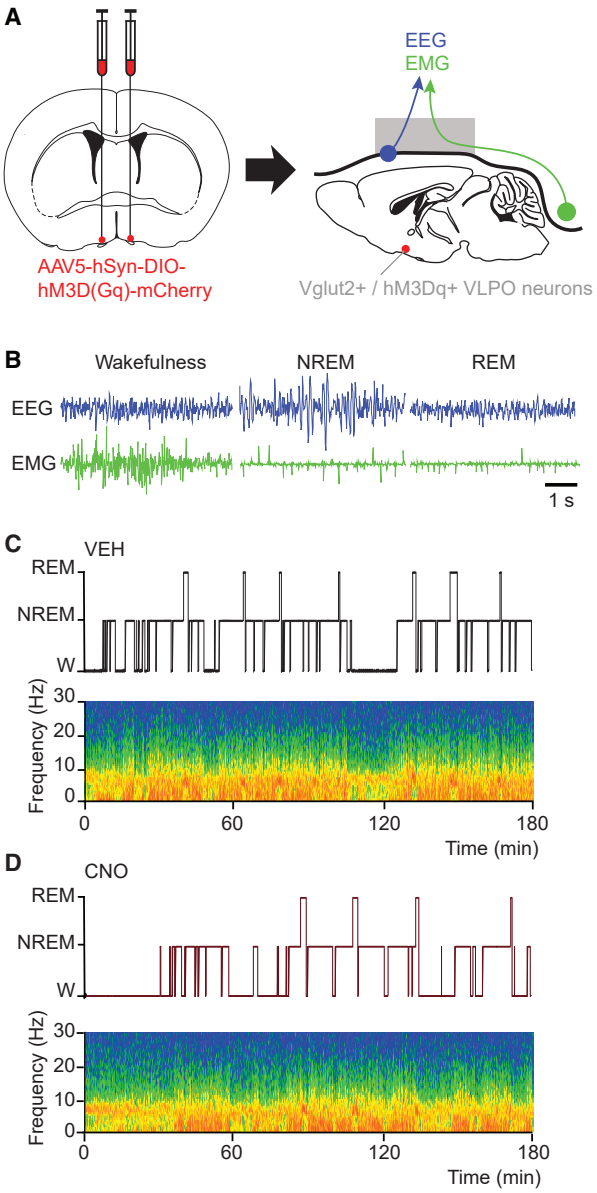

Figure 6. Chemogenetic Stimulation of Glutamatergic Neurons in the VLPO Increased Wakefulness and Decreased Sleep

(A) Schematic representation of bilateral AAV injections into the VLPO for expression of the excitatory designer receptor hM3Dq. Following the expression of hM3Dq receptors in the VLPO, mice were implanted with electrodes for recording the EEG (blue) and EMG (green).

(B) Representative EEG and EMG signals recorded from the same Vglut2-Cre mouse during wakefulness, NREM sleep, and REM sleep.

(C and D) Hypnograms displaying the time course of sleep and wakefulness during the 3-h recording period after VEH (C) and CNO (D) injection. The spectrograms below each hypnogram show state-specific changes in frontal power density (red, maximum; blue, minimum) across the respective recording session. Time 0 on the abscissa indicates the time at which VEH or CNO (1.0 mg/kg) was injected.

(E–G) Effect of CNO administration on the duration (in s) of W (E), NREM sleep (F), and REM sleep (G) over the 3-h recording period. Asterisk indicates a significant difference (*$p < 0.05$) from vehicle control using a two-tailed Wilcoxon test. Data are shown as mean ± SEM.

See also Figures S3 and S5.

SUPPLEMENTAL INFORMATION

Supplemental Information can be found online at https://doi.org/10.1016/j.cub.2019.12.063.

ACKNOWLEDGMENTS

The authors thank Mary A. Norat from the Department of Anesthesiology, University of Michigan for expert assistance. We are grateful to Drs. Carol F. Elias and David Garcia-Galiano from the Department of Molecular & Integrative Physiology, University of Michigan for their guidance to identify the reproductive cycle stage in female mice. This work was funded by the National Institutes of Health (R01 GM124248 to G.V. and G.A.M.), Bethesda, MD, USA, and the Department of Anesthesiology, University of Michigan Medical School, Ann Arbor.

AUTHOR CONTRIBUTIONS

G.V. and G.A.M. designed the experiments, interpreted the data, and wrote the manuscript; G.V., M.B., M.M., A.M., I.C., A.V.C., and V.S.H.-W. conducted the experiments; and G.V., M.B., A.M., I.C., M.P., V.C., A.V.C., and V.S.H.-W. analyzed the data. All authors read and approved the manuscript.

DECLARATION OF INTERESTS

The authors declare no competing interests.

Received: March 5, 2019
Revised: November 11, 2019
Accepted: December 19, 2019
Published: February 20, 2020

REFERENCES

1. Lydic, R., and Biebuyck, J.F. (1994). Sleep neurobiology: relevance for mechanistic studies of anaesthesia. Br. J. Anaesth. *72*, 506–508.
2. Moore, J.T., Chen, J., Han, B., Meng, Q.C., Veasey, S.C., Beck, S.G., and Kelz, M.B. (2012). Direct activation of sleep-promoting VLPO neurons by volatile anesthetics contributes to anesthetic hypnosis. Curr. Biol. *22*, 2008–2016.
3. Nelson, L.E., Guo, T.Z., Lu, J., Saper, C.B., Franks, N.P., and Maze, M. (2002). The sedative component of anesthesia is mediated by GABA(A) receptors in an endogenous sleep pathway. Nat. Neurosci. *5*, 979–984.
4. Lu, J., Nelson, L.E., Franks, N., Maze, M., Chamberlin, N.L., and Saper, C.B. (2008). Role of endogenous sleep-wake and analgesic systems in anesthesia. J. Comp. Neurol. *508*, 648–662.
5. Tung, A., Bluhm, B., and Mendelson, W.B. (2001). The hypnotic effect of propofol in the medial preoptic area of the rat. Life Sci. *69*, 855–862.
6. Eikermann, M., Vetrivelan, R., Grosse-Sundrup, M., Henry, M.E., Hoffmann, U., Yokota, S., Saper, C.B., and Chamberlin, N.L. (2011). The ventrolateral preoptic nucleus is not required for isoflurane general anesthesia. Brain Res. *1426*, 30–37.
7. McCarren, H.S., Chalifoux, M.R., Han, B., Moore, J.T., Meng, Q.C., Baron-Hionis, N., Sedigh-Sarvestani, M., Contreras, D., Beck, S.G., and Kelz, M.B. (2014). α2-adrenergic stimulation of the ventrolateral preoptic nucleus destabilizes the anesthetic state. J. Neurosci. *34*, 16385–16396.
8. Han, B., McCarren, H.S., O'Neill, D., and Kelz, M.B. (2014). Distinctive recruitment of endogenous sleep-promoting neurons by volatile anesthetics and a nonimmobilizer. Anesthesiology *121*, 999–1009.
9. Chung, S., Weber, F., Zhong, P., Tan, C.L., Nguyen, T.N., Beier, K.T., Hörmann, N., Chang, W.C., Zhang, Z., Do, J.P., et al. (2017). Identification of preoptic sleep neurons using retrograde labelling and gene profiling. Nature *545*, 477–481.
10. Harding, E.C., Yu, X., Miao, A., Andrews, N., Ma, Y., Ye, Z., Lignos, L., Miracca, G., Ba, W., Yustos, R., et al. (2018). A neuronal hub binding sleep initiation and body cooling in response to a warm external stimulus. Curr. Biol. *28*, 2263–2273.e4.
11. Alam, M.A., Kumar, S., McGinty, D., Alam, M.N., and Szymusiak, R. (2014). Neuronal activity in the preoptic hypothalamus during sleep deprivation and recovery sleep. J. Neurophysiol. *111*, 287–299.
12. Suntsova, N., Szymusiak, R., Alam, M.N., Guzman-Marin, R., and McGinty, D. (2002). Sleep-waking discharge patterns of median preoptic nucleus neurons in rats. J. Physiol. *543*, 665–677.
13. Rezai Amin, S., Gruszczynski, C., Guiard, B.P., Callebert, J., Launay, J.M., Louis, F., Betancur, C., Vialou, V., and Gautron, S. (2019). Viral vector-mediated Cre recombinase expression in substantia nigra induces lesions of the nigrostriatal pathway associated with perturbations of dopamine-related behaviors and hallmarks of programmed cell death. J. Neurochem. *150*, 330–340.
14. Lu, J., Bjorkum, A.A., Xu, M., Gaus, S.E., Shiromani, P.J., and Saper, C.B. (2002). Selective activation of the extended ventrolateral preoptic nucleus during rapid eye movement sleep. J. Neurosci. *22*, 4568–4576.
15. Kroeger, D., Absi, G., Gagliardi, C., Bandaru, S.S., Madara, J.C., Ferrari, L.L., Arrigoni, E., Münzberg, H., Scammell, T.E., Saper, C.B., and Vetrivelan, R. (2018). Galanin neurons in the ventrolateral preoptic area promote sleep and heat loss in mice. Nat. Commun. *9*, 4129.
16. Vanini, G., Watson, C.J., Lydic, R., and Baghdoyan, H.A. (2008). Gamma-aminobutyric acid-mediated neurotransmission in the pontine reticular formation modulates hypnosis, immobility, and breathing during isoflurane anesthesia. Anesthesiology *109*, 978–988.
17. Zhang, Z., Ferretti, V., Güntan, İ., Moro, A., Steinberg, E.A., Ye, Z., Zecharia, A.Y., Yu, X., Vyssotski, A.L., Brickley, S.G., et al. (2015). Neuronal ensembles sufficient for recovery sleep and the sedative actions of α2 adrenergic agonists. Nat. Neurosci. *18*, 553–561.
18. Ma, Y., Miracca, G., Yu, X., Harding, E.C., Miao, A., Yustos, R., Vyssotski, A.L., Franks, N.P., and Wisden, W. (2019). Galanin neurons unite sleep homeostasis and α2-adrenergic sedation. Curr. Biol. *29*, 3315–3322.e3.
19. Gvilia, I., Xu, F., McGinty, D., and Szymusiak, R. (2006). Homeostatic regulation of sleep: a role for preoptic area neurons. J. Neurosci. *26*, 9426–9433.
20. Tung, A., Szafran, M.J., Bluhm, B., and Mendelson, W.B. (2002). Sleep deprivation potentiates the onset and duration of loss of righting reflex induced by propofol and isoflurane. Anesthesiology *97*, 906–911.
21. Pal, D., Lipinski, W.J., Walker, A.J., Turner, A.M., and Mashour, G.A. (2011). State-specific effects of sevoflurane anesthesia on sleep homeostasis: selective recovery of slow wave but not rapid eye movement sleep. Anesthesiology *114*, 302–310.
22. Tung, A., Lynch, J.P., and Mendelson, W.B. (2001). Prolonged sedation with propofol in the rat does not result in sleep deprivation. Anesth. Analg. *92*, 1232–1236.
23. Pick, J., Chen, Y., Moore, J.T., Sun, Y., Wyner, A.J., Friedman, E.B., and Kelz, M.B. (2011). Rapid eye movement sleep debt accrues in mice exposed to volatile anesthetics. Anesthesiology *115*, 702–712.
24. Gelegen, C., Miracca, G., Ran, M.Z., Harding, E.C., Ye, Z., Yu, X., Tossell, K., Houston, C.M., Yustos, R., Hawkins, E.D., et al. (2018). Excitatory pathways from the lateral habenula enable propofol-induced sedation. Curr. Biol. *28*, 580–587.e5.
25. Jiang-Xie, L.-F., Yin, L., Zhao, S., Prevosto, V., Han, B.-X., Dzirasa, K., and Wang, F. (2019). A common neuroendocrine substrate for diverse general anesthetics and sleep. Neuron *102*, 1053–1065.e4.
26. Takahashi, K., Lin, J.S., and Sakai, K. (2009). Characterization and mapping of sleep-waking specific neurons in the basal forebrain and preoptic hypothalamus in mice. Neuroscience *161*, 269–292.
27. Sakai, K. (2011). Sleep-waking discharge profiles of median preoptic and surrounding neurons in mice. Neuroscience *182*, 144–161.
28. Sherin, J.E., Elmquist, J.K., Torrealba, F., and Saper, C.B. (1998). Innervation of histaminergic tuberomammillary neurons by GABAergic and galaninergic neurons in the ventrolateral preoptic nucleus of the rat. J. Neurosci. *18*, 4705–4721.
29. Moffitt, J.R., Bambah-Mukku, D., Eichhorn, S.W., Vaughn, E., Shekhar, K., Perez, J.D., Rubinstein, N.D., Hao, J., Regev, A., Dulac, C., and Zhuang, X. (2018). Molecular, spatial, and functional single-cell profiling of the hypothalamic preoptic region. Science *362*, eaau5324.
30. Vong, L., Ye, C., Yang, Z., Choi, B., Chua, S., Jr., and Lowell, B.B. (2011). Leptin action on GABAergic neurons prevents obesity and reduces inhibitory tone to POMC neurons. Neuron *71*, 142–154.
31. Kroeger, D., Ferrari, L.L., Petit, G., Mahoney, C.E., Fuller, P.M., Arrigoni, E., and Scammell, T.E. (2017). Cholinergic, glutamatergic, and GABAergic neurons of the pedunculopontine tegmental nucleus have distinct effects on sleep/wake behavior in mice. J. Neurosci. *37*, 1352–1366.
32. Anaclet, C., Pedersen, N.P., Ferrari, L.L., Venner, A., Bass, C.E., Arrigoni, E., and Fuller, P.M. (2015). Basal forebrain control of wakefulness and cortical rhythms. Nat. Commun. *6*, 8744.
33. Abbott, S.B., Machado, N.L., Geerling, J.C., and Saper, C.B. (2016). Reciprocal control of drinking behavior by median preoptic neurons in mice. J. Neurosci. *36*, 8228–8237.
34. Krashes, M.J., Shah, B.P., Madara, J.C., Olson, D.P., Strochlic, D.E., Garfield, A.S., Vong, L., Pei, H., Watabe-Uchida, M., Uchida, N., et al. (2014). An excitatory paraventricular nucleus to AgRP neuron circuit that drives hunger. Nature *507*, 238–242.
35. Geerling, J.C., Yokota, S., Rukhadze, I., Roe, D., and Chamberlin, N.L. (2017). Kölliker-Fuse GABAergic and glutamatergic neurons project to distinct targets. J. Comp. Neurol. *525*, 1844–1860.
36. Krashes, M.J., Koda, S., Ye, C., Rogan, S.C., Adams, A.C., Cusher, D.S., Maratos-Flier, E., Roth, B.L., and Lowell, B.B. (2011). Rapid, reversible

activation of AgRP neurons drives feeding behavior in mice. J. Clin. Invest. *121*, 1424–1428.

37. Alkire, M.T., McReynolds, J.R., Hahn, E.L., and Trivedi, A.N. (2007). Thalamic microinjection of nicotine reverses sevoflurane-induced loss of righting reflex in the rat. Anesthesiology *107*, 264–272.
38. Tung, A., Herrera, S., Szafran, M.J., Kasza, K., and Mendelson, W.B. (2005). Effect of sleep deprivation on righting reflex in the rat is partially reversed by administration of adenosine A1 and A2 receptor antagonists. Anesthesiology *102*, 1158–1164.
39. Pal, D., Silverstein, B.H., Lee, H., and Mashour, G.A. (2016). Neural correlates of wakefulness, sleep, and general anesthesia: an experimental study in rat. Anesthesiology *125*, 929–942.
40. Hudetz, A.G., Vizuete, J.A., and Pillay, S. (2011). Differential effects of isoflurane on high-frequency and low-frequency γ oscillations in the cerebral cortex and hippocampus in freely moving rats. Anesthesiology *114*, 588–595.
41. Kelz, M.B., Sun, Y., Chen, J., Cheng Meng, Q., Moore, J.T., Veasey, S.C., Dixon, S., Thornton, M., Funato, H., and Yanagisawa, M. (2008). An essential role for orexins in emergence from general anesthesia. Proc. Natl. Acad. Sci. USA *105*, 1309–1314.
42. Vanini, G., Nemanis, K., Baghdoyan, H.A., and Lydic, R. (2014). GABAergic transmission in rat pontine reticular formation regulates the induction phase of anesthesia and modulates hyperalgesia caused by sleep deprivation. Eur. J. Neurosci. *40*, 2264–2273.
43. Guidera, J.A., Taylor, N.E., Lee, J.T., Vlasov, K.Y., Pei, J., Stephen, E.P., Mayo, J.P., Brown, E.N., and Solt, K. (2017). Sevoflurane induces coherent slow-delta oscillations in rats. Front. Neural Circuits *11*, 36.
44. Taylor, N.E., Van Dort, C.J., Kenny, J.D., Pei, J., Guidera, J.A., Vlasov, K.Y., Lee, J.T., Boyden, E.S., Brown, E.N., and Solt, K. (2016). Optogenetic activation of dopamine neurons in the ventral tegmental area induces reanimation from general anesthesia. Proc. Natl. Acad. Sci. USA *113*, 12826–12831.
45. Sciolino, N.R., Plummer, N.W., Chen, Y.W., Alexander, G.M., Robertson, S.D., Dudek, S.M., McElligott, Z.A., and Jensen, P. (2016). Recombinase-dependent mouse lines for chemogenetic activation of genetically defined cell types. Cell Rep. *15*, 2563–2573.
46. Caligioni, C.S. (2009). Assessing reproductive status/stages in mice. Curr. Protoc. Neurosci. *4* (Appendix), 4I.
47. Gonzalez, G. (2016). Determining the stage of the estrous cycle in female mice by vaginal smear. Cold Spring Harb. Protoc. *2016*, https://doi.org/10.1101/pdb.prot094474.
48. Paxinos, G., and Franklin, K.B.J. (2001). The Mouse Brain in Stereotaxic Coordinates, Second Edition (Academic).

STAR★METHODS

KEY RESOURCES TABLE

REAGENT or RESOURCE	SOURCE	IDENTIFIER
Antibodies		
Rat monoclonal anti-mCherry	Fisher Scientific	M11217; RRID:AB_2536611
Donkey anti-rat, Alexa Fluor 594	Fisher Scientific	A-21209; RRID:AB_2535795
Rabbit polyclonal anti-cFos	Milipore Sigma	ABE457; RRID not available
Donkey anti-rabbit, Alexa Fluor 488	Fisher Scientific	A-21206; RRID:AB_2535792
Bacterial and Virus Strains		
AAV5-hSyn-DIO-hM3D(Gq)-mCherry	Addgene	50459-AAV5
Chemicals, Peptides, and Recombinant Proteins		
Clozapine-N-oxide	Sigma-Aldrich	C0832-5MG
Dimethyl sulfoxide	Sigma-Aldrich	276855
Isoflurane	Hospira, Inc., Lake Forest, IL, USA	N/A
Carprofen (Rimadyl®)	Pfizer UK	N/A
Dental Acrylic	GC America, Inc., Alsip, IL, USA	335201
Phosphate Buffered Saline	Fisher Scientific	BP3994
Formalin (Buffered, 10%)	Fisher Scientific	SF100-4
Tissue-Plus O.C.T. Compound	Fisher Scientific	23-730-571
Sucrose	Fisher Scientific	S25590
Triton X-100	Sigma-Aldrich	X100
Normal goat serum	Vector Laboratories	S-1000
SlowFade Diamond Antifade Mountant	Fisher Scientific	S36972
SlowFade Diamond Antifade Mountant with DAPI	Fisher Scientific	S36973
Experimental Models: Organisms/Strains		
Vgat-IRES-Cre: *Slc32a1*$^{tm2(cre)Lowl}$/J	Jackson Laboratories	Stock # 016962
Vglut2-IRES-Cre: *Slc17a6*$^{tm2(cre)Lowl}$/J	Jackson Laboratories	Stock # 016963
Software and Algorithms		
Prism	GraphPad	Version 7
Spike2	Cambridge Electronic Design Ltd.	Version 7
Other		
EEG screw electrodes	Plastics One	8IE3632016XE, E363/20/1.6/SPC
EMG electrodes	Plastics One	8IE36376XXXE, E363/76/SPC
Six-pin electrode pedestal	Plastics One	MS363

LEAD CONTACT AND MATERIALS AVAILABILITY

This study did not generate any new unique materials. Further information and requests for resources and reagents should be directed to and will be fulfilled by the Lead Contact, Giancarlo Vanini (gvanini@umich.edu).

EXPERIMENTAL MODEL AND SUBJECT DETAILS

Mice

All procedures using animals were approved by the Institutional Animal Care and Use Committee, the Institutional Biosafety Committee, and were conducted following recommendations from the Guide for the Care and Use of Laboratory Animals. We studied adult Vgat-IRES-Cre: *Slc32a1*$^{tm2(cre)Lowl}$/J (JAX® mice, Stock # 016962) [9, 10, 30–33], and Vglut2-IRES-Cre: *Slc17a6*$^{tm2(cre)Lowl}$/J (JAX® mice, Stock # 016963) [31–35] mice (16-20 weeks old, weighing 18 – 25 g at the time of surgery; 27 male, 26 female Vgat-Cre and 32 male, 22 female Vglut2-Cre). Mice were bred at the institutional breeding colony facility and housed in a 12-h light:dark cycle with unrestricted access to food and water. All mice were genotyped (Transnetyx) before use.

METHOD DETAILS

Viral Vector and Chemicals

For selective expression of excitatory hM3Dq designer receptors in Vgat+ (GABAergic) and Vglut2+ (glutamatergic) neurons of the MnPO and VLPO we used the Cre-inducible adeno-associated viral vector AAV5-hSyn-DIO-hM3D(Gq)-mCherry [36]. The vector was purchased from the University of North Carolina Vector Core (Chapel Hill, NC, USA) and Addgene (Cat.# 50459-AAV5) and had a titer concentration of 3.7 to 7.8 X 10^{12} genome copies per ml.

Clozapine-N-oxide (CNO) and dimethyl sulfoxide (DMSO) were purchased from Sigma-Aldrich (St. Louis, MO, USA). CNO was dissolved in sterile saline containing DMSO. A stock solution of CNO (0.1 mg/ml in saline and 0.5% DMSO) was made, divided in aliquots, and stored at −20°C for subsequent use. For each experiment, one aliquot of the CNO stock solution was allowed to thaw at room temperature protected from the light until use; for the 0.5 mg/kg dose, the CNO solution was diluted in sterile saline to achieve the desired final concentration. The injection volume was 0.1 mL per 10 g of mouse weight.

Surgical Procedures for Stereotaxic Viral Vector Injection and Sleep Studies

The procedure for vector injection into the MnPO and VLPO was conducted under sterile conditions and general anesthesia. Briefly, mice were anesthetized in an acrylic induction chamber with 5.0% isoflurane (Hospira, Inc., Lake Forest, IL, USA) in 100% O_2. The delivered concentration of isoflurane was monitored continuously by spectrometry (Cardiocap/5; Datex-Ohmeda, Louisville, CO, USA). When anesthetized, mice received an injection of carprofen (5 mg/kg, subcutaneous) for preemptive analgesia and were positioned within a Kopf Model 962 stereotaxic frame fitted with a mouse adaptor (Model 922) and a mouse anesthesia mask (Model 907) (David Kopf Instruments, Tujunga, CA, USA). The concentration of isoflurane was then reduced to 1.6 to 2.0% for the remainder of the surgical procedure. Core body temperature was maintained at 37-38°C using a water-filled pad connected to a heat pump (Gaymar Industries, Orchard Park, NY, USA). Based on pilot microinjection studies, we determined that microinjecting 50 nL of the undiluted viral vector was optimal for achieving a robust and sustained receptor expression localized to the MnPO. For VLPO experiments, mice received microinjections of 36 nL of AAV5-hSyn-DIO-hM3D(Gq)-mCherry [15]. For MnPO studies, the vector was microinjected at stereotaxic coordinates 0.40 mm anterior to bregma, 0.0 mm relative to the midline, and 4.75 mm ventral to bregma (Figures 1A and 2A). For VLPO studies, the vector was microinjected bilaterally at stereotaxic coordinates 0.15 mm anterior to bregma, ± 0.5 mm relative to the midline, and 5 mm below the dura (Figures 5A and 6A). The virus injection (5 nl/min) was performed using a Hamilton Neuros Syringe 7000 (5 μL; Hamilton Company, Reno, NV, USA) mounted on a microinjection syringe pump connected to a digital Micro2T controller (Model UMP3T-2; World Precision Instruments, Sarasota, FL, USA). Following the injection procedure, the syringe was kept in position for an additional 5 minutes to avoid vector reflux. Three weeks after the vector injection, a subset of mice used for sleep studies was implanted with screw electrodes (8IE3632016XE, E363/20/1.6/SPC; Plastics One, Roanoke, VA, USA) to record the electroencephalogram (EEG) from frontal (1.5 mm anterior to bregma and ± 2.0 mm relative to the midline), and occipital (3.2 mm posterior to bregma and ± 3.0 mm relative to the midline) cortices (Figures 2A and 6A). A screw electrode implanted over the cerebellum was used as reference for monopolar EEG recordings, and two electrodes (8IE36376XXXE, E363/76/SPC; Plastics One) implanted bilaterally in the dorsal neck muscles were used to record the electromyogram (EMG). Thereafter, all electrodes were inserted into a six-pin electrode pedestal (MS363; Plastics One) and cemented to the skull using dental acrylic (Fast Cure Powder/Liquid, Product# 335201; GC America, Inc., Alsip, IL, USA). Isoflurane delivery was discontinued, and mice were kept warm and monitored until fully ambulatory. Analgesia was maintained with carprofen for a minimum of 48 h post-surgery. All mice were housed with their littermates and allowed to recover for at least two weeks before conditioning began.

Experimental Protocols

Quantification of Anesthetic State Transitions

Mice were conditioned to being handled and to the gas-tight testing chamber for 5 days, and were given at least 4 weeks between vector injection and experimentation. All studies were conducted between 11:30 AM and 3:30 PM (lights on at 6:00 AM). We used a within-subject study design so each mouse received all treatments and served as its own control in paired-wise comparisons. Experiments in the same mouse were separated by a wash out period of at least 3 days. On the day of the experiment, mice received randomized intraperitoneal injections of vehicle solution or CNO (0.5 or 1.0 mg/kg) and were placed back in their home cage until testing. Thereafter (60 min post-injection, MnPO experiments; 30 min post-injection, VLPO experiments), mice were anesthetized in a gas-tight acrylic chamber pre-filled with 1.5% or 1.2% isoflurane in oxygen, and anesthesia was maintained for 30 minutes. The concentration of isoflurane was measured continuously using a B40v3 monitor (GE Healthcare, Datex-Ohmeda, Inc., Pittsburgh, PA, USA). The temperature at the bottom of the chamber was maintained between 37 – 38°C during the experiment. Anesthetic induction and recovery were quantified, respectively, as the time to loss and resumption of righting response; both are widely used surrogate measures of loss and resumption of consciousness in rodent experiments [6, 16, 17, 37–44]. Additionally, all the experiments were video-recorded for subsequent analysis by an observer who was blinded to the treatment condition and mouse line. Agreement in the quantification of loss and resumption of consciousness between experimenters (real time assessment) and blinded investigator (offline assessment) was greater than 95%. Times to loss and resumption of consciousness from MnPO experiments are illustrated in Figures 1B–1E and VLPO experiments in Figures 5B–5E (Cre mice expressing hM3Dq receptors) and Figures S1 and S2 (control Cre mice that did not express hM3Dq receptors, sham-injected and naive).

Measurements of Body Temperature After Activation of GABAergic or Glutamatergic Neurons in the MnPO

Temperature experiments were conducted after MnPO anesthesia and sleep experiments. Vgat-Cre and Vglut2-Cre mice were briefly and gently restrained for measurements of body temperature using a lubricated mouse rectal probe (Model# 600-1000, Barnant Company, Barrington, IL, USA). Temperature was measured before and after an intraperitoneal injection of CNO (1 mg/kg) in 10-min intervals for 90 minutes [45]. Hypothermic mice were placed back in their cages under a heating lamp between testing intervals. Changes in core body temperature after CNO administration are shown in Figure 3.

Electroencephalographic - Electromyographic Recordings and Analysis of Sleep-Wakefulness States

Three weeks after vector injection, mice were conditioned to tethering in the recording setup for 5 days before sleep experiments began. Thereafter, mice received an intraperitoneal injection (10:00 AM) of vehicle or CNO (1.0 mg/kg), and EEG/EMG signals were recorded continuously for 3 hours –the duration of anesthesia experiments– post-injection. Monopolar EEG signals and EMG signals were recorded and digitized using a Model 1700 AC amplifier (A-M Systems, Sequim, WA, USA), a Micro3 1401 acquisition unit and Spike2 software (Cambridge Electronic Design, Cambridge, UK). Electrophysiologic signals were bandpass filtered between 0.1 – 500 Hz (EEG) and 10 – 500 Hz (EMG). A video recording time-synchronized with our EEG-EMG recordings was used for behavioral assessments during sleep/wake analysis. States of wakefulness, non-rapid eye movement (NREM) sleep and rapid eye movement (REM) sleep were manually scored offline in 5 s epochs using standard criteria (Figures 2B and 6B). Wakefulness was recognized by the presence of low-amplitude, high-frequency EEG activity, with high muscle tone and active movements. NREM sleep was identified by the presence of high-amplitude, low-frequency EEG activity with reduced muscle tone. REM sleep was recognized by low-amplitude, high-frequency EEG activity with prominent theta waveforms, along with sustained muscle atonia. The total time spent in wakefulness, NREM sleep and REM sleep was compared between treatment conditions in Cre mice expressing hM3Dq receptors (Figures 2 and 6) and sham-injected controls (Figure S3).

Identification of Reproductive Cycle Stage

After each anesthesia experiment, female mice were briefly restrained and vaginal smear samples were collected following a published protocol [46, 47]. The unstained material was immediately observed using low-illumination light microscopy under a 10x objective (Primo Star, Carl Zeiss Microscopy, LLC, Thornwood, NY, USA). The cycle stage was identified as proestrus, estrus, metestrus and diestrus, according to standard histologic criteria [46].

Immunohistochemistry for Localization of Vector Injection Sites (mCherry) and Assessment of CNO-induced Neuronal Activation (cFos)

For cFos/mCherry immunohistochemistry (Figure 4), mice received an intraperitoneal injection of vehicle or CNO (1 mg/kg) 90 minutes before euthanasia. Mice were deeply anesthetized with isoflurane, perfused transcardially with 0.1 M phosphate buffered saline pH 7.4 (PBS) followed by 5% formalin in PBS using a MasterFlex perfusion pump (Cole Palmer, Vernon Hills, IL, USA). The brains were removed and post-fixed in 5% formalin overnight at 4°C. Thereafter, brains were cryoprotected with 20% sucrose in PBS for 3 to 5 days, frozen in Tissue–Plus (Fisher Healthcare, Houston, TX, USA), and sectioned coronally at 40 μm using a cryostat (CM3050S, Leica Microsystems, Nussloch, Germany). A series of brain sections containing the MnPO were blocked in PBS containing 0.25% Triton X-100 and 3% normal goat serum (Vector Laboratories, Burlingame, CA, USA) for 60 min at room temperature. Sections were then processed for mCherry immunolabeling, or sequentially processed for double immunohistochemistry for mCherry and cFos. For mCherry, sections were incubated in primary antiserum overnight at room temperature. We used a rat monoclonal anti-mCherry (1:30000; Thermo Fisher Scientific, Cat.#: M11217). The next morning, sections were washed in PBS and incubated in a donkey anti-rat secondary antiserum (1:500; Alexa Fluor 594, Thermo Fisher Scientific, Cat.#: A-21209) for 2 h at room temperature. For cFos, sections were incubated in a rabbit polyclonal anti-cFos (1:5000; Millipore Sigma, Cat.#: ABE457) overnight at room temperature. The next morning, slices were washed in PBS and incubated in a donkey anti-rabbit secondary antiserum (1:500; Alexa Fluor 488, Thermo Fisher Scientific, Cat.#: A-21206) for 2 h at room temperature. Following incubation in the respective secondary antisera, tissues were washed in PBS, float-mounted on glass slides and coverslipped with SlowFade Diamond (S36972 or S36973; Thermo Fisher Scientific). All brain sections were examined using fluorescence microscopy (BX43, Olympus America Inc., Waltham, MA, USA). Only brains in which the expression of the designer receptor hM3Dq was localized to the MnPO or VLPO were included in the analysis (Figures S4 and S5). A mouse brain atlas [48] was used for reference. The number mCherry-positive neurons that expressed cFos was quantified as the percentage of total neurons expressing mCherry in the MnPO (Figures 4A and 4B).

QUANTIFICATION AND STATISTICAL ANALYSIS

Data analyses were performed using PRISM v7.0 (GraphPad Software Inc., La Jolla, CA). All data were tested for normality and reported as mean ± standard error of the mean. A P *value* < 0.05 was considered statistically significant. The time to loss and resumption of consciousness is reported as the time in seconds. Differences in the time to loss and resumption of consciousness in MnPO-anesthesia experiments in which 3 concentrations of CNO were used (data shown in Figures 1B, 1C, and S1) were assessed by a Friedman test followed, when applicable, by a Dunn's multiple comparison test. All pairwise comparisons (i.e., vehicle versus 1.0 mg/kg CNO) of time to loss and resumption of consciousness were evaluated by a two-tailed Wilcoxon test. Changes in the time spent in wakefulness, NREM sleep and REM sleep were assessed by a one-tailed (MnPO Vgat and Vglut2, and VLPO Vgat)

or two-tailed (VLPO Vglut2) Wilcoxon test. Differences in body temperature as a function of treatment, time and mouse line were evaluated by a two-way analysis of variance (ANOVA) followed by a Bonferroni's multiple comparisons test. Last, the percentage of active cells (cFos+) after vehicle and CNO administration was compared by a one-tailed Mann Whitney test.

DATA AND CODE AVAILABILITY

The datasets supporting the current study have not been deposited in a public repository but are available from the Lead Contact on request. This study did not generate any code.

Current Biology, Volume *30*

Supplemental Information

Activation of Preoptic GABAergic or Glutamatergic Neurons Modulates Sleep-Wake Architecture, but Not Anesthetic State Transitions

Giancarlo Vanini, Marina Bassana, Megumi Mast, Alejandra Mondino, Ivo Cerda, Margaret Phyle, Vivian Chen, Angelo V. Colmenero, Viviane S. Hambrecht-Wiedbusch, and George A. Mashour

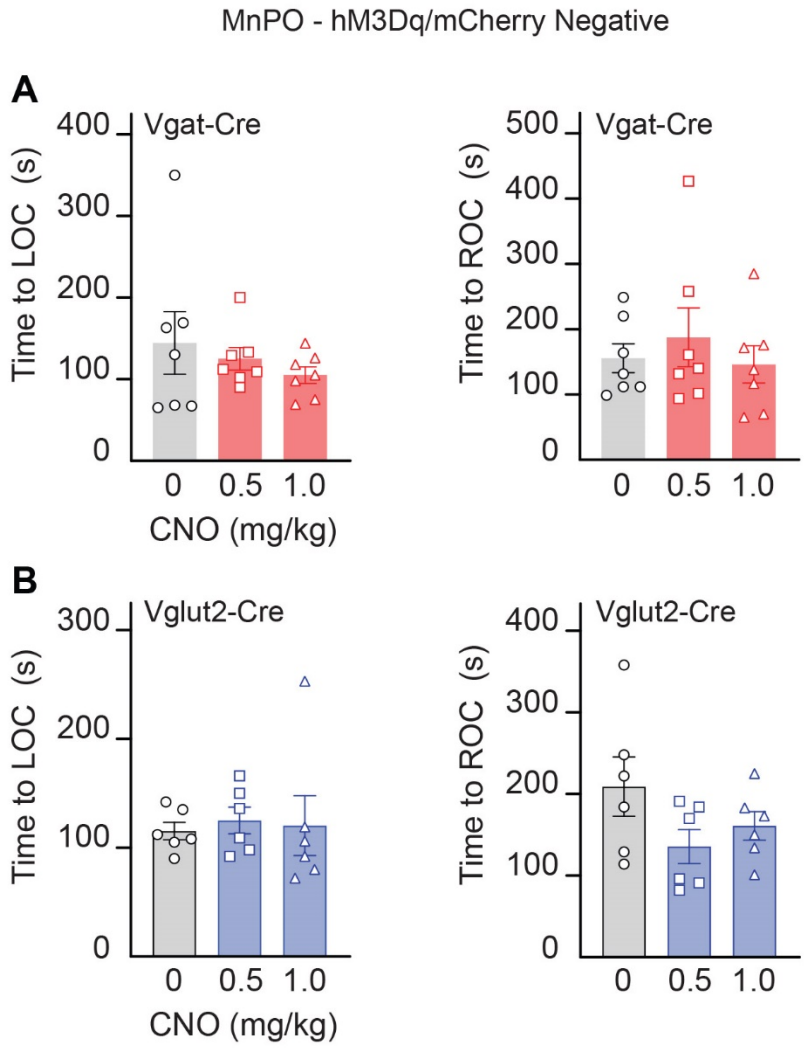

Figure S1. CNO administration to control mice without designer receptor expression did not alter anesthetic state transitions, Related to Figure 1

Time to loss and resumption of consciousness (left and right panels, respectively) in Vgat-Cre (panels in **A**) and Vglut2-Cre (panels in **B**) mice that received vector injections into the MnPO but did not express hM3Dq receptors (negative controls). Statistical comparisons were conducted using a Friedman test. Data are shown as mean ± standard error of the mean.

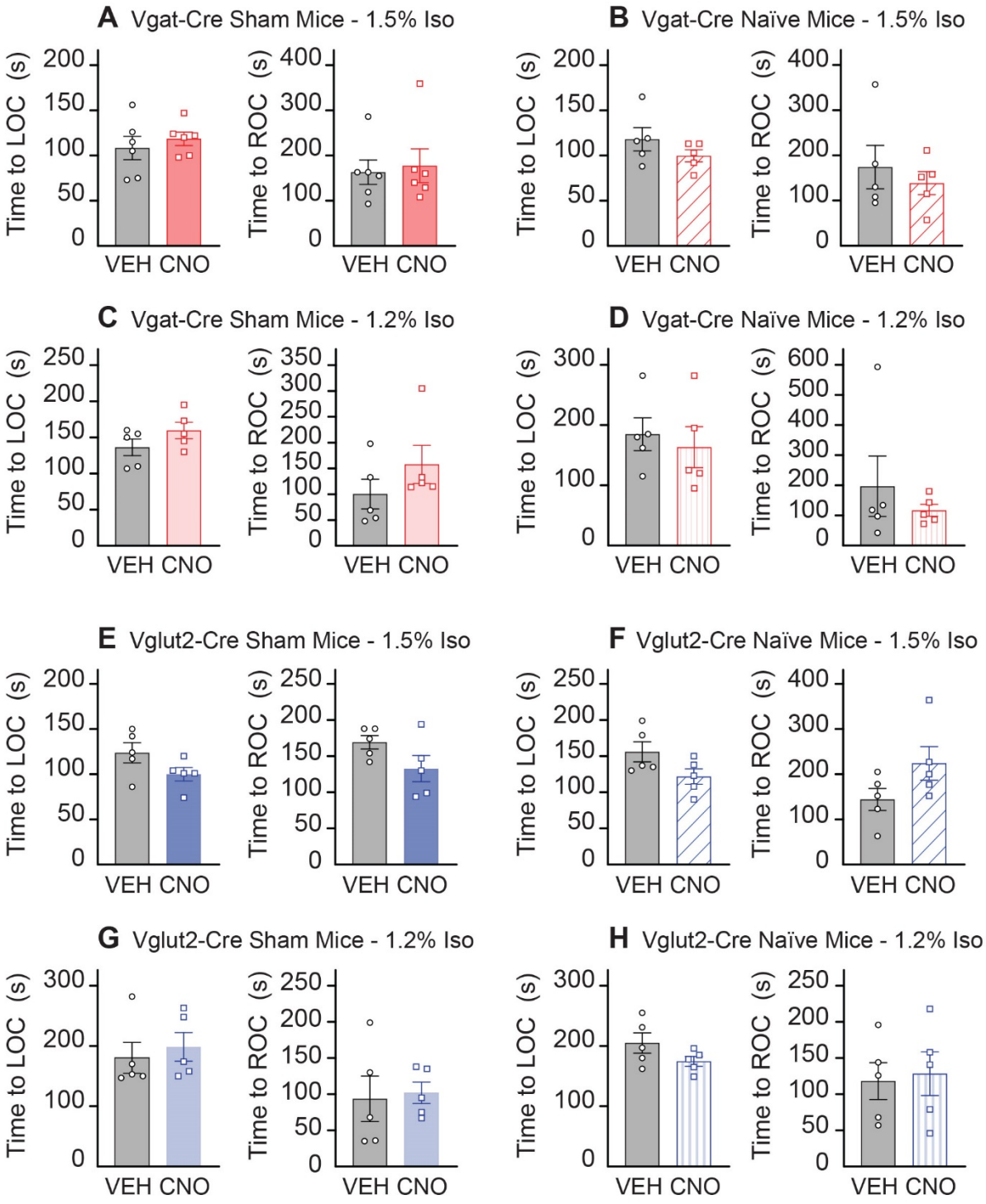
A Vgat-Cre Sham Mice - 1.5% Iso
B Vgat-Cre Naïve Mice - 1.5% Iso
C Vgat-Cre Sham Mice - 1.2% Iso
D Vgat-Cre Naïve Mice - 1.2% Iso
E Vglut2-Cre Sham Mice - 1.5% Iso
F Vglut2-Cre Naïve Mice - 1.5% Iso
G Vglut2-Cre Sham Mice - 1.2% Iso
H Vglut2-Cre Naïve Mice - 1.2% Iso
Time to LOC (s)
Time to ROC (s)
VEH CNO

Figure S2. CNO administration to sham and naïve control mice did not alter anesthetic state transitions, Related to Figures 1 and 5

Time to loss and resumption of consciousness (left and right panels, respectively) in sham (**A**) and naïve (**B**) Vgat-Cre mice exposed to 1.5% isoflurane. **C** and **D** show the time to loss and resumption of consciousness in sham and naïve Vgat-Cre mice exposed to 1.2% isoflurane. Time to loss and resumption of consciousness (left and right panels, respectively) in sham (**E**) and naïve (**F**) Vglut2-Cre mice exposed to 1.5% isoflurane. **G** and **H** show the time to loss and resumption of consciousness in sham and naïve Vglut2-Cre mice exposed to 1.2% isoflurane. Statistical comparisons were conducted using a two-tailed Wilcoxon test. Data are shown as mean ± standard error of the mean.

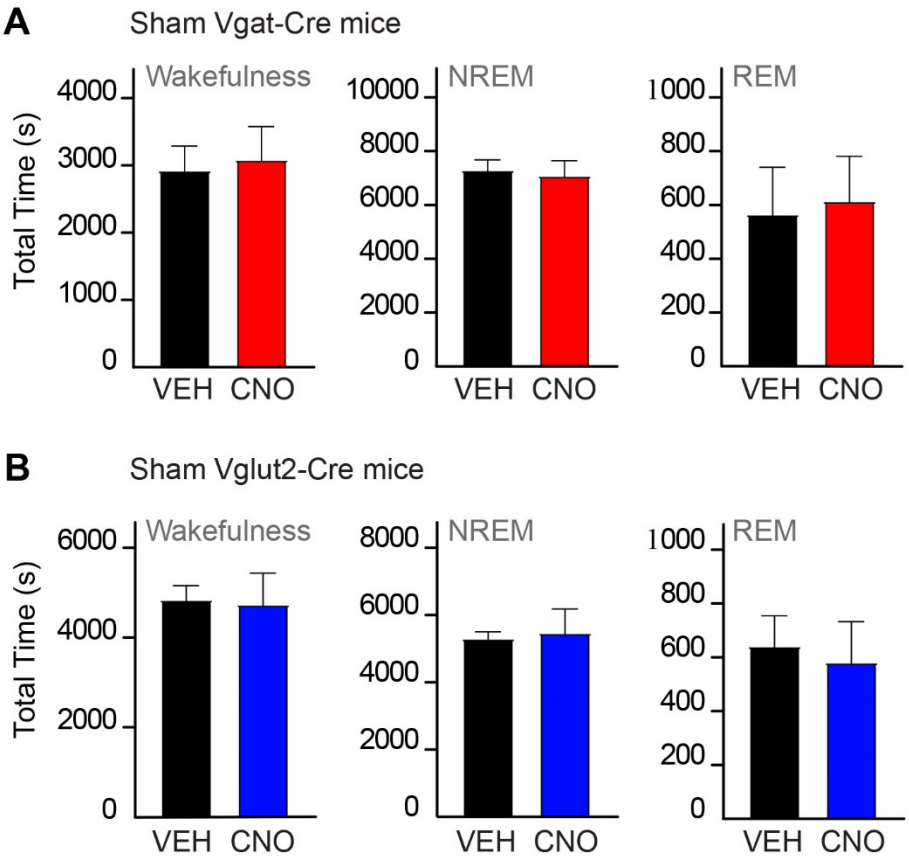

Figure S3. CNO administration to sham control mice did not alter sleep architecture, Related to Figures 2 and 6

Total time in wakefulness, non-rapid eye movement (NREM) sleep and rapid eye movement (REM) sleep in sham-operated (without AAV injection) Vgat-Cre (panels in **A**) and Vglut2-Cre mice (panels in **B**) after injection of vehicle control (VEH) or clozapine-N-oxide (CNO; 1.0 mg/kg). Data are shown as mean ± standard error of the mean.

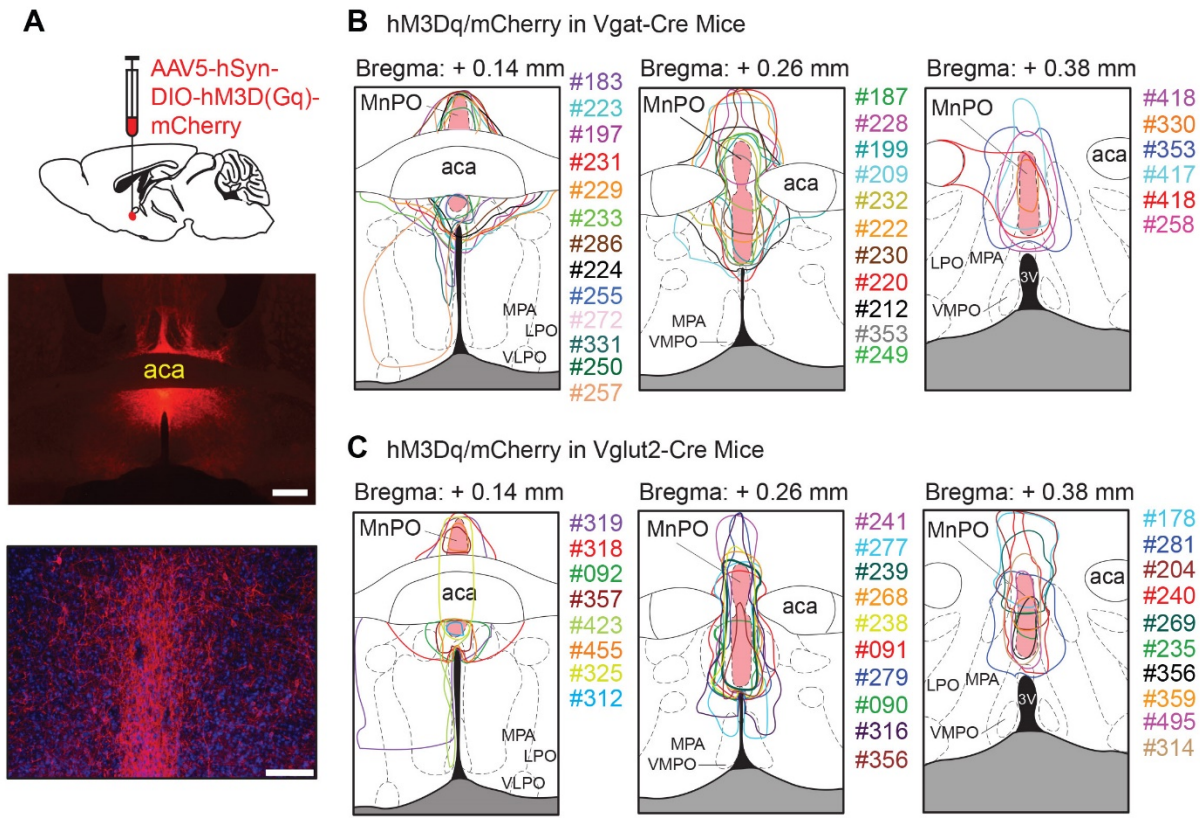

Figure S4. Vector injection sites in the MnPO, Related to Figures 1, 2 and 3

A. Schematic representation of AAV injection into the median preoptic nucleus (MnPO). In the top panel (low magnification photograph), mCherry immunohistochemical staining (red) indicates the expression of the excitatory designer receptor hM3Dq within the MnPO of a Vglut2-Cre mouse. The bottom panel is a representative high magnification photograph demonstrating mCherry immunohistochemical staining (red) and DAPI nuclear staining (blue) in the MnPO. **B.** Color-coded vector injection sites (i.e., area of hM3Dq receptor expression) within the MnPO of Vgat-Cre mice used for anesthesia, sleep and temperature experiments are represented on coronal schematics of the preoptic area modified from a mouse brain atlas [S1]. Color-matched identification numbers for each mouse are listed on the right side of each panel.

C. Vector injection sites within the MnPO of Vglut2-Cre mice used for anesthesia experiments. Abbreviations: aca, anterior commissure; LPO, lateral preoptic area; MnPO, median preoptic nucleus; MPA, medial preoptic area; 3V, third ventricle; VLPO, ventrolateral preoptic nucleus; VMPO, ventromedial preoptic nucleus. Calibration bars in A, 200 μm (top) and 100 μm (bottom).

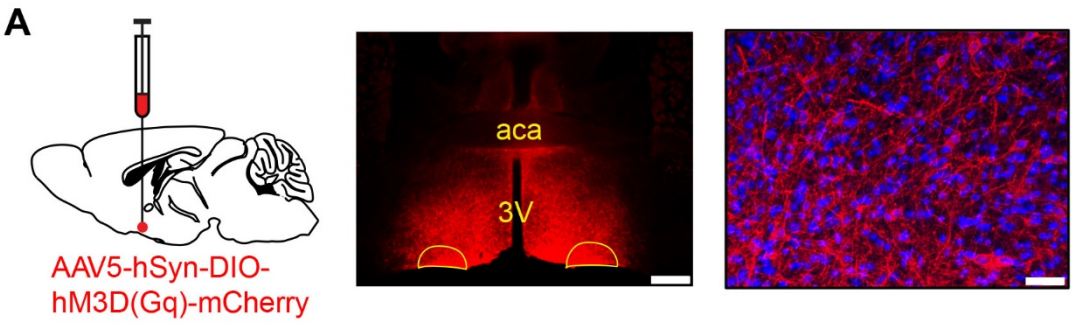
A
aca
3V
AAV5-hSyn-DIO-
hM3D(Gq)-mCherry
B hM3Dq/mCherry in Vgat-Cre Mice
C hM3Dq/mCherry in Vglut2-Cre Mice
Bregma: + 0.14 mm
#301
#274
#264
#303
#304
#449
MPO
MPA
LPO
VLPO
VMPO
Bregma: + 0.02 mm
#300
#262
#500
oc
Bregma: -0.10 mm
#276
3V
#320
#336
#337
#360
#361
#326

Figure S5. Vector injection sites in the VLPO, Related to Figures 5 and 6

A. The first panel is a schematic representation of AAV injection into the ventrolateral preoptic nucleus (VLPO). In the center panel (low magnification photograph), mCherry immunohistochemical staining (red) indicates the expression of the excitatory designer receptor hM3Dq within the VLPO of a Vglut2-Cre mouse. The third panel is a representative high magnification photograph demonstrating mCherry immunohistochemical staining (red) and DAPI nuclear staining (blue) in the VLPO. **B.** Color-coded vector injection sites (i.e., area of hM3Dq receptor expression) within the VLPO of Vgat-Cre mice used for anesthesia and sleep experiments are represented on coronal schematics of the preoptic area modified from a mouse brain atlas [S1]. Color-matched identification numbers for each mouse are listed on the right side of each panel. **C.** Vector injection sites within the VLPO of Vglut2-Cre mice used for anesthesia and sleep experiments. Abbreviations: aca, anterior commissure; LPO, lateral preoptic area; MnPO, median preoptic nucleus; MPA, medial preoptic area; 3V, third ventricle; VLPO, ventrolateral preoptic nucleus; VMPO, ventromedial preoptic nucleus. Calibration bars in A, 200 μm (center panel) and 20 μm (right side panel).

Supplemental Reference

S1. Paxinos, G. and Franklin, K.B.J. (2001). The Mouse Brain in Stereotaxic Coordinates, Second Edition (San Diego: Academic).

Comentarios adicionales al artículo

Este trabajo demostró que la activación tanto de neuronas GABAérgicas como glutamatérgicas en el VLPO y MnPO si bien tienen un rol en el ciclo sueño-vigilia no influencian la inducción o recuperación anestésica. Este hallazgo cuestiona la hipótesis de los mecanismos compartidos entre anestesia y sueño, ampliamente apoyada durante muchos años. Esto llevó a la publicación de un artículo editorial titulado ¨Sleep and Anesthesia: The Shared Circuit Hypothesis Has Been Put to Bed¨ (Eikermann *et al.*, 2020). En este trabajo, los autores comentan que su grupo había demostrado previamente que las principales neuronas promotoras de sueño del área preóptica no eran requeridas para la anestesia general con isoflurano (Eikermann *et al.*, 2011). Los autores comentan que existe mayor evidencia que apoya que los sedantes, pero no los anestésicos, como por ejemplo la dexmedetomidina actuarían sobre estas áreas somnogénicas (Nelson *et al.*, 2003). En este trabajo, también se utilizó una dosis de isoflurano subanestésica (1.2%) ya que a esa dosis se provoca principalmente sedación, sin embargo, tampoco se observó un efecto de la activación de las neuronas glutamatérgicas en los tiempos de inducción o recuperación. De todas maneras, los anestésicos aún podrían estar actuando en otras regiones promotoras de sueño, o inhibiendo áreas (o grupos neuronales específicos) generadores de vigilia (Reitz & Kelz, 2021). De hecho, recientemente, se ha comprobado que neuronas hipotalámicas del núcleo supraóptico y sus alrededores (conocidas como neuronas activadas por anestésicos) serían un sustrato neural común para el sueño y la anestesia. Interesantemente, la mayoría de estas neuronas son principalmente células neuroendócrinas, productoras de péptidos tales como vasopresina, dinorfina y galanina(Jiang-Xie *et al.*, 2019). Adicionalmente, neuronas glutamatérgicas de la habénula lateral son capaces de modular tanto el sueño como la anestesia general(Gelegen *et al.*, 2018; Liu *et al.*, 2021). Por último, la corteza prefrontal podría ser también una región clave, ya que ha sido

demostrado que esta área posee un rol clave en la generación de vigilia, y que estaría inhibida durante el sueño NREM y la anestesia (Pal *et al.*, 2018; Parkar *et al.*, 2020). De hecho, la inhibición de esta corteza genera un retraso en la recuperación de la anestesia con sevoflurano (Huels *et al.*, 2021).

Es importante destacar, que en este trabajo obtuvimos un resultado inesperado; las neuronas glutamatérgicas del VLPO (un área que ha sido considerada durante mucho tiempo como somnogénica) producen vigilia, fragmentan el sueño NREM e inhiben el sueño REM. Este hallazgo nos llevó a querer estudiar el rol de estas neuronas en el ciclo sueño-vigilia con más detalle, particularmente en relación a las transiciones entre los distintos estados comportamentales y su rol en la regulación de la actividad cortical, lo cual ha sido desarrollado en el siguiente capítulo.

Capítulo 4. Rol de las neuronas glutamatérgicas del área preóptica del hipotálamo en el ciclo sueño-vigilia.

El área preóptica del hipotálamo es un área compleja que se encarga de diversas funciones además de la regulación del ciclo sueño-vigilia como, por ejemplo, la termorregulación, el comportamiento sexual y maternal y la homeostasis de fluidos en el organismo (Gvilia *et al.*, 2005; Hull & Dominguez, 2006; McKinley *et al.*, 2021; Rivas *et al.*, 2021; Rothhaas & Chung, 2021; Tsuneoka & Funato, 2021). Como fue mencionado anteriormente, en cuanto a la regulación del ciclo sueño-vigilia, durante muchos años fue considerada un área exclusivamente somnogénica. Sin embargo, en el capítulo anterior, demostramos que las neuronas glutamatérgicas del área medial-lateral del hipotálamo (pero no del núcleo mediano) generan vigilia, fragmentan el sueño NREM y suprimen el sueño REM. La hipótesis de este trabajo fue que la activación de las neuronas glutamatérgicas del área medial-lateral del hipotálamo, además de fragmentar el sueño NREM, afectan la actividad eléctrica cortical durante este estado, provocando un sueño más ligero. El objetivo del siguiente trabajo fue evaluar el rol de estas neuronas en más detalle, determinando además como afectan la actividad eléctrica cortical durante los estados de vigilia y sueño.

Systems/Circuits

Glutamatergic Neurons in the Preoptic Hypothalamus Promote Wakefulness, Destabilize NREM Sleep, Suppress REM Sleep, and Regulate Cortical Dynamics

Alejandra Mondino,[1,2,4] Viviane S. Hambrecht-Wiedbusch,[1,2] Duan Li,[1,2] A. Kane York,[1,3] Dinesh Pal,[1,2,3] Joaquin González,[4] Pablo Torterolo,[4] George A. Mashour,[1,2,3] and Giancarlo Vanini[1,2,3]

[1]Department of Anesthesiology, University of Michigan, Ann Arbor, Michigan 48109-5615, [2]Center for Consciousness Science, University of Michigan, Ann Arbor, Michigan 48109, [3]Neuroscience Graduate Program, University of Michigan, Ann Arbor, Michigan 48109-2215, and [4]Departamento de Fisiología, Facultad de Medicina, Universidad de la República, Montevideo, 11200, Uruguay

Clinical and experimental data from the last nine decades indicate that the preoptic area of the hypothalamus is a critical node in a brain network that controls sleep onset and homeostasis. By contrast, we recently reported that a group of glutamatergic neurons in the lateral and medial preoptic area increases wakefulness, challenging the long-standing notion in sleep neurobiology that the preoptic area is exclusively somnogenic. However, the precise role of these subcortical neurons in the control of behavioral state transitions and cortical dynamics remains unknown. Therefore, in this study, we used conditional expression of excitatory hM3Dq receptors in these preoptic glutamatergic (Vglut2^{+}) neurons and show that their activation initiates wakefulness, decreases non-rapid eye movement (NREM) sleep, and causes a persistent suppression of rapid eye movement (REM) sleep. We also demonstrate, for the first time, that activation of these preoptic glutamatergic neurons causes a high degree of NREM sleep fragmentation, promotes state instability with frequent arousals from sleep, decreases body temperature, and shifts cortical dynamics (including oscillations, connectivity, and complexity) to a more wake-like state. We conclude that a subset of preoptic glutamatergic neurons can initiate, but not maintain, arousals from sleep, and their inactivation may be required for NREM stability and REM sleep generation. Further, these data provide novel empirical evidence supporting the hypothesis that the preoptic area causally contributes to the regulation of both sleep and wakefulness.

Key words: **arousal; consciousness; DREADDs; gamma; sleep fragmentation; slow oscillations**

Significance Statement

Historically, the preoptic area of the hypothalamus has been considered a key site for sleep generation. However, emerging modeling and empirical data suggest that this region might play a dual role in sleep-wake control. We demonstrate that chemogenetic stimulation of preoptic glutamatergic neurons produces brief arousals that fragment sleep, persistently suppresses REM sleep, causes hypothermia, and shifts EEG patterns toward a "lighter" NREM sleep state. We propose that preoptic glutamatergic neurons can initiate, but not maintain, arousal from sleep and gate REM sleep generation, possibly to block REM-like intrusions during NREM-to-wake transitions. In contrast to the long-standing notion in sleep neurobiology that the preoptic area is exclusively somnogenic, we provide further evidence that preoptic neurons also generate wakefulness.

Received Oct. 24, 2020; revised Jan. 24, 2021; accepted Feb. 22, 2021.

Author contributions: G.V. and G.A.M. designed research; G.V., A.M., D.L., A.K.Y., D.P., J.G., P.T., and G.A.M. analyzed data; G.V. and A.M. wrote the first draft of the paper; G.V., A.M., V.S.H.-W., D.L., A.K.Y., D.P., J.G., P.T., and G.A.M. edited the paper; G.V., A.M., D.P., P.T., and G.A.M. wrote the paper; A.M. and V.S.H.-W. performed research.

This work was supported by National Institutes of Health R01 GM124248 to G.V. and G.A.M., and the Department of Anesthesiology, University of Michigan Medical School. We thank Leonor Floran-Garduno, Megumi Mast, and Mary Norat (Department of Anesthesiology, University of Michigan) for expert assistance; and Dr. Corey Powell (Consulting for Statistics, Computing & Analytics Research, University of Michigan) for input on statistical analyses.

The authors declare no competing financial interests.

Correspondence should be addressed to Giancarlo Vanini at gvanini@umich.edu.

https://doi.org/10.1523/JNEUROSCI.2718-20.2021

Introduction

Since the beginning of the last century, the preoptic area of the hypothalamus has been considered a critical site for sleep generation. In the early 1900s, von Economo's work revealed that patients suffering severe insomnia after encephalitis lethargica had extensive lesions within the rostral hypothalamus (von Economo, 1930). Consistent with this observation, subsequent studies demonstrated that lesioning of the preoptic area causes a prolonged, severe insomnia in cats (Sallanon et al., 1989) and rats (Nauta, 1946; John et al., 1994; Lu et al., 2000; Eikermann et al., 2011), and transplantation of fetal preoptic cells into the preoptic area partially restored sleep quantity in previously lesioned

insomniac rats (John et al., 1998). Infusion of adenosine (or adenosine analogs) into the preoptic region increases sleep and decreases wakefulness (Ticho and Radulovacki, 1991; Mendelson, 2000), whereas pharmacologic inhibition of this region reduces sleep (Lin et al., 1989; M. N. Alam and Mallick, 1990; Benedetto et al., 2012). Additionally, evidence from single-cell recording and cFos studies confirmed that the median preoptic nucleus (MnPO) as well as ventrolateral and medial preoptic area contain neurons that are mainly active during non-rapid eye movement (NREM) sleep (Koyama and Hayaishi, 1994; Szymusiak et al., 1998; Suntsova et al., 2002; Takahashi et al., 2009; Sakai, 2011; M. A. Alam et al., 2014; Zhang et al., 2015; Chung et al., 2017; Harding et al., 2018) and, to a lesser extent, during rapid eye movement (REM) sleep (Koyama and Hayaishi, 1994; Lu et al., 2002; Suntsova et al., 2002; Gvilia et al., 2006; Dentico et al., 2009; Sakai, 2011; M. A. Alam et al., 2014). Importantly, a subset of these cells increases its activity during periods of prolonged wakefulness with increased sleep pressure, suggesting a role in the regulation of both NREM and REM sleep homeostasis (Gvilia et al., 2006; Dentico et al., 2009; Todd et al., 2010; M. A. Alam et al., 2014; Gvilia et al., 2017).

Several lines of evidence show that a group of GABAergic neurons (some of which coexpress galanin) distributed within the median, medial-lateral, and ventrolateral preoptic area are sleep-active and innervate monoaminergic arousal-promoting systems (Sherin et al., 1998; Gaus et al., 2002; Uschakov et al., 2006; Hsieh et al., 2011; Chung et al., 2017). Activation of preoptic GABAergic and galaninergic neurons promotes NREM sleep (Chung et al., 2017; Harding et al., 2018; Kroeger et al., 2018; Vanini et al., 2020) and lesion (Lu et al., 2000; Ma et al., 2019), or neuromodulation of these neurons (Harding et al., 2018; Kroeger et al., 2018) alters the EEG during sleep-wake states. Furthermore, a recent study using activity-dependent tagging and subsequent stimulation of previously tagged neurons showed that a subgroup of glutamatergic neurons within the median and medial preoptic nucleus of the hypothalamus promotes body cooling and NREM sleep (Harding et al., 2018). However, contrary to the prevailing idea in the field that virtually all preoptic neurons that regulate sleep-wake states are somnogenic, we recently reported that a region including the ventrolateral preoptic nucleus (VLPO) and the ventral half of the medial and lateral preoptic area, collectively referred in the current study as medial-lateral preoptic region, contains glutamatergic neurons that promote wakefulness (Vanini et al., 2020).

Here we used a chemogenetic stimulation approach to investigate further the role of these preoptic glutamatergic neurons in the regulation of sleep-wake states as well as state transitions and cortical dynamics, which have not yet been examined. We show that stimulation of glutamatergic neurons in the medial-lateral preoptic region causes a transient increase in wakefulness and a decrease in both NREM and REM sleep. Activation of these neurons also produces a high degree of NREM sleep fragmentation and state instability, a "lighter" NREM sleep state, and a long-lasting suppression of REM sleep. Thus, our data suggest that a subset of preoptic glutamatergic neurons may initiate, but not maintain, arousal from sleep, and their inactivation might be required for NREM stability and REM sleep generation. Furthermore, these results provide novel empirical evidence that the preoptic area plays a dual role in the regulation of both sleep and wakefulness.

Materials and Methods

Mice

Vglut2-IRES-Cre (Slc17a6tm2(cre)Lowl/J; stock #016963) mice were purchased from The Jackson Laboratory, bred at the University of Michigan animal care facility, and genotyped (Transnetyx) before weaning. Adult male mice used in this study ($n = 41$) were housed in groups in a 12 h light:dark cycle (lights on at 6:00 A.M.) with free access to food (PicoLab Laboratory Rodent Diet 5LOD; LabDiet) and water. The temperature in the housing and testing rooms was maintained at 22°C. All experiments were approved by the Institutional Animal Care and Use Committee and the Institutional Biosafety Committee, and were conducted in accordance with the recommendations published in the *Guide for the care and use of laboratory animals* (Ed 8, National Academies Press, Washington, DC, 2001).

Viral vector and drugs

For Cre-recombinase-dependent expression of the excitatory designer receptor hM3Dq in preoptic glutamatergic (Vglut2$^+$) neurons, we used the adeno-associated viral vector AAV-hSyn-DIO-hM3D(Gq)-mCherry (Addgene; catalog #50459-AAV5) (Krashes et al., 2011; Vanini et al., 2020). In a separate group of Vglut-Cre mice used for control experiments, we used the Cre-dependent vector AAV-hSyn-DIO-mCherry (Addgene; catalog #50459-AAV5) that lacked the coding sequence for the designer receptor and only contained the fluorescent reporter mCherry. The titer of the viral solutions was $3.7\text{-}7.8 \times 10^{12}$ copies per ml. DMSO and clozapine-N-oxide (CNO, catalog #C0832-5MG; agonist at hM3Dq receptors) were purchased from Sigma Millipore. A stock solution of CNO (0.1 mg/ml in saline solution containing 0.5% DMSO) was prepared and stored in aliquots, and then frozen at −20°C until use. Before each experiment, an aliquot of the stock solution was thawed at room temperature protected from the light until injection time. Mice received 1 mg/kg CNO or a vehicle control solution (VEH, saline with 0.5% DMSO) by intraperitoneal injection; the injection volume was 0.1 ml per 10 g of body weight (Vanini et al., 2020).

Viral injection and electrode implantation for sleep studies

The procedure for vector injection into the preoptic area was performed as described previously (Vanini et al., 2020). Mice were anesthetized in an induction chamber with 5.0% isoflurane (Hospira) in 100% O_2. The delivered concentration of isoflurane was monitored continuously by spectrometry (Cardiocap/5; Datex-Ohmeda). Following anesthetic induction, mice received preemptive analgesia (5 mg/kg carprofen; s.c.), and were immediately placed in a Kopf model 962 stereotaxic frame fitted with a mouse adaptor and a mouse anesthesia mask (models 922 and 907, respectively; David Kopf Instruments). Thereafter, the concentration of isoflurane was reduced and maintained at 1.6%-2.0% throughout the surgical procedure. Core body temperature was maintained at 37°C-38°C with a water-filled pad connected to a heat pump (Gaymar Industries). For the medial-lateral preoptic region, vector injections were performed bilaterally (36 nl on each side at the stock concentration provided by Addgene); stereotaxic coordinates: AP = 0.15 mm, ML = ±0.5 mm and DV = −5.0 mm from bregma (Vanini et al., 2020). Injections were performed at a rate of 5 nl/min using a Hamilton Neuros Syringe 7000 (5 ml) mounted on a microinjection syringe pump, driven by a digital Micro2T controller (model UMP3T-2; World Precision Instruments). After each injection, the syringe was maintained in position for an additional 5 min to avoid vector reflux. We previously confirmed that this volume, stereotaxic coordinates, and injection procedure yielded a reliable expression of hM3Dq receptors in the target region (Vanini et al., 2020). The scalp incision was closed with sutures, and mice were placed under a controlled heat source until full recovery. Mice were then returned to the vivarium and group-housed with their respective littermates. Analgesia was maintained with carprofen (5 mg/kg every 24 h) for a minimum of 48 h after surgery.

Three weeks following vector injection, mice were anesthetized with isoflurane and EEG electrodes (8IE3632016XE, E363/20/1.6/SPC; Plastics One) were implanted above the right frontal (AP = 1.5 mm, ML = 2.0 mm from bregma) and occipital (AP = −3.2 mm, ML = 3.0

mm from bregma) cortices. A reference screw electrode was implanted over the cerebellum, and a pair of EMG electrodes (8IE36376XXXE, E363/76/SPC; Plastics One) was inserted bilaterally into the dorsal neck muscles. All electrode pins were then inserted into an electrode pedestal (MS363; Plastics One) that was affixed to the skull with dental cement (Fast Cure Powder/Liquid, Product #335201; GC America). Thereafter, the delivery of isoflurane was discontinued, and mice were allowed to recover following the same postoperative care protocol outlined above. Mice were allowed a minimum of 10 d before experiments began.

EEG/EMG data acquisition

At least 1 week after the surgery for implantation of EEG/EMG electrodes, mice were conditioned to handling, simulating drug injection and tethering in the recording setup for 5 d. On the day of the experiment, mice received an injection of VEH or CNO and EEG/EMG signals were recorded for 6 h. The injection and recording start time was 10:00 A.M. (ZT04), when homeostatic sleep pressure is high, an optimal time to study the wakefulness-promoting effect of the targeted neurons. Monopolar EEG and bipolar EMG signals were amplified (×1000) and digitized (sampling rate = 1024 Hz), respectively, with a model 1700 AC amplifier (A-M Systems) and a Micro3 1401 acquisition unit and Spike2 software (Cambridge Electronic Design); notch filters were used for each mouse recording (both after VEH and CNO) when 60 Hz electrical noise was present. All signals were bandpass filtered between 0.1 and 500 Hz (EEG) and between 10 and 500 Hz (EMG). Mouse behaviors were video recorded, in synchrony with the electrophysiologic recordings in Spike2.

Analysis of sleep-wake states

States of wakefulness, NREM sleep, and REM sleep were manually scored in Spike2 in 5 s epochs using standard criteria described previously (Vanini et al., 2020). Wakefulness was defined by low-amplitude, high-frequency EEG activity accompanied by an active EMG characterized by high tone with phasic movements. NREM sleep was recognized by high-amplitude, low-frequency EEG waveforms along with a low muscle tone. REM sleep was identified by low-amplitude, high-frequency EEG signals with prominent, regular theta rhythm (particularly evident in the occipital cortex), and EMG atonia. Total time spent in wakefulness, NREM sleep, and REM sleep, the average duration and number of bouts for each vigilance state, was analyzed over the 6 h recording period, as well as in 1 h bins to assess the mean duration of the treatment effect. The mean latency to NREM sleep and REM sleep onset was compared between treatment conditions. Additionally, we reanalyzed sleep recordings from a group of Vglut2-Cre mice used in a recent study with confirmed hM3Dq receptor expression within the MnPO of the hypothalamus (Vanini et al., 2020). The reanalysis extended the assessment of sleep recordings from 3 to 6 h and was performed by the same investigator using the same scoring criteria as in the study by Vanini et al. (2020). Furthermore, the viral vector, surgical procedures, experimental design, and dose of CNO were identical in both studies. These mice served in the current study as a site-control group.

Sleep fragmentation analysis

An initial exploratory analysis revealed that chemogenetic activation of preoptic glutamatergic neurons substantially increased the number and decreased the duration of wakefulness and NREM sleep bouts, revealing a robust sleep fragmentation. Therefore, to further characterize this phenomenon, we calculated the stability of wake and NREM sleep states, between- and within-state transition probabilities, as well as a fragmentation index (FI). First, the mean number of transitions from NREM to wakefulness was quantified over the 6 h recording period and for every 1 h bin. The stability of each state was calculated using a Markov memoryless model. This is a regression-like method in which variables are modeled as a function of the previous observations (J. W. Kim et al., 2009; Perez-Atencio et al., 2018). In this formalism, the probability of being in one state is determined by the previous state and the transition probability from one state to another. The probability of each specific state was calculated by the number of times that this state was scored over the total number of epochs recorded and the transition probability was obtained as the conditional probability P(X/Y), that is, the number of times that State Y transitioned to State X in the following epoch, divided by the number of epochs of the Y state. Next, we calculated an FI for wakefulness and NREM sleep (codes are available at https://github.com/joaqgonzar/Fragmentation_Index). We defined FI as FI = 1 − p(X/X), that is, 1 minus the probability of transitioning from the State X to the same State X. This implies that FI = 1 only if the state is completely fragmented, in other words, if the probability of transitioning to the same state equals 0. Finally, as the sleep-wake cycle is characterized by bouts of short and long duration, we generated histograms of bout length for wakefulness and NREM sleep. These plots were obtained by counting the number of events that occurred in each increment of 10 s for wakefulness and 50 s for NREM sleep.

Determination of changes in body temperature after activation of glutamatergic neurons in the medial-lateral preoptic region

The effect of the activation of medial-lateral preoptic glutamatergic neurons on core body temperature was evaluated in two different experiments using a separate group of mice. The first set of experiments tested whether stimulation of these neurons alters body temperature. Mice were briefly and gently restrained for 10-15 s each time, and core body temperature was measured using a lubricated mouse rectal probe (model 600-1000, Barnant). After obtaining a stable temperature reading, the probe was removed and the animal was returned to its cage until the next measurement. Temperature measurements were obtained before the injection of VEH or CNO (1.0 mg/kg) and in 10 min intervals for 90 min after injection. If a temperature drop was detected, mice were placed under a heating lamp in their respective home cages between testing intervals. The second set of experiments was designed to evaluate the duration of temperature changes after CNO administration, relative to the duration of the sleep studies. Using the same procedure described above, temperature measurements were obtained in 30 min intervals for 6 h after CNO injection.

EEG signal processing and analysis

EEG analysis (power, coherence, connectivity, and complexity; 0.1-115 Hz) was conducted on artifact-free, nontransition epochs during the initial 3 h block after VEH and CNO injection. Digitized, raw EEG signals in frontal and occipital channels were exported from Spike2 software into MATLAB (version 2019b; The MathWorks) and downsampled to 512 Hz (resample.m function in MATLAB signal processing toolbox). Because notch filters were applied to EEG channels in some recordings (always in VEH/CNO pairs, for consistency), frequencies between 45 and 75 Hz were not considered for the analysis. The power-line interference (60 and 120 Hz), if present, was removed using multitaper regression technique and Thomas *F* statistics implemented in Cleanline plugin for EEGLAB toolbox (Delorme and Makeig, 2004). The 3-h-long recording blocks were segmented into 5 s windows with no overlap. All EEG measures were calculated from $n = 10$ mice (#541 was excluded because of poor signal quality that precluded its use in these analyses) in each window and then averaged over all available windows to obtain the mean values for each vigilance state, treatment condition, and mouse.

Spectral power and coherence analysis. The EEG power spectrum was estimated using the multitaper method in Chronux analysis toolbox (Mitra and Bokil, 2008) with a window length = 5 s without overlap, time-bandwidth product = 2, and number of tapers = 3. For each mouse in each treatment group, the mean power spectrum in each behavioral state (wake, NREM, REM) was obtained by averaging the power spectra across all available windows in frontal and occipital channels, respectively. Furthermore, the power values were calculated for slow oscillations (0.5-1 Hz) as well as δ (1-4 Hz), theta (4-9 Hz), σ (9-15 Hz), β (15-30 Hz), low γ (30-45 Hz), and high γ (75-115 Hz) frequency bands. Power values were normalized for each mouse as the mean power of each frequency band divided by the sum of the power in all bands (i.e., total power).

Cortical coherence (a measure of undirected functional connectivity) between frontal and occipital channels was quantified by the multitaper time-frequency coherence method in Chronux analysis toolbox (Mitra and Bokil, 2008), with the same parameters described above for the

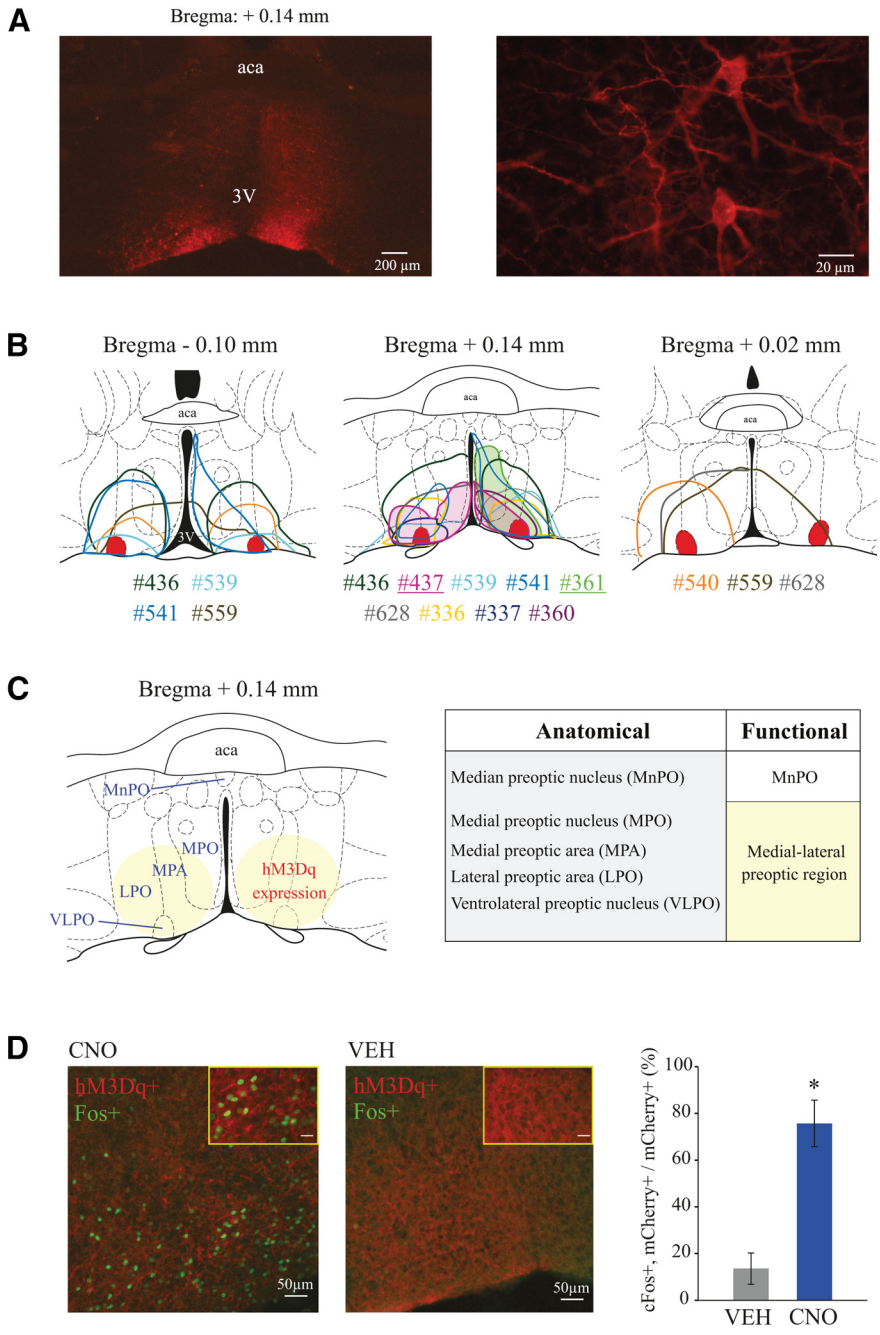

Figure 1. Histologic confirmation of hM3Dq receptor expression in the preoptic area of Vglut2-Cre mice used in sleep studies, and confirmation of neuronal activation caused by CNO administration. ***A***, Left, Right, Examples of low- and high-magnification photographs, respectively, of mCherry immunohistochemical staining (red), indicating the expression of the excitatory designer receptor hM3Dq within the VLPO of a Vglut2-Cre mouse. ***B***, Color-coded depiction of the area of hM3Dq receptor expression is represented on coronal schematics of the preoptic area modified from a mouse brain atlas (Paxinos and Franklin, 2001). Middle, Filled areas of hM3Dq expression highlight mice #437 and #361 (also indicated by underlined numbers below the brain schematic), which had the largest increase in sleep and wakefulness, respectively. For anatomic reference, solid red represents the bilateral sites corresponding to the VLPO. Color-matched identification numbers for each mouse used in the sleep studies ($n = 11$) are listed below each panel. ***C***, Schematic of the preoptic area illustrating relevant anatomic subdivisions and main area of designer receptor expression (yellow circles). Right, Chart compares the anatomic subdivisions and functional nomenclature used in this study. Based on the uniform response to chemogenetic stimulation, different from that observed in MnPO studies (Vanini et al., 2020), the area of hM3Dq receptor expression in the current study is referred to as the medial-lateral preoptic region. ***D***, cFos expression (green nuclei) in mCherry-positive (red) neurons in the medial-lateral preoptic region after CNO (1.0 mg/kg; $n = 4$ mice) and VEH ($n = 4$) administration. Graph plots the percentage (mean ± SEM) of mCherry-positive neurons that also expressed cFos over the total count of mCherry-positive neurons. Two-tailed unpaired t test was used for statistical comparison between treatment conditions. *Significant difference ($p < 0.05$) relative to control. Scale bars: high-magnification photographs (insets), 20 µm. aca, Anterior commissure; 3V, third ventricle.

spectral power analysis. The frontal-occipital coherence as a function of frequency was thus obtained by averaging the coherence over time in each behavioral state, for each mouse and treatment group. Coherence values were normalized by the Fisher's z-transform (Miranda de Sá et al., 2009). The same frequency bands used in the spectral power analysis were assessed in the coherence analysis.

Analysis of directed connectivity. We used normalized symbolic transfer entropy (NSTE) to assess directed connectivity between frontal and occipital cortices. NSTE is an information theoretic measure, and our previous studies have validated its use to measure cortical connectivity changes in humans (Lee et al., 2013) and rats (Borjigin et al., 2013; Pal et al., 2016, 2020). In the calculation of NSTE, three parameters are required: embedding dimension (d_E), time delay (τ), and transfer time (δ). We filtered the frontal and occipital EEG signals into the frequency bands as described above and segmented the filtered data into nonoverlapped 5 s windows. We followed the methods used in previous studies (D. Li et al., 2017; Pal et al., 2020) and fixed the embedding dimension $d_E = 3$; as the time delay τ defines a broad frequency-specific window of sensitivity for NSTE (Jordan et al., 2013; Sitt et al., 2014; Ranft et al., 2016), we used $\tau = 64, 28, 17, 9, 6, 2$, corresponding to δ (0.5-4 Hz), theta, σ, β, low- and high-γ, respectively. For each window, we searched the transfer time δ = 1-50 (corresponding to ~2-100 ms) and selected the one that generated maximum feedback (from frontal to occipital) and feedforward (from occipital to frontal) NSTE, respectively. For statistical comparisons, the averaged connectivity values were calculated over the studied behavioral states for each mouse and treatment group.

Complexity analysis. We used Lempel-Ziv complexity (LZc) to quantify the dynamic changes in EEG signals from frontal and occipital cortices in the different behavioral states between the two treatment conditions. LZc is a method of symbolic sequence analysis (Lempel and Ziv, 1976) that has been shown to be a valuable tool to investigate the temporal or spatiotemporal complexity of brain activity (Schartner et al., 2017; D. Li and Mashour, 2019; Brito et al., 2020; Pal et al., 2020). Given the limited number of EEG channels in this study, we assessed only temporal complexity in frontal and occipital channels; spatiotemporal complexity was not evaluated. EEG signals were detrended using local linear regression (locdetrend function in Chronux analysis software) and a lowpass filter was applied at 115 Hz (but excluding the frequencies at 45-75Hz) via Butterworth filter of order 4 (butter and filtfilt functions in MATLAB signal processing toolbox). The Hilbert transform of the signal was used to calculate the instantaneous amplitude, which was then segmented into 5 s windows without overlapping and binarized using its mean value as the threshold for each channel (Schartner et al., 2017). LZc analysis

estimates the complexity of a finite series of numbers by computing the number of times that a different subsequence of consecutive characters, or "word," is found within that series. To assess the signal complexity beyond the spectral changes, we generated surrogate data through phase randomization while preserving the spectral profiles of the signal (Schartner et al., 2015, 2017; Brito et al., 2020; Pal et al., 2020), and normalized the original LZc by the mean of the LZc values from $N = 50$ surrogate time series for each recording. The resultant LZc values were then averaged across all the windows as the estimate of the complexity for wakefulness, NREM sleep, and REM sleep. Higher values of LZc reflect higher complexity of the EEG signal. Analysis of spectral power, connectivity, and complexity during REM sleep was precluded by the profound suppression of REM sleep in the CNO group, which led to an insufficient sample size.

Immunohistochemistry and histologic verification of designer receptor expression; confirmation of neuronal activation after CNO administration

After the last sleep experiment, mice were deeply anesthetized with isoflurane and perfused transcardially with ice-cold 0.1 M PBS, pH 7.4, followed by 5% formalin for 10 min using a MasterFlex perfusion pump (Cole Palmer). A subset of mice previously injected with AAV-hM3Dq-mCherry (not used for sleep or temperature experiments) was perfused 90 min after an injection of VEH or CNO ($n = 4$ mice in each treatment group) for analysis of cFos expression in glutamatergic neurons of the medial-lateral preoptic region; the time of perfusion was 2:00 P.M. (ZT08) to minimize spontaneous cFos expression in the preoptic area. After perfusion, the brains were removed and postfixed in 5% formalin overnight at 4°C. Subsequently, brains were cryoprotected with 20% sucrose in PBS for 1-2 d, and then transferred to 30% sucrose for an additional 2-3 d. Thereafter, brains were frozen in Tissue–Plus (Fisher Healthcare) and sectioned coronally at 40 µm using a cryostat (CM1950, Leica Microsystems). Brain sections that contained the VLPO were collected and blocked in PBS containing 0.25% Triton X-100 and 3% normal donkey serum (Vector Laboratories) for 60 min at room temperature. Thereafter, sections were immunolabeled for mCherry, or sequentially processed for double immunohistochemistry for mCherry and cFos. First, we incubated the tissues overnight at room temperature in primary antiserum (rat monoclonal anti-mCherry 1:30,000; Thermo Fisher Scientific, catalog #M11217). For cFos detection, sections were incubated in a rabbit polyclonal anti-cFos (1:5000; Sigma Millipore, catalog #ABE457) overnight at room temperature. Next, sections were washed in PBS and incubated for 2 h at room temperature in a donkey anti-rat secondary antiserum (1:500; AlexaFluor-594, Thermo Fisher Scientific, catalog #A-21209 for mCherry and 1:500; AlexaFluor-488, Thermo Fisher Scientific, catalog #A-21206 for cFos). Last, brain sections were washed with PBS, float-mounted on glass slides, and coverslipped with SlowFade Diamond (S36972 or S36973; Invitrogen). Brain sections containing the target region were then examined by means of fluorescence microscopy (BX43, Olympus America). The brain regions in which the designer receptor hM3Dq were expressed were identified with the aid of a mouse brain atlas (Paxinos and Franklin, 2001). For stimulation experiments, only those mice that had reliable expression of designer receptors within the VLPO and adjacent areas were included in the analysis. The number mCherry-positive neurons that expressed cFos was visually examined by an experienced investigator and was quantified as the percentage of total neurons expressing mCherry in the medial-lateral preoptic region. Vglut2-Cre mice that received an AAV-hSyn-DIO-hM3D(Gq)-mCherry injection but did not express designer receptors were used as controls in the sleep studies described above.

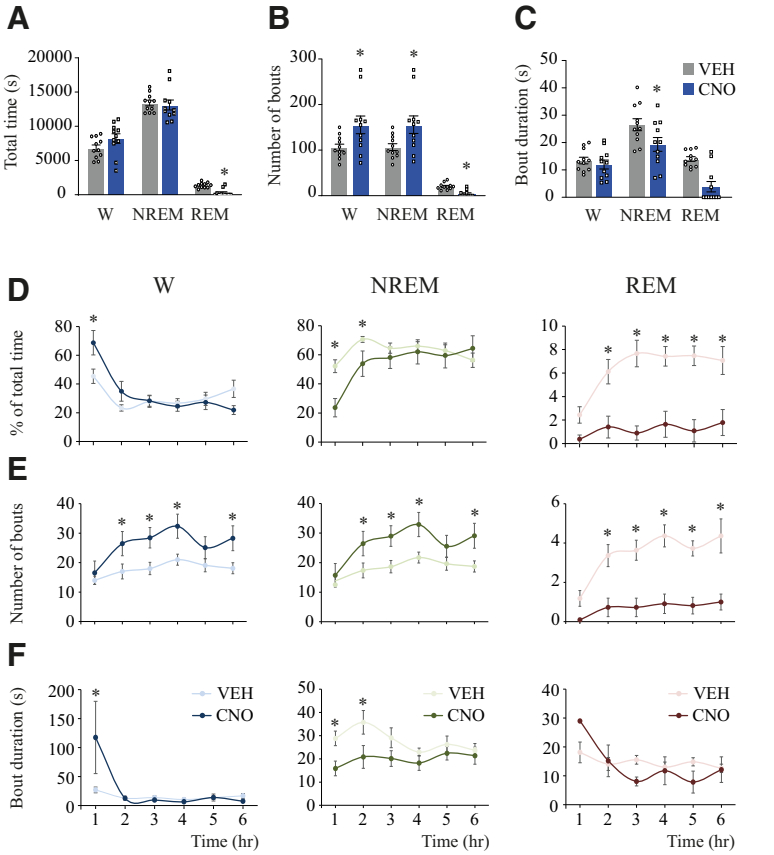

Figure 2. Chemogenetic activation of glutamatergic neurons in the medial-lateral preoptic region increased wakefulness and decreased NREM and REM sleep. ***A***, Time spent in wakefulness, NREM sleep, and REM sleep, averaged across the 6 h recording period, after administration of VEH and CNO (1.0 mg/kg) in $n = 11$ mice. ***B***, Effect on the number of wakefulness, NREM sleep, and REM sleep bouts. ***C***, Changes in the mean duration of wake, NREM sleep, and REM sleep bouts. Additionally, analyses of sleep-wake parameters were conducted in 1 h blocks after VEH (lighter color) and CNO (darker color) injection. ***D***, Percent of total time in wakefulness, NREM sleep, and REM sleep. ***E***, Number of bouts per state. ***F***, Mean duration of wake, NREM sleep, and REM sleep bouts. ***A–C***, A one-tailed paired *t* test with Bonferroni correction was used for statistical comparisons. ***D–F***, Two-way, repeated-measures ANOVA followed by a Sidak test adjusted for multiple comparisons was used to statistically compare sleep-wake parameters shown as a function of time and treatment condition. Data are mean ± SEM. *Significant difference ($p < 0.05$) relative to control.

Statistical analyses

Statistical comparisons were performed with PRISM version 7.0 (GraphPad Software). All data were tested for normality and are presented as mean ± SEM; *t* test and ANOVA results are reported as "*t* (DF) = ..." and "*F*(DFn, DFd) = ...," respectively. A $p < 0.05$ was considered statistically significant. The effect of stimulation of preoptic glutamatergic neurons on total state duration, number of bouts, bout duration, and number of NREM-to-W transitions over the 6 h recording period was assessed by a one-tailed paired *t* test (Bonferroni correction was used for analysis of the data reported in Figs. 2*A-C*, 7*A-C*, and 8*A-C*). The directional hypothesis that predicted the nature of the effects of chemogenetic stimulation of preoptic glutamatergic neurons on these sleep-wake parameters was based on previously published data (Vanini et al., 2020). Differences in sleep-wake parameters for each 1 h block were evaluated by a two-way repeated-measures ANOVA followed by a Bonferroni multiple-comparisons test. The effect of CNO injection on the latency to NREM sleep and REM sleep onset was analyzed by a one-tailed paired *t* test and by survival analysis. The effect of CNO administration on core body temperature was assessed by a two-way ANOVA followed by Dunnett (within-group comparisons) and Tukey (between-group comparisons) tests. The treatment effect on EEG

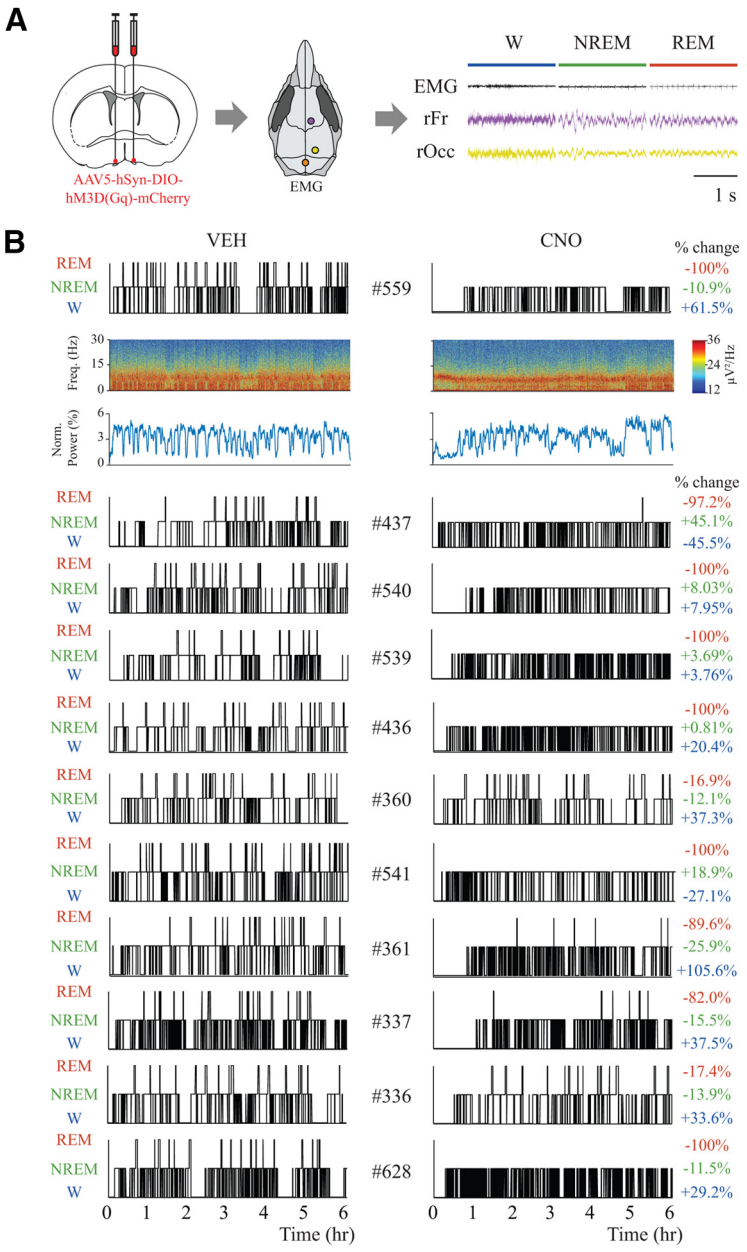

Figure 3. Chemogenetic activation of glutamatergic neurons in the medial-lateral preoptic region altered sleep-wake patterns. ***A***, Schematic representation of bilateral injections of a Cre-dependent adeno-associated virus for expression of the excitatory designer receptor hM3Dq into the medial-lateral preoptic region of Vglut2-Cre mice. Three weeks after the injection, mice were implanted with electrodes for recording the EEG from the right frontal (purple) and right occipital (yellow) cortex. A reference electrode was placed over the cerebellum (orange), and two electrodes were also implanted bilaterally in the neck muscles for recording the EMG. Right, Representative EEG and EMG signals from a mouse during wakefulness, NREM sleep, and REM sleep. ***B***, Hypnogram pairs illustrate the temporal organization of sleep-wake states after VEH (left panels) and 1.0 mg/kg CNO (right panels) for each mouse ($n = 11$). The height of the bars (from lowest to highest) represents the occurrence of wakefulness (W), NREM sleep, and REM sleep. Time 0 on the abscissa indicates the time at which the mouse received the injection of VEH or CNO. Mouse identification numbers are listed between each pair of hypnograms. Individual differences relative to control (% change) in the time spent in wakefulness (blue), NREM sleep (green), and REM sleep (red) after CNO injection are shown to the right of each CNO hypnogram. Representative spectrograms and power plots below the top two hypnograms corresponding to Mouse #559 show, respectively, state- and treatment-specific changes in frontal power density and normalized δ power with median filter across the 6 h recording session.

spectral power, Z'coherence, and NSTE (connectivity measures) for each frequency band was also assessed by a two-way repeated-measures ANOVA followed by a Bonferroni multiple-comparisons test. Changes in LZc were analyzed by a two-tailed paired t test. The effect of CNO administration on the FI over the 6 h recording period was determined by a Wilcoxon signed-rank test; the Benjamini-Hochberg correction for multiple-comparisons with a false discovery rate of 0.05 was used for the hour-by-hour analysis. Differences between treatment conditions in the distribution histograms were compared by the Kolmogorov-Smirnov test. Last, the relationship between REM sleep time (averaged for each mouse across the 6 h recording period) and the FI or the number of NREM-wake transitions was estimated using the Spearman correlation coefficient.

Results

Anatomical localization of designer receptors and confirmation of neuronal activation by designer receptors

As described in our previous publication (Vanini et al., 2020), histologic examination of vector injection sites revealed that neurons expressing hM3Dq receptors were localized within the VLPO and the adjacent region encompassing (from medial to lateral) the ventral aspect of the medial preoptic nucleus as well as medial and lateral preoptic area (Fig. 1). As stated above, in the current study, we refer to this region collectively as medial-lateral preoptic. There was no correlation between the area of receptor expression within the preoptic region and the stimulation effects on sleep-wake variables. Importantly, there was no receptor expression in glutamatergic neurons, nor in fibers, within any structure of the basal forebrain region (i.e., horizontal limb of the diagonal band of Broca and substantia innominata), just lateral to the preoptic region of the hypothalamus. Analysis of cFos expression confirmed that, relative to control, CNO administration activated glutamatergic neurons in the medial-lateral preoptic region (two-tailed t test, $t_{(6)} = 5.17$; $p = 0.0021$).

Activation of medial-lateral preoptic glutamatergic neurons increased wakefulness and reduced NREM and REM sleep

Previously published data validated the viral vector for stimulation of preoptic neurons and showed that activation of preoptic glutamatergic neurons causes a robust increase in wakefulness (Vanini et al., 2020). The present study used a chemogenetic stimulation method and thorough analysis to better understand the role of these neurons in the regulation of behavioral states, sleep-wake state transitions, and cortical dynamics. Figure 2 summarizes the effect of stimulation of preoptic glutamatergic neurons on sleep-wake variables (time spent in wakefulness, NREM sleep, and REM sleep as well as the mean number and duration of bouts for each state) averaged across the 6 h postinjection period. Compared with VEH, CNO administration significantly reduced the time spent in REM sleep ($t_{(10)} = 6.72$; $p < 0.0001$) (Fig. 2*A*); this state was completely abolished in 6 of the 11 mice studied (Fig. 3). There was

no significant difference in the time spent in wakefulness ($t_{(10)} = 0.58$; $p = 0.2870$) and NREM sleep ($t_{(10)} = 1.27$; $p = 0.1166$). Activation of preoptic glutamatergic neurons significantly increased the number of wakefulness and NREM sleep bouts ($t_{(10)} = 2.58$; $p = 0.0136$ and $t_{(10)} = 2.53$; $p = 0.0149$, respectively), and decreased the number of REM sleep bouts ($t_{(10)} = 4.99$; $p = 0.0003$) (Fig. 2*B*). Furthermore, the duration of NREM sleep bouts was significantly reduced during the 6 h recording period following CNO injection ($t_{(10)} = 2.56$; $p = 0.0141$); there were no changes in wakefulness bout duration ($t_{(10)} = 0.65$; $p = 0.2656$) (Fig. 2*C*). Because of the reduced number of mice that had REM sleep after CNO administration and the scarcity of REM sleep bouts in this group, the treatment effect on REM sleep bout duration was not statistically analyzed (VEH vs CNO: 13.98 ± 0.86 vs 10.64 ± 2.75; Fig. 2*C*).

Figure 2*D* illustrates hour-by-hour changes in the time spent in wakefulness, NREM sleep, and REM sleep (expressed as the percent of total time) as a function of treatment condition during the 6 h after injection. Two-way, repeated-measures ANOVA indicated a significant time effect and treatment condition × time interaction for wakefulness ($F_{(5,50)} = 15.36$; $p < 0.0001$ and $F_{(5,50)} = 4.98$; $p = 0.0009$) and NREM sleep ($F_{(5,50)} = 12.18$; $p < 0.0001$ and $F_{(5,50)} = 5.49$; $p = 0.0004$). CNO administration caused a significant increase in the time in wakefulness during the first hour after injection ($p = 0.0014$) and a reduction of NREM sleep duration during hours 1 ($p < 0.0001$) and 2 ($p = 0.0188$) after injection. For REM sleep, ANOVA revealed a significant time ($F_{(5,50)} = 5.35$; $p = 0.0005$) and drug ($F_{(1,10)} = 45.12$; $p < 0.0001$) effect as well as a treatment × time interaction ($F_{(5,50)} = 2.69$; $p = 0.0316$).

Activation of preoptic glutamatergic neurons caused a significant decrease in the time spent in REM sleep between hours 2-6 after CNO injection ($p = 0.002$, $p < 0.0001$, $p < 0.0001$, $p < 0.0001$, and $p < 0.0001$). Figure 2*E* shows that, relative to control, CNO altered the number of wakefulness, NREM sleep, and REM sleep bouts. ANOVA showed a significant drug and time effect on the number of wake ($F_{(1,10)} = 6.82$; $p = 0.0260$ and $F_{(5,50)} = 5.32$; $p = 0.0005$) and NREM sleep bouts ($F_{(1,10)} = 6.29$; $p = 0.0311$ and $F_{(5,50)} = 6.77$; $p < 0.0001$), and no significant effect on treatment condition × time interaction ($F_{(5,50)} = 1.41$; $p = 0.2380$ and $F_{(5,50)} = 1.62$; $p = 0.1725$). The hour-by-hour *post hoc* analysis revealed that CNO significantly increased the number of wake ($p = 0.0103$, $p = 0.0036$, $p = 0.0013$, and 0.0048) and NREM sleep ($p = 0.0129$, $p = 0.0033$, $p = 0.0013$, and $p = 0.0033$) bouts during hours 2, 3, 4, and 6 after injection. Additionally, there was a significant effect of CNO administration on the number of REM sleep bouts ($F_{(1,10)} = 26.43$; $p = 0.0004$), a significant time effect ($F_{(5,50)} = 7.26$; $p < 0.0001$), and a significant treatment × time interaction ($F_{(5,50)} = 2.55$; $p = 0.0391$). Congruent with the decrease in REM sleep time, the mean number of REM sleep bouts was significantly reduced between hours 2-6 after CNO administration ($p < 0.0001$, $p < 0.0001$, $p < 0.0001$, $p < 0.0001$, and $p < 0.0001$). Figure 2*F* plots the mean bout duration for wakefulness, NREM sleep, and REM sleep. Two-way, repeated-measures ANOVA indicated a significant time effect on the bout duration for wakefulness ($F_{(5,50)} = 3.74$; $p = 0.0059$) and a significant drug effect on bout duration for NREM sleep ($F_{(1,10)} = 8.14$; $p = 0.0172$). *Post hoc* Bonferroni showed that CNO significantly increased the duration of wake bouts ($p = 0.0067$) during the first hour after injection, which accounts for the increase in the time in wakefulness shown in Figure 2*A*. Of note, the large deviation in the mean episode duration is related to 1 mouse that remained awake for the entire hour after injection; removal of this mouse's VEH and CNO data points did not affect statistical significance. Bonferroni tests revealed that NREM sleep episode duration was significantly decreased during hours 1 ($p = 0.0010$) and 2 ($p = 0.0006$) after CNO injection. There were no significant changes in REM sleep episode duration. Figure 3 illustrates the sleep-wake architecture in each Vglut2-Cre mouse ($n = 11$) expressing excitatory hM3Dq receptors in glutamatergic neurons of the medial-lateral preoptic region, after injection of VEH or CNO.

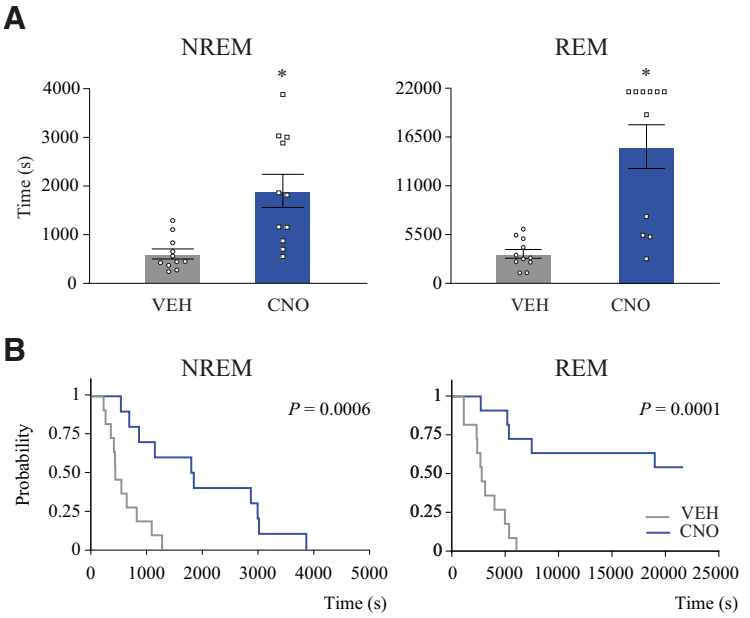

Figure 4. Activation of glutamatergic neurons in the medial-lateral preoptic region increased the latency to NREM and REM sleep. ***A***, Effect of CNO (1.0 mg/kg) injection on NREM (left) and REM sleep (right) latencies in $n = 11$ mice. Data are mean ± SEM. One-tailed paired *t* test was used for statistical comparisons. *Significant difference ($p < 0.05$) relative to control. ***B***, Graphs represent the probability of no NREM sleep (left) and REM sleep (right) generation after injection of VEH or CNO. Survival analysis demonstrated that the probability of no REM sleep occurring remained increased throughout the 6 h recording period and was significantly different between treatment condition in both NREM ($p = 0.0006$) and REM sleep ($p = 0.0001$).

Activation of medial-lateral preoptic glutamatergic neurons increased NREM and REM sleep latency

Figure 4 illustrates sleep latencies measured after VEH and CNO injection. The Figure 4*A* graphs plot NREM and REM sleep latencies averaged across the 6 h recording period for all mice. Animals that did not have REM sleep after CNO administration ($n = 6$) were assigned the maximum possible time (total recording time = 21,600 s) as the latency to REM sleep. Relative to VEH, CNO injection significantly increased the latency to both NREM (mean ± SEM = 604.55 ± 102.51 vs 1796.36 ± 378.39, $t_{(10)} = 2.88$; $p = 0.0081$) and REM sleep (3334.55 ± 494.74 vs 15 419.55 ± 2463.17, $t_{(10)} = 4.76$; $p = 0.0004$). Because several mice did not have REM sleep after CNO injection, changes in the latency to the first REM sleep bout (also the latency to NREM sleep onset) were assessed by survival analysis (Vanini and Baghdoyan, 2013). The Figure 4*B* graphs plot the probability of not having NREM sleep and REM sleep after CNO

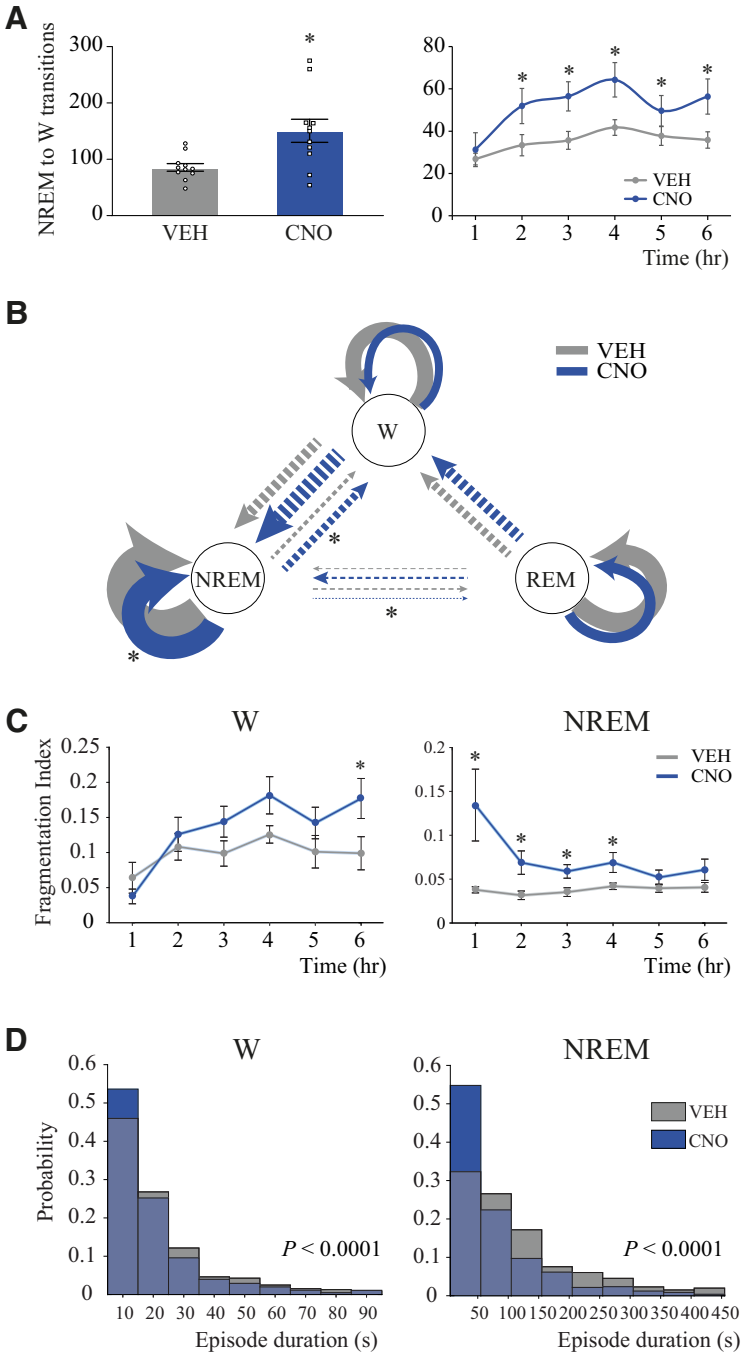

Figure 5. Activation of glutamatergic neurons in the medial-lateral preoptic region increased NREM to wake transitions and caused NREM sleep fragmentation. ***A***, Number of transitions from NREM to wakefulness (W) averaged across the 6 h recording period (left) and per 1 h block (right) after injection of VEH or CNO in $n = 11$ mice. Data are mean ± SEM. One-tailed paired *t* test (6 h block) and two-way repeated-measures ANOVA followed by a Sidak test to correct for multiple comparisons (1 h block analysis) was used for statistical comparisons between treatment conditions. *Significant difference ($p < 0.05$) relative to control. ***B***, Diagram of the Markov model for wakefulness (W)–NREM sleep–REM sleep dynamics after VEH and CNO (1.0 mg/kg) injection in $n = 11$ mice. Circular arrows indicate the probability of remaining within the same state. Straight arrows indicate the probability of transitioning from one state to another. The thickness of the arrows is proportional to the corresponding probability. Two different scales were used: one for the circular arrows and another one for straight arrows; that is, circular arrows were designed with continuous lines, whereas straight arrows were designed with dotted lines. Differences between VEH and CNO were analyzed by means of Wilcoxon matched-pairs rank tests. *Significant difference ($p < 0.05$) relative to control. ***C***, FI calculated from $n = 11$ mice for each 1 h block during wakefulness and NREM sleep after VEH or CNO injection. We defined FI as FI = 1 − p(X/X), being p(X/X) the probability of transitioning from the State X to the same State X. This implies that FI = 1 only if the state is completely fragmented, that is, if the probability of transitioning to the same state equals 0. Error bars indicate SEM. Differences between VEH and CNO were analyzed by means of Wilcoxon matched-pairs rank tests. *p* values were corrected by the Benjamini-Hochberg for a false discovery rate of 5%. *Significant difference ($p < 0.05$) relative to control. ***D***, Histograms represent the probability distribution of episode durations calculated from $n = 11$ mice in units of 10 s of wakefulness and in units of 50 s of NREM sleep. VEH and CNO histograms were overlapped to better appreciate the differences. The difference in the distribution of episode duration between VEH and CNO injection was analyzed by means of a Kolmogorov-Smirnov test. Episode duration after CNO and VEH had a different distribution in both wakefulness ($p < 0.0001$) and NREM sleep ($p < 0.0001$), with increased short and reduced long bouts after CNO administration.

administration. Activation of preoptic glutamatergic neurons significantly increased the probability of not having NREM sleep ($p = 0.0006$) and REM sleep ($p = 0.0001$). Furthermore, relative to control, the probability of REM sleep not occurring after CNO administration remained elevated (>50%) until the end of the recording period.

Activation of medial-lateral preoptic glutamatergic neurons increased NREM to wake transitions and caused a robust NREM sleep fragmentation

Because activation of preoptic glutamatergic neurons increased the number of wake and NREM sleep bouts, we compared the number of transitions from NREM sleep to wakefulness as a function of treatment condition and time. Figure 5*A* (left) plots the mean number of NREM to wake transitions averaged across the 6 h recording period for all mice. CNO injection significantly increased the number of transitions by 76% ($t_{(10)} = 3.36$; $p = 0.0036$). Figure 5*A* (right) illustrates hour-by-hour changes in NREM to wake transitions during 6 h after VEH and drug administration. ANOVA revealed a significant effect of treatment ($F_{(1,10)} = 11.35$; $p = 0.0071$). There was no treatment × time interaction ($F_{(5,50)} = 1.96$; $p = 0.1012$). Multiple-comparisons *post hoc* tests showed that the number of transitions was significantly increased between postinjection hours 2-6 ($p = 0.0014$, $p = 0.0001$, $p < 0.0001$, $p = 0.0168$, and $p = 0.0002$). There was no significant correlation between REM sleep time and the number of NREM to wake transitions ($r = -0.4808$; $p = 0.1364$).

Based on (1) the increase in the number of NREM sleep bouts, (2) the reduction of NREM sleep bout duration, and (3) the increment in the number of NREM to wake transitions after CNO injection, we hypothesized that the activation of preoptic glutamatergic neurons causes NREM sleep instability. We tested this hypothesis using three different approaches. First, we calculated the state transition probability after VEH and CNO administration by means of a Markov model. Figure 5*B* depicts the probability of transitioning between/within states of wakefulness, NREM sleep, and REM sleep. Consistent with a previous study (Perez-Atencio et al., 2018), the probability of remaining in one state was much higher than the probability of transitioning into a different

state. Relative to VEH, activation of glutamatergic neurons in the medial-lateral preoptic region significantly reduced the probability of remaining in NREM sleep (mean ± SEM = 0.9384 ± 0.009 vs 0.9621 ± 0.003, W [probability vector value] = −7; p = 0.0186), while there was no significant change in the probability of remaining in wakefulness (0.8983 ± 0.0491 vs 0.9205 ± 0.0069, W = −24; p = 0.1602) or REM sleep (0.9052 ± 0.040 vs 0.9621 ± 0.003, W = −7; p = 0.2188). Consistent with this evidence, there was an increased probability of transitioning from NREM sleep to wakefulness (0.060 ± 0.010 vs 0.031 ± 0.003, W = 64; p = 0.0010), while the probability of transitioning from wakefulness to NREM sleep was not affected (0.1017 ± 0.015 vs 0.079 ± 0.007, W = 24.0; p = 0.1602). Furthermore, as expected because of the drastic reduction in the amount of REM sleep, CNO significantly decreased the probability of transitioning from NREM to REM sleep (0.0017 ± 0.001 vs 0.0072 ± 0.001, W = −60; p = 0.0024). The probability of entering either wakefulness or NREM sleep from REM sleep was not affected by the activation of the glutamatergic neurons of the medial-lateral preoptic region (0.0833 ± 0.032 vs 0.0625 ± 0.008, W = 7; p = 0.2188 and 0.011 ± 0.009 vs 0.003 ± 0.001, W = 2; p = 0.3750, respectively). None of the mice entered REM sleep from wakefulness after VEH, as expected, or CNO administration. Second, to evaluate the stability of sleep-wake states in each 1 h block, we calculated an FI; FI = 1 indicates that the state is maximally unstable and fragmented. Because of the scarcity of REM sleep after CNO administration, we only performed this analysis for wakefulness and NREM sleep states. Figure 5*C* shows that, compared with VEH, stimulation of glutamatergic neurons in the medial-lateral preoptic region significantly fragmented NREM sleep during the first 4 h of the recording period (W = 45, p = 0.0294; W = 54, p = 0.0294; W = 48, p = 0.0315; W = 46, p = 0.0315). There was no significant correlation between REM sleep time and FI NREM values (r = −0.3569; p = 0.2785). Additionally, wakefulness was only fragmented during the last hour of the 6-h-long recording period (W = 64, p = 0.0060). Third, to understand better the effect of the activation of preoptic glutamatergic neurons on sleep and wake episode duration, we compared the distribution of NREM sleep and wake bout duration after VEH and CNO injection. Figure 5*D* shows that the activation of glutamatergic neurons of the medial-lateral preoptic region significantly altered the probability distribution of bout duration by increasing the number of short bouts and decreasing the number of long bouts during both NREM sleep ($p < 0.0001$) and wakefulness ($p < 0.0001$).

Activation of medial-lateral preoptic glutamatergic neurons reduces body temperature

Activation of MnPO glutamatergic (Abbott and Saper, 2017; Vanini et al., 2020) and VLPO galaninergic neurons (Kroeger et al., 2018) has been shown in mice to cause hypothermia, which can increase wakefulness and reduce NREM and REM sleep duration (Parmeggiani, 1987). Thus, the effect of glutamatergic neurons in the medial-lateral preoptic region on core body temperature was evaluated before and after CNO injection (n = 10 mice), compared with a VEH control group (n = 5), and relative to previously published data obtained after activation of glutamatergic neurons in the MnPO (n = 9) (Fig. 6). MnPO temperature values used here are from the data reported previously (Vanini et al., 2020). Relative to baseline, a two-way ANOVA revealed a significant time ($F_{(9,210)}$ = 2.17; p = 0.0252) and treatment ($F_{(2,210)}$ = 19.03; $p < 0.0001$) effect. A Dunnett's test demonstrated that, relative to baseline, the activation of glutamatergic neurons in the medial-lateral preoptic region significantly reduced body

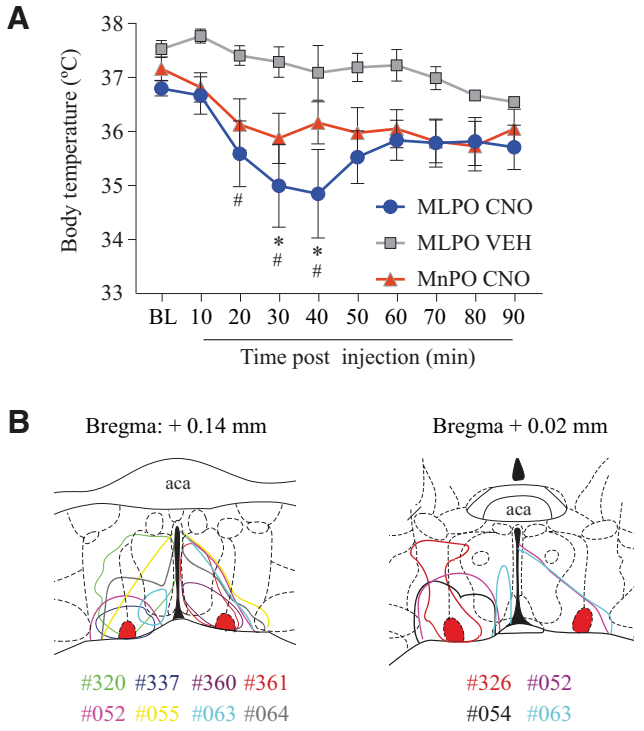

Figure 6. Activation of glutamatergic neurons in the medial-lateral preoptic region causes hypothermia in awake mice. ***A***, The time course of core body temperature in awake mice before and after injection of VEH control solution (n = 5 mice) or CNO (1.0 mg/kg) for activation of glutamatergic neurons within the MnPO (n = 9) and medial-lateral preoptic region (MLPO; n = 10). Temperature values for the MnPO are from Vanini et al. (2020, their Fig. 3; see also their Fig. S4 showing the distribution of the excitatory designer receptor hM3Dq within the MnPO of Vglut2-Cre mice used in that study). Data are mean ± SEM. Two-way ANOVA followed by a *post hoc* Dunnett's test corrected for multiple-comparisons was used for statistical comparisons of mean temperature levels after VEH and CNO injection relative to baseline (BL). Differences in temperature levels between the VEH and the medial-lateral preoptic group, and medial-lateral preoptic versus MnPO glutamatergic group were assessed by Tukey's and Sidak's *post hoc* tests. *Significant difference ($p < 0.05$) in the medial-lateral preoptic group relative to baseline. $^{\#}$Significant difference relative to VEH. ***B***, Color-coded area of hM3Dq receptor expression within the medial-lateral preoptic region of Vglut2-Cre mice used for temperature experiments, represented on coronal schematics of the preoptic area modified from a mouse brain atlas (Paxinos and Franklin, 2001).

temperature at 30 and 40 min after injection (p = 0.0238 and p = 0.0104). Compared with VEH, CNO injection caused hypothermia between 20 and 40 min (Tukey's test; p = 0.0340, p = 0.0051, and p = 0.0064). Relative to the MnPO, there was no significant difference in temperature at any time point. Furthermore, the mean temperature decrease after CNO injection (from min 20-90) was 1.28 ± 0.48°C (mean ± SEM) in the medial-lateral preoptic group and 1.19 ± 0.26°C in the MnPO group, and there was no significant difference in the magnitude of temperature change between both groups ($t_{(0.1738)}$ = 13.71; p = 0.8645). In a separate experiment, we investigated the time course of mean temperature changes induced by the activation of glutamatergic neurons in the medial-lateral preoptic region (n = 5), with respect to the duration of the sleep studies described above. Temperature measurements were obtained before and after CNO injection, every 30 min for 6 h. A one-way, repeated-measures ANOVA showed a significant treatment effect ($F_{(2.428,9.710)}$ = 20.08; p = 0.0003). *Post hoc* Dunnett's test demonstrated that there was a sustained, significant reduction in body temperature between minute 30 and 360 after CNO administration (p = 0.0049, p = 0.0235, p = 0.0085, p = 0.0046, p = 0.0131, p = 0.0012,

Table 1. Sleep-wake parameters obtained from individual, negative control groups as a function of treatment condition[a]

	AAV-mCherry ("empty" control vector)		AAV without hM3Dq expression	
	VEH	CNO	VEH	CNO
Time spent in wake (s)	7919 ± 633.5	7730 ± 353.3	7250 ± 484.3	7347 ± 435.4
Time spent in NREM sleep (s)	12443 ± 516.9	12321 ± 347.5	12803 ± 482.7	13166 ± 374.3
Time spent in REM sleep (s)	1239 ± 312.3	1549 ± 77.55	1547 ± 55.6	1087 ± 262.3
No. of wake bouts	126.8 ± 17.54	109.3 ± 5.22	107.2 ± 15.68	100.0 ± 13.88
No. of NREM sleep bouts	126.8 ± 17.72	108.8 ± 5.28	107.8 ± 15.62	100.6 ± 14.09
No. of REM sleep bouts	17.50 ± 2.46	19.75 ± 3.42	20.6 ± 2.22	16.40 ± 3.95
Duration of wake bout (s)	12.84 ± 1.01	14.30 ± 1.22	14.29 ± 1.63	15.36 ± 1.23
Duration of NREM sleep bout (s)	20.93 ± 3.13	22.75 ± 1.04	25.60 ± 3.40	28.56 ± 4.32
Duration of REM sleep bout (s)	14.18 ± 3.17	17.13 ± 2.84	15.52 ± 1.22	12.60 ± 1.70
Latency to NREM sleep (s)	356.3 ± 237.1	278.8 ± 139.6	320 ± 199.2	855 ± 154.7
Latency to REM sleep (s)	4256 ± 1993	1813 ± 125.6	2949 ± 1128	7423 ± 3735

[a]Data ($n = 9$ Vglut2-Cre mice) are mean ± SEM. Relative to control (VEH), there were no significant differences. CNO (hM3Dq receptor agonist; 1.0 mg/kg).

$p = 0.0027$, $p = 0.0003$, $p = 0.0005$, $p = 0.0022$, $p = 0.0030$, and $p = 0.0017$).

CNO administration to control mice without designer receptors did not alter sleep-wake states

To rule out any nonspecific effect of CNO or its active metabolites (Ilg et al., 2018), as well as from the cell damage caused by the injection procedure or vector-associated toxicity (Rezai Amin et al., 2019), we included two negative control groups. The effect of 1.0 mg/kg CNO on sleep-wake states was evaluated in a group of mice that received the vector injection into the medial-lateral preoptic region but did not express hM3Dq receptors ($n = 5$), and in a second group injected with the "empty" control vector that only contained the fluorescent reporter mCherry ($n = 4$). Consistent with previous work (Vanini et al., 2020), CNO injection did not alter sleep-wake states in either group. Therefore, the data from all 9 mice were pooled for statistical analysis. The data corresponding to each control group (6 h average) are shown in Table 1. Figure 7*A–C* summarizes group data averaged across the 6 h recording period and shows that CNO injection did not modify the time in wakefulness ($t_{(8)} = 0.069$; $p = 0.9460$), NREM sleep ($t_{(8)} = 0.351$; $p = 0.7344$), or REM sleep ($t_{(8)} = 0.506$; $p = 0.6265$). Neither the number of bouts nor their duration was altered during wakefulness ($t_{(8)} = 1.182$; $p = 0.2710$ and $t_{(8)} = 1.850$; $p = 0.1014$), NREM sleep ($t_{(8)} = 1.209$; $p = 0.2613$ and $t_{(8)} = 1.215$; $p = 0.2589$), or REM sleep ($t_{(8)} = 0.525$; $p = 0.6137$ and $t_{(8)} = 0.142$; $p = 0.8909$). Furthermore, there were no significant changes in the total time (expressed as the percent of total time) in wakefulness, NREM sleep, and REM sleep in the hour-by-hour analysis (Fig. 7*D–F*). Two-way, repeated-measures ANOVA showed no significant effect of the treatment, or treatment × time interaction in wakefulness ($F_{(1,8)} = 0.005$; $p = 0.9460$ and $F_{(5,40)} = 0.125$; $p = 0.9860$), NREM sleep ($F_{(1,8)} = 0.124$; $p = 0.7344$ and $F_{(5,40)} = 0.054$; $p = 0.9980$), and REM sleep ($F_{(1,8)} = 0.257$; $p = 0.6260$ and $F_{(5,40)} = 2.17$; $p = 0.0767$). The latency to NREM or REM sleep was not significantly altered by CNO, as shown in Figure 7*G* (mean time in s ± SEM = 336.1 ± 143.0 vs 598.9 ± 142.0, $t_{(8)} = 1.986$; $p = 0.0823$ and 3530 ± 1034 vs 4929 ± 2202, $t_{(8)} = 0.662$; $p = 0.5268$, respectively). Importantly, neither wakefulness nor NREM sleep was fragmented during the 6 h period after CNO injection (0.075 ± 0.005 vs 0.068 ± 0.003, $W = -27$; $p = 0.1289$; and 0.046 ± 0.005 vs 0.040 ± 0.003, $W = -21$; $p = 0.2500$). Accordingly, no fragmentation was found in any of the six 1 h block analyses for wakefulness ($W = -27$, $p = 0.1289$; $W = -3.0$, $p = 0.9102$; $W = -11$, $p = 0.5703$; $W = 1.0$, $p > 0.9999$; $W = -19$, $p = 0.3008$; $W = 1.0$, $p > 0.9999$) or NREM sleep ($W = -15$, $p = 0.4258$; $W = -27$, $p = 0.1289$; $W = -11$, $p = 0.5703$; $W = 9.0$, $p = 0.6523$; $W = -13$, $p = 0.4961$; $W = 7.0$, $p = 0.7344$) as shown in Figure 7*H*, *I*.

Activation of glutamatergic neurons in the MnPO did not substantially alter sleep-wake states

To test whether the effects of the activation of glutamatergic neurons in the medial-lateral preoptic region were site-specific, we reanalyzed sleep-wake data from a previous study in which we used the same chemogenetic methods and experiment design to stimulate MnPO glutamatergic neurons in Vglut2-Cre mice (Vanini et al., 2020). Figure 8*A–C* shows that activation of glutamatergic neurons within the MnPO ($n = 7$ mice) did not modify the time in wakefulness ($t_{(6)} = 0.253$; $p = 0.8087$), NREM sleep ($t_{(6)} = 0.748$; $p = 0.2412$), and REM sleep ($t_{(6)} = 1.738$; $p = 0.066$). CNO administration did not alter the number of bouts or bout duration of wakefulness ($t_{(6)} = 0.577$; $p = 0.2925$ and $t_{(6)} = 0.630$; $p = 0.5519$), NREM ($t_{(6)} = 0.635$; $p = 0.2745$ and $t_{(6)} = 0.223$; $p = 0.8312$), and REM sleep ($t_{(6)} = 2.294$; $p = 0.0616$ and $t_{(6)} = 0.889$; $p = 0.4082$). Additionally, there were no significant changes in the time (expressed as the percent of total time) spent in wake, NREM sleep, and REM sleep in the 1 h block analysis (Fig. 8*D–F*). Two-way, repeated-measures ANOVA revealed no significant effect of treatment or treatment × time interaction for wakefulness ($F_{(1,6)} = 0.06$; $p = 0.809$ and $F_{(5,30)} = 0.37$; $p = 0.866$), NREM sleep ($F_{(1,6)} = 0.16$; $p = 0.7059$ and $F_{(5,30)} = 0.41$; $p = 0.8386$), and REM sleep ($F_{(1,6)} = 3.02$; $p = 0.1328$ and $F_{(5,30)} = 0.91$; $p = 0.4860$). Figure 8*G* shows that activation of glutamatergic neurons in the MnPO did not alter the latency to NREM (mean time in s ± SEM = 568.6 ± 136.5 vs 680.0 ± 199.0, $t_{(6)} = 0.619$; $p = 0.558$) or REM sleep (2676 ± 330.3 vs 4496 ± 777.0, $t_{(6)} = 2.14$; $p = 0.076$). Furthermore, activation of MnPO glutamatergic neurons did not cause fragmentation of wake or NREM sleep states (Fig. 8*H*,*I*).

Activation of medial-lateral preoptic glutamatergic neurons altered EEG features during wakefulness and NREM sleep

This study aimed to determine whether the activation of preoptic glutamatergic neurons, in addition to altering sleep-wake patterns, alters cortical dynamics (i.e., oscillations, connectivity, and complexity) associated with sleep and wakefulness. We thus evaluated local and network-level cortical activity by means of power spectrum, functional and directed connectivity between frontal and occipital cortices, as well as the complexity of EEG signals. Figure 9 shows the mean spectral power from frontal and occipital cortices during wakefulness and NREM sleep. There was a significant treatment effect (CNO) on the spectral power in the

occipital cortex during wakefulness ($F_{(1,9)} = 18.79$; $p = 0.0019$), and in the frontal cortex during NREM sleep ($F_{(1,9)} = 6.46$; $p = 0.0317$). There was a significant drug × EEG frequency band interaction for the occipital cortex during wakefulness ($F_{(6,54)} = 9.33$; $p < 0.0001$) and during NREM sleep ($F_{(6,54)} = 6.41$; $p < 0.0001$). No significant treatment effect or treatment × EEG frequency band interaction was found in the frontal cortex during wakefulness ($F_{(1,9)} = 3.40$; $p = 0.0985$ and $F_{(6,54)} = 2.19$; $p = 0.0952$); there was a significant EEG frequency effect ($F_{(6,54)} = 166.3$; $p <$ 0.0001). *Post hoc* (Bonferroni) multiple-comparisons analysis revealed that CNO injection significantly decreased the power of slow oscillations (0.5-1 Hz) during wakefulness ($p = 0.0077$, frontal, and $p < 0.0001$, occipital) and NREM sleep ($p < 0.0001$, frontal, and $p < 0.0001$, occipital), and increased δ power during NREM sleep ($p = 0.0051$, frontal, and $p = 0.0198$, occipital). However, the increase in δ power is mainly driven by only 1 mouse that had a relatively large increase after normalization (128%; corrected p value after removal of this outlier is 0.0761, frontal, and 0.2480, occipital; Cohen's $d = 0.6$ and 0.4).

Figure 10 plots Z'coherence between frontal and occipital cortices as a function of EEG frequency band and treatment condition. ANOVA revealed a significant treatment × EEG frequency band interaction during wakefulness ($F_{(6,54)} = 3.34$; $p = 0.0072$) and NREM sleep ($F_{(6,54)} = 6.13$; $p < 0.0001$). Furthermore, a *post hoc* multiple-comparisons test demonstrated an increase in high-γ coherence during wakefulness ($p = 0.0449$), as well as δ ($p = 0.0163$), theta ($p < 0.0001$), and high-γ ($p =$ 0.0209) Z'coherence during NREM sleep. In accordance with the changes in Z'coherence (undirected functional connectivity), CNO administration altered NSTE (directed connectivity). Mean feedforward and feedback NSTE values for each frequency band during wake and NREM states are shown in Table 2. Compared with VEH, CNO injection significantly altered feedforward connectivity during NREM sleep ($F_{(1,9)} = 6.60$; $p =$ 0.0302) but not during wakefulness ($F_{(1,9)} =$ 1.86; $p = 0.2059$). Moreover, there was a significant drug × frequency band interaction for the frontal-to-occipital NSTE during NREM ($F_{(5,45)} = 4.05$; $p = 0.0040$) and for the occipital-to-frontal NSTE during wakefulness ($F_{(5,45)} = 3.71$; $p = 0.0068$) and NREM sleep ($F_{(5,45)} = 4.95$; $p = 0.0011$). *Post hoc* multiple-comparisons tests demonstrated that theta frontal-to-occipital connectivity was increased during NREM sleep ($p = 0.0003$). Additionally, theta occipital-to-frontal connectivity was increased during NREM ($p < 0.0001$) and wakefulness ($p = 0.0052$).

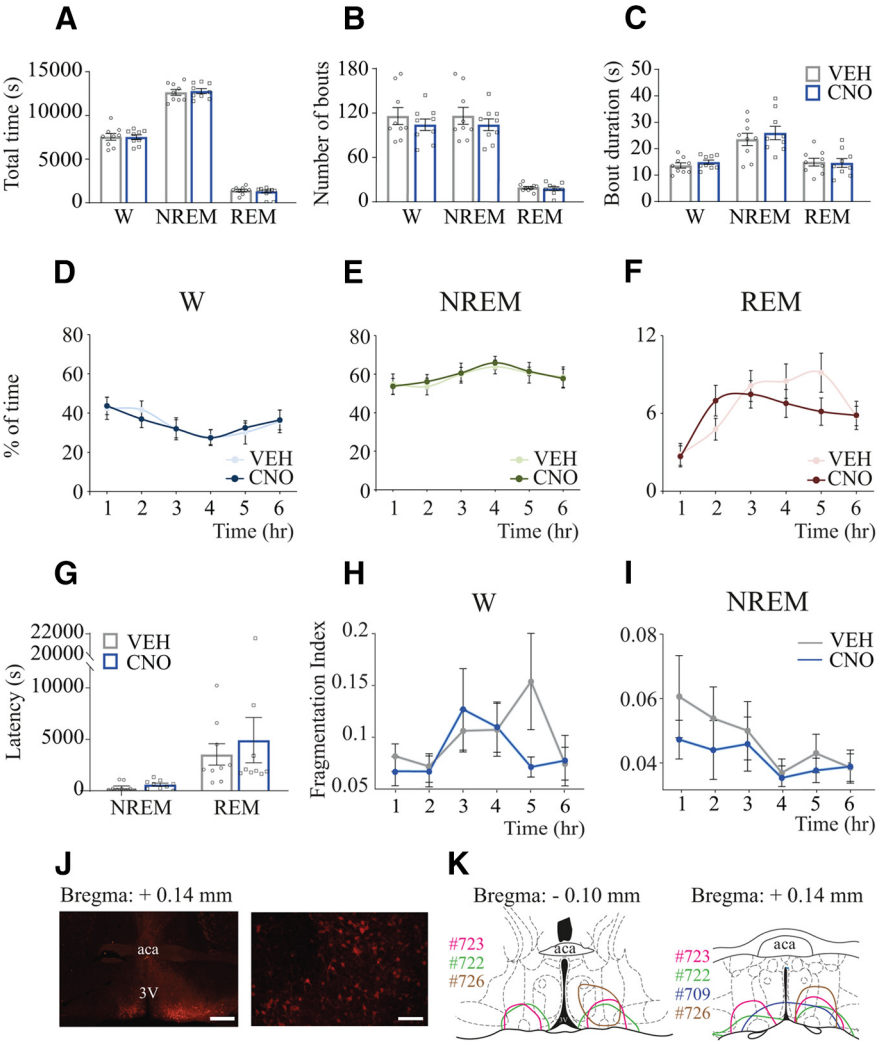

Figure 7. CNO administration to Vglut2-Cre mice that did not express designer receptors did not alter sleep-wake states. Sleep data from Vglut2-Cre mice injected with (1) AAV-hSyn-DIO-hM3D(Gq)-mCherry into the preoptic area but did not express designer receptors ($n = 5$) and (2) the control vector AAV-hSyn-DIO-mCherry ($n = 4$) were pooled together and used as negative controls. ***A***, Group data summarizing total time in wakefulness, NREM sleep, and REM sleep after VEH or CNO (1.0 mg/kg) injection. ***B***, Number of bouts of wakefulness, NREM sleep, and REM sleep. ***C***, Comparison of mean episode duration per state. A one-tailed paired *t* test with Bonferroni correction was used for statistical comparisons between treatment conditions. ***D–F***. Graphs plot the mean time (expressed as percent of total recording time) in wakefulness, NREM sleep, and REM sleep, respectively, for each 1 h block after VEH and CNO administration. Two-way repeated-measures ANOVA followed by a Bonferroni test was used for statistical comparisons. ***G***, Latency to NREM and REM sleep. A one-tailed paired *t* test was used for statistical comparisons between treatment conditions. ***H***, ***I***, FI calculated for NREM and REM sleep, respectively, plotted for each 1 h block after VEH and CNO injection. Wilcoxon matched-pairs rank tests were used for statistical comparisons between treatment conditions. Data are mean ± SEM. ***J***, Left, Right, Low- and high-magnification photographs, respectively, of mCherry immunohistochemical staining (red) corresponding to the fluorescent reporter of the control vector within the VLPO of a Vglut2-Cre mouse. Scale bars: Left, 500 μm; Right, 100 μm. ***K***, Color-coded depiction of control vector injection area, represented on coronal schematics of the preoptic area modified from a mouse brain atlas (Paxinos and Franklin, 2001). Color-matched identification numbers for each mouse used in this study are listed on the left side of each panel. aca, Anterior commissure; 3V, third ventricle.

Compared with VEH injection, CNO did not modify feedforward NSTE during NREM in δ ($p = 0.0759$), σ, β, low-γ, and high-γ ($p > 0.9999$ for each frequency band), as well as the feedback NSTE during wakefulness or NREM in δ ($p = 0.8974$ and $p > 0.9999$, respectively), σ, β, low-γ, and high-γ ($p > 0.9999$ for each frequency band and each behavioral state). To summarize, activation of preoptic glutamatergic neurons enhanced both undirected and directed connectivity in the theta frequency band during NREM sleep as well as undirected functional connectivity in the high-γ band during wakefulness and NREM sleep.

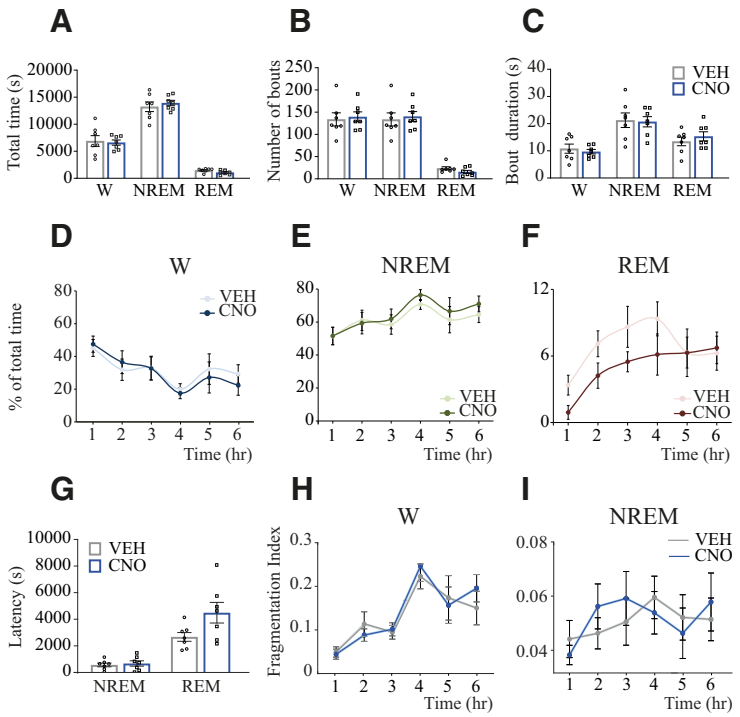

Figure 8. Activation of glutamatergic neurons in the MnPO of the hypothalamus did not substantially alter sleep-wake states. Sleep data from a previous study (collected using identical procedures and experiment design) (Vanini et al., 2020) were reanalyzed and used in the current study as a site-control group. All Vglut2-Cre mice ($n = 7$) included in this control group had confirmed hM3Dq receptor expression in MnPO glutamatergic neurons (for information on the distribution of the excitatory designer receptor hM3Dq within the MnPO, see Vanini et al., 2020, their Fig. S4). ***A***, Group data summarizing total time in wakefulness, NREM sleep, and REM sleep after VEH or CNO (1.0 mg/kg) injection. ***B***, Number of bouts of wakefulness, NREM sleep, and REM sleep. ***C***, Comparison of mean episode duration per state. A one-tailed paired *t* test with Bonferroni correction was used for statistical comparisons between treatment conditions. ***D–F***, Graphs represent the mean time (expressed as percent of total recording time) in wakefulness, NREM sleep, and REM sleep, respectively, for each 1 h block after VEH and CNO administration. Two-way repeated-measures ANOVA followed by a Bonferroni test was used for statistical comparisons. ***G***, Latency to NREM and REM sleep. A one-tailed paired *t* test was used for statistical comparisons. ***H***, ***I***, FI calculated for NREM and REM sleep, respectively, plotted for each 1 h block after VEH and CNO injection. Wilcoxon matched-pairs rank tests were used for statistical comparisons between treatment conditions. Data are mean ± SEM.

Changes in temporal complexity of the signals evaluated by a corrected LZc analysis are summarized in Figure 11. Relative to VEH injection, CNO increased EEG signal complexity during wakefulness in both frontal (mean ± SEM = 0.9782 ± 0.005 vs 0.9618 ± 0.005; $t_{(9)} = 2.47$, $p = 0.0354$) and occipital regions (0.9891 ± 0.007 vs 0.968 ± 0.007; $t_{(9)} = 3.72$, $p = 0.0048$). Additionally, CNO increased the EEG complexity during NREM sleep in frontal (0.9728 ± 0.009 vs 0.947 ± 0.003; $t_{(9)} = 3.29$, $p = 0.0094$) and occipital regions (0.9708 ± 0.009 vs 0.948 ± 0.003; $t_{(9)} = 3.13$, $p = 0.0122$). Interestingly, EEG complexity levels during NREM sleep after CNO were not significantly different from during wakefulness in the control treatment condition (frontal cortex: $t_{(9)} = 0.94$; $p = 0.3719$ and occipital cortex: $t_{(9)} = 0.26$ $p = 0.8029$).

Discussion

This study demonstrates that chemogenetic activation of preoptic glutamatergic neurons within the medial-lateral preoptic region of the hypothalamus increases wakefulness, decreases NREM sleep, causes NREM sleep fragmentation and state instability, reduces body temperature, and suppresses REM sleep. Furthermore, these neurons influence cortical oscillations, connectivity, and complexity. The effect on state transitions and cortical dynamics are both novel aspects of this study and significantly advance our understanding on the role of these neurons in arousal state control. A dual role for preoptic neurons in sleep-wake regulation was recently predicted by modeling simulations based on EEG dynamics across the sleep-wake cycle of rats with VLPO neuronal lesions (Lombardi et al., 2020). Together with our previous work (Vanini et al., 2020), and evidence demonstrating that optogenetic stimulation of VLPO glutamatergic neurons projecting to the tuberomammillary nucleus increases wakefulness (Chung et al., 2017), this is among the first studies to empirically identify a subset of preoptic neurons that promotes wakefulness. Importantly, activation of glutamatergic neurons in the MnPO (control site) had no substantial effect on sleep-wake duration, sleep latency, and consolidation. The nonsignificant trend toward an increase in the latency and decrease in the duration of REM sleep during the first 4 h after CNO injection is congruent with previous work from our group showing that (in an analysis of only 3 h after CNO administration) MnPO glutamatergic neurons only reduced REM sleep quantity (Vanini et al., 2020). Together, these data suggest that glutamatergic neurons in the MnPO destabilize REM sleep and support the conclusion that the effect of the activation of glutamatergic neurons in the medial-lateral preoptic region on sleep-wake states is site-specific.

The preoptic area contributes to REM sleep regulation. Cell-specific excitotoxic lesions in a region medial and dorsal to the VLPO (termed "extended" VLPO) decreases REM sleep (Lu et al., 2002). Subsets of preoptic neurons are maximally active during spontaneous REM sleep bouts, during periods of sleep restriction when REM sleep pressure is the highest, and during REM sleep rebound following REM sleep deprivation (Lu et al., 2002; Suntsova et al., 2002; Gvilia et al., 2006; Takahashi et al., 2009; Sakai, 2011; M. A. Alam et al., 2014). Furthermore, activation of preoptic GABAergic neurons that innervate the tuberomammillary nucleus increases REM sleep (Chung et al., 2017). Here we show that activation of glutamatergic neurons in the medial-lateral preoptic region decreased REM sleep time. Indeed, this state was eliminated for 6 h in 55% of the mice. To the best of our knowledge, this is the first direct demonstration that preoptic glutamatergic neurons can, directly or indirectly, suppress REM sleep generation. The remarkable reduction in REM sleep may result from several factors. First, the profound sleep fragmentation induced by activation of preoptic glutamatergic neurons can reduce REM sleep because its propensity builds up during prior NREM sleep bouts and spontaneous REM sleep generation requires NREM sleep occurrence (Benington and Heller, 1994; Le Bon, 2020). This is particularly evident in 2 mice that had a substantial increase in NREM sleep (45% in #559 and 19% in #541), but their sleep was highly fragmented and REM sleep was virtually eliminated. However, while NREM sleep fragmentation had a duration of 4 h, REM sleep quantity was reduced or totally suppressed for 6 h after CNO administration; and there was no negative correlation between REM sleep time and sleep fragmentation or the number

of NREM-wake transitions. Furthermore, there was no REM homeostatic response after sleep fragmentation, as both number and duration of REM sleep bouts remained unchanged. Another potential mechanism is by a direct or indirect activation of brain circuits that inhibit REM sleep generation. The preoptic region is reciprocally connected with wake-promoting monoaminergic systems and hypocretin/orexin-containing neurons in the perifornical region of the hypothalamus (Zardetto-Smith and Johnson, 1995; Sherin et al., 1998; Chou et al., 2002; Uschakov et al., 2006). Furthermore, the ventrolateral periaqueductal gray receives projections from preoptic neurons (Uschakov et al., 2009; Hsieh et al., 2011) and GABAergic neurons within the periaqueductal gray region exert a powerful inhibitory control on REM sleep generation (Sastre et al., 1996; Vanini et al., 2007; Sapin et al., 2009; Weber et al., 2018). Identification of local and distant target neurons of wake-promoting glutamatergic neurons in the medial-lateral preoptic region will be critical for a circuit-based understanding of their role in REM sleep control. This is especially important because the ability of these neurons to promote wakefulness as well as enhance cortical dynamics while suppressing REM sleep might serve the function of preventing REM-like intrusions after the initiation of waking consciousness. Last, preoptic neurons play an important role in thermoregulation (McGinty et al., 2001). Activation of MnPO glutamatergic (Abbott and Saper, 2017; Vanini et al., 2020) and VLPO galaninergic neurons (Kroeger et al., 2018) induces significant hypothermia in mice, and exposure to cold temperature increases wakefulness and reduces REM sleep in rodents (Roussel et al., 1984; Amici et al., 1998; Baracchi et al., 2008; Sato et al., 2015). Glutamatergic neurons that cause hypothermia (some of which also promote sleep) are mainly localized within the MnPO and medial preoptic area (Zhang et al., 2015; Abbott and Saper, 2017; Harding et al., 2018; Vanini et al., 2020). Here we demonstrate that activation of glutamatergic neurons in the medial-lateral preoptic region causes hypothermia and that the reduction of body temperature was sustained during the 6 h recording period. Interestingly, the severity of the hypothermia induced by activation of glutamatergic neurons in the MnPO and medial-lateral preoptic region was comparable (i.e., there was no significant difference), and CNO administration to MnPO mice did not cause sleep fragmentation or REM suppression. These results suggest that hypothermia and sleep fragmentation caused by activation of glutamatergic neurons in the medial-lateral preoptic region may not be dissociated and may causally contribute to the prevention of REM sleep generation.

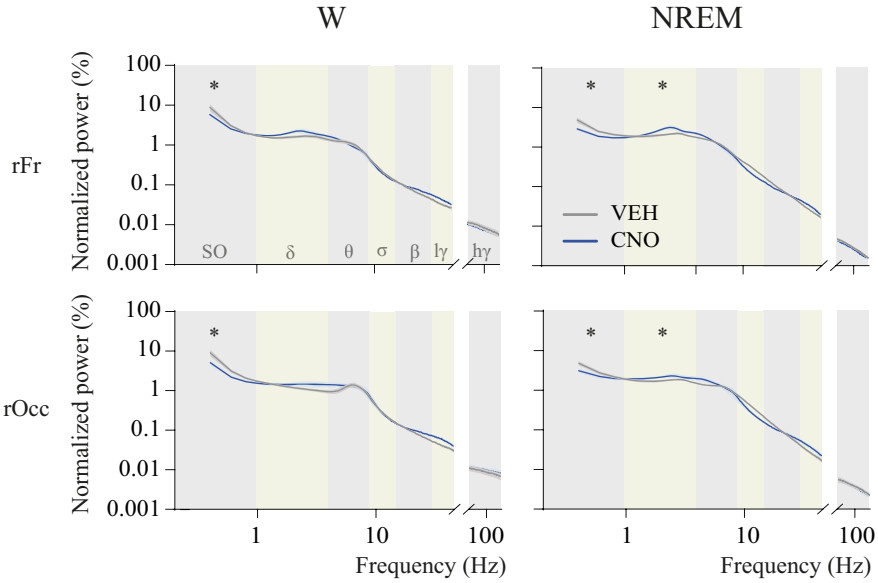

Figure 9. Activation of glutamatergic neurons in the medial-lateral preoptic region decreased the spectral power of slow oscillations and increased δ power. Graphs plot normalized spectral power in the right frontal (rFr) and occipital (rOcc) regions during wakefulness (W) and NREM sleep, after injection of VEH or CNO (1.0 mg/kg) in $n = 10$ mice. Traces represent mean values (thin, dark lines) $\pm$ the SEM (shaded area above and below the mean). Alternating vertical-colored bands in the background of the graphs represent frequency ranges. Because notch filters were applied to some recording pairs (i.e., VEH and CNO recordings from the same mouse), frequencies between 45 and 75 Hz were excluded from the analysis. Two-way repeated-measures ANOVA followed by a Sidak test corrected for multiple comparisons was used for statistical comparison of spectral power in each frequency band. *Significant difference ($p < 0.05$) relative to control. SO, Slow oscillations; lγ, low-γ; hγ, high-γ.

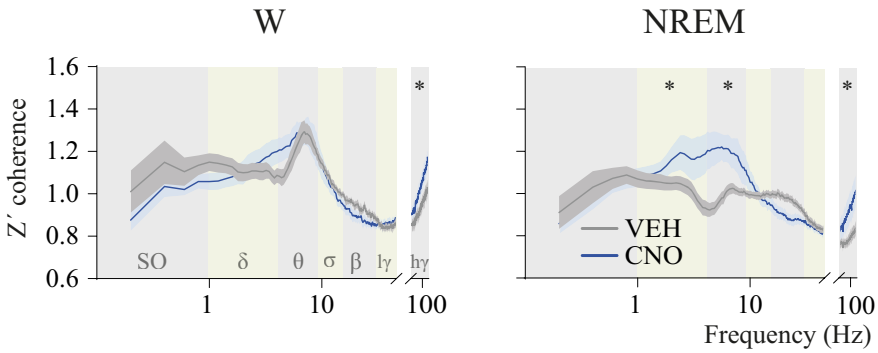

Figure 10. Activation of glutamatergic neurons in the medial-lateral preoptic region increased cortical connectivity. Mean Z′coherence (undirected connectivity) profile between right frontal and occipital as a function of state (wakefulness [W] and NREM sleep) and treatment (VEH and CNO 1.0 mg/kg) in $n = 10$ mice. Traces represent mean values (thin, dark lines) $\pm$ the SEM (shaded area above and below the mean). Alternating vertical-colored bands in the background of the graphs represent frequency ranges. Because notch filters were applied to some recording pairs (i.e., VEH and CNO recordings from the same mouse), frequencies between 45 and 75 Hz were excluded from the analysis. *Significant difference ($p < 0.05$) relative to control. SO, Slow oscillations; lγ, low-γ; hγ, high-γ.

This study shows that activation of glutamatergic neurons in the medial-lateral preoptic region causes a transient increase in wakefulness and a reduction in NREM sleep. Additionally, there was a robust, long-lasting NREM sleep fragmentation and state instability resembling the disrupted sleep pattern observed in sleep apnea (Guilleminault et al., 1976; Kimoff, 1996), Alzheimer's disease (Lim et al., 2014), and aging (Lim et al., 2014; J. Li et al., 2018). Similarly, chemogenetic stimulation of cholinergic neurons in the basal forebrain, lateral to the preoptic area, increases wakefulness and fragments sleep (Anaclet et al., 2015); and optical stimulation of basal forebrain parvalbumin neurons induces brief, rapid arousals from sleep (McKenna et al.,

Table 2. Directed cortical connectivity during NREM and wake states, by EEG frequency band and as a function of treatment condition[a]

	Occipital-to-frontal (feedback connectivity)				Frontal-to-occipital (feedforward connectivity)			
	Wakefulness		NREM sleep		Wakefulness		NREM sleep	
EEG frequency band	VEH	CNO	VEH	CNO	VEH	CNO	VEH	CNO
δ (0.5-4 Hz)	0.033 ± 0.002	0.029 ± 0.002	0.028 ± 0.001	0.031 ± 0.003	0.037 ± 0.002	0.048 ± 0.007	0.052 ± 0.008	0.038 ± 0.002
Theta (4-9 Hz)	0.049 ± 0.003	0.059 ± 0.004	0.035 ± 0.001	0.051 ± 0.004*	0.086 ± 0.006	0.090 ± 0.009*	0.073 ± 0.010	0.050 ± 0.003*
Sigma (9-15 Hz)	0.049 ± 0.002	0.047 ± 0.005	0.049 ± 0.003	0.047 ± 0.005	0.049 ± 0.003	0.050 ± 0.007	0.040 ± 0.004	0.039 ± 0.001
Beta (15-30 Hz)	0.026 ± 0.024	0.023 ± 0.002	0.027 ± 0.001	0.023 ± 0.001	0.0250 ± 0.001	0.022 ± 0.001	0.021 ± 0.001	0.027 ± 0.001
Low γ (30-45 Hz)	0.021 ± 0.001	0.024 ± 0.002	0.022 ± 0.001	0.023 ± 0.001	0.018 ± 0.001	0.019 ± 0.001	0.019 ± 0.001	0.019 ± 0.001
High γ (75-115 Hz)	0.017 ± 0.001	0.020 ± 0.001	0.011 ± 0.001	0.015 ± 0.002	0.020 ± 0.001	0.025 ± 0.001	0.019 ± 0.002	0.014 ± 0.001

[a]Data ($n = 10$ Vglut2-Cre mice) are mean ± SEM. A two-way repeated-measures ANOVA followed by Sidak multiple-comparisons test was used for statistical comparisons. CNO (agonist at hM3Dq receptors; 1.0 mg/kg).
*Significant differences relative to control ($p < 0.05$).

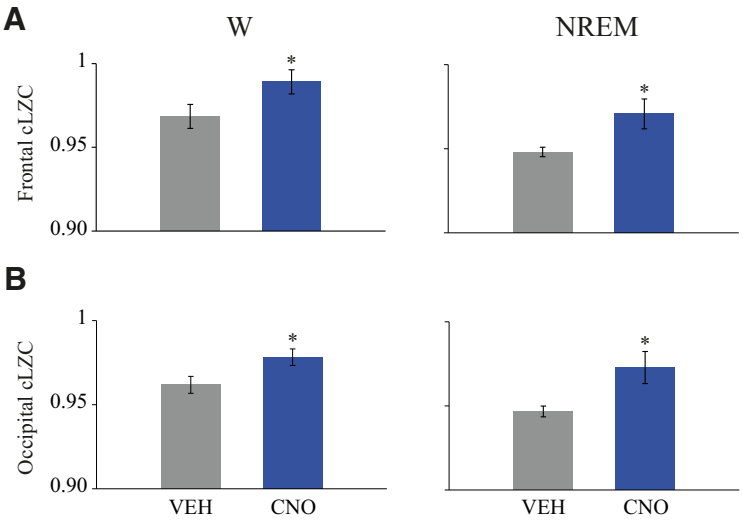

Figure 11. Activation of glutamatergic neurons in the medial-lateral preoptic region increased EEG signal complexity. Graphs plot corrected LZc (cLZc) values during wakefulness (W) and NREM sleep for frontal (***A***) and occipital (***B***) regions. Data are mean ± SEM. Differences between VEH and CNO (1.0 mg/kg) in $n = 10$ mice were analyzed by two-tailed paired *t* tests. *Significant difference ($p < 0.05$) relative to control.

2020). Relative to basal forebrain glutamatergic neurons, optogenetic stimulation increases wakefulness (Xu et al., 2015), whereas activation of these neurons using chemogenetic strategies did not significantly alter sleep-wake states (Anaclet et al., 2015). Importantly, none of the mice in this study expressed excitatory designer receptors in the basal forebrain region, confirming again the specificity of the effects of our stimulation region. Given the frequent and brief arousals from sleep observed after CNO administration, we speculate that glutamatergic neurons in the medial-lateral preoptic region may initiate, but not maintain, wakefulness. Furthermore, these neurons may be part of a brain network that produces rapid arousals from sleep in response to endogenous or environmental alert signals.

Given the considerable diversity of preoptic neurons, genetically targeting glutamatergic/Vglut2 neurons for optogenetic or chemogenetic studies of this region does not necessarily restrict the manipulation to a single functional cell group. For example, Moffitt et al. (2018) reported that many excitatory neurons (Vglut2$^+$) expressed GABA synthetic genes, and a few Vglut2$^+$ neurons in the preoptic area also express the vesicular GABA transporter. Based on this evidence, we cannot rule out that more than one neuronal type was stimulated in the present work, which may explain the substantive increase in NREM sleep time observed in 2 of the mice contrasting with the rest of the cohort in the sleep study. Thus, it is becoming evident that further studies will require a more nuanced approach, identifying and manipulating these neurons based on specific projection sites or neurochemical markers (Chung et al., 2017; Harding et al., 2018; Reitz et al., 2020).

Glutamatergic neurons in the medial-lateral preoptic altered several sleep and wake EEG features related to cortical dynamics. Specifically, CNO administration increased (1) theta and γ coherence, (2) cortical connectivity, and (3) EEG complexity during NREM sleep. These are electrophysiologic traits of more activated states. Indeed, EEG theta and γ coherence, directed connectivity, and complexity are typically highest during wakefulness (Abasolo et al., 2015; Pal et al., 2016, 2020; Brito et al., 2020; Mondino et al., 2020) and progressively decline as sleep deepens (Abasolo et al., 2015; Pal et al., 2016; Bandt, 2017; Gonzalez et al., 2019, 2020; Migliorelli et al., 2019). Together, these EEG changes and the reduction of the spectral power of slow oscillations after CNO injection provide evidence for a "lighter" NREM sleep state. Increased EEG complexity and high-γ coherence are, respectively, suggestive of a higher number of brain network interactions (Guevara Erra et al., 2016) and more alertness during wakefulness (Castro et al., 2013). In the current study, we indeed found that CNO administration increased high-γ coherence, EEG complexity, and feedback connectivity, while reducing the power of slow oscillations during wakefulness. Therefore, these data support the interpretation that activation of glutamatergic neurons in the medial-lateral preoptic region produces an activated EEG state with features that correlate with enhanced wakefulness. Sleep consolidation (Ward et al., 2009) and sleep quality (i.e., slow wave activity and slow oscillations during NREM sleep) (Bellesi et al., 2014; Schreiner et al., 2018; J. Kim et al., 2019; Hahn et al., 2020) as well as REM sleep (Boyce et al., 2017) are crucial for normal cognition. Thus, because of the substantial disruption of sleep patterns and cortical dynamics produced during NREM sleep by the activation of preoptic glutamatergic neurons, further studies are needed to examine the impact on attention and memory processes.

Collectively, our results support the interpretation that glutamatergic neurons in the medial-lateral preoptic region may

initiate, but not maintain, wakefulness from sleep, and their inactivation may be necessary for NREM stability and REM sleep initiation. The present work is limited by including only male mice and stimulation strategies as well as by the lack of data on the effects of these preoptic neurons on sleep-wake states during the dark phase. Additionally, future studies are needed to identify relevant projection pathways and neuronal targets mediating their wakefulness-promoting effects. Furthermore, these findings encourage future circuit-based studies to examine the relevance of these neurons in the generation of wakefulness in response to endogenous or environmental alert signals during sleep, while suppressing REM-like intrusions. These data also have translational implications as they potentially inform the etiology of debilitating, disrupted sleep patterns observed in aging, sleep apnea, and dementia. Last, this study advances sleep neurobiology by providing empirical evidence supporting the hypothesis that the preoptic area is not exclusively somnogenic but rather plays a dual role in the regulation of both sleep and wakefulness.

References

Abasolo D, Simons S, Morgado da Silva R, Tononi G, Vyazovskiy VV (2015) Lempel-Ziv complexity of cortical activity during sleep and waking in rats. J Neurophysiol 113:2742–2752.

Abbott SB, Saper CB (2017) Median preoptic glutamatergic neurons promote thermoregulatory heat loss and water consumption in mice. J Physiol 595:6569–6583.

Alam MA, Kumar S, McGinty D, Alam MN, Szymusiak R (2014) Neuronal activity in the preoptic hypothalamus during sleep deprivation and recovery sleep. J Neurophysiol 111:287–299.

Alam MN, Mallick BN (1990) Differential acute influence of medial and lateral preoptic areas on sleep-wakefulness in freely moving rats. Brain Res 525:242–248.

Amici R, Zamboni G, Perez E, Jones CA, Parmeggiani PL (1998) The influence of a heavy thermal load on REM sleep in the rat. Brain Res 781:252–258.

Anaclet C, Pedersen NP, Ferrari LL, Venner A, Bass CE, Arrigoni E, Fuller PM (2015) Basal forebrain control of wakefulness and cortical rhythms. Nat Commun 6:8744.

Bandt C (2017) A new kind of permutation entropy used to classify sleep stages from invisible EEG microstructure. Entropy 19:197.

Baracchi F, Zamboni G, Cerri M, Del Sindaco E, Dentico D, Jones CA, Luppi M, Perez E, Amici R (2008) Cold exposure impairs dark-pulse capacity to induce REM sleep in the albino rat. J Sleep Res 17:166–179.

Bellesi M, Riedner BA, Garcia-Molina GN, Cirelli C, Tononi G (2014) Enhancement of sleep slow waves: underlying mechanisms and practical consequences. Front Syst Neurosci 8:208.

Benedetto L, Chase MH, Torterolo P (2012) GABAergic processes within the median preoptic nucleus promote NREM sleep. Behav Brain Res 232:60–65.

Benington J, Heller HC (1994) REM-sleep timing is controlled homeostatically by accumulation of REM-sleep propensity in non-REM sleep. Am J Physiol Regul Integr Comp Physiol 266:1992–2000.

Borjigin J, Lee U, Liu T, Pal D, Huff S, Klarr D, Sloboda J, Hernandez J, Wang MM, Mashour GA (2013) Surge of neurophysiological coherence and connectivity in the dying brain. Proc Natl Acad Sci USA 110:14432–14437.

Boyce R, Williams S, Adamantidis A (2017) REM sleep and memory. Curr Opin Neurobiol 44:167–177.

Brito MA, Li D, Mashour GA, Pal D (2020) State-dependent and bandwidth-specific effects of ketamine and propofol on electroencephalographic complexity in rats. Front Syst Neurosci 14:50.

Castro S, Falconi A, Chase MH, Torterolo P (2013) Coherent neocortical 40-Hz oscillations are not present during REM sleep. Eur J Neurosci 37:1330–1339.

Chou TC, Bjorkum AA, Gaus SE, Lu J, Scammell TE, Saper CB (2002) Afferents to the ventrolateral preoptic nucleus. J Neurosci 22:977–990.

Chung S, Weber F, Zhong P, Tan CL, Nguyen TN, Beier KT, Hormann N, Chang WC, Zhang Z, Do JP, Yao S, Krashes MJ, Tasic B, Cetin A, Zeng H, Knight ZA, Luo L, Dan Y (2017) Identification of preoptic sleep neurons using retrograde labelling and gene profiling. Nature 545:477–481.

Delorme A, Makeig S (2004) EEGLAB: an open source toolbox for analysis of single-trial EEG dynamics including independent component analysis. J Neurosci Methods 134:9–21.

Dentico D, Amici R, Baracchi F, Cerri M, Del Sindaco E, Luppi M, Martelli D, Perez E, Zamboni G (2009) c-Fos expression in preoptic nuclei as a marker of sleep rebound in the rat. Eur J Neurosci 30:651–661.

Eikermann M, Vetrivelan R, Grosse-Sundrup M, Henry ME, Hoffmann U, Yokota S, Saper CB, Chamberlin NL (2011) The ventrolateral preoptic nucleus is not required for isoflurane general anesthesia. Brain Res 1426:30–37.

Gaus SE, Strecker RE, Tate BA, Parker RA, Saper CB (2002) Ventrolateral preoptic nucleus contains sleep-active, galaninergic neurons in multiple mammalian species. Neuroscience 115:285–294.

Gonzalez J, Cavelli M, Mondino A, Pascovich C, Castro-Zaballa S, Torterolo P, Rubido N (2019) Decreased electrocortical temporal complexity distinguishes sleep from wakefulness. Sci Rep 9:18457.

Gonzalez J, Cavelli M, Mondino A, Pascovich C, Castro-Zaballa S, Rubido N, Torterolo P (2020) Electrocortical temporal complexity during wakefulness and sleep: an updated account. Sleep Science 13:47–50.

Guevara Erra R, Mateos DM, Wennberg R, Perez Velazquez JL (2016) Towards a statistical mechanics of consciousness: maximization of number of connections is associated with conscious awareness. Phys Rev E 94:052402-1–052402-9.

Guilleminault C, Tilkian A, Dement WC (1976) The sleep apnea syndromes. Annu Rev Med 27:465–484.

Gvilia I, Turner A, McGinty D, Szymusiak R (2006) Preoptic area neurons and the homeostatic regulation of rapid eye movement sleep. J Neurosci 26:3037–3044.

Gvilia I, Suntsova N, Kostin A, Kalinchuk A, McGinty D, Basheer R, Szymusiak R (2017) The role of adenosine in the maturation of sleep homeostasis in rats. J Neurophysiol 117:327–335.

Hahn MA, Heib D, Schabus M, Hoedlmoser K, Helfrich RF (2020) Slow oscillation-spindle coupling predicts enhanced memory formation from childhood to adolescence. Elife 9:e53730.

Harding EC, Yu X, Miao A, Andrews N, Ma Y, Ye Z, Lignos L, Miracca G, Ba W, Yustos R, Vyssotski AL, Wisden W, Franks NP (2018) A neuronal hub binding sleep initiation and body cooling in response to a warm external stimulus. Curr Biol 28:2263–2273.e2264.

Hsieh KC, Gvilia I, Kumar S, Uschakov A, McGinty D, Alam MN, Szymusiak R (2011) c-Fos expression in neurons projecting from the preoptic and lateral hypothalamic areas to the ventrolateral periaqueductal gray in relation to sleep states. Neuroscience 188:55–67.

Ilg AK, Enkel T, Bartsch D, Bahner F (2018) Behavioral effects of acute systemic low-dose clozapine in wild-type rats: implications for the use of DREADDs in behavioral neuroscience. Front Behav Neurosci 12:173.

John J, Kumar VM, Gopinath G, Ramesh V, Mallick H (1994) Changes in sleep-wakefulness after kainic acid lesion of the preoptic area in rats. Jpn J Physiol 44:231–242.

John J, Kumar VM, Gopinath G (1998) Recovery of sleep after fetal preoptic transplantation in medial preoptic area-lesioned rats. Sleep 21:601–606.

Jordan D, Ilg R, Riedl V, Schorer A, Grimberg S, Neufang S, Omerovic A, Berger S, Untergehrer G, Preibisch C, Schulz E, Schuster T, Schroter M, Spoormaker V, Zimmer C, Hemmer B, Wohlschlager A, Kochs EF, Schneider G (2013) Simultaneous electroencephalographic and functional magnetic resonance imaging indicate impaired cortical top-down processing in association with anesthetic-induced unconsciousness. Anesthesiology 119:1031–1042.

Kim J, Gulati T, Ganguly K (2019) Competing roles of slow oscillations and delta waves in memory consolidation versus forgetting. Cell 179:514–526.e513.

Kim JW, Lee JS, Robinson PA, Jeong DU (2009) Markov analysis of sleep dynamics. Phys Rev Lett 102:178104.

Kimoff J (1996) Sleep fragmentation in obstructive sleep apnea. Sleep 19: S61– S66.

Koyama Y, Hayaishi O (1994) Firing of neurons in the preoptic/anterior hypothalamic areas in rat: its possible involvement in slow wave sleep and paradoxical sleep. Neurosci Res 19:31–38.

Krashes MJ, Koda S, Ye C, Rogan SC, Adams AC, Cusher DS, Maratos-Flier E, Roth BL, Lowell BB (2011) Rapid, reversible activation of AgRP neurons drives feeding behavior in mice. J Clin Invest 121:1424–1428.

Kroeger D, Absi G, Gagliardi C, Bandaru SS, Madara JC, Ferrari LL, Arrigoni E, Munzberg H, Scammell TE, Saper CB, Vetrivelan R (2018) Galanin neurons in the ventrolateral preoptic area promote sleep and heat loss in mice. Nat Commun 9:4129.

Le Bon O (2020) Relationships between REM and NREM in the NREM-REM sleep cycle: a review on competing concepts. Sleep Med 70:6–16.

Lee U, Ku S, Noh G, Baek S, Choi B, Mashour GA (2013) Disruption of frontal-parietal communication by ketamine, propofol, and sevoflurane. Anesthesiology 118:1264–1275.

Lempel A, Ziv J (1976) On the complexity of finite sequences. IEEE Trans Inform Theory 22:75–81.

Li D, Mashour GA (2019) Cortical dynamics during psychedelic and anesthetized states induced by ketamine. Neuroimage 196:32–40.

Li D, Hambrecht-Wiedbusch VS, Mashour GA (2017) Accelerated recovery of consciousness after general anesthesia is associated with increased functional brain connectivity in the high-gamma bandwidth. Front Syst Neurosci 11:16.

Li J, Vitiello MV, Gooneratne NS (2018) Sleep in normal aging. Sleep Med Clin 13:1–11.

Lim AS, Ellison BA, Wang JL, Yu L, Schneider JA, Buchman AS, Bennett DA, Saper CB (2014) Sleep is related to neuron numbers in the ventrolateral preoptic/intermediate nucleus in older adults with and without Alzheimer's disease. Brain 137:2847–2861.

Lin JS, Sakai K, Vanni-Mercier G, Jouvet M (1989) A critical role of the posterior hypothalamus in the mechanisms of wakefulness determined by microinjection of muscimol in freely moving cats. Brain Res 479:225–240.

Lombardi F, Gomez-Extremera M, Bernaola-Galvan P, Vetrivelan R, Saper CB, Scammell TE, Ivanov PC (2020) Critical dynamics and coupling in bursts of cortical rhythms indicate non-homeostatic mechanism for sleep-stage transitions and dual role of VLPO neurons in both sleep and wake. J Neurosci 40:171–190.

Lu J, Greco MA, Shiromani P, Saper CB (2000) Effect of lesions of the ventrolateral preoptic nucleus on NREM and REM sleep. J Neurosci 20:3830–3842.

Lu J, Bjorkum AA, Xu M, Gaus SE, Shiromani PJ, Saper CB (2002) Selective activation of the extended ventrolateral preoptic nucleus during rapid eye movement sleep. J Neurosci 22:4568–4576.

Ma Y, Miracca G, Yu X, Harding EC, Miao A, Yustos R, Vyssotski AL, Franks NP, Wisden W (2019) Galanin neurons unite sleep homeostasis and alpha2-adrenergic sedation. Curr Biol 29:3315–3322.e3313.

McGinty D, Alam MN, Szymusiak R, Nakao M, Yamamoto M (2001) Hypothalamic sleep-promoting mechanisms: coupling to thermoregulation. Arch Ital Biol 139:63–75.

McKenna JT, Thankachan S, Uygun DS, Shukla C, McNally JM, Schiffino FL, Cordeira J, Katsuki F, Zant JC, Gamble MC, Deisseroth K, McCarley RW, Brown RE, Strecker RE, Basheer R (2020) Basal forebrain parvalbumin neurons mediate arousals from sleep induced by hypercarbia or auditory stimuli. Curr Biol 30:2379–2385.e2374.

Mendelson WB (2000) Sleep-inducing effects of adenosine microinjections into the medial preoptic area are blocked by flumazenil. Brain Res 852:479–481.

Migliorelli C, Bachiller A, Andrade AG, Alonso JF, Mananas MA, Borja C, Gimenez S, Antonijoan RM, Varga AW, Osorio RS, Romero S (2019) Alterations in EEG connectivity in healthy young adults provide an indicator of sleep depth. Sleep 42:zsz081.

Miranda de Sá AM, Ferreira DD, Dias E, Mendes EM, Felix LB (2009) Coherence estimate between a random and a periodic signal: bias, variance, analytical critical values, and normalizing transforms. J Franklin Inst 346:841–853.

Mitra P, Bokil H (2008) Observed brain dynamics. New York: Oxford UP.

Moffitt JR, Bambah-Mukku D, Eichhorn SW, Vaughn E, Shekhar K, Perez JD, Rubinstein ND, Hao J, Regev A, Dulac C, Zhuang X (2018) Molecular, spatial, and functional single-cell profiling of the hypothalamic preoptic region. Science 362:eaau5324.

Mondino A, Cavelli M, Gonzalez J, Osorio L, Castro-Zaballa S, Costa A, Vanini G, Torterolo P (2020) Power and coherence in the EEG of the rat: impact of behavioral states, cortical area, lateralization and light/dark phases. Clocks Sleep 2:536–556.

Nauta WJ (1946) Hypothalamic regulation of sleep in rats: an experimental study. J Neurophysiol 9:285–316.

Pal D, Silverstein BH, Lee H, Mashour GA (2016) Neural correlates of wakefulness, sleep, and general anesthesia: an experimental study in rat. Anesthesiology 125:929–942.

Pal D, Li D, Dean JG, Brito MA, Liu T, Fryzel AM, Hudetz AG, Mashour GA (2020) Level of consciousness is dissociable from electroencephalographic measures of cortical connectivity, slow oscillations, and complexity. J Neurosci 40:605–618.

Parmeggiani PL (1987) Interaction between sleep and thermoregulation: an aspect of the control of behavioral states. Sleep 10:426–435.

Paxinos G, Franklin KB (2001) The mouse brain in stereotaxic coordinates, Ed 2. San Diego: Academic.

Perez-Atencio L, Garcia-Aracil N, Fernandez E, Barrio LC, Barios JA (2018) A four-state Markov model of sleep-wakefulness dynamics along light/dark cycle in mice. PLoS One 13:e0189931.

Ranft A, Golkowski D, Kiel T, Riedl V, Kohl P, Rohrer G, Pientka J, Berger S, Thul A, Maurer M, Preibisch C, Zimmer C, Mashour GA, Kochs EF, Jordan D, Ilg R (2016) Neural correlates of sevoflurane-induced unconsciousness identified by simultaneous functional magnetic resonance imaging and electroencephalography. Anesthesiology 125:861–872.

Reitz SL, Wasilczuk AZ, Beh GH, Proekt A, Kelz MB (2020) Activation of preoptic tachykinin 1 neurons promotes wakefulness over sleep and volatile anesthetic-induced unconsciousness. Curr Biol 31:394–405.e4.

Rezai Amin S, Gruszczynski C, Guiard BP, Callebert J, Launay JM, Louis F, Betancur C, Vialou V, Gautron S (2019) Viral vector-mediated Cre recombinase expression in substantia nigra induces lesions of the nigrostriatal pathway associated with perturbations of dopamine-related behaviors and hallmarks of programmed cell death. J Neurochem 150:330–340.

Roussel B, Turrillot P, Kitahama K (1984) Effect of ambient temperature on the sleep-waking cycle in two strains of mice. Brain Res 294:67–73.

Sakai K (2011) Sleep-waking discharge profiles of median preoptic and surrounding neurons in mice. Neuroscience 182:144–161.

Sallanon M, Denoyer M, Kitahama K, Aubert C, Gay N, Jouvet M (1989) Long-lasting insomnia induced by preoptic neuron lesions and its transient reversal by muscimol injection into the posterior hypothalamus in the cat. Neuroscience 32:669–683.

Sapin E, Lapray D, Berod A, Goutagny R, Leger L, Ravassard P, Clement O, Hanriot L, Fort P, Luppi PH (2009) Localization of the brainstem GABAergic neurons controlling paradoxical (REM) sleep. PLoS One 4:e4272.

Sastre JP, Buda C, Kitahama K, Jouvet M (1996) Importance of the ventrolateral region of the periaqueductal gray and adjacent tegmentum in the control of paradoxical sleep as studied by muscimol microinjections in the cat. Neuroscience 74:415–426.

Sato N, Marui S, Ozaki M, Nagashima K (2015) Cold exposure and/or fasting modulate the relationship between sleep and body temperature rhythms in mice. Physiol Behav 149:69–75.

Schartner M, Seth A, Noirhomme Q, Boly M, Bruno MA, Laureys S, Barrett A (2015) Complexity of multi-dimensional spontaneous EEG decreases during propofol induced general anaesthesia. PLoS One 10:e0133532.

Schartner MM, Carhart-Harris RL, Barrett AB, Seth AK, Muthukumaraswamy SD (2017) Increased spontaneous MEG signal diversity for psychoactive doses of ketamine, LSD and psilocybin. Sci Rep 7:46421.

Schreiner T, Doeller CF, Jensen O, Rasch B, Staudigl T (2018) Theta phase-coordinated memory reactivation reoccurs in a slow-oscillatory rhythm during NREM sleep. Cell Rep 25:296–301.

Sherin JE, Elmquist JK, Torrealba F, Saper CB (1998) Innervation of histaminergic tuberomammillary neurons by GABAergic and galaninergic neurons in the ventrolateral preoptic nucleus of the rat. J Neurosci 18:4705–4721.

Sitt JD, King JR, El Karoui I, Rohaut B, Faugeras F, Gramfort A, Cohen L, Sigman M, Dehaene S, Naccache L (2014) Large scale screening of neural signatures of consciousness in patients in a vegetative or minimally conscious state. Brain 137:2258–2270.

Suntsova N, Szymusiak R, Alam MN, Guzman-Marin R, McGinty D (2002) Sleep-waking discharge patterns of median preoptic nucleus neurons in rats. J Physiol 543:665–677.

Szymusiak R, Alam N, Steininger TL, McGinty D (1998) Sleep-waking discharge patterns of ventrolateral preoptic/anterior hypothalamic neurons in rats. Brain Res 803:178–188.

Takahashi K, Lin JS, Sakai K (2009) Characterization and mapping of sleep-waking specific neurons in the basal forebrain and preoptic hypothalamus in mice. Neuroscience 161:269–292.

Ticho SR, Radulovacki M (1991) Role of adenosine in sleep and temperature regulation in the preoptic area of rats. Pharmacol Biochem Behav 40:33–40.

Todd WD, Gibson JL, Shaw CS, Blumberg MS (2010) Brainstem and hypothalamic regulation of sleep pressure and rebound in newborn rats. Behav Neurosci 124:69–78.

Uschakov A, Gong H, McGinty D, Szymusiak R (2006) Sleep-active neurons in the preoptic area project to the hypothalamic paraventricular nucleus and perifornical lateral hypothalamus. Eur J Neurosci 23:3284–3296.

Uschakov A, McGinty D, Szymusiak R, McKinley MJ (2009) Functional correlates of activity in neurons projecting from the lamina terminalis to the ventrolateral periaqueductal gray. Eur J Neurosci 30:2347–2355.

Vanini G, Baghdoyan HA (2013) Extrasynaptic GABAA receptors in rat pontine reticular formation increase wakefulness. Sleep 36:337–343.

Vanini G, Torterolo P, McGregor R, Chase MH, Morales FR (2007) GABAergic processes in the mesencephalic tegmentum modulate the occurrence of active (rapid eye movement) sleep in guinea pigs. Neuroscience 145:1157–1167.

Vanini G, Bassana M, Mast M, Mondino A, Cerda I, Phyle M, Chen V, Colmenero AV, Hambrecht-Wiedbusch VS, Mashour GA (2020) Activation of preoptic GABAergic or glutamatergic neurons modulates sleep-wake architecture, but not anesthetic state transitions. Curr Biol 30:779–787.e774.

von Economo C (1930) Sleep as a problem of localization. J Nerv Mental Dis 71:249–259.

Ward CP, McCoy JG, McKenna JT, Connolly NP, McCarley RW, Strecker RE (2009) Spatial learning and memory deficits following exposure to 24 h of sleep fragmentation or intermittent hypoxia in a rat model of obstructive sleep apnea. Brain Res 1294:128–137.

Weber F, Hoang Do JP, Chung S, Beier KT, Bikov M, Saffari Doost M, Dan Y (2018) Regulation of REM and non-REM sleep by periaqueductal GABAergic neurons. Nat Commun 9:354.

Xu M, Chung S, Zhang X, Zhong P, Ma C, Chang WC, Weissbourd B, Sakai N, Luo L, Nishino S, Dan Y (2015) Basal forebrain circuit for sleep-wake control. Nat Neurosci 18:1641–1647.

Zardetto-Smith AM, Johnson AK (1995) Chemical topography of efferent projections from the median preoptic nucleus to pontine monoaminergic cell groups in the rat. Neurosci Lett 199:215–219.

Zhang Z, Ferretti V, Guntan I, Moro A, Steinberg EA, Ye Z, Zecharia AY, Yu X, Vyssotski AL, Brickley SG, Yustos R, Pillidge ZE, Harding EC, Wisden W, Franks NP (2015) Neuronal ensembles sufficient for recovery sleep and the sedative actions of alpha2 adrenergic agonists. Nat Neurosci 18:553–561.

Comentarios adicionales al artículo

En este trabajo demostramos que la activación de estas neuronas produce frecuentes despertares de corta duración fragmentando el sueño NREM y suprime el sueño REM. Además de esto, la activación de estas neuronas genera un sueño más ligero de acuerdo con los parámetros electroencefalográficos encontrados. Por último, demostramos que, además de su rol en el ciclo sueño-vigilia, la activación de estas neuronas produce hipotermia. En este sentido, consideramos que la región medial-lateral del hipotálamo tendría un rol dual en el ciclo sueño-vigilia, con neuronas generadoras de sueño y otras generadoras de vigilia. Esto también fue demostrado por Chung et al. 2017, quien activando mediante optogenética las neuronas glutamatérgicas del VLPO que proyectaban al núcleo tuberomamilar produjo un incremento de vigilia (Chung *et al.*, 2017). Además, otros autores, comprobaron que la activación de neuronas productoras de Taquiquinina 1 también genera vigilia, en este caso una vigilia de mayor duración y más estable, que la provocada por la estimulación de las neuronas glutamatérgicas hallada en nuestro estudio (Reitz *et al.*, 2021). Por último, un trabajo de nuestro laboratorio demostró que la administración de Bicuculina, un antagonista competitivo GABA en el VLPO provoca un aumento de vigilia, una reducción del sueño REM y un aumento de algunos comportamientos maternales activos (Benedetto *et al.*, 2021). Los autores proponen que la administración de Bicuculina estaría desinhibiendo neuronas del VLPO, posiblemente neuronas glutamatérgicas.

<u>Termorregulación y ciclo sueño-vigilia</u>

En este trabajo observamos que además de los efectos sobre el ciclo sueño-vigilia, la activación de las neuronas glutamatérgicas en la región medial-lateral del área preóptica del hipotálamo genera hipotermia. Por lo tanto, no es posible descartar la posibilidad de que algunos de los cambios observados en el ciclo sueño-vigilia sean debidos a la hipotermia. Se ha demostrado que

existe un gran solapamiento entre el ciclo sueño-vigilia y la termorregulación (Harding *et al.*, 2020). La temperatura corporal de los mamíferos disminuye previo a dormir, y la probabilidad de entrar en sueño NREM es mayor cuando la caída de temperatura es máxima. De hecho, existen comportamientos específicos preparatorios para el sueño, siendo uno de ellos la realización del nido con la finalidad de mantener la termo-neutralidad durante el sueño (Harding *et al.*, 2018). Se requieren futuros estudios que determinen si la regulación del sueño y de la temperatura corporal por las neuronas glutamatérgicas esta dada por diferentes subgrupos neuronales, o sí, por el contrario, las mismas neuronas cumplen un rol en ambas funciones.

Conclusiones generales

En este trabajo abordamos la relación neurobiológica y electrofisiológica entre el sueño y la anestesia general. En primer lugar, realizamos un análisis de la potencia y coherencia espectral durante el ciclo sueño-vigilia con el fin de conocer en detalle la actividad eléctrica cortical para luego poder comprarla con la de la anestesia general. Este trabajo fue además complementado con el trabajo de Osorio *et al.* (2020). Pudimos observar que la potencia y coherencia del EEG durante el sueño varía de acuerdo al ciclo luz-oscuridad. Adicionalmente, demostramos diferencias entre distintas áreas corticales e incluso entre ambos hemisferios. Por lo tanto, cuando se compara la actividad eléctrica cortical del ciclo sueño-vigilia con otro estado, es de gran importancia utilizar la misma disposición de electrodos, así como realizar los registros en la misma etapa del día.

Adicionalmente, si bien durante muchos años se ha sostenido que la anestesia general comparte grandes similitudes con el sueño y que actúa mediante los mismos circuitos neurales, en este trabajo hemos colectado evidencia que contradice estas teorías. Por un lado, existen claras

diferencias electroencefalográficas entre la anestesia con uretano (considerada un modelo farmacológico de sueño) y el sueño (tanto No-REM como REM). Por otro lado, la activación del área preóptica del hipotálamo, un área esencial en la generación de sueño no modifica la sensibilidad al isoflurano (un anestésico general ampliamente utilizado).

Por último, el estudio del área preóptica en el sueño y la anestesia general nos permitió desafiar el concepto de que las neuronas involucradas en el ciclo sueño-vigilia del área preóptica del hipotálamo son exclusivamente somnogénicas al comprobar que las neuronas glutamatérgicas del área medial y ventrolateral de la región preóptica generan vigilia, fragmentan el sueño No-REM e inhiben el sueño REM.

Referencias

Akeju, O. & Brown, E.N. (2017) Neural oscillations demonstrate that general anesthesia and sedative states are neurophysiologically distinct from sleep. *Curr Opin Neurobiol*, **44**, 178-185.

Akeju, O., Song, A.H., Hamilos, A.E., Pavone, K.J., Flores, F.J., Brown, E.N. & Purdon, P.L. (2016) Electroencephalogram signatures of ketamine anesthesia-induced unconsciousness. *Clin Neurophysiol*, **127**, 2414-2422.

Alkire, M., Hudetz, A.G. & Tononi, G. (2008) Consciousness and Anesthesia. *Science*, **322**, 876-880.

Avigdor, T., Minert, A., Baron, M. & Devor, M. (2021) Paradoxical anesthesia: Sleep-like EEG during anesthesia induced by mesopontine microinjection of GABAergic agents. *Exp Neurol*, **343**, 113760.

Benedetto, L., Chase, M.H. & Torterolo, P. (2012) GABAergic processes within the median preoptic nucleus promote NREM sleep. *Behav Brain Res*, **232**, 60-65.

Benedetto, L., Rivas, M., Pena, F., Serantes, D., Ferreira, A. & Torterolo, P. (2021) Local administration of bicuculline into the ventrolateral and medial preoptic nuclei modifies sleep and maternal behavior in lactating rats. *Physiol Behav*, **238**, 113491.

Bernard, C.L. (1875) *sur les anesthesique et sur l'asphyxsie*. JB Balliere et Fils, Paris

Boucetta, S., Cisse, Y., Mainville, L., Morales, M. & Jones, B.E. (2014) Discharge profiles across the sleep-waking cycle of identified cholinergic, GABAergic, and glutamatergic neurons in the pontomesencephalic tegmentum of the rat. *J Neurosci*, **34**, 4708-4727.

Bullock, T. & McClune, M. (1989) Lateral coherence of the electrocorticogram: a new measure of brain synchrony. *Electroencephalography and clinical Neurophysiology*, **73**, 479-498.

Carskadon, M.A. & Dement, W.C. (2011) Monitoring and staging human sleep. In Kryger, M.H., Roth, T., Dement, W.C. (eds) *Principles and practice of sleep medicine*. Elseiver Saunders, St Louis, pp. 16-26.

Castro-Zaballa, S., Cavelli, M.L., Gonzalez, J., Nardi, A.E., Machado, S., Scorza, C. & Torterolo, P. (2018) EEG 40 Hz Coherence Decreases in REM Sleep and Ketamine Model of Psychosis. *Front Psychiatry*, **9**, 766.

Cavelli, M., Castro-Zaballa, S., Mondino, A., Gonzalez, J., Falconi, A. & Torterolo, P. (2017) Absence of EEG gamma coherence in a local activated cortical state: a conserved trait of REM sleep. *Translational Brain Rhythmicity*, **2**.

Cavelli, M., Castro, S., Schwarzkopf, N., Chase, M.H., Falconi, A. & Torterolo, P. (2015) Coherent neocortical gamma oscillations decrease during REM sleep in the rat. *Behav Brain Res*, **281**, 318-325.

Cavelli, M., Rojas-Libano, D., Schwarzkopf, N., Castro-Zaballa, S., Gonzalez, J., Mondino, A., Santana, N., Benedetto, L., Falconi, A. & Torterolo, P. (2018) Power and coherence of cortical high-frequency oscillations during wakefulness and sleep. *Eur J Neurosci*, **48**, 2728-2737.

Chung, S., Weber, F., Zhong, P., Tan, C.L., Nguyen, T.N., Beier, K.T., Hormann, N., Chang, W.C., Zhang, Z., Do, J.P., Yao, S., Krashes, M.J., Tasic, B., Cetin, A., Zeng, H., Knight, Z.A., Luo, L. & Dan, Y. (2017) Identification of preoptic sleep neurons using retrograde labelling and gene profiling. *Nature*, **545**, 477-481.

Clement, E.A., Richard, A., Thwaites, M., Ailon, J., Peters, S. & Dickson, C.T. (2008) Cyclic and sleep-like spontaneous alternations of brain state under urethane anaesthesia. *PLoS One*, **3**, e2004.

Eikermann, M., Akeju, O. & Chamberlin, N.L. (2020) Sleep and Anesthesia: The Shared Circuit Hypothesis Has Been Put to Bed. *Curr Biol*, **30**, R219-R221.

Eikermann, M., Vetrivelan, R., Grosse-Sundrup, M., Henry, M.E., Hoffmann, U., Yokota, S., Saper, C.B. & Chamberlin, N.L. (2011) The ventrolateral preoptic nucleus is not required for isoflurane general anesthesia. *Brain Res*, **1426**, 30-37.

Franks, N.P. (2008) General anaesthesia: from molecular targets to neuronal pathways of sleep and arousal. *Nat Rev Neurosci*, **9**, 370-386.

Gelegen, C., Miracca, G., Ran, M.Z., Harding, E.C., Ye, Z., Yu, X., Tossell, K., Houston, C.M., Yustos, R., Hawkins, E.D., Vyssotski, A.L., Dong, H.L., Wisden, W. & Franks, N.P. (2018) Excitatory Pathways from the Lateral Habenula Enable Propofol-Induced Sedation. *Curr Biol*, **28**, 580-587 e585.

Guang, J., Baker, H., Ben-Yishay Nizri, O., Firman, S., Werner-Reiss, U., Kapuller, V., Israel, Z. & Bergman, H. (2021) Toward asleep DBS: cortico-basal ganglia spectral and coherence activity during interleaved propofol/ketamine sedation mimics NREM/REM sleep activity. *NPJ Parkinsons Dis*, **7**, 67.

Gugino, L.D., Chabot, R.J., Prichep, L.S., John, E.R., Formanek, V. & Aglio, L.S. (2001) Quantitative EEG changes associated with loss and return of consciousness in healthy adult volunteers anaesthetized with propofol or sevoflurane. *Br J Anaesth*, **87**, 421-428.

Gvilia, I., Angara, C., McGinty, D. & Szymusiak, R. (2005) Different neuronal populations of the rat median preoptic nucleus express c-fos during sleep and in response to hypertonic saline or angiotensin-II. *J Physiol*, **569**, 587-599.

Gvilia, I., Suntsova, N., Angara, B., McGinty, D. & Szymusiak, R. (2011) Maturation of sleep homeostasis in developing rats: a role for preoptic area neurons. *Am J Physiol Regul Integr Comp Physiol*, **300**, R885-894.

Han, B., McCarren, H., O'Neill, D. & Kelz, M.B. (2014) Distinctive Recruitment of Endogenous Sleep-promoting Neurons by Volatile Anesthetics and a Nonimmobilizer. *Anesthesiology*, **121**.

Harding, E.C., Franks, N.P. & Wisden, W. (2020) Sleep and thermoregulation. *Curr Opin Physiol*, **15**, 7-13.

Harding, E.C., Yu, X., Miao, A., Andrews, N., Ma, Y., Ye, Z., Lignos, L., Miracca, G., Ba, W., Yustos, R., Vyssotski, A.L., Wisden, W. & Franks, N.P. (2018) A Neuronal Hub Binding Sleep Initiation and Body Cooling in Response to a Warm External Stimulus. *Curr Biol*, **28**, 2263-2273 e2264.

Horner, R.L. & Kubin, L. (1999) Pontine Carbachol Elicits Multiple Rapid Eye Movement Sleep-Like Neural Events in Urethane-Anesthetized Rats. *Neuroscience*, **93**, 215-226.

Hudetz, A.G., Liu, X., Pillay, S., Boly, M. & Tononi, G. (2016) Propofol anesthesia reduces Lempel-Ziv complexity of spontaneous brain activity in rats. *Neurosci Lett*, **628**, 132-135.

Huels, E.R., Groenhout, T., Fields, C.W., Liu, T., Mashour, G.A. & Pal, D. (2021) Inactivation of Prefrontal Cortex Delays Emergence From Sevoflurane Anesthesia. *Front Syst Neurosci*, **15**, 690717.

Hull, E.M. & Dominguez, J.M. (2006) Getting his act together: roles of glutamate, nitric oxide, and dopamine in the medial preoptic area. *Brain Res*, **1126**, 66-75.

Jiang-Xie, L.F., Yin, L., Zhao, S., Prevosto, V., Han, B.X., Dzirasa, K. & Wang, F. (2019) A Common Neuroendocrine Substrate for Diverse General Anesthetics and Sleep. *Neuron*, **102**, 1053-1065 e1054.

Jing, W., Wang, Y., Fang, G., Chen, M., Xue, M., Guo, D., Yao, D. & Xia, Y. (2016) EEG Bands of Wakeful Rest, Slow-Wave and Rapid-Eye-Movement Sleep at Different Brain Areas in Rats. *Front Comput Neurosci*, **10**, 79.

Kaisti, K., Metsähonkala, L., Teräs, M., Oikonen, V., Aalto, S., Jääskeläinen, S., Hinkka, S. & Scheinin, H. (2002) Effects of Surgical Levels of Propofol and Sevoflurane Anesthesia on Cerebral Blood Flow in Healthy Subjects Studied with Positron Emission Tomography. *Anesthesiology*, **96**, 1358-1370.

Keifer, J.C., Baghdoyan, H.A. & Lydic, R. (1996) Pontine Cholinergic Mechanisms Modulate the Cortical Electroencephalographic Spindles of Halothane Anesthesia. *Anesthesiology*, **84**, 945-954.

Kroeger, D., Absi, G., Gagliardi, C., Bandaru, S.S., Madara, J.C., Ferrari, L.L., Arrigoni, E., Munzberg, H., Scammell, T.E., Saper, C.B. & Vetrivelan, R. (2018) Galanin neurons in the ventrolateral preoptic area promote sleep and heat loss in mice. *Nat Commun*, **9**, 4129.

Lee, M.G., Manns, I., Alonso, A. & Jones, B. (2004) Sleep-Wake Related Discharge Properties of Basal Forebrain Neurons Recorded With Micropipettes in Head-Fixed Rats. *J Neurophysiol*, **92**, 1182-1198.

Liu, C., Liu, J., Zhou, L., He, H., Zhang, Y., Cai, S., Yuan, C., Luo, T., Zheng, J., Yu, T. & Zhang, M. (2021) Lateral Habenula Glutamatergic Neurons Modulate Isoflurane Anesthesia in Mice. *Front Mol Neurosci*, **14**, 628996.

Lu, J., Nelson, L.E., Franks, N., Maze, M., Chamberlin, N.L. & Saper, C.B. (2008) Role of endogenous sleep-wake and analgesic systems in anesthesia. *J Comp Neurol*, **508**, 648-662.

Lydic, R. & Biebuyck, J.F. (1994) Sleep neurobiology: relevance for mechanistic studies of anaesthesia. *Br J Anaesth*, **72**, 506-508.

Maquet, P. (2000) Functional neuroimaging of normal human sleep by positron emission tomography. *J Sleep Res*, **9**, 207-231.

Mashour, G.A. (2006) Integrating the science of consciousness and anesthesia. *Anesth Analg*, **103**, 975-982.

Mashour, G.A. (2011) Sleep, Anesthesia, and Consciousness. *Sleep*, **34**, 283-291.

Mashour, G.A. & Hudetz, A.G. (2018) Neural Correlates of Unconsciousness in Large-Scale Brain Networks. *Trends Neurosci*, **41**, 150-160.

Mashour, G.A., Lipinski, W.J., Matlen, L.B., Walker, A.J., Turner, A.M., Schoen, W., Lee, U. & Poe, G.R. (2010) Isoflurane anesthesia does not satisfy the homeostatic need for rapid eye movement sleep. *Anesth Analg*, **110**, 1283-1289.

Mashour, G.A. & Pal, D. (2012) Interfaces of sleep and anesthesia. *Anesthesiology Clinics*, **30**, 385-398.

McKinley, M.J., Pennington, G.L. & Ryan, P.J. (2021) Chapter 29 - The median preoptic nucleus: A major regulator of fluid, temperature, sleep, and cardiovascular homeostasis. In Swaab, D.F., Kreier, F., Lucassen, P.J., Salehi, A., Buijs, R.M. (eds) *Handbook of Clinical Neurology*. Elsevier, pp. 435-454.

Melloni, L., Molina, C., Pena, M., Torres, D., Singer, W. & Rodriguez, E. (2007) Synchronization of neural activity across cortical areas correlates with conscious perception. *J Neurosci*, **27**, 2858-2865.

Modirrousta, M., Mainville, L. & Jones, B.E. (2004) Gabaergic neurons with alpha2-adrenergic receptors in basal forebrain and preoptic area express c-Fos during sleep. *Neuroscience*, **129**, 803-810.

Moore, J.T., Chen, J., Han, B., Meng, Q.C., Veasey, S.C., Beck, S.G. & Kelz, M.B. (2012) Direct activation of sleep-promoting VLPO neurons by volatile anesthetics contributes to anesthetic hypnosis. *Curr Biol*, **22**, 2008-2016.

Murphy, M., Bruno, M., Riedner, B., Boveroux, P., Noirhomme, Q., Landsness, E., Brichant, J., Phillips, C., Massimini, M., Laureys, S., Tononi, G. & Boly, M. (2011) Propofol Anesthesia and Sleep: A High-Density EEG Study. *Sleep*, **34**, 283-291.

Nelson, L., Lu, J., Guo, T., Sapper, C., Franks, N. & Maze, M. (2003) The Alpha 2-Adrenoceptor Agonist Dexmedetomidine Converges on an Endogenous Sleep-promoting Pathway to Exert Its Sedative Effects. *Anesthesiology*, **98**, 428-436.

Neves, R.M., van Keulen, S., Yang, M., Logothetis, N.K. & Eschenko, O. (2018) Locus coeruleus phasic discharge is essential for stimulus-induced gamma oscillations in the prefrontal cortex. *J Neurophysiol*, **119**, 904-920.

Osorio, L., Mondino, A., Cavelli, M., González, J., Torterolo, P. & Costa, A. (2020) EEG power spectrum daily variations in sleep and wakefulness. *Sleep Science*.

Pace-Schott, E.F. & Hobson, J.A. (2002) The neurobiology of sleep: genetics, cellular physiology and subcortical networks. *Nat Rev Neurosci*, **3**, 591-605.

Pagliardini, S., Gosgnach, S. & Dickson, C.T. (2013) Spontaneous sleep-like brain state alternations and breathing characteristics in urethane anesthetized mice. *PLoS One*, **8**, e70411.

Pal, D., Dean, J.G., Liu, T., Li, D., Watson, C.J., Hudetz, A.G. & Mashour, G.A. (2018) Differential Role of Prefrontal and Parietal Cortices in Controlling Level of Consciousness. *Curr Biol*, **28**, 2145-2152 e2145.

Pal, D., Lipinski, W.J., Walker, A.J., Turner, A.M. & Mashour, G.A. (2011) State-specific Effects of Sevoflurane Anesthesia on Sleep Homeostasis. *Anesthesiology*, **114**, 302-310.

Pal, D., Silverstein, B.H., Lee, H. & Mashour, G.A. (2016) Neural Correlates of Wakefulness, Sleep, and General Anesthesia: An Experimental Study in Rat. *Anesthesiology*, **125**, 929-942.

Parkar, A., Fedrigon, D.C., Alam, F., Vanini, G., Mashour, G.A. & Pal, D. (2020) Carbachol and Nicotine in Prefrontal Cortex Have Differential Effects on Sleep-Wake States. *Front Neurosci*, **14**, 567849.

Pick, J., Chen, Y., Moore, J.T., Sun, Y., Wyner, A.J., Friedman, E.B. & Kelz, M.B. (2011) Rapid eye movement sleep debt accrues in mice exposed to volatile anesthetics. *Anesthesiology*, **115**, 702-712.

Reitz, S.L. & Kelz, M.B. (2021) Preoptic Area Modulation of Arousal in Natural and Drug Induced Unconscious States. *Front Neurosci*, **15**, 644330.

Reitz, S.L., Wasilczuk, A.Z., Beh, G.H., Proekt, A. & Kelz, M.B. (2021) Activation of Preoptic Tachykinin 1 Neurons Promotes Wakefulness over Sleep and Volatile Anesthetic-Induced Unconsciousness. *Curr Biol*, **31**, 394-405 e394.

Rivas, M., Serantes, D., Pena, F., Gonzalez, J., Ferreira, A., Torterolo, P. & Benedetto, L. (2021) Role of Hypocretin in the Medial Preoptic Area in the Regulation of Sleep, Maternal Behavior and Body Temperature of Lactating Rats. *Neuroscience*, **475**, 148-162.

Roth, B.L. (2016) DREADDs for Neuroscientists. *Neuron*, **89**, 683-694.

Rothhaas, R. & Chung, S. (2021) Role of the Preoptic Area in Sleep and Thermoregulation. *Front Neurosci*, **15**, 664781.

Saper, C.B., Fuller, P.M., Pedersen, N.P., Lu, J. & Scammell, T.E. (2010) Sleep state switching. *Neuron*, **68**, 1023-1042.

Saper, C.B., Scammell, T.E. & Lu, J. (2005) Hypothalamic regulation of sleep and circadian rhythms. *Nature*, **437**, 1257-1263.

Siegel, J.M. (2005) Clues to the functions of mammalian sleep. *Nature*, **437**, 1264-1271.

Singer, W. (2006) Consciousness and the Binding Problem. *Annals of the New York Academy of Sciences*, **929**, 123-146.

Sleigh, J.W., Scheib, C.M. & Sanders, R.D. (2011) General anaesthesia and electroencephalographic spindles. *Trends in Anaesthesia and Critical Care*, **1**, 263-269.

Smith, K.S., Bucci, D.J., Luikart, B.W. & Mahler, S.V. (2016) DREADDS: Use and application in behavioral neuroscience. *Behav Neurosci*, **130**, 137-155.

Suntsova, N., Guzman-Marin, R., Kumar, S., Alam, M.N., Szymusiak, R. & McGinty, D. (2007) The median preoptic nucleus reciprocally modulates activity of arousal-related and sleep-related neurons in the perifornical lateral hypothalamus. *J Neurosci*, **27**, 1616-1630.

Suntsova, N., Szymusiak, R., Alam, M.N., Guzman-Marin, R. & McGinty, D. (2002) Sleep-waking discharge patterns of median preoptic nucleus neurons in rats. *J Physiol*, **543**, 665-677.

Szymusiak, R., Gvilia, I. & McGinty, D. (2007) Hypothalamic control of sleep. *Sleep Med*, **8**, 291-301.

Szymusiak, R. & McGinty, D. (2008) Hypothalamic regulation of sleep and arousal. *Ann N Y Acad Sci*, **1129**, 275-286.

Taniguchi, H. (2014) Genetic dissection of GABAergic neural circuits in mouse neocortex. *Front Cell Neurosci*, **8**, 8.

Torterolo, P., Benedetto, L., Lagos, P., Sampogna, S. & Chase, M.H. (2009) State-dependent pattern of Fos protein expression in regionally-specific sites within the preoptic area of the cat. *Brain Res*, **1267**, 44-56.

Torterolo, P., Castro-Zaballa, S., Cavelli, M. & Gonzalez, J. (2019) Arousal and normal conscious cognition *Arousal in Neurological and Psychiatric Diseases*, pp. 1-24.

Torterolo, P., Gonzalez, J., Castro-Zaballa, S., Cavelli, M., Mondino, A., Pascovich, C., Rubido, N., Murillo-Rodriguez, E. & Vanini, G. (2022) Polysomnography in humans and animal models: basic procedures and analysis. In Murillo-Rodriguez, E. (ed) *Methodological Approaches for Sleep and Vigilance Research*. Academic Press, Elseiver, London, Uk.

Tsuneoka, Y. & Funato, H. (2021) Cellular Composition of the Preoptic Area Regulating Sleep, Parental, and Sexual Behavior. *Front Neurosci*, **15**, 649159.

Tung, A., Bergmann, B.M., Herrera, S., Cao, D. & Mendelson, W. (2004) Recovery from Sleep Deprivation Occurs during Propofol Anesthesia. *Anesthesiology*, **100**, 1419-1426.

Tung, A., Bluhm, B., Wallace, B. & Mendelson, W. (2001) The hypnotic effect of propofol in the medial preoptic area of the rat. *Life Sciences*, **69**, 855-862.

Tung, A., Szafran, M., Bluhm, B. & Mendelson, W. (2002) Sleep Deprivation Potentiates the Onset and Duration of Loss of Righting Reflex Induced by Propofol and Isoflurane. *Anesthesiology*, **97**, 906-911.

Uchida, S., Atsumi, Y. & Kojima, T. (1994) Dynamic Relationships Between Sleep Spindles and Delta Waves During a NREM Period. *Brain Research Bulletin*, **33**, 351-355.

Vacas, S., Kurien, P. & Maze, M. (2013) Sleep and Anesthesia - Common mechanisms of action. *Sleep Med Clin*, **8**, 1-9.

Van Dort, C.J., Zachs, D.P., Kenny, J.D., Zheng, S., Goldblum, R.R., Gelwan, N.A., Ramos, D.M., Nolan, M.A., Wang, K., Weng, F.J., Lin, Y., Wilson, M.A. & Brown, E.N. (2015) Optogenetic activation of cholinergic neurons in the PPT or LDT induces REM sleep. *Proc Natl Acad Sci U S A*, **112**, 584-589.

Vanini, G., Torterolo, P., Baghdoyan, H.A. & Lydic, R. (2011) The Shared Circuits of Sleep and Anesthesia. In Mashour, G.A. (ed) *Neuroscientific Foundations of Anestesiology*. Oxford University Press., New York, pp. 33-44.

von Economo, C. (1930) Sleep as a Problem of Localization. *The Journal of Nervous and Mental Disease*, **71**, 249-259.

Vyazovskiy, V.V. & Tobler, I. (2008) Handedness leads to interhemispheric EEG asymmetry during sleep in the rat. *J Neurophysiol*, **99**, 969-975.

Wang, J., Noh, G.J., Choi, B.M., Ku, S.W., Joo, P., Jung, W.S., Kim, S. & Lee, H. (2017) Suppressed neural complexity during ketamine- and propofol-induced unconsciousness. *Neurosci Lett*, **653**, 320-325.

Whissell, P.D., Tohyama, S. & Martin, L.J. (2016) The Use of DREADDs to Deconstruct Behavior. *Front Genet*, **7**, 70.

Xu, M., Chung, S., Zhang, S., Zhong, P., Ma, C., Chang, W.C., Weissbourd, B., Sakai, N., Luo, L., Nishino, S. & Dan, Y. (2015) Basal forebrain circuit for sleep-wake control. *Nat Neurosci*, **18**, 1641-1647.

Yagishita, H., Nishimura, Y., Noguchi, A., Shikano, Y., Ikegaya, Y. & Sasaki, T. (2020) Urethane anesthesia suppresses hippocampal subthreshold activity and neuronal synchronization. *Brain Res*, **1749**, 147137.

Zhou, H., Zhang, Y., Suter, R., Gong, H., Fang, Q., Zhou, P. & Hickford, J.G.H. (2017) A nucleotide substitution in exon 8 of the glucosylceramidase beta gene is associated with Gaucher disease in sheep. *Anim Genet*, **48**, 733-734.

Anexo 1

SPECIAL ISSUE

XV Latin American Symposium on Chronobiology 2019
Colonia del Sacramento - Uruguay

EEG power spectrum daily variations in sleep and wakefulness

Lucía Osorio [1]
Alejandra Mondino [1,2]
Matías Cavelli [1,3]
Joaquín González [1]
Pablo Torterolo [1]
Alicia Costa [1*]

[1]Laboratorio de Neurobiología del Sueño, Departamento de Fisiología, Facultad de Medicina, Universidad de la República, Montevideo, Uruguay.
[2]Department of Anesthesiology, University of Michigan, Ann Arbor, MI, USA.
[3]Department of Psychiatry, University of Wisconsin, Madison, WI, USA.

ABSTRACT

Objective: To study the differences in electrocortical activity during wakefulness (W), NREM and REM sleep throughout the subjective day and night of the rat. **Methods:** 24-hours of continuous polysomnographic recordings were performed on seven male rats, using neocortical superficial electrodes in a 12h light/12h dark condition. The daily variation of the power spectrum (0.1-200 Hz) was analyzed for each behavioral state. **Results:** In comparison to the dark phase, W during the day was characterized by increases in the relative power of frequencies slower than 30 Hz while higher frequencies were lower. NREM sleep showed marked increases in frequencies higher than 20Hz during the night in comparsion with the light phase; while the delta band (0.5-4Hz) was prominent in diurnal NREM. While the relative power spectrum of REM sleep was homogeneous during the day, it variates in a complex manner during the night. **Discussion:** Electrocortical EEG profile of W and sleep is highly dependent on the time of the day.

Keywords: Rem Sleep; NREM; EEG; Circadian; Rhythm; Delta; Gamma

Corresponding author:
Alicia Costa
E-mail: acosta@fmed.edu.uy

DOI: 10.5935/1984-0063.20200017

INTRODUCTION

The sleep-wake cycle is a critical physiological process and one of the most preserved biological rhythms throughout evolution. This cycle is composed of different behavioral states, commonly distinguished by their electrophysiological signatures and behavioral characteristics. These states correspond to wakefulness (W), non-rapid eye movement (NREM) sleep and rapid eye movement (REM) sleep. W and sleep are associated with different brain functional states, which can be captured by electroencephalographic (EEG) signals containing a broad frequency spectrum.

The EEG reflects the interrelated multicomponent activity of numerous cortical and subcortical neuronal ensembles[1]. EEG activity consists of various frequency bands that vary during the sleep-wake cycle in a characteristic fashion. In the rat, the EEG during W is characterized by low voltage fast waves as well as theta rhythm (4.5-9 Hz) in posterior cortices mainly during active W. NREM sleep EEG is recognized by the occurrence of high-amplitude slow waves (0.5 to 4 Hz) and electrographic events of 0.5-2 seconds in duration known as sleep spindles, that have an intra-event frequency of 9-15 Hz[2,3]. EEG during REM sleep shows a high-frequency rhythm that is nested in very regular and prominent theta activity[4,5].

In contrast to humans, rodents show a strong ultradian component in their sleep, with no single period of consolidated W during the active (night) period or consolidated sleep during the rest (diurnal) period[6]. This polyphasic nature of their sleep-wake cycle allows us to study the features of the EEG during W, NREM and REM sleep at different times of the day.

Previous works in rodents and humans have shown the existence of diurnal variations in the EEG activity at low-frequency bands (up to 30 Hz) (i.e. 7, 2, 8, 9). However, to the best of our knowledge, a continuous recording and analysis of the diurnal variations of the high-frequency bands of the EEG are lacking. Hence, the aim of this report is to convey an initial descriptive analysis of the changes in the EEG power spectra (0.1-200 Hz) of sleep and W occurring at different times of the day. For this purpose, we performed an hour-to-hour analysis of the power spectrum in each behavioral state over a 24h period and illustrate it as the Z-score variation from the mean.

MATERIAL AND METHODS

Experimental animals

Seven adults male Wistar rats (275-330 g) were used in this study. The animals were obtained from and determined to be in good health by the Institutional Animal Care Facility. The experimental procedures were conducted in accordance with the Guide for the Care and Use of Laboratory Animals (8th edition, National Academy Press, Washington, DC, 2010) and approved by the Institutional Animal Care Commission (protocol No. 070153-000332-16, Facultad de Medicina, Universidad de la República). Adequate measures were taken to minimize pain, discomfort or stress of the animals, and efforts were made to use the smallest number of animals necessary to obtain reliable data.

Surgical procedures

The animals were chronically implanted with electrodes to monitor the states of sleep and W. We employed surgical procedures like those used in our previous studies (e.g., 10). Anesthesia was induced with a mixture of ketamine-xylazine (90 mg/kg; 5 mg/kg i.p., respectively). The rat was positioned in a stereotaxic frame, and the skull was exposed. To record the EEG, stainless steel screw electrodes (1 mm diameter) were screwed on craniotomies to have their tips touching the brain's surface (above the dura mater) in different cortices. The arrangement of electrodes is depicted in Figure 1. Six electrodes were located bilaterally in the primary motor cortex (M1: L ± 2.5 mm, AP +2.5 mm), the primary somatosensory cortex (S1: L ± 2.5 mm, AP −2.5 mm) and secondary visual cortex (V2: L ± 2.5 mm, AP −7.5 mm). The reference electrode was placed in the cerebellum (Figure 1 A). Bipolar electrodes were inserted into the neck muscles in order to record the electromyogram (EMG). The electrodes were connected to a plug that was bonded to the skull with acrylic cement. At the end of the surgical procedures, an analgesic (Ketoprofen, 1 mg/kg, subcutaneously) was administered. Incision margins were kept clean and a topical antibiotic was applied daily. After the animals recovered from the preceding surgical procedures, they were adapted to the recording chamber for one week.

Experimental sessions

All animals were housed individually in transparent cages (40 x 30 x 20 cm) containing wood shavings in a temperature-controlled room (21- 24 °C) with 12:12h light-dark cycle, light (50 lux) beginning at 08:00h (ZT0), with water and food *ad libitum*. The recordings were performed through a rotating connector, to allow the rats to move freely within the recording box.

All the data was collected continuously over a 24h period recordings starting at ZT0. Bioelectric signals were amplified (×1000), the filters were set at 0.1 Hz and 200 Hz. EEG and EMG activity were captured and stored directly on a PC computer through a National Instruments data acquisition card of 16 bits with a sampling rate of 1024 Hz by means of DASYLab software (Measurement Computing). The animals were left undisturbed during all the recordings.

Data analysis

Behavioral states were determined in 10 s epochs. W was defined as low voltage fast waves in the frontal cortex, sometimes with theta rhythm in occipital cortex and relatively high EMG activity. Light sleep (LS) was defined as high voltage slow cortical waves interrupted by low voltage fast electroencephalographic activity, while slow-wave sleep (SWS) was identified by continuous high amplitude slow (1-4 Hz) frontal, parietal and occipital waves and sleep spindles combined with a reduced EMG activity. For the daily power spectrum analysis, LS and SWS were pooled together and classified as NREM sleep. REM sleep was defined as low voltage fast frontal waves, a regular theta rhythm in the parietal and occipital cortices, and a silent EMG except for occasional myoclonic twitching.

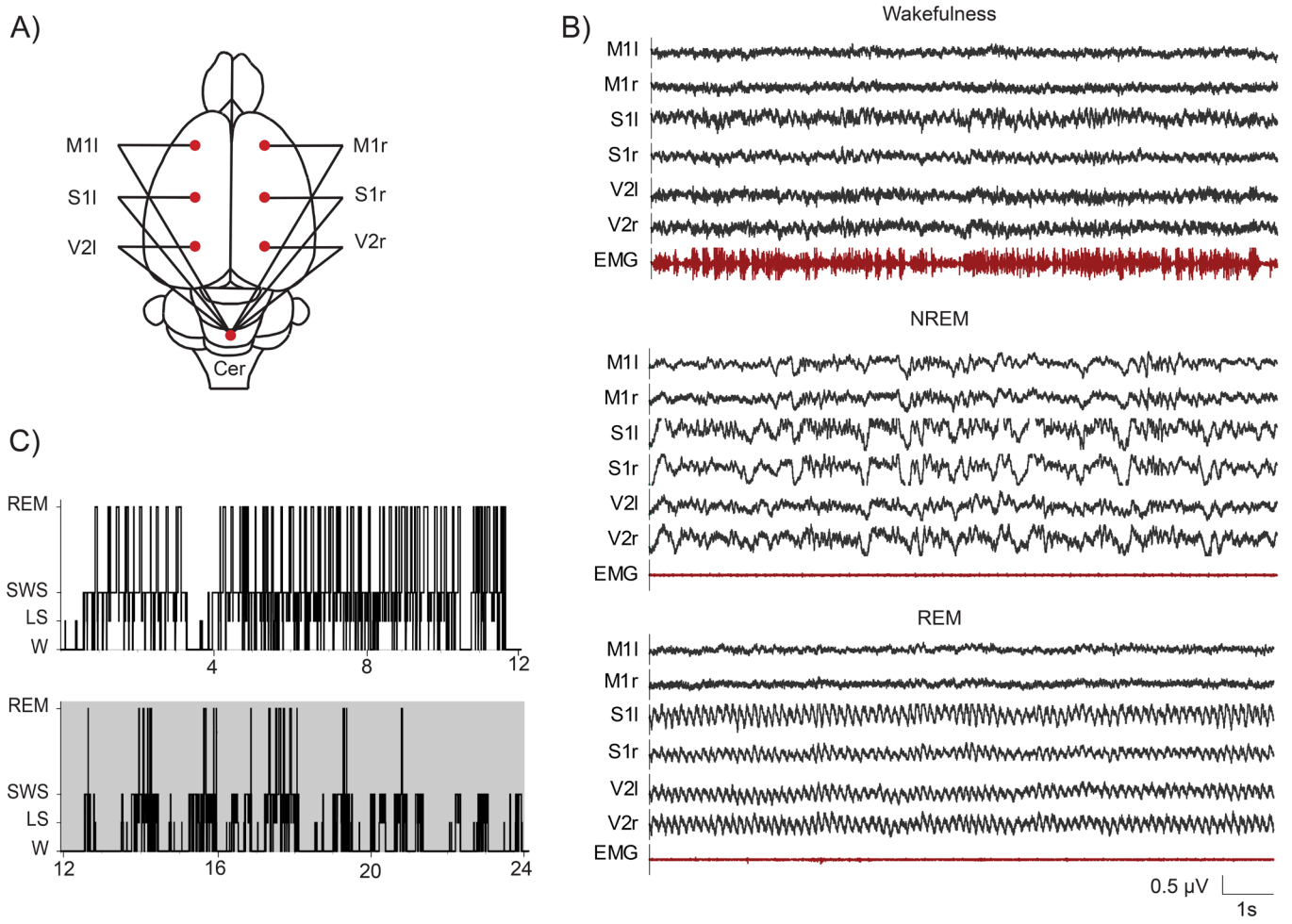

Figure 1. A) Representative scheme showing the position of the recording electrodes. The electrodes were referred to a common electrode that was located over the cerebellum (Cer). M1, primary motor cortex; S1, primary somatosensory cortex; V2, secondary visual cortex; r, right; l, left. B) Polysomnographic recordings of a representative animal in wakefulness, NREM sleep, and REM sleep. EMG: electromyogram. C) Representative hypnogram of the 24h period (0 is 8:00 AM: ZT0). The shaded area indicates the lights-off period.

In order to analyze the power spectrum in each EEG channel, we used procedures like those applied in our previous studies (e.g., 10). The power spectrum was estimated on Matlab using the Welch function (Hamming window, window size 10 s, with an overlap of 2.5 s, a frequency sample of 1024 Hz and a resolution of 0.5 Hz). The mean power of all 6 electrodes and 7 rats, was used to calculate the relative power. This was determined by dividing the power value for each frequency band in each time point, by the sum of the total power for that frequency in the 24 hs. Z transformations were made in order to express the values as deviations from the mean. It is important to note that in the REM sleep analysis the last hour was not computed due to a coincidental lack of this behavioral state in all animals during that period.

RESULTS

Polysomnographic recordings

The simultaneous electrocortical activity of different brain areas was recorded continuously over a 24h period. Representative recordings of these areas during W, NREM, and REM sleep are shown (Figure 1B). The polycyclic nature of the sleep-wake cycle of the rat can be observed in a representative hypnogram (Figure 1C). The animals showed a clear preference for sleep during the light period (72% of total sleep time; 59% in NREM and 13% in REM sleep) and to be awake at night (61% in W; 32% in NREM and 4% in REM sleep).

Daily power spectrum during wakefulness

Figure 2A shows the hour-to-hour analysis of the percentage of W; the daily variation in the percentage of W is readily observed.

The EEG power spectrum during W has robust daily variations, as shown in the spectrograms (grand average of animals and channels) (Figure 2B and C). The main observation was that diurnal and nocturnal W differ in their electrocortical activity profiles. The relative power of the high-frequency rhythms (30 - 200 Hz) was higher both at the beginning (between ZT12 and ZT16) and at the end of the dark phase, reaching values that were 2 to 3 standard deviations (SD or Z-units) over the mean (Figure 2B).

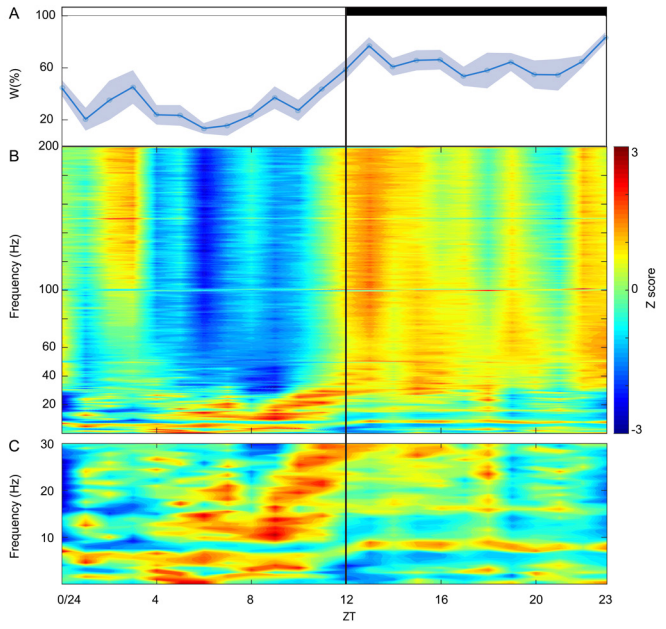

Figure 2. EEG relative power spectra during wakefulness. A) Percentage of time spent in W throughout the 24h period. The shaded outline indicates 1 SD. The top bar indicates light and dark periods. B) Z-score of the relative power spectrogram of W during the 24h period. The black vertical line indicates lights-off onset. C) Zoomed inset showing the Z-score of the relative power spectrogram for the 0-30Hz band. ZT0 = 8AM. Panels B and C share the same z-score color scale. All Y-axis starting at 0.

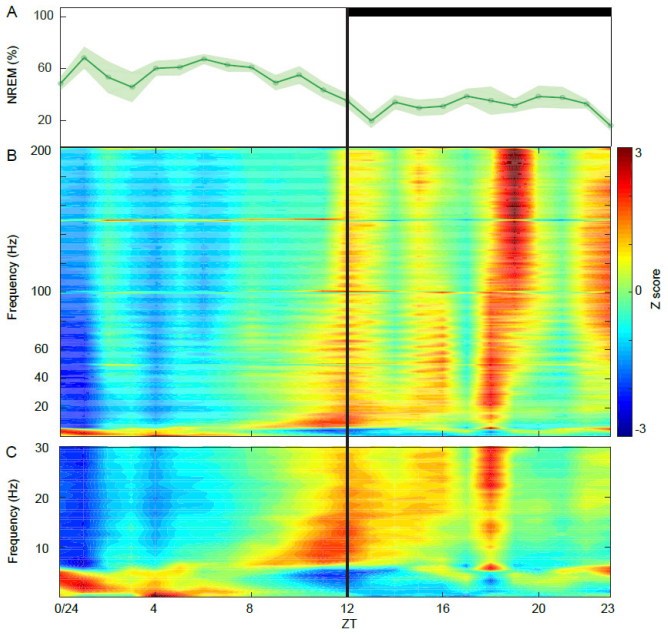

Figure 3. EEG relative power spectra during NREM sleep. A) Top panel: Percentage of time spent in NREM throughout the 24h period. The shaded outline indicates 1 SD. The top bar indicates light and dark phases. B) Z-score for the relative power spectrogram of NREM during the 24h period. The black vertical line indicates lights-off onset. C) Zoomed inset showing the Z-score of the relative power spectrogram for the 0-30Hz band. ZT0=8AM. Panels B and C share the same z-score color scale. All Y-axis starting at 0.

In addition, their lower values were observed in the ZT4-ZT10 window (light phase). Inspecting the frequencies up to 30Hz we observed higher relative power values (2 to 3 SD over the mean) mainly from Z4 up to Z12 (Figure 2C). Note that from ZT8 to ZT12 there is a progressive increase in the relative power of frequencies in the 12-30 Hz range. Another interesting observation is that theta-band activity (5 to 9 Hz) seemed to be faster during the nighttime.

Daily power spectrum during NREM sleep

As it is shown in Figure 3A NREM sleep predominates during the light phase. During the light phase, from ZT0 to ZT6, NREM was characterized by an increase in the relative power of the activity up to 5Hz (mainly slow-wave activity, SWA), and a decrease in the higher frequencies (Figure 3B and C). From ZT8 a progressive increase in power in 9-15 Hz oscillations (sleep spindles) was observed. The SWA relative power reached a minimum value two hours before lights-off. During the dark period, NREM was characterized by an increase in the relative power of frequencies higher than 6 Hz and up to 200Hz (Figure 3B and C); however, these changes were not homogenous throughout the night.

Daily power spectrum during REM sleep

Figure 4A shows the hour-to-hour analysis of the percentage of REM sleep. This behavioral state was more prominent during the light phase, no presence of REM sleep was detected in the last hour of the recordings.

The relative power spectrogram during the lights-on period showed no marked changes in relation to the mean (Figure 4B); however, it was highly variable during the dark phase.

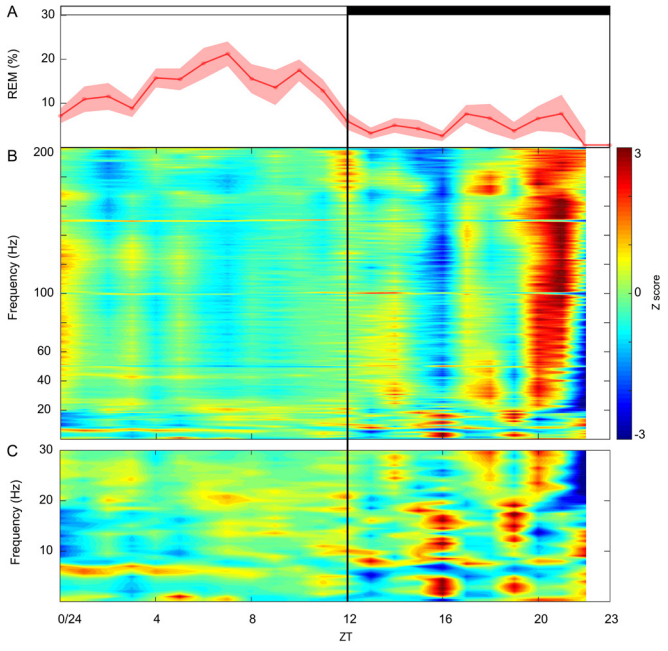

Figure 4. EEG relative power spectra during REM sleep. A) Percentage of time spent in REM throughout the 24h period. The shaded outline indicates 1 SD. The top bar indicates light and dark phases. B) Z-score for the relative power spectrogram during the 24h period. The black vertical line indicates lights-off onset. C) Zoomed inset showing the Z-score of the relative power spectrogram for the 0-30Hz band. ZT0=8AM. Panels B and C share the same z-score color scale. All Y-axis starting at 0.

In fact, the relative power of frequencies up to 30Hz changed with short time increases and decreases over the mean. Also, the most remarkable fact was the increase in the relative power of frequencies in the 20-200 Hz range, at the end of the nighttime (Figure 4B). During the day, theta frequency appears to be slower than during the dark- phase. (Figure 4C). Note that the last hour in the spectrogram is blank due to the lack of REM sleep during this period.

DISCUSSION

In this preliminary study, we performed a descriptive analysis of the daily variations in the EEG power spectrum (0.1 – 200 Hz) of W, NREM and REM sleep of the rat. We demonstrated the presence of an important daily variation in the spectrographic profile of both W and sleep. This variation was evident both within and between the light and dark phases.

Previous studies showed diurnal variations in the EEG of the rat on frequencies up to 30 Hz[7, 4, 11]. In fact, our results support the pioneer studies of Rosenberg et al.,[12] and Steinfels et al.[7], that showed that the highest spectral values can be found during the day in the delta band for NREM sleep and in the theta band for REM sleep. However, we chose to use relative power in order to analyze differences within each frequency band throughout the 24hs for each behavioral state. These previous studies were limited to study frequencies lower than 30Hz, while in this report we also analyze the higher frequencies (up to 200Hz).

Our results showed that diurnal W was heterogeneous with the main changes being a decrease in the relative power of high frequency oscillations (> 30 Hz), and bouts of increase in the relative power of slower rhythms. Nocturnal W was characterized by a larger relative power in the high-frequency rhythms (> 30 Hz) while slower oscillations, apart from the theta band, showed not main changes. This result suggests that nocturnal W presents greater cortical arousal than diurnal W.

Human electrocortical activity has been shown to exhibit important diurnal and circadian variations. Cacot et al.[13] found a clear diurnal variation in the power of EEG rhythms up to 30 Hz during W, with maximum achieved at noon or in the afternoon. In addition, classic studies by Kleitman have shown ultradian differences in behavior during W, what was called basic rest-activity cycle[14]; however, the electrophysiological counterpart of this ultradian cycle has not been studied in detail.

Regarding NREM sleep, in comparison to nighttime, diurnal activity presented a higher power in lower frequencies (mainly below 5 Hz), while the power of the high frequencies (> 30 Hz) was lower. Hence, suggesting that NREM sleep during the day is deeper than during the night. In accordance with Bergmann et al.[2], our data showed that as NREM sleep time increases, slow-wave incidence and amplitude increase. Fluctuations in the elctrocortical activity, probably reflecting the level of arousal, also occur during night NREM sleep. In humans, a cyclic alternating pattern (CAP), characterized by the regular alternation of EEG patterns that represents a complex form of periodic activity, was described during NREM sleep see [15, 16]. In fact, Terezano et al.[17], showed the existence of a CAP in NREM sleep characterized by changes at the level of arousal to sensory stimuli.

An important fact, is that during W and NREM, an opposite correlation between high frequency (> 30 Hz) and low-frequency oscillations (mainly in the delta, 0.5-4 Hz band) was evident. This result agrees with Maloney et al.[18] who showed that gamma activity was negatively correlated with delta across all behavioral states.

Regarding REM sleep, our results showed a mostly homogeneous profile during the light-phase. This is in accordance with previous results by Borbély et al.[4], who showed no clear variations in the relative EEG power density of REM during the day. Hence, REM sleep is a highly stable behavioral state during the light phase. During the night REM sleep the spectrogram has a changing profile with alternations between bouts of slow (< 20Hz) and high (30 - 200 Hz) electrocortical activity. Our results agree with those of Steinfels et al.[7] where a clear increase in the EEG spectral power was observed at the end of the dark period. Finally, it was readily observed that during the first half of the light period, the frequency of the peak of the theta band during REM sleep was lower that in the dark period; probably this fact could be related with a more active REM sleep during the night[19].

CONCLUSIONS AND FUTURE DIRECTIONS

In the present report, we demonstrated a clear difference in the power spectrum profile both in W and sleep during the light and dark phases among a wide range of electrocortical oscillations (0.1-200 Hz). However, further analysis needs to be done in order to better understand if the observed variations depend on external cues, circadian and/or homeostatic process (processes C and S, respectively; see Borbély et al., 20). Sleep deprivation, as well as recording in free-running conditions, will be optimal to answer these interrogations.

In addition, another future direction is to perform a detailed analysis of the daily variation of the activity of different neocortical and archicortical (olfactory bulb) areas as well as of their functional connectivity.

ACKNOWLEDGMENTS

This work was supported by Agencia Nacional de Investigación e Innovación (ANII), (Proyecto FCE_1_2017_1_136550); Comisión Sectorial de Investigación Científica (CSIC) (Proyecto I+D 2016_589); and Programa de Desarrollo de Ciencias Básicas (PEDECIBA)-Uruguay.

REFERENCES

1. da Silva FL. Neural mechanisms underlying brain waves: from neural membranes to networks. Electroencephalography and clinical neurophysiology. 1991 Aug 1;79(2):81-93.
2. Bergmann BM, Winter JB, Rosenberg RS, Rechtschaffen A. NREM sleep with low-voltage EEG in the rat. Sleep. 1987 Jan 1;10(1):1-1.
3. Etevenon P, Giannella F. Waking and sleeping states in the rat from an EEG data analysis point of view. Waking & Sleeping. 1980 Jan-Mar;4(1):33-45.
4. Borbély AA, Tobler I, Hanagasioglu M. Effect of sleep deprivation on sleep and EEG power spectra in the rat. Behavioural brain research. 1984 Dec 1;14(3):171-82.
5. Young GA, Steinfels GF, Khazan N, Glaser EM. Cortical EEG power spectra associated with sleep-awake behavior in the rat. Pharmacology Biochemistry and Behavior. 1978 Jan 1;8(1):89-91.

6. Yasenkov R, Deboer T. Circadian modulation of sleep in rodents. In: Progress in brain research 2012 Jan 1 (Vol. 199, pp. 203-218). Elsevier.
7. Steinfels GF, Young GA, Khazan N. Diurnal variations in REM and NREM sleep EEG power spectra in the rat. Brain research. 1980 Jan 13;181(2):425-32.
8. Grasing K, Szeto H. Diurnal variation in continuous measures of the rat EEG power spectra. Physiology & behavior. 1992 Feb 1;51(2):249-54.
9. Dijk DJ. Circadian variation of EEG power spectra in NREM and REM sleep in humans: dissociation from body temperature. Journal of sleep research. 1999 Sep;8(3):189-95.
10. Cavelli M, Castro-Zaballa S, Mondino A, Gonzalez J, Falconi A, Torterolo P. Absence of EEG gamma coherence in a local activated cortical state: a conserved trait of REM sleep. Translational Brain Rhythmicity. 2017;21132017.
11. Grasing K, Szeto H. Diurnal variation in continuous measures of the rat EEG power spectra. Physiology & behavior. 1992 Feb 1;51(2):249-54.
12. Rosenberg RS, Bergmann BM, Rechtschaffen A. Variations in slow wave activity during sleep in the rat. Physiology & behavior. 1976 Dec 1;17(6):931-8.
13. Cacot P, Tesolin B, Sebban C. Diurnal variations of EEG power in healthy adults. Electroencephalography and clinical neurophysiology. 1995 May 1;94(5):305-12
14. Kleitman N. The basic rest-activity cycle and physiological correlates of dreaming. Experimental neurology. 1967 Dec 1;19:2-4.
15. Gaches J. Activités périodiques en EEG. Revue d'Electroencéphalographie et de Neurophysiologie Clinique. 1971 Jan 1;1(1):9-33.
16. Terzano MG, Mancia D, Manzoni Gc. Periodic activities in Creutzfeldt-Jakob disease and epilepsy. In: Nisticb G, Di Perri R, Meinardi H, eds. Epilepsy: an update on research and therapy. New York: Alan R. Liss, 1983:199-226.
17. Terzano MG, Mancia D, Salati MR, Costani G, Decembrino A, Parrino L. The cyclic alternating pattern as a physiologic component of normal NREM sleep. Sleep. 1985 Jun 1;8(2):137-45.
18. Maloney KJ, Cape EG, Gotman J, Jones BE. High-frequency γ electroencephalogram activity in association with sleep-wake states and spontaneous behaviors in the rat. Neuroscience. 1997 Jan 1;76(2):541-55.
19. Sei H, Morita Y. Acceleration of EEG theta wave precedes the phasic surge of arterial pressure during REM sleep in the rat. Neuroreport. 1996 Nov 25;7(18):3059-62.
20. Borbély AA, Daan S, Wirz-Justice A, Deboer T. The two-process model of sleep regulation: a reappraisal. Journal of sleep research. 2016 Apr;25(2):131-43.